MODELING STUDY OF NONLINEAR DYNAMICS IN THE GROWTH OF AQUATIC PHYTOPLANKTON

by

Qing Guo

BSc., Jilin Agricultural University, 2015
MSc., Wenzhou University, 2018

DISSERTATION SUBMITTED IN PARTIAL
FULFILLMENT OF THE REQUIREMENTS FOR THE
DEGREE OF DOCTOR OF PHILOSOPHY
IN
NATURAL RESOURCES AND ENVIRONMENTAL STUDIES

UNIVERSITY OF NORTHERN BRITISH COLUMBIA

July 2023

ABSTRACT

Phytoplankton bloom has become a growing global concern in recent years due to the excessive growth of algae, causing significant negative impacts on aquatic ecosystem and threatening human health. Growing evidence suggests that algal blooms are a consequence of the interplay of various hydrodynamical, chemical, and biological processes in aquatic systems. The complexity and nonlinearity of aquatic ecosystems, and the complexity of climatic and hydrographic events, make interpreting and predicting the blooms a very challenging task. In recent years, many different strategies have been adopted to manage algal blooms. Among them, mathematical models are advantageous because they can capture the ubiquitous stoichiometric constraints for modeling species growth and interaction. Thus, mathematical models have been widely used to investigate the dynamics of phytoplankton growth. In this study, five mathematical models were developed based on population dynamics, ecological dynamics, dynamic modeling, and probability theory. The models were investigated theoretically and numerically in terms of the theory of partial differential equations, stochastic differential equations, impulsive differential equations, and numerical simulation. The objective of this dissertation research was to gain insight into plankton dynamics and explore potential management strategies for excessive algal growth in aquatic systems. The main results are presented as follows:

Firstly, a nutrient-plankton model incorporating delay and diffusion was developed. The theoretical analysis revealed that delay can trigger the nutrient-plankton oscillation via a Hopf bifurcation. Especially, the stability switches for positive equilibrium occur with increasing delay, which indicates that delay can generate and suppress the unstable coexistence of species population. Numerical results reveal that the stability switches for positive equilibrium indeed exist in the model, and the homogeneous multiple periodic solutions, as well as chaos, can occur with different values of delay, which implies that the model

exhibits delay-induced complex dynamics.

Secondly, a stochastic Leslie-Gower phytoplankton-zooplankton model with prey refuge was developed. The dynamical analysis revealed the sufficient conditions for the persistence and extinction of plankton populations. The numerical simulations showed that environmental noise and prey refuge play a crucial role in the survival of plankton species. The results further demonstrate that prey refuge can enhance the oscillation range of phytoplankton population, but the variance of zooplankton tends to increase and then decrease as prey refuge increased.

Thirdly, considering seasonal disturbances in aquatic ecosystem, a stochastic nutrient-phytoplankton model with seasonal fluctuation was developed. The results indicate that periodic solutions exist under certain conditions, suggesting that plankton populations are associated with periodic oscillations. Furthermore, numerical results showed that seasonal fluctuation can trigger periodic blooms of phytoplankton and promote the coexistence of plankton species. Specifically, the results indicate that phytoplankton is more sensitive to nutrient than to seasonal fluctuation.

Fourthly, a stochastic nutrient-plankton model with regime-switching was developed by considering regime-switching plankton mortality. The results showed that the model admits a stationary distribution under certain conditions. Then the numerical analysis revealed that the persistence and extinction of plankton populations are sensitive to variations in nutrient input. The numerical results also indicate that regime-switching plankton mortality contributes to the survival of plankton populations in the aquatic system.

Finally, a stochastic nutrient-plankton model with impulsive control was developed. The theoretical analysis established sufficient conditions for the existence of periodic solutions. In addition, the numerical analysis showed that nutrient impulse plays an important role in preventing and controlling algal blooms, and appropriate environmental fluctuation can promote the coexistence of phytoplankton and zooplankton populations. However, excess intensity noise can

result in the collapse of the entire ecosystem.

CO-AUTHORSHIP

This dissertation was primarily conducted by me, as I was responsible for developing overarching research goals and aims, creating models, and developing software. I also wrote the manuscripts and incorporated comments and feedback during revisions. Dr. Jianbing Li supervised the research progress and provided valuable feedback during manuscript revisions. Dr. Min Zhao supervised field data collection and provided computing resources and analysis tools. Dr. Chuanjun Dai provided computer code, supporting algorithms, and computing resources, and contributed to the manuscript revisions. Dr. He Liu also provided valuable input to improve the manuscripts. All resulting publications include authorship from Dr. Jianbing Li, Dr. Min Zhao, Dr. Chuanjun Dai, and Dr. He Liu. Additionally, Dr. Hengguo Yu, Dr. XiuXiu Sun, Dr. Yi Wang, Dr. Pankaj Kumar Tiwari, Dr. Zhan Jin, and MS. Lijun Wang provided manuscript reviews and suggestions, and as a result, they were included as co-authors on some of the publications.

Publication and authorships from this dissertation (Published or prepared for submission):

Guo, Q., Dai, C.J., Yu, H.G., Liu, H., Sun, X.X., Li, J., Zhao, M., 2020. Stability and bifurcation analysis of a nutrient-phytoplankton model with time delay. Mathematical Methods in the Applied Sciences. 43, 3018-3039. DOI: 10.1002/mma.6098.

Guo, Q., Wang, L.J., Liu, H., Wang, Y., Li, J., Tiwari, P.K., Zhao, M., Dai, C.J., 2022. Stability switches and chaos induced by delay in a nutrient-plankton model with diffusion. Submitted to Journal of Biological Dynamics on October 9, 2022 (Revision Required on June 27, 2023). (Chapter 3)

Guo, Q., Dai, C.J., Wang, L.J., Liu, H., Wang, Y., Li, J., Zhao, M., 2021. Dynamics of a stochastic Leslie-Gower phytoplankton-zooplankton model with prey refuge. (Prepared), (Chapter 4)

Guo, Q., Dai, C.J., Wang, L.J., Liu, H., Wang, Y., Li, J., Zhao, M., 2022. Stochastic periodic solution of a nutrient-plankton model with seasonal fluctuation. Journal of Biological Systems. 30, 695-720. DOI: 10.1142/S0218339022500255. (Chapter 5)

Guo, Q., Wang, Y., Dai, C.J., Wang, L.J., Liu, H., Li, J., Tiwari, P.K., Zhao, M., 2023. Dynamics of stochastic nutrient-plankton model with regime-switching. Ecological Modelling. 477, 110249. DOI: 10.1016/j.ecolmodel.2022.110249. (Chapter 6)

Guo, Q., Liu, H., Wang, Y., Li, J., Zhao, M., Tiwari, P.K., Jin, Z., Dai, C.J., 2023. Dynamics of a stochastic nutrient-plankton model with impulsive control strategy. European Physical Journal Plus. 138, 470. DOI: 10.1140/epjp/s13360-023-04111-0. (Chapter 7)

Zhao, X., Wang, L.J., Tiwari, P.K., Liu, H., Wang, Y., Li, J., Zhao, M., Dai, C.J., Guo, Q., 2023.

Investigation of a nutrient-plankton model with stochastic fluctuation and impulsive control. Mathematical Biosciences and Engineering. Accepted on July 5, 2023.

Liu, H., Dai, C.J., Yu, H.G., Guo, Q., Li, J., Hao, A.M., Kikuchi, J., Zhao, M., 2021. Dynamics induced by environmental stochasticity in a phytoplankton-zooplankton system with toxic phytoplankton. Mathematical Biosciences and Engineering. 18, 4101-4126. DOI: 10.3934/mbe.2021206.

Liu, H., Dai, C.J., Yu, H.G., Guo, Q., Li, J., Hao, A.M., Kikuchi, J., Zhao, M., 2022. Dynamics of a stochastic phytoplankton–toxic phytoplankton–zooplankton system under regime switching. Mathematical Methods in the Applied Sciences. 45, 9769-9786. DOI: 10.1002/mma.8334.

Liu, H., Dai, C.J., Yu, H.G., Guo, Q., Li, J., Hao, A.M., Kikuchi, J., Zhao, M., 2023. Dynamics of a stochastic non-autonomous phytoplankton–zooplankton system involving toxin-producing phytoplankton and impulsive perturbations. Mathematics and Computers in Simulation. 203, 368-386. DOI: 10.1016/j.matcom.2022.06.012.

TABLE OF CONTENTS

LIST OF TABLES

LIST OF FIGURES

ACKNOWLEDGEMENT

First and foremost, I would like to express to my supervisor, Dr. Jianbing Li, and co-supervisor, Dr. Min Zhao, for their invaluable guidance, encouragement, and support throughout this study. Without their advice and support, I would not have been able to complete this research. I would also like to thank my supervisory committee members, Dr. Ron Thring and Dr. Youmin Tang, for their insightful guidance and encouragement.

I would also like to extend my special appreciation to Dr. Chuanjun Dai from Wenzhou University for generously sharing his expertise and insights in research and providing selfless assistance in both my research and personal life. Dr. Dai consistently offered valuable suggestions and resources that greatly contributed to my research. My heartfelt thanks also go to Dr. Bill McGill, Dr. Darwyn Coxson, and Dr. Ellen Petticrew for their supervision during my first year of the PhD program. Their guidance inspired me to approach my research from a broader perspective and instilled in me a positive and optimistic outlook on life. Additionally, I am grateful to all the staff and faculty members at UNBC for their help, which made my life and studies at UNBC more comfortable.

This research received support from multiple organizations, including the National Natural Science Foundation of China, the National Key Research and Development Program of China, the Zhejiang Provincial Natural Science Foundation of China, the UNBC Graduate Entrance Research Award (GERA), Wenzhou University Joint Doctoral Stipend, Wenzhou Huang Mengqi Dandelion Charity Foundation, and the PhD Dissertation Completion Award.

I would like to express my thanks to Dr. Youqin Wang for providing me with lab equipment, supplies, and the necessary resources for my simulation work at UNBC. I am also grateful to Dr. Yuan Tian, Dr. Jingjing Shi, and Dr. He Liu for their encouragement and selfless help. I would like to acknowledge my classmates at UNBC for sharing their knowledge, skills, and thoughtful discussions. Special thanks go to Dr. Xiufeng Yan, Dr. Mingjiang Wu, Dr. Zengling Ma, Dr.

Xiangyong Zheng, Dr. Qi Wang, Dr. Min Wang, Dr. Wenli Qin, and Dr. Hengguo Yu for their support and professional advice regarding water sampling and data analysis at Wenzhou University.

I extend my gratitude to all my friends in China and Canada, with a special thanks to Ms. Jingjing Su, Ms. Lijun Wang, Mr. Lei Shen, Mr. Jess, and all my teammates who supported me through many challenging times during my PhD studies. Lastly, I would like to express my heartfelt thanks to my family for their unconditional support and love. I am especially grateful to my parents, my elder brother, my cousins, and my relatives, who consistently support and understand my choices, brightening my life with their presence.

Chapter 1

GENERAL INTRODUCTION

1.1. Background

Aquatic planktonic ecosystems are natural systems formed by the interaction between planktonic organisms and the abiotic environment. They encompass a specific spatiotemporal range, and are an integral part of aquatic ecosystems. Plankton, a group of organisms that passively float in the water layer under water movement, form the foundation of productivity in the water. Plankton can be classified into six distinct groups based on their size: picoplankton (< 2 μm), nanoplankton (2-20 μm), microplankton (20-200 μm), mesoplankton (0.2-2 mm), macroplankton (2-20 mm), and megaplankton (> 20 mm) (Baretta-Bekker et al., 1998; Medvinsky et al., 2002; Raymont, 1980). Additionally, the functional classification of plankton is significantly influenced by their trophic level, size, and distribution (Medvinsky et al., 2002). Based on the nutritional approach, plankton can be divided into two categories: phytoplankton and zooplankton species.

Phytoplankton are commonly known as floating plant species that inhabit various water environments, including fresh-water lakes, larger rivers, and the pelagic zone of the sea (Moruff et al., 2016). Phytoplankton are autotrophic plankton that produce organic matter through photosynthesis by absorbing light energy and carbon dioxide. Phytoplankton, such as diatoms, cyanobacteria, and methanogens, are unicellular and microscopic in size. They serve as the primary producers in aquatic ecosystems and are the primary food source for zooplankton. In contrast, zooplankton are consumers and secondary producers in aquatic ecosystems.

Apart from their role as the base of the food chain in aquatic ecosystems, phytoplankton also contribute to our climate by absorbing harmful carbon dioxide from the atmosphere and producing oxygen through photosynthesis. Additionally, phytoplankton recycle phosphorus, nitrogen, and

sulphur (Lobus et al., 2023). However, there is growing evidence of an increasing trend in the frequency, intensity, and duration of algal blooms over the past decades. This includes the emergence of more toxic species and the adverse effects on fisheries resources (Anderson, 2009; Fang et al., 2022).

Algal blooms are characterized by rapid accumulation followed by an equally rapid decline (Guo et al., 2023). Experimental and modeling studies suggest that excessive nutrient input (Zhang et al., 2020), suitable temperature (Ralston and Moore, 2020), and favorable light intensity (Tian et al., 2018) are likely to affect the characteristics of algal blooms, such as frequency, intensity, and duration. Due to the abundance and diversity of phytoplankton, the scale and timing of blooms are highly stochastic, with some occurring in spring and others in summer, and some localized in bays or estuaries for a few weeks, while others are massive and last for years (Anderson, 1997; Fang et al., 2019; Kim et al., 2022). These events can generally be categorized into two types: spring blooms and red tides. Spring blooms are mainly induced by seasonal changes in temperature or nutrient availability, influenced by seasonal variations in thermocline depth and strength (Ho and Michalak, 2020; Leruste et al., 2019). In contrast, red tides occur independently of specific regions or high water temperatures and are localized outbreaks commonly observed in coastal waters, estuaries, and fronts (Li et al., 2021; Truscott and Brindley, 1994).

Algal blooms can have a negative impact on aquatic ecosystems (Huang et al., 2019). For example, cyanobacteria can cause waterbodies to produce an unpleasant smell and form green scum layers, significantly reducing water transparency and interfering with recreational activities and the quality of drinking water reservoirs (Huisman et al., 2018; Sultana et al., 2022). In addition, during the bloom phase, hypoxia and anoxia can be induced by a significant increase in sediment oxygen consumption due to the microbial degradation of senescent blooms, resulting in the death of fish and benthic invertebrates (Kumari et al., 2022). Some cyanobacterial blooms can produce

potent toxins that can cause various gastrointestinal and neurological illnesses in humans through the food chain (Mello et al., 2018; Pradhan et al., 2022).

In recent decades, various countermeasures have been developed to control algal blooms, including chemical treatments, physical contact between prey and predator, and biological control. However, most of these methods have achieved limited success. For example, copper algicides have proven effective in controlling harmful algal blooms in drinking water supplies, but they are toxic to other aquatic microorganisms and can induce the release of toxins due to cyanobacterial cell lysis (Shen et al., 2019). Similarly, while sonication is applicable for water treatment systems, it is not suitable for large water bodies (Gallardo-Rodríguez et al., 2019). The underlying processes of phytoplankton bloom formation are still not fully understood, and further knowledge is needed to improve the understanding of algal blooms and develop effective control methods.

1.2. Statement of the problem

Due to the rapid development of industry and agriculture, a significant amount of industrial wastewater and domestic sewage containing large amounts of nutrients are discharged into water, resulting in severe eutrophication problems in recent years (Hansen et al., 2017). China has more than 2300 natural lakes covering a surface area larger than 1 km^2, mainly used for irrigation, drinking water, aquaculture, and tourism (Liu and Qiu, 2007; Yang et al., 2016). Over the past decades, increased nutrient inputs have significantly boosted the production of phytoplankton and other microorganisms, leading to the deterioration of the normal functioning of water bodies (Dubey and Dutta, 2020).

Under natural conditions, some phytoplankton species, such as *Microcystis*, the most common freshwater cyanobacterial genus, typically form colonies (Xiao et al., 2018). Colony formation of algae contributes to preventing algal species from being grazed by zooplankton, reducing damage

from ultraviolet radiation, resisting severe water turbulence, and providing protection from heavy metals (Lürling, 2021; Xiao et al., 2018; Yamamoto et al., 2011). Additionally, the colony formation of some phytoplankton species is important for their dominance and even bloom formation (Yamamoto et al., 2011). Blooms are characterized by a sharp increase in the number of large colonies, which is directly attributable to the population increase. Thus, restraining the growth of phytoplankton is an effective way to prevent and control algal blooms. However, the extent to which influencing factors affect algal growth mechanisms remains unclear.

In recent years, numerous field or experimental studies have been conducted to explore the key drivers of the bloom phenomenon. Extensive studies support the notion that reducing nutrient inputs to aquatic ecosystems is an efficient way to decrease the frequency and intensity of blooms (Huisman et al., 2018). Additionally, the nitrogen to phosphorus ratio has been considered a key driver in controlling phytoplankton growth and seasonal succession (Liu et al., 2021b). Bharathi et al. (2018) experimentally suggest that low salinity and a high N:P ratio favor the growth of blue-green algae. However, there is evidence suggesting that this may be an incomplete explanation for the presence or absence of blooms. Bloom occurrence is ultimately a random phenomenon resulting from a combination of climatic and hydrographic events (Guo et al., 2023; McGowan, 2017). For example, Ralston and Moore (2020) indicated that global warming expressed as an increase in summer temperatures can increase the risk of phytoplankton bloom. Beaulieu et al. (2013) suggested that some blooms, such as cyanobacterial blooms, are favored by warm temperatures. Light intensity and carbon supply may also contribute to the formation of algal blooms (Huang et al., 2019; Liao et al., 2018; Tian et al., 2018). These studies indicate that the bloom phenomenon is much more complex than we expected.

Growing evidence reveals that rapid algal growth is a consequence of the interplay of various hydrodynamics, chemical processes, and biological processes (Chen and Mynett, 2006; Guo et al.,

2023), making it difficult to understand the mechanism of phytoplankton growth based solely on experimental and field observations. Moreover, the nonlinearity and complexity of aquatic ecosystems make it challenging to develop management systems and improvement measures. Therefore, mathematical modeling of plankton populations as an important alternative methodology has drawn increasing attention (Dai et al., 2019).

One of the interesting problems in the dynamical analysis of phytoplankton growth models is the oscillation behavior of plankton populations. While many phytoplankton growth models suggest that plankton populations can coexist at equilibrium globally under certain conditions (Dai et al., 2019; Deng et al., 2015), the results from Sherratt and Smith (2008) reveal that a constant population density may not exist in reality due to the presence of environmental noise and physical factors such as water temperature, light, and hydrodynamics. Moreover, experimental results support that the physical factors, such as reduced vertical mixing, can generate oscillations and chaos in phytoplankton biomass (Huisman et al., 2006).

In recent years, the dynamical behaviors, including regular, irregular, and chaotic spatiotemporal oscillations, have gained significant attention in numerous experimental and modeling studies of aquatic ecosystems. A long-term experimental study with a complex food web was conducted by Benincà et al. (2008), and the results revealed that species interactions in food webs can generate chaos. Furthermore, a nutrient-plankton model developed by Wang et al. (2016) indicated that periodic oscillation and chaotic behaviors of plankton biomass can be induced by delays resulting from phytoplankton absorbing nutrients. It is worth noting that compared to experimental studies, mathematical models have the advantage of being able to capture these ubiquitous stoichiometric constraints for modeling species growth and interaction.

Although various phytoplankton growth dynamical models have been explored to investigate the mechanism of algal growth, the dynamic mechanism of phytoplankton growth remains a

challenge due to the complex and highly nonlinear nature of the planktonic ecosystem. It is therefore important to gain a better understanding of the underlying mechanisms for this phenomenon.

1.3. Objectives of the study

The main objective of this research is to investigate plankton dynamics using mathematical models. Theoretical and numerical analyses are conducted to examine the dynamic properties of the models. A summary schematization of the research content is shown in Figure 1.1.

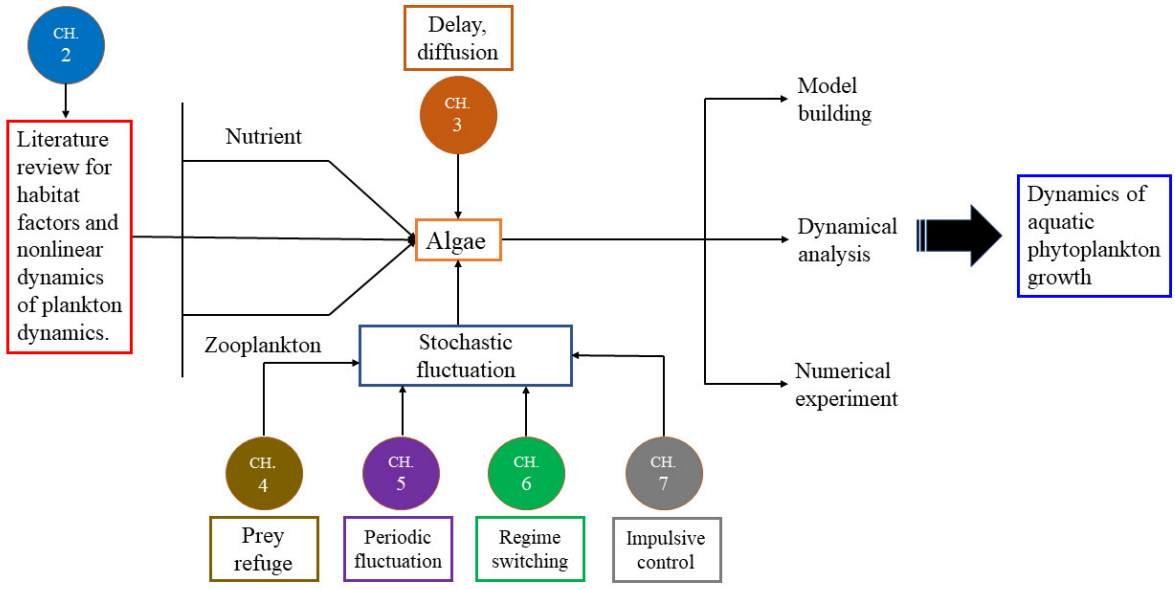

Figure 1.1. Schematization of research content.

The specific objectives of this dissertation include:

- Investigating how the delay caused by phytoplankton's nutrient absorption affects the nutrient-plankton interaction dynamics. Sufficient conditions for the stability switches of the positive equilibrium were derived and the direction of Hopf bifurcation and the stability of the bifurcation periodic solutions were tracked. In addition, chaotic behavior induced by delay was

investigated through simulation.

- Examining the joint effect of prey refuge and stochastic fluctuation on plankton growth dynamics. The existence of the global positive solution of the model was studied, and the conditions for the model to admit an ergodic stationary distribution were derived. Moreover, numerical results were presented to further explore the effect of noise density and prey refuge on the intensity of planktonic oscillation.
- Investigating how seasonal fluctuation affects the bloom events of phytoplankton under stochastic environments. The survival analysis of plankton populations was conducted and the sufficient conditions for the existence of a positive periodic solution were derived. Additionally, numerical analysis was conducted to explore the effect of seasonal fluctuation on phytoplankton growth.
- Developing a stochastic nutrient-plankton model under regime switching to analyze the effect of regime-switching plankton mortality on plankton dynamics. Theoretical analysis was conducted to derive the sufficient conditions for the stationary distribution of the model. Additionally, numerical simulations were conducted to investigate the sensitivity of plankton dynamics to parameters. The plankton dynamics in response to shifting plankton mortality and stochastic fluctuation were investigated.
- Investigating a stochastic nutrient-plankton model with impulsive control both theoretically and numerically. The sufficient conditions for the existence of a global positive solution and periodic solutions were derived. Furthermore, numerical analysis was carried out to investigate how plankton dynamics respond to stochastic fluctuation and impulsive control.

1.4. Organization of the dissertation

The dissertation is organized as follows: literature review is presented in Chapter 2; in

Chapters 3-7, the mathematical analyses for five different phytoplankton growth models are developed, including the delayed nutrient-plankton model with diffusion (Chapter 3), the stochastic Leslie-Gower phytoplankton-zooplankton model with prey refuge (Chapter 4), the stochastic nutrient-plankton model with seasonal fluctuation (Chapter 5), the stochastic nutrient-plankton model under regime switching (Chapter 6), and the stochastic nutrient-plankton model with impulsive control (Chapter 7); in Chapter 8, some conclusions and recommendations for future research are provided.

Chapter 2

LITERATURE REVIEW

2.1. The causes of algal blooms

Algal bloom is a significant sign of extreme eutrophication in aquatic ecosystems, drawing increasing attention from researchers. Over the last several decades, the frequency, intensity, and geographic distribution of such events have shown an increasing trend (Anderson et al., 2021), and most coastal countries have experienced an escalating and worrisome trend in the incidence of phytoplankton blooms. Extensive research has revealed that the formation of phytoplankton blooms is a consequence of the interplay of various physical, geological, biological, chemical, and hydrodynamic processes (Brandenburg et al., 2017; Chen and Mynett, 2006), contributing to the difficulty in understanding how phytoplankton growth responds to environmental factors.

2.1.1. Nutrient supply of nitrogen (N) and phosphorus (P)

Phytoplankton growth process is primarily limited by the availability of nitrogen (N) (demanded for protein synthesis) and phosphorus (P) (demanded for DNA, RNA, and energy transfer) among multiple nutrients (Conley et al., 2009). Numerous studies have suggested that eutrophication is typically caused by excess nitrogen and phosphorus inputs (Rathore et al., 2016), resulting in the rate of primary production exceeding the rate at which it is utilized by secondary consumers. Under high nutrient availability, specific algal species can become dominant through nutrient uptake, leading to algal blooms. In addition to the overall level of nutrient input, the nitrogen to phosphorus ratio is also an important driver of phytoplankton blooms, due to the differing nutrient requirements of different algal species (Orihel et al., 2015). The results reported by Paerl et al. (2018) indicated that while phytoplankton growth indeed requires nitrogen and

phosphorus, reducing nitrogen input (or phosphorus input) alone does not necessarily lead to noticeable improvements in water quality related to eutrophication. Moreover, Zhang et al. (2020) demonstrated that controlling both nitrogen (N) and phosphorus (P) in water is necessary for improving the aquatic environment.

2.1.2. Light intensity

Light intensity is a crucial environmental factor that affects the growth rate and carrying capacity of primary producers as algae are primarily photoautotrophs (Tian et al., 2018; Zohdi and Abbaspour, 2019). Furthermore, Tian et al. (2018) revealed an important fact that different algal species exhibit varying sensitivity to light intensity, as evidenced by their trace element uptake (e.g., Mn, Zn, and Fe) and photosynthesis responses. While high light intensity is generally assumed to increase water temperature and promote the photosynthetic rate of algae, ultimately leading to a large increase in algal biomass. Yang et al. (2012) demonstrated that some cyanobacteria prefer low irradiance and are vulnerable to photoinhibition. Moreover, increased light intensity can enhance the growth rates of certain species such as *Prorocentrum micans* Ehrenberg, *Cryptomonas* sp., and diatoms, but eventually reach a plateau (saturation) (Tian et al., 2018). Growing evidence suggests that light intensity is closely linked to phytoplankton bloom events, and the growth responses of algae to varying light intensities are highly variable (Cui et al., 2015; Winder et al., 2012).

2.1.3. Water temperature

Water temperature, under nutrient-sufficient and adequate light conditions, is a key factor in the occurrence of phytoplankton blooms (Araki et al., 2018). Reinl et al. (2023) demonstrated that although increasing lake surface temperature can promote cyanobacterial growth, “cold-water cyanobacterial bloom” was also observed when the water temperature is $< 15℃$. In addition,

Winder et al. (2012) reported that changes in water temperature are a key driver of the launch of plankton blooms in spring, and higher water temperatures may result in earlier bloom events for many functional plankton groups. It is widely observed that seasonal changes often lead to the formation of different dominant phytoplankton species (Guo et al., 2014; Xiao et al., 2016), with periodic changes in water temperature being one of the obvious reasons. To sum up, water temperature is one of the main factors in triggering algal blooms.

2.1.4. Biotic factor

Limiting factors of phytoplankton blooms also include trophic cascades via top-down control of phytoplankton by zooplankton (Gianuca et al., 2016; Mao et al., 2020). Some zooplankton such as daphnia and copepod zooplankton, are effective predators of algae, which not only affect the phytoplankton biomass but also the diversity of multiple trophic levels (Birtel and Mattews, 2016; Duggan et al., 2015). Under resource limitations, herbivores may enhance primary production by decreasing interspecific competitors (Ger et al., 2018). Thus, maintaining the dominance of such zooplankton species may be an effective way to control algal growth. Furthermore, intraspecific competition in algal populations can also affect the internal structure of the plankton community. For example, toxin release from *Microcystis* can impact the growth of zooplankton and other algae, resulting in their dominance in the waters (Jester et al., 2009). In fact, biotic factors affecting algal blooms extend well beyond those mentioned above, and the mechanisms of coupling between various biological factors affecting planktonic systems are still the focus of current research.

2.1.5. Climate and hydrology

Extensive research has suggested that the bloom phenomenon is subject to climate and hydrographic events (Havens et al., 2019). For example, the inflow of trace elements and nutrients into the water due to rainfall can result in excessive growth of algae. In addition, during the rainfall

season, high water temperature and air temperature can create favorable conditions for algae growth. Hydrodynamic motion, such as horizontal transport, mixing, and stirring, also plays a significant role in plankton dynamics (Hernández-Carrasco et al., 2018; Jaccod et al., 2021; Sandulescu et al., 2007). Deng et al. (2016) demonstrated that horizontal migration can trigger phytoplankton blooms and have an important influence on the competition and coexistence of different plankton species. In fact, climate conditions, wave disturbances, and wind effects all affect algal growth, and the seasonal fluctuation of environmental changes can result in the scale and timing of blooms being highly stochastic. Some blooms occur in spring, while others in summer or winter. Some blooms are localized, occurring in bays, while others are massive, covering thousands of square kilometers. Some blooms occur at the same time and place each year, lasting a few weeks, while others happen randomly, lasting years (Anderson, 1997; Silva et al., 2021). Therefore, the variability of climate and hydrology poses a challenge for studying the mechanisms of algal growth.

2.1.6. Human activities

Over the last few decades, excessive human activities, such as the discharge of untreated domestic sewage, industrial wastewater, and agricultural wastewater, have seriously deteriorated water quality, and the increase in nutrient loadings in lakes or rivers contributes to the process of eutrophication. Zhao et al. (2019) demonstrated that due to the increased intensity of human activities frequent outbreaks of algal blooms have become typical events affecting the Earth's atmosphere. Furthermore, Bhagowati et al. (2020) suggested that natural eutrophication is a gradual aging process of aquatic ecosystems, occurring over thousands of years. However, human activities or cultural influences, such as high agricultural activities, sewage, and industrial discharges, have significantly accelerated eutrophication, leading to profound changes in the

structure and function of water bodies (Ansari et al., 2011). Lane-Medeiros et al. (2023) also revealed that overexploitation of piscivorous fisheries may favor phytoplankton blooms through capturing top predators.

The factors affecting algal blooms are not limited to those mentioned. Other factors include water pH and transparency (Amorim and Moura, 2021; Lane-Medeiros et al., 2023). Phytoplankton blooms have been considered as the consequence of synergistic effects of internal and external regulatory factors. Although extensive investigations have been conducted to study how these factors affect the bloom phenomenon, the underlying mechanisms of phytoplankton growth remain a challenge. Because aquatic ecosystems are much more complex than expected, there is still much to investigate regarding the causes of algal blooms.

2.2. The characteristics of algal blooms

Phytoplankton blooms are characterized by high densities of algae, often reaching millions of cells per liter due to the proliferation and occasional dominance of these phytoplankton species under favorable environmental conditions (Sarkar, 2018). During the bloom phase, the number of algae grows exponentially, rather than following the general population growth characteristics (Menden-Deuer and Montalbano, 2015), and the blooms are often visible as a discoloration of the water. For example, *Microcystis* blooms typically turn the water green. Algal blooms can be divided into four phases: the initial phase, development phase, maintenance phase, and decline phase.

In aquatic ecosystems, two important forms of algae are unicellular individuals and colonies. Some phytoplankton species, such as *Microcystis*, normally form colonies under natural conditions, which is thought to contribute to bloom formation; for example, colony formation promotes the *Microcystis* dominated blooms (Xiao et al., 2018). Thus, colony formation may indeed play an

important role in the dominance and formation of blooms in some algae, which has been extensively investigated by many researchers (Cao and Yang, 2010; Mars Brisbin and Mitarai, 2019; Yamamoto et al., 2011).

Interestingly, blooms are generally followed by a sudden decline in population numbers (Guo et al., 2023). There is a growing body of literature that recognizes the effect of phytoplankton mortality on the termination of algal blooms (Choi et al., 2017), and phytoplankton mortality normally shows a dramatic increase in the decline phase, leading to blooms that are generally followed shortly by a sudden collapse, whereby the phytoplankton population returns to its original low level (Mukhopadhyay and Bhattacharyya, 2006). In addition, Garcés et al. (2005) designed a dilution experiment of natural single *Alexandrium* spp. to observe cells during the development, maintenance, and decline phases of blooms, and they found the highest mortality rates during the decline phase. One obvious reason for this is that fast-growing algae can cause a dramatic decrease in dissolved oxygen levels, as evidenced by rapid oxygen consumption through metabolism of algae and a sharp decrease in oxygen production in bottom water due to decreased light penetration (Raj et al., 2020). Furthermore, excessive oxygen depletion is often responsible for massive organism deaths (Chislock et al., 2013).

2.3. Algal bloom impacts

Algal blooms can be classified into two categories: toxic and non-toxic, both of which can pose serious threats to public health and the function of aquatic ecosystems (Treuer et al., 2021). Although only a few dozen toxic phytoplankton species exist, they have the capacity to produce potent toxins that can cause severe diseases in humans (Curran and Richlen, 2019). After the toxic phytoplankton is consumed by shellfish, the toxic substances can accumulate in shellfish bodies to levels that can have human health impacts. For example, paralytic shellfish poisons (PSP) can be

caused by *Gymnodinium catenatum*, and it has been shown that PSP can easily accumulate in shellfish and could be fatal to humans (Hallegraeff, 1993). Additionally, based on the symptoms observed in human intoxications, algal toxins can be classified into several types, such as diarrhetic shellfish poisoning (DSP), amnesic shellfish poisoning (ASP), neurotoxic shellfish poisoning (NSP), Ciguatera fish poisoning, and azasporacid poisoning (AZP) (Grattan et al., 2016; Wang and Wu, 2009). In recent years, there has been an increasing trend of human poisoning due to the consumption of fish or shellfish during algal bloom events, which are becoming more frequent around the world.

In contrast, non-toxic algal species do not produce toxins but can still cause harm in various ways, such as marine fauna kills due to excessive oxygen depletion or disturbance of the marine food web (Shen et al., 2012). Excessive growth of non-toxic algal species can also result in unpleasant smells and discoloration of the water, forming a thick layer on the water surface and preventing light penetration to the bottom. Additionally, during the decline phase of blooms, the massive biomass decay can lead to a dramatic increase in oxygen depletion, leading to widespread mortalities of plants and animals in the affected area (Anderson, 2009; He, 2015). Excessive growth of non-toxic algae can also destroy the water body's landscape and cause serious damage to aquatic ecosystems. Villacorte et al. (2015) suggests that these "high biomass" blooms can occur in pristine water or in response to excessive pollution inputs.

In addition to the public health and ecological risks, phytoplankton blooms can also have a variety of economic impacts. The rapid growth of algae can have a significant impact on fisheries, leading to reductions in seafood sales and an increase in wild and farmed aquatic product mortalities (Sanseverino et al., 2016). Anderson et al. (2015) demonstrated that unfavorable changes in the plankton ecosystems may have undesirable effects on fisheries. Moreover, algal blooms can significantly impact tourism and tourism-related businesses in the bloom-affected

areas, and the increasing risk of human illness due to the consumption of contaminated shellfish or fish leads to higher medical costs (Sanseverino et al., 2016). All these phenomena are responsible for direct or indirect economic impacts of phytoplankton bloom events.

2.4. Bloom control

Although the prevention and control of phytoplankton blooms have drawn significant attention in recent years, the diversity of blooms makes bloom control continuing to be one of the most challenging and controversial tasks for bloom management (Nelson et al., 2018). Strategies for controlling blooms can generally be classified into five categories: mechanical, biological, chemical, genetic and environmental control (Anderson et al., 2017).

Recently, a variety of mechanical control methods have been investigated and applied in field applications. For example, clay can be used to remove algal cells (Alshahri et al., 2021; Li et al., 2023). Since the clay particles can aggregate with phytoplankton cells and sink to the bottom through sedimentation, this method has already been applied in several countries such as Japan, Australia, and South Korea to control HABs in the field (Ibrahim et al., 2022). However, the clay application can threaten benthic fauna and burial of resident populations (Anderson et al., 2017). Furthermore, the higher cost, increased ecological impact, and greater logistic challenges limit the application of this method outside the laboratory (Anderson, 2009; Yu et al., 2017).

Biological control (biocontrol) agents represent another approach for controlling phytoplankton blooms. Although a variety of biological methods have been reported in recent years, laboratory success is predominant, and the success rate of field management appears to be quite low (Pal et al., 2020). Biocontrol has not been explored in algal bloom control due to logistical problems, although it has been widely explored in field applications in agriculture, such as insect pest control. Although there are many successful cases where such an approach has been both

effective and environmentally benign on land, considerable efforts are needed in aquatic ecosystems.

In contrast, chemical control of algal blooms is operated by releasing toxic chemicals, including titanium dioxide (Chang et al., 2018), sophorolipids (Balaji-Prasath et al., 2022), copper (Schoffman et al., 2016). Although chemical treatments have been widely reported and have shown massive success in small systems, some chemical precipitants could become problematic. For example, the release of endotoxins can be induced by massive algal cell lysis caused by copper sulfate (Nwankwegu et al., 2019). Additionally, Schoffman et al. (2016) found that the sensitivity of algal blooms to copper ions differs significantly among different phytoplankton species. In practice, chemical control has not been actively pursued for algal bloom control since it may cause the widespread mortality of other aquatic organisms, and the full range of sensitive environmental concerns is still challenging (Nwankwegu et al., 2019).

Genetic control is a method of introducing purposefully designed species to alter the habits of harmful species, such as environmental tolerances and reproduction. Similar to biological control, genetic control in terrestrial agriculture has shown remarkable success, but issues occur in aquatic ecosystems, as evidenced by the possible negative impacts of introducing a non-indigenous organism to a water area. The issue of genetic control may be more of a societal concern, and the hypothetical impacts would make it exceedingly difficult to obtain approval for such approaches in the near future (Anderson, 2009).

Finally, for environmental manipulation, the aim of such approaches is to affect the target species or introduce bio-controlled species through chemical or physical modifications of the environment (Anderson, 2009). Nutrient level may be an important indicator of environmental manipulation and might involve large-scale manipulation. However, due to long-term storage of nutrients in sediments and alteration in the biogeochemistry of systems after years of nutrient

loading, such an approach may not achieve the desired effect on shorter time scales (Tang et al., 2016).

In summary, while some treatments like copper ions can effectively control phytoplankton blooms, they may also lead to the release of endotoxins. Other treatments like clay may be more environmentally friendly but have high costs. It has now been broadly acknowledged that a sustainable technique for algal bloom control needs to be both environmentally effective and economically affordable (Li et al., 2013; Zhang et al., 2018). However, most current strategies for bloom control do not represent a sustainable development approach, and one obvious reason is that the diversity and complexity of the bloom phenomenon resulting in the dynamics of phytoplankton growth are currently not well understood. It is therefore important to gain a better understanding of these factors to develop new techniques for controlling blooms that provide additional environmental and economic benefits.

2.5. Nonlinear dynamics of planktonic ecosystems

Phytoplankton and herbivorous zooplankton are known to be the basis for all food chains and webs of aquatic ecosystems (Titocci et al., 2022; Yannawar, 2022). Considerable field and experimental studies have focused on plankton growth. However, the complexity and nonlinearity of aquatic ecosystems contribute to the difficulty in understanding phytoplankton growth dynamics based solely on field and experimental studies (Dai et al., 2019). Mathematical models have made important contributions to the study of phytoplankton growth by providing quantitative insights into the dynamic mechanism of phytoplankton growth (Guo et al., 2020; Malerba et al., 2012). In recent years, there has been a growing body of literature that recognizes the importance of mathematical models in the study of plankton dynamics (Sekerci and Petrovskii, 2015; Thakur and Ojha, 2020).

Contemporary mathematical modeling of phytoplankton growth dates back to Fleming (1939), who provided the first mathematical model of a planktonic system investigating phytoplankton blooming controlled by zooplankton grazing. Later, Riley et al. (1949) established a vertical, one-dimensional ecodynamic model to simulate the seasonal variation of aquatic plankton in the North Sea of Europe. Based on the work of Fleming (1939) and Riley et al. (1949), numerous phytoplankton growth models have been developed, such as bottom-up control (nutrient-phytoplankton) and top-down control (zooplankton-phytoplankton) plankton models (Mao et al., 2020; Sandhu et al., 2020; Ward et al., 2014).

Additionally, the functional response describing the response of the consumption of prey by individual predators (Dawes and Souza, 2013) has been shown to play an important role in modeling studies of plankton. Holling (1959a) presented the first functional response named the Holling-type, followed by various forms of functional response such as the Beddington–DeAngelis functional response (Beddington, 1975; DeAngelis et al., 1975), Crowley-Martin functional response (Crowley and Martin, 1989), and so on. In recent years, various plankton growth models have been developed by introducing various functional responses in the classical predator-prey models (Meng and Li, 2020; Thakur et al., 2020).

The aim of investigating phytoplankton growth models is to reveal the key factors that affect algal growth through dynamic studies from a quantitative analysis perspective. Two main model structures are used to describe population growth, mortality, predation or prey relationships, intraspecific competition, and other factors. They include ordinary differential equations and partial differential equations. Growing evidence suggests that the planktonic ecosystem's response to impact factors is regulated by complex nonlinear processes, and nonlinearity has been recognized as an inherent property of planktonic ecosystems (Cael et al., 2021; McGillicuddy Jr, 2010).

In the past decades, a variety of phytoplankton growth models have been developed to provide a deeper understanding of the structure of planktonic ecosystems (Camara et al., 2019; Dai et al., 2019). Extensive research has demonstrated that various dynamic behaviors exist in plankton models, such as steady-state behavior (Chen et al., 2019; Li and Lin, 2010), bifurcation behaviors (Chen et al., 2020a; Dai and Zhao, 2020), pattern formation (Han and Dai, 2019; Righetti et al., 2019), among others. Although a considerable number of phytoplankton growth models have been developed, only a few models are able to predict longer-term dynamical behavior due to the existence of chaotic behavior (Song et al., 2014; Tian, 2012; Wang et al., 2016). Furthermore, numerous mathematical models have predicted that chaotic behavior in plankton ecosystems can be generated by species interactions, such as competition and predation (Benincà et al., 2015; Huisman et al., 2006).

In natural aquatic ecosystems, phytoplankton growth is extremely complex, with many physical-chemical processes affecting the distribution of phytoplankton populations, such as delayed nutrient recycling, diffusion process, environmental fluctuations, impulsive control, and others. For instance, changes in plankton population biomass can be attributed to the daily variation in temperature and light. Many researchers have dedicated their efforts to investigating plankton dynamics, and many interesting developments have been reported.

2.5.1. Delay-induced nonlinear dynamics

Extensive studies have demonstrated that under certain conditions, plankton populations can coexist around equilibrium globally (Deng et al., 2015; Lv et al., 2014). However, due to the existence of random fluctuations, phytoplankton population density usually exhibits oscillatory behavior, indicating that the phytoplankton population density is not constant but changes over time (Fussmann et al., 2000; Huisman et al., 2006). Additionally, most studies of plankton models

assume that phytoplankton populations respond instantaneously to interactions with other species, such as the conversion of nutrients by phytoplankton (Chakraborty et al., 2015; Chen et al., 2020c; Yu et al., 2019a). It may be doubtful whether there is a time lag in the growth response of phytoplankton over a large area. However, the pioneering work conducted by Caperon (1969) suggested that the growth response of *Isochrysis galbana* is subject to a time lag in a variable nitrate environment, supporting the idea that time delay may indeed exist in the phytoplankton growth process.

Time delay can be classified into two categories: distributed and discrete time-delays, both of which have been extensively investigated by many researchers. For example, Ruan (1995) revised the model of Beretta et al. (1990) with a discrete time delay due to gestation and a distributed time delay that describes nutrient recycling. The author demonstrated that the effect of the distributed time delay is somewhat weaker than that of the discrete time delay since nutrient-plankton oscillation can be induced by the discrete time delay rather than the distributed time delay. Moreover, it is shown that both the discrete time delay and distributed time delay are "harmless" in some models, as the conditions for uniform persistence are the same as those for the instantaneous case (Li and Liu, 2010).

Time delay not only plays a crucial role in the growth of phytoplankton but also significantly influences the oscillatory behavior of phytoplankton biomass (Rehim and Imran, 2012; Singh et al., 2023). It is now well recognized from a variety of studies, that delay can destabilize the positive equilibrium via Hopf bifurcation and induce various dynamic behaviors, such as periodic oscillation (Meng et al., 2020), stability switch (Thakur et al., 2021), and chaos (Wang et al., 2016). Dai et al. (2019) investigated a nutrient-phytoplankton model with multiple delays, and the results showed that the unique positive equilibrium is globally asymptotically stable when there is no delay. However, if the delay is beyond a critical value, the unique positive equilibrium may lose

its stability via Hopf bifurcation, and then periodic solutions emerge.

Moreover, in most studies of delayed phytoplankton growth models, many authors demonstrated that the equilibrium is always unstable when the delay increases beyond a critical value (Shi et al., 2020; Zhao et al., 2015). However, the results reported by Song et al. (2014) implied that delay can not only generate but also suppress the instability coexistence of species populations, that is, the stability switch of species coexistence. Furthermore, the stability switch of species coexistence has been explored by many authors (Du and Yang, 2022; Zhuang et al., 2021) to control the stable coexistence of species populations.

In real natural ecosystems, chaotic behavior may exist in population dynamics due to the inherent nonlinearities of the system (Song et al., 2014). However, empirical evidence of chaos in real ecosystems is relatively scarce, and one possible explanation for this might be that the food webs contain many weak links between species, which may stabilize food-web dynamics (Neutel et al., 2002; Wootton and Stouffer, 2016). Additionally, external fluctuations, such as seasonal perturbations, contribute to the lack of suitable data to test for chaos in food webs (Benincà et al., 2008; Song et al., 2014). Benincà et al. (2008) designed the first long-term experiment with a complex food web consisting of bacteria, several phytoplankton species, herbivorous and predatory zooplankton species, and detritivores, and their results implied that species interactions in food webs can generate chaos, indicating that chaotic behavior may indeed exist in real aquatic ecosystems.

In contrast to experimental attention, the studies of chaos in population dynamical models date back to the work of May (1974), in which the author found that complex chaotic dynamics can be generated in a simple population model. Growing evidence reveals that species interactions such as competition for limiting resources and predation, can generate chaotic behavior (Chen et al., 2017; Levy et al., 2016). In recent years, many different routes to chaotic dynamics have been

explored, and evidence suggests that delay is one of the most important factors for the emergence of chaos in population dynamical models. Many researchers have shown increasing interest in delay-induced chaotic behavior (Song et al., 2014; Wang et al., 2016). For instance, a nutrient-plankton model with a single delay can generate chaotic behavior with increasing delay (Sharma et al., 2014), while gestation delays induce chaos in a plankton-fish model as studied by Thakur et al. (2020). Dai et al. (2019) examined chaos in a nutrient-phytoplankton model with multiple delays. Furthermore, there is evidence that typical chaotic behavior is characterized by the sensitivity of the plankton oscillations to initial conditions due to the coexistence of a chaotic attractor and a limit cycle (Sadhu and Thakur, 2017), suggesting that it might be fundamentally impossible to predict phytoplankton biomass.

The study of phytoplankton growth models also includes an interesting topic of delay-induced spatiotemporal dynamics known as “patchiness”. It has been recognized that the emergence of patchiness is closely connected to the spatial heterogeneity of plankton distribution (Medvinsky et al., 2002). The spatiotemporal pattern formation was accidentally discovered by Turing (1952), who demonstrated that spatial structure can be induced by the nonlinear interaction of two or more agents with different diffusion coefficients, which is called Turing instability (Giricheva, 2019). Segel and Jackson (1972) first introduced Turing’s ideas into population dynamics to investigate the dissipative instability in the prey-predator interaction of phytoplankton and herbivorous copepods with higher herbivore motility, and later Levin and Segel (1976) suggested that this scenario of spatial pattern formation might be a possible explanation for planktonic patchiness. Furthermore, Medvinsky et al. (2001) demonstrated that conceptual reaction-diffusion mathematical models are appropriate tools for understanding the underlying mechanisms of plankton pattern formation and complex spatiotemporal plankton dynamics. They also revealed that turbulence, advective currents, and wind, etc., can affect the formation of spatial structures in

plankton communities. Extensive research has been carried out in recent years to better understand the mechanisms resulting in plankton spatial patterns (Sekerci and Petrovskii, 2018; Tian and Ruan, 2019).

Despite the Turing mechanism, non-Turing mechanisms underlying spatial pattern formation have also drawn growing attention (Hu et al., 2015). Banerjee and Petrovskii (2011) demonstrated that irregular spatiotemporal patterns can emerge around the Turing-Hopf bifurcation in a ratio-dependent prey-predator model. Delay-induced spatiotemporal patterns have also attracted a lot of attention due to the prevalence of the delay effect in aquatic ecosystems (Dai et al., 2016; Tian, 2012; Tian and Zhang, 2013). Grill et al. (1995) experimentally studied the effect of delay feedback on pattern formation using the light-sensitive Belousov-Zhabotinsky reaction. Tian (2012) revealed that delay can induce spatial patterns in a delayed plankton allelopathic system, and the results showed that the delay significantly affects pattern selection. Additionally, Dai et al. (2016) suggested that the delay can promote the formation of patchiness (an irregular pattern) via Hopf bifurcation.

2.5.2. Stochastic population dynamics

In real ecosystems, population systems are often subject to environmental noise (Dean and Shnerb, 2020; Lee, 2020). May (2019) pointed out that carrying capacities, birth rates, and other parameters exhibit random fluctuations. Thus, models that ignore the stochastic nature may not reflect the true dynamical behavior of phytoplankton growth. Moreover, there is a growing body of literature that recognizes the key role of environmental noises in ecological systems, such as white noise (Belabbas et al., 2021) and colored noise (Guo et al., 2023). White noise is characterized by many small, independent random fluctuations such as rainfall, wind, or day to night transitions. Colored noise, say telegraph noise, is considered a switching between two or

more environmental regimes. For example, in aquatic ecosystems, the growth environment in winter will be much different from that in summer, resulting in seasonal changes in the diversity of phytoplankton. All of these perturbations have an impact on changes in population density, and one effective method to study this problem is to develop stochastic dynamics models that can capture the pattern of random effects on the population and provide a more accurate quantitative insight into population growth.

The study of stochastic population dynamics dates back to Hasminskii (1980), who introduced two white noise sources to stabilize an unstable two-dimensional linear system. Later, Mao et al. (2002) revealed an important fact that stochastic noise can suppress potential explosions in population dynamics, while Deng et al. (2008) pointed out that noise can suppress or express exponential growth. Furthermore, it is now recognized that stochastic effects, such as those resulting from rainfall, windy conditions, and temperature variations, are widely present in the phytoplankton growth process (Song et al., 2020a). In recent years, stochastic prey-predator plankton models have been widely explored (Camara et al., 2019; Chen et al., 2020b; Song et al., 2020b). Stochastic plankton growth models incorporating constant and periodic toxin-producing phytoplankton have been analyzed by Wang and Liu (2020) and Jang and Allen (2015), respectively. Zhao et al. (2016) developed a non-autonomous toxic-producing phytoplankton allelopathy model with white noise fluctuations and derived sufficient conditions for the existence of the boundary periodic solution and the nontrivial positive stochastically periodic solution. Stochastic chemostat models with white noise fluctuations have also been widely explored (Sun et al., 2017; Xu et al., 2021; Xu and Yuan, 2016).

In addition, seasonal fluctuation is a crucial factor among stochastic effects. It is widely accepted that the vital rates of plankton populations often undergo seasonal variations due to the periodicity of the natural environment (Song et al., 2019). Growing evidence suggests that seasonal

changes in abiotic factors such as temperature, light intensity, and nutrient enrichment (Baek et al., 2019; Lind et al., 2016; Vanderley et al., 2021) result in apparent seasonality of rapid phytoplankton growth. Recently, many studies have been reported on how seasonal fluctuations affect the dynamics of phytoplankton growth within random environments (Guo et al., 2022; Zhao et al., 2020). The results from Huisman (2006) suggest that seasonal environments can trigger more complex dynamics than constant environments.

While many stochastic phytoplankton growth models have focused on white noise, it has been discovered that phytoplankton growth can switch between two or more environmental regimes, which differ by factors such as nutrition or rainfall. For example, algal blooms are often followed by rapid collapses (Ma et al., 2018), and phytoplankton mortality has been found to be much higher in the decline phase compared to the development phase (Garcés et al., 2005), which cannot be adequately described by white noise. Moreover, the decomposition of dead algae quickly leads to a rapid depletion of dissolved oxygen, subsequently leading to hypoxic or anoxic "dead zone" lacking sufficient oxygen to support most organisms (Morro et al., 2022). This phenomenon may result in an increasing trend of zooplankton mortality in the bloom phase (Anderson et al., 2021).

It is widely accepted that the switching phenomenon described above can be mathematically described by the so-called colored noise, namely telegraph noise, which can be described by a finite-state Markov chain switching between two or more environmental regimes. Typically, the switching among different environments is memoryless, and the waiting time for the next switch follows an exponential distribution (Pan et al., 2015; Wang and Jiang, 2018; Zou and Wang, 2014). Zhao et al. (2016) proposed a stochastic phytoplankton allelopathy model under regime switching and demonstrated that both white and colored noises have great impacts on the evolution of phytoplankton populations. Additionally, Yu et al. (2019a) studied a nutrient-plankton model with the effect of regime switching and the results showed that the Markov chain is beneficial for the

survival of plankton.

In summary, researchers have long sought to understand how phytoplankton growth responds to random fluctuations in aquatic ecosystems. Stochastic models of plankton populations have been meaningfully used to investigate the mechanisms of bloom formation (Cai et al., 2020; Liu et al., 2021a; Yu et al., 2019b). Modeling studies not only deepen our quantitative understanding of plankton growth but also provide theoretical foundations for the prevention and control of algal blooms. Despite significant progress in the field of stochastic phytoplankton growth models, the complexity and nonlinearity of aquatic ecosystems under random fluctuations present ongoing challenges for further research.

2.5.3. The dynamics of impulsive control system under environmental fluctuation

In natural ecosystems, the state of ecosystems can change abruptly due to environmental fluctuations and human activity interventions, such as catching adult fish and releasing fry. Typically, these changes occur over a relatively short period, and are often described mathematically as impulsive control. In addition, many impulsive controls involve human interventions that introduce or remove some members from a population at a given time or when the state of the species satisfies certain criteria (Akhmet et al., 2006). Extensive research has suggested that impulsive differential equations are useful tools for studying these phenomena because they have the advantage of reflecting the features of transient changes in the system's status.

In recent years, impulsive dynamical systems have received considerable attention due to the increasing frequency of human interventions in natural ecosystems, which often leads to transient changes. The study of impulsive dynamical systems can be traced back to Milman and Myshkis (1960). The impulsive control has since been widely used in many scientific fields in recent

decades, such as orbital transfer of satellites, epidemic control, ecological systems, and population models. Recently, impulsive dynamical systems have been widely developed in the study of population dynamics. Notably, impulses control may contribute to the changes in the dynamics of a model (Li et al., 2019). Specifically, Li et al. (2019) demonstrated an important finding that appropriate impulse control can promote species survival.

It is important to note that various strategies have been implemented to prevent and control phytoplankton blooms, including planting and harvesting, which can result in transient changes in the state of aquatic ecosystems. Therefore, the study of prevention and control of phytoplankton blooms has incorporated impulsive differential equations as they provide a natural description of observed phenomena in real-world ecosystems. In addition, it is of great interest to investigate complex dynamics for impulsive perturbations in plankton dynamics. For instance, Lürling et al. (2018) reported that nutrient impulses are crucial for the survival of phytoplankton species. However, these models primarily focused on how impulsive control affects phytoplankton growth, while not accounting for the prevalent random perturbations in aquatic ecosystems. In reality, both environmental fluctuation and impulsive control significantly influence plankton dynamics, and therefore, the stochastic model coupled with impulsive control has received growing attention. Feng et al. (2021) demonstrated that nutrient pulses play an important role in the stochastic dynamics of phytoplankton growth. Furthermore, Liu et al. (2023) revealed an important fact that both environmental fluctuation and impulsive control can directly influence population extinction and persistence in the mean (the population can survive in the system).

Although some research studies have been conducted on the coupling effects between environmental fluctuation and impulsive control on plankton dynamics, there is still very little scientific understanding of how plankton dynamics respond to impulsive perturbations under environmental fluctuation. Understanding these dynamical behaviors is crucial for developing

effective strategies to prevent and control algal blooms. Therefore, gaining insight into the coupling effects between environmental fluctuation and impulsive control on plankton dynamics is of great importance.

2.6. Summary of literature review

Phytoplankton, as the primary producer in aquatic ecosystems, plays crucial role in assessing water quality and determining the production capacity of water bodies. Phytoplankton is inextricably linked to various aspects of human life, such as fisheries, medicine, agriculture, and more. However, in recent years, there has been an increasing discharge of domestic sewage, as well as industrial and agricultural wastewater, leading to accelerated eutrophication in many water bodies. Phytoplankton blooms are considered the primary symptom of eutrophication, disrupting the aquatic food webs and upsetting the balance of ecological structure and function. While various treatments for bloom control have been explored, achieving a balance between cost and environmental health has proven challenging due to a limited understanding of the underlying mechanisms of algal blooms.

To investigate the dynamics of algal growth, phytoplankton growth models have attracted widespread attention as an effective method due to the high nonlinearity and complexity of aquatic ecosystems. Phytoplankton growth models incorporate various functional responses into classical prey-predator models have been widely adopted and provide a broader perspective on phytoplankton growth dynamics. Furthermore, nonlinear dynamics induced by delay, stochastic fluctuations, and impulsive control have emerged as particularly important factors, as delay and random disturbances are inherent in the phytoplankton growth process. Despite considerable efforts to investigate the effects of delay, stochastic fluctuations, and impulsive control on the underlying mechanism of phytoplankton growth, the extent of these effects on plankton growth

dynamics remains unclear due to the diversity of aquatic ecosystems and the complexity of habitat environments.

Previous studies on chaotic behavior induced by delay have primarily focused on plankton dynamics without considering diffusion. Thus, in Chapter 3, the spatiotemporal dynamics are investigated and the results show that chaotic behavior appear in a spatiotemporal nutrient-plankton model. In addition, most stochastic phytoplankton growth models have been investigated without considering the effects of prey refuge and seasonal fluctuations. In the present research, the effects of prey refuge and seasonal fluctuations under noise turbulation are studied (Chapter 4 & 5). Previous research has mostly focused on constant plankton mortality rather than regime-switching plankton mortality. However, due to the impact of algal blooms on aquatic ecosystems, regime-switching plankton mortality is more realistic, which is investigated in Chapter 6. Most studies on nutrient-plankton models with impulsive control have been conducted in a constant environment, ignoring the stochastic effects on aquatic ecosystems. Thus, a stochastic nutrient-plankton model with impulsive control is developed and analyzed in Chapter 7. The results obtained from Chapter 7 may provide valuable insights into the possible management of excessive algal growth in aquatic systems.

It is important to note that some phytoplankton growth models may only offer abstractions of real-world phenomena and may not be applicable for predicting bloom events. However, they can provide an understanding of specific key processes underlying the growth of phytoplankton. Particularly, research on bloom-triggering mechanisms contributes to the development of effective prevention and control measures to improve water quality and restore aquatic ecosystems.

Chapter 3

STABILITY SWITCHES AND CHAOS INDUCED BY DELAY IN A NUTRIENT-PLANKTON MODEL WITH DIFFUSION[1]

Abstract

In this chapter, a reaction-diffusion model considering nutrient, phytoplankton, and zooplankton as dynamic variables was investigated. The impact of time delay that involved in the growth of phytoplankton after the uptake of nutrients was studied. The theoretical findings indicated that delay in the growth of phytoplankton could trigger the emergence of persistent oscillations in the model via a Hopf bifurcation. In addition, the theoretical analysis tracked the direction of Hopf bifurcation and the stability of bifurcating periodic solutions. The simulation results showed that stability switches occur for the positive equilibrium with an increasing value of the time lag. The findings showed that the model experienced homogeneous periodic-2 & 3 solutions as well as chaos. Overall, the results showed that the presence of time delay in the growth of phytoplankton could bring forth dynamical complexity in the nutrient-plankton model of the aquatic habitat.

Keywords: Nutrient-plankton model, time delay, Hopf bifurcation, stability switches, multiple periodic solutions, chaos

[1] Guo, Q., Wang, L.J., Liu, H., Wang, Y., Li, J., Tiwari, P.K., Zhao, M., Dai, C.J., 2022. Stability switches and chaos induced by delay in a nutrient-plankton model with diffusion. Submitted to Journal of Biological Dynamics on October 9, 2022 (Revision required on June 27, 2023).

3.1. Introduction

Algal blooms occur in aquatic systems due to the massive growth of phytoplankton, which can lead to significant water-quality problems and have adverse effects on the human health (Hallegraeff, 1993; Medvinsky et al., 2002; Mukhopadhyay and Bhattacharyya, 2006). The occurrence of algal blooms is the result of the interplay of various hydrodynamics, chemical processes, and biological processes (Chen and Mynett, 2006). It is well established that algal blooms are influenced by nutrients level and the predation of zooplankton (Dacey and Wakeham, 1986). Experiment conducted by Vanni (1987) has shown that even small changes in zooplankton size can have a significant impact on the phytoplankton community, although nutrient levels play a more substantial role in phytoplankton growth compared to zooplankton. Despite extensive research on phytoplankton growth dynamics, the process by which phytoplankton bloom occurs is not clearly understood yet. A deeper understanding of the nutrient-plankton interaction is necessary. However, studying the mechanisms of phytoplankton growth solely through experimental or field observations is challenging (Dai et al., 2019).

Researchers have employed mathematical models to gain quantitative insights into the dynamics of planktonic blooms in aquatic reservoirs (Edwards and Brindley, 1999; Guo et al., 2020; Guo et al., 2023; Mandal et al., 2021a). Tiwari et al. (2022) observed that the nutrient-plankton model destabilizes with an increase in nutrient input and recycling of dead phytoplankton biomass into nutrients. The toxins liberation by phytoplankton species and the intraspecific competition among themselves have the potentials to terminate persistent oscillations and stabilize the ecosystem. Biswas et al. (2020b) found that the presence of free-viruses and environmental toxins in aquatic systems could drive the zooplankton population to a very low equilibrium value, but the ecological balance of the aquatic food web could be maintained by modulating the decay (depletion) rate of free-viruses (environmental toxins). Mandal et al. (2021b) demonstrated that

environmental toxins could be reduced to a low level, thereby maintaining the equilibrium of the planktonic ecosystem. Through sophisticated sensitivity analysis technique, Guo et al. (2023) reported that the biomass of phytoplankton in aquatic reservoirs was highly sensitive to the uptake rate by zooplankton and least sensitive to the re-mineralization of dead plankton biomass into nutrients. Their numerical results also revealed that the persistence and extinction of plankton populations highly depended on nutrient levels in the aquatic system.

Experimental evidence suggests that a time lag occurs in the growth response of *Isochrysis galbana* under high nutrient availability (Caperon, 1969), indicating a delay exists in the growth of phytoplankton. therefore, it is reasonable to consider the effect of time delay in phytoplankton growth models. Both experimental and field observations have shown that changes in plankton population density often exhibit oscillatory behavior due to the existence of internal factors (Fussmann et al., 2000; Huisman et al., 2006), indicating that the population density of phytoplankton in aquatic reservoirs is not constant but changes over time in the realistic scenario (Sherrattand and Smith, 2008). Several previous studies have introduced time delay into the study of phytoplankton growth dynamics (Agnihotri and Kaur, 2019; Chen et al., 2020a; Das and Ray, 2008; Sharma et al., 2014; Yuan, 2012). The growing body of evidence suggests that plankton models with time delay exhibit rich and complex dynamical behaviors. Previous studies have demonstrated that delay can destabilize a model via Hopf bifurcation, induce periodic solutions (Bentounsi et al., 2018; Chen et al., 2013; Song and Wei, 2005), create stability switches (Thakur et al., 2021; Wang et al., 2016), and even lead to chaotic dynamics (Adak et al., 2020; Shu et al., 2015).

Moreover, it is well established that nutrients and plankton are able to disperse in aquatic reservoirs due to currents and turbulent diffusion. Previous studies have suggested that plankton growth and distribution can be characterized by spatial variation. Based on the work of Medvinsky

et al. (2002) and Holmes et al. (1994), it is recognized that appropriate partial differential equations can be used to model a variety of ecological phenomena, including complex spatio-temporal dynamics of plankton populations. Segel and Jackson (1972) were the first to introduce spatial structure in population dynamical models., and since then, numerous plankton models have considered the effect of diffusion (Agmour et al., 2021; Dai et al., 2015; Han and Dai, 2019; Upadhyay et al., 2012; Zhao et al., 2019). Chakraborty et al. (2015) investigated the spatial dynamics of a nutrient-phytoplankton model considering the toxicity of phytoplankton. Their findings showed that in the presence of toxicity, the distributions of nutrient and phytoplankton in the aquatic ecosystem become spatially heterogeneous, resulting in different patterns such as stripes, spots, and their mixtures, depending on the level of toxicity. Chakraborty et al. (2015) also observed spatio-temporal oscillations in the distributions of nutrient and phytoplankton under certain toxicity level.

Ecological systems possess all the elements to produce chaotic dynamics (May, 1987). The chaotic situations may arise from an equilibrium state for various reasons. Although chaos is commonly predicted by mathematical models, evidence for its existence in the natural world is scarce and inconclusive. The characteristics of chaos and its presence in nature have been extensively discussed in the field of ecology (Godfray and Grenfell, 1993; Hastings et al., 1993; Jorgensen, 1995; Perry et al., 1993). Recent developments in dynamical modeling theory consider chaotic fluctuations of a model as highly desirable because they allow for easy control. To assess the ecological implications of chaotic dynamics in different natural systems, it is important to explore changes in the dynamics when structural assumptions of the system are varied. One approach to studying of the dynamics of ecological communities is through their food webs and the coupling of interacting species (Hastings and Powell, 1991). Chattopadhyay and Sarkar (2003) applied the idea of Hastings and Powell (1991) to a plankton model with toxic effects. Jorgensen

(1995) demonstrated that chaos can occur in planktonic systems due to variation in the size of zooplankton species. More information on the ecological implications of body size can be found in Peters (1983). Mandal et al. (2006) applied thermodynamic principles to a plankton-fish model and found that gradually decreasing the size of zooplankton changes the model's dynamics from an equilibrium state to chaotic conditions. Biswas et al. (2020a) found that when viral infection triggers chaotic dynamics in an ecosystem, a high avoidance intensity of zooplankton can stabilize the system. Biswas et al. (2022) considered a time delay in the viral replication process in a lysis event, and found that infection and replication of free viruses were seasonally forced. They found that time delay could account for recurrent stability switching event in the model. They also observed chaotic oscillations in the seasonally forced delayed model, which indicates the emergence of harmful algal blooms. Their investigations suggested that increasing the strength of toxic compounds exuded by phytoplankton species may suppress chaotic disorder and drive the system into a zooplankton-free zone (Biswas et al., 2022). However, the intensity of selective grazing by zooplankton can change the state of chaos to order and promote a disease-free aquatic ecosystem.

It is worth noting that although the spatio-temporal dynamics of nutrient-plankton models have been widely investigated, the influence of time delay in the growth of phytoplankton after nutrient uptake on the spatial distributions of nutrient, phytoplankton, and zooplankton in aquatic ecosystems remains unclear. Therefore, in this study, the role of such time delay in a diffusive nutrient-plankton model is explored by considering the fact that some species of phytoplankton may release toxic chemicals to reduce predation pressure by zooplankton. The remaining portion of this chapter is organized as follows: Chapter 3.2 proposes a model for the combined actions of delay and diffusion in an aquatic ecosystem is proposed. Chapter 3.3 analyzes the dynamics of the model mathematically, including the equilibrium points in the absence of time delay, and the

stability behavior of the model in the presence of delay and diffusion. Existence of Hopf bifurcation and direction and stability of the bifurcating periodic solutions are also analyzed. In Chapter 3.4, numerical simulations are performed to illustrate the analytical findings and gain further insights into the dynamics of the delayed-diffusive nutrient-plankton model. In the end, conclusions of this study are presented in Chapter 3.5.

3.2. The mathematical model

In this chapter, a mathematical model is constructed to examine the impact of delay in the growth of phytoplankton after nutrient uptake in a diffusive nutrient-plankton model of an aquatic ecosystem. The model incorporates nutrient concentration, phytoplankton biomass, and the zooplankton biomass as dynamical variables. The growth dynamics of the phytoplankton and zooplankton population mainly depend on the availability of nutrient and the phytoplankton, respectively. The concentration of nutrient in the aquatic system depends on its input and washout rates, as well as uptake by the phytoplankton population. For the phytoplankton population, its biomass is determined by nutrient uptake, grazing by zooplankton, and mortality, either natural or due to nutrient shortage. A more appropriate functional form to describe the predation of phytoplankton by zooplankton is the Holling type II (Holling, 1959a). Finally, the zooplankton biomass in the aquatic reservoir depends on the grazing of phytoplankton, toxin liberation by phytoplankton, and loss due to mortality.

Let $N(t,x)$, $P(t,x)$, and $Z(t,x)$ respectively represent the concentration of nutrient, biomass of phytoplankton, and biomass of zooplankton at any time $t > 0$ and position x. The model is built based on the following assumptions.

(1) There is a constant input of nutrient to the aquatic system. The nutrient depletes naturally at a rate b and is uptaken by the phytoplankton following the bilinear law of interaction.

(2) Let c denote the maximum uptake rate of phytoplankton by zooplankton. The predation rate of zooplankton on phytoplankton is described by the Holling type II functional form (Holling, 1959a), $\frac{cPZ}{h+P}$, where h is the half saturation constant.

(3) The parameters m and k represents the natural mortality rates of phytoplankton and zooplankton species, respectively. Besides natural mortality, phytoplankton also experience death due to competition for available nutrients in the aquatic system. Furthermore, intraspecies competition among phytoplankton species, resulting from limited resources, is considered.

(4) The rate of conversion of phytoplankton biomass into zooplankton biomass is denoted by d. Toxin-producing phytoplankton species release toxic chemicals at a rate ρ, leading to a reduction in the biomass of zooplankton at a rate $\frac{\rho PZ}{h+P}$.

(5) A delay is incorporated in the growth response of phytoplankton after nutrient uptake.

(6) In aquatic system, nutrient and plankton disperse due to the currents and turbulent diffusion.

Based on these assumptions, a schematic of the model expressing the interactions of nutrient and plankton is presented in Figure 3.1. Then the following reaction-diffusion nutrient-plankton model with delay is obtained:

$$\begin{cases} \frac{\partial N}{dt} = \alpha - bN - eNP + d_1\Delta N, \\ \frac{\partial P}{dt} = \beta N(t-\tau)P - \frac{cPZ}{h+P} - mP - rP^2 + d_2\Delta P, \\ \frac{\partial Z}{dt} = \frac{dPZ}{h+P} - kZ - \frac{\rho PZ}{h+P} + d_3\Delta Z, \end{cases} \tag{3.1}$$

In the above model, the parameter τ represents the delay, which denotes the time required by phytoplankton to absorb nutrients and reproduce. The constants d_1, d_2 and d_3 denote the self-diffusion coefficients of nutrient, phytoplankton and zooplankton, respectively. Let $x \in \Omega = [0,\ l\pi]$, and for $t \in [-\tau,\ 0]$, $N(x,\ t) = \varphi_1(x,\ t) \geq 0$, $P(x,\ t) = \varphi_2(x,\ t) \geq 0$ and $Z(x,\ t) =$

$\varphi_3(x,\ t) \geq 0$. All the parameters in model (3.1) are assumed to be positive, and their biological meanings are listed in Table 3.1.

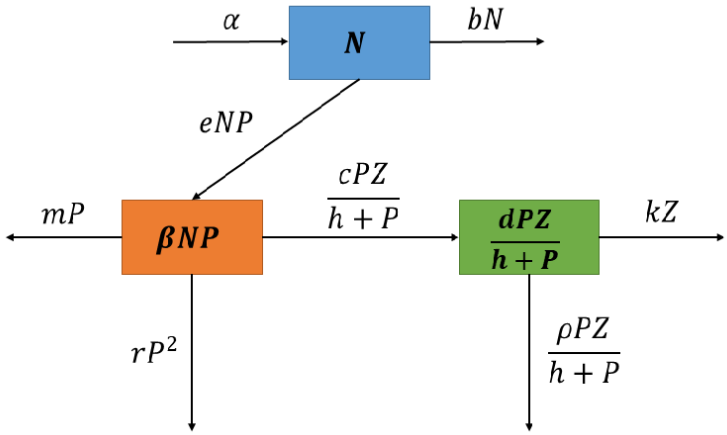

Figure 3.1. The scheme representation of the model (3.1).

3.3. The main results

In this chapter, the existence of ecologically meaningful equilibria of model (3.1) is discussed by ignoring the delay and diffusion factors. Then, the linear stability and bifurcation analysis are performed by taking time delay as bifurcation parameter.

3.3.1. The existence of equilibria

Model (3.1) does not have any trivial solution, but it has a non-trivial solution $E^0 = (N^0, P^0, Z^0)$, where $P^0 = \frac{\beta N^0 - m}{r}$, $Z^0 = 0$ and N^0 is the positive solution of the following quadratic equation:

$$e\beta {N^0}^2 + (br - em)N^0 - \alpha r = 0.$$

Obviously, the above equation has only one positive root that is given by

$$N^0 = \frac{(em - br) + \sqrt{(br - em)^2 + 4e\beta\alpha r}}{2e\beta}.$$

Additionally, if the following conditions are satisfied:

$$\alpha > \frac{(m(d-k-\rho)+hkr)(b(d-k-\rho)+ehk)}{\beta(d-k-\rho)^2}, d > k+\rho$$

then model (3.1) has a unique positive equilibrium $E^*(N^*, P^*, Z^*)$ whose components are given by

$$P^* = \frac{hk}{(d-k-\rho)}, N^* = \frac{\alpha}{(b+eP^*)}, Z^* = \frac{(\beta N^* - m - rP^*)(h+P^*)}{c}.$$

From an ecological point of view, the positive equilibrium E^* is very important as all the considered dynamical variables are presented here. So, this research is mainly focus on the dynamics of model (3.1) around this equilibrium point in the forthcoming chapters.

3.3.2. Stability and Hopf bifurcation

In this subchapter, the stability of positive equilibrium $E^*(N^*, P^*, Z^*)$ and Hopf bifurcation in model (3.1) are analyzed. Let $(\boldsymbol{H1})$:$\frac{a_{11}}{a_{22}} d_2 < d_1 < \left(\frac{a_{11}a_{22}+a_{12}a_{21}}{a_{23}a_{32}}\right) d_3$, and one can get the following result:

Theorem 3.1. If $b > \max\left\{d-p, \frac{\alpha\beta}{m}\right\}$ and $(\boldsymbol{H1})$ holds, then the positive equilibrium E^* of model (3.1) without delay is locally asymptotically stable for any $j \in \mathbb{N}_0$.

The proof is given in Appendix A. Furthermore, by direct computing, the following lemma obtained

Lemma 3.1. *Let $b > max\left\{d-p, \frac{\alpha\beta}{m}\right\}$ and $(\boldsymbol{H1})$ holds. Then, following two cases are obtained.*

(i) If $\Delta_1 = M_{1,j_0}^2 - 3M_{2,j_0} \leq 0$ for any $j \in \mathbb{N}_0$, then Eq. (B2) does not have any positive roots.

(ii) If there exists a $j_0 \in \mathbb{N}_0$ such that $\Delta_1 = M_{1,j_0}^2 - 3M_{2,j_0} > 0$, then Eq. (B2) possesses two positive roots if and only if $x_{j_0,1} > 0$ and $f(x_{j_0,1}) < 0$.

The proof is given in Appendix B. Now, the following lemma, which states the transversality condition required for the presence of Hopf bifurcation in model (3.1), is presented.

Lemma 3.2. *If Lemma 3.1 (ii) holds, then*

$$\frac{dRe\lambda(\tau)}{d\tau}|_{\tau=\tau_{j_0,1}^s} > 0,$$

$$\frac{dRe\lambda(\tau)}{d\tau}|_{\tau=\tau_{j_0,2}^s} < 0,$$

$$s = 0, 1, 2, \ldots.$$

The proof is given in Appendix C. By Lemma 3.2, Hopf bifurcation occurs in model (3.1) at the critical value $\tau = \tau_c$, which means that the positive equilibrium E^* becomes unstable when τ is larger than τ_c. Thus, the following theorem obtained.

Theorem 3.2. For model (3.1), one can obtain that

(i) If Lemma 3.1 (i) holds, then the positive equilibrium E^* of model (3.1) is locally asymptotically stable for all values of $\tau \geq 0$.

(ii) If Lemma 3.1 (ii) holds, then there exists a nonnegative integer n such that the positive equilibrium E^* of model (3.1) is locally asymptotically stable when $\tau \in \left[0, \tau_{j_0,1}^0\right) \cup \left(\tau_{j_0,2}^0, \tau_{j_0,1}^1\right) \cup \cdots \cup \left(\tau_{j_0,2}^{n-1}, \tau_{j_0,1}^n\right)$, and is unstable when $\tau \in \left(\tau_{j_0,1}^0, \tau_{j_0,2}^0\right) \cup \left(\tau_{j_0,1}^1, \tau_{j_0,2}^1\right) \cup \cdots \cup \left(\tau_{j_0,1}^{n-1}, \tau_{j_0,2}^{n-1}\right) \cup \left(\tau_{j_0,1}^n, +\infty\right)$. Further, model (3.1) undergoes Hopf bifurcation around E^* at every $\tau = \tau_{j_0,p}^s$ for $p = 1, 2$ and $s = 0,1,2,\cdots$.

Now, the following results, which are based on the center manifold theorem and the normal form theory, are stated.

Theorem 3.3. The Hopf bifurcation is characterized by the signs of μ_2, β_2, and T_2 as follows.

(i) If $\mu_2 > 0 (< 0)$, Hopf bifurcation is supercritical (subcritical) at $\tau = \tau^*$;

(ii) If $\beta_2 < 0 (> 0)$, the bifurcated periodic solutions are stable (unstable);

(iii) If $T_2 > 0 (< 0)$, the period of the bifurcating periodic solutions increases (decreases).

A detailed proof of Theorem 3.3 is provided in Appendix D.

Table 3.1. Biological explanations of variables and parameters in model (3.1), and numerical values used for simulation results

Parameter	Description	Unit	Value	Source
N	Nutrient concentration	$\mu g/L$		
P	Phytoplankton biomass	$\mu g/L$		
Z	Zooplankton biomass	$\mu g/L$		
α	Nutrient input rate to the aquatic system	$\mu g/L/day$	[0.1]	2[(a)]
b	Natural washout rate of nutrient	day^{-1}	0.4	0.4[(a)]
e	Uptake rate of nutrient by phytoplankton	$L/\mu g/day$	0.09	0.1[(b)]
β	Conversion rate of nutrient concentration into the biomass of phytoplankton	$L/\mu g/day$	0.95	0.9677[(c)]
c	Uptake rate of phytoplankton by zooplankton	day^{-1}	0.09	0.1[(b)]
d	Conversion rate of phytoplankton biomass into the biomass of zooplankton	day^{-1}	0.95	0.9661[(c)]
h	Half-saturation constant	$\mu g/L$	3	3.5[(b)]
m	Natural mortality rate of phytoplankton	day^{-1}	0.19	0.2-0.65[(d)]
k	Natural mortality rate of phytoplankton	day^{-1}	0.2	0.2[(a)]
r	Strength of interspecies competition among the phytoplankton population	$L/\mu g/day$	0.2	Assumed
ρ	Rate of toxin liberation by toxin producing phytoplankton	day^{-1}	[0.1]	0.22/0.3/0.92[(e)]

(a) Ruan (1993); (b) Wang et al. (2016); (c) Rehim et al. (2016); (d) Garcés et al. (2005); (e) Javidi and Ahmad (2015).

3.4. Numerical simulation

In this chapter, the effect of time delay on the dynamics of model (3.1) is further discussed. For the numerical investigations of model (3.1), the following parameter values are chosen, which are in accordance with the values mentioned in Table 3.1:

$$b = 0.4, e = 0.09, \beta = 0.95, c = 0.09, h = 3, m = 0.01,$$

$$r = 0.2, d = 0.95, k = 0.2, d_1 = d_2 = 0.01, d_3 = 0.02.$$

The above set of parameter values is used throughout this chapter if not mentioned in the text. The parameters α, ρ, and τ are chosen as control parameters in the nutrient-plankton model (3.1). Furthermore, the initial values for nutrient, phytoplankton, and zooplankton are selected as 0.9, 0.9, and 22, respectively.

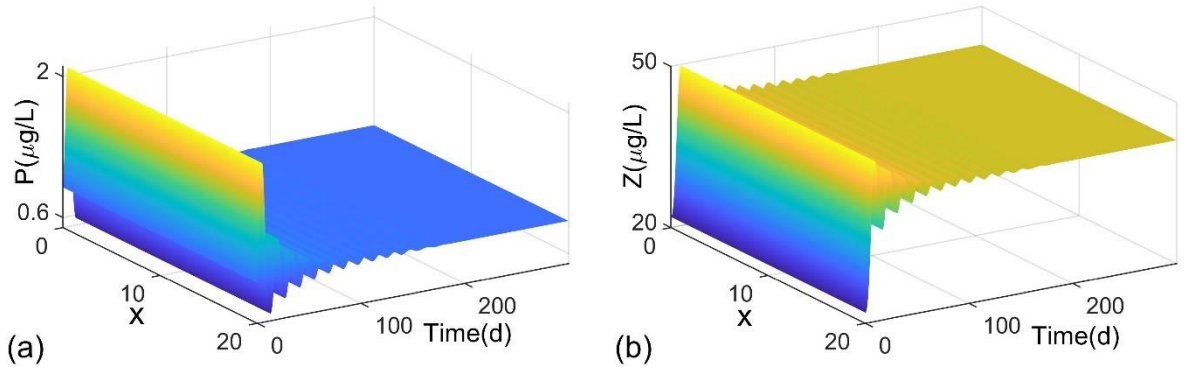

Figure 3.2. Biomass distributions of (a) phytoplankton and (b) phytoplankton populations in model (3.1) over time and space for $\tau = 0$.

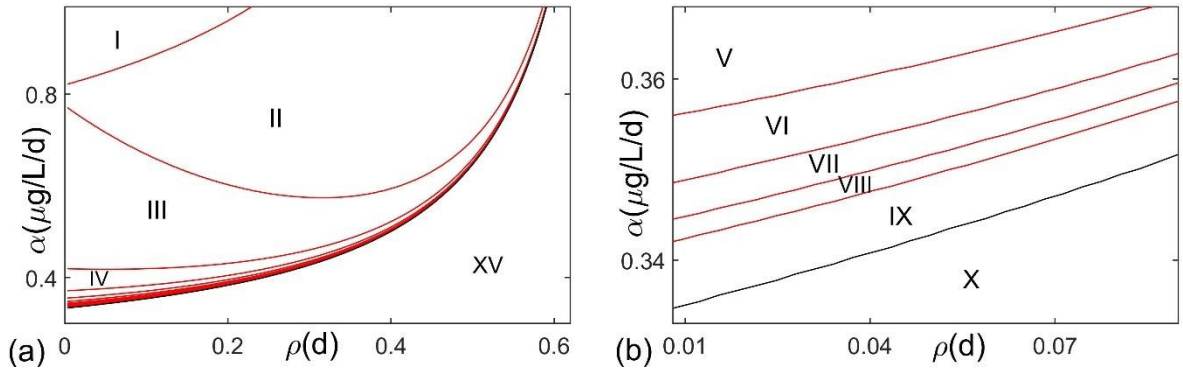

Figure 3.3. (a) The number of stability switches of the positive equilibrium of model (3.1) in the $\rho - \alpha$ plane. Stability switches occur once in region III, twice in region IV, three times in region V, four times in region VI, five times in region VII, six times in region VIII and seven times in region IX. (b) The partial enlarge diagram of (a).

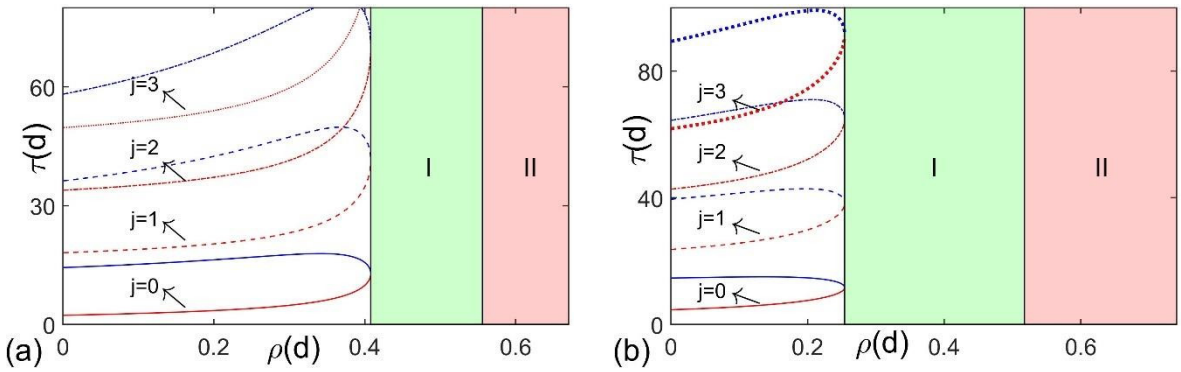

Figure 3.4. Bifurcation diagrams of model (3.1) with respect to ρ and τ for (a) $\alpha = 0.45$ and (b) $\alpha = 0.35$. In the figures, the solid, dashed, dash-dot, and dotted curves represent the critical values of τ for $j = 0, 1, 2, 3$ respectively.

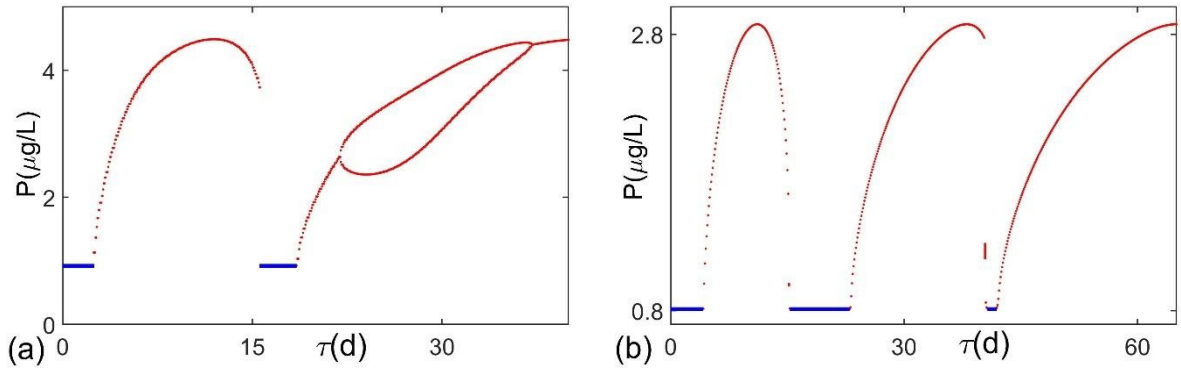

Figure 3.5. Bifurcation diagrams of model (3.1) with respect to τ for (a) $\alpha = 0.45$ and $\rho = 0.1$, and (b) $\alpha = 0.35$ and $\rho = 0.05$. In the figure, the solid blue line and the dotted red line represent the stable positive equilibrium and the maximum biomass of phytoplankton, respectively.

Firstly, the dynamics of model (3.1) in the absence of time delay are investigated. Figure 3.2 shows the biomasses of phytoplankton and zooplankton populations over time and space by setting $\tau = 0$ in model (3.1). It is evident from the figure that the corresponding equilibrium point is asymptotically stable, indicating that the biomasses of plankton populations do not change over time. However, theoretical analysis indicates that Hopf bifurcation may occur when there is a time lag in the growth of phytoplankton after nutrient uptake. The nutrient-plankton model may also exhibit stability switches with a gradual increase in such time delay. Furthermore, in the simulation process, the results show that the natural mortality of phytoplankton species does not significantly

affect the model's dynamics much. Therefore, to highlight the dynamical behaviors of stability switches, Figure 3.3(a) shows the number of stability switches that the model experiences around the positive equilibrium by simultaneously varying the parameters ρ and α under $m = 0.19$. In Figure 3.3(a), region I corresponds to the unstable domain of the positive equilibrium. In region X, the positive equilibrium is stable if it exists. In region II, the positive equilibrium loses its stability when τ crosses a critical value τ_0. It is important to note that there are no stability switches for positive equilibrium in region II, despite the fact that Eq. (B2) has two positive roots. However, stability switches emerge in region III. In Figure 3.3(b), an enlarged view of Figure 3.3(a) is presented to explore the characteristics of the stability switches for the positive equilibrium of model (3.1).

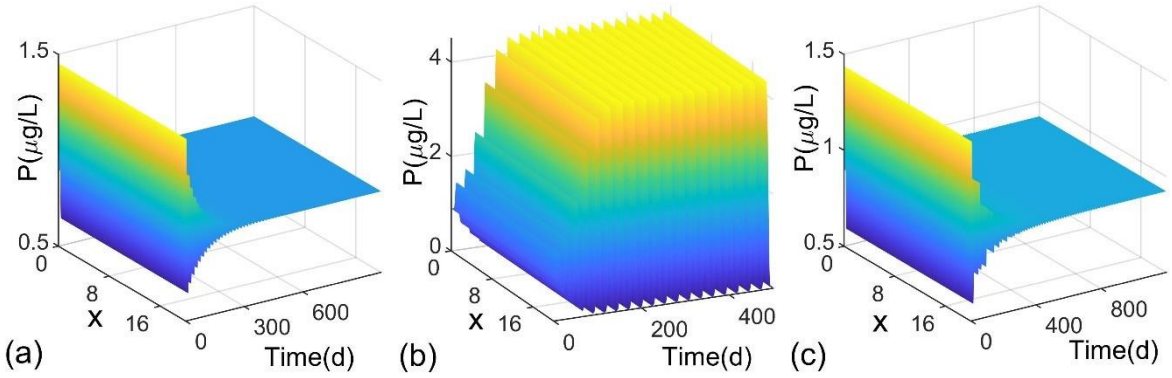

Figure 3.6. Biomass distribution of phytoplankton population in model (3.1) over time and space for $\alpha = 0.45, \rho = 0.1$ and different values of τ: (a) $\tau = 2$, (b) $\tau = 10$ and (c) $\tau = 18$.

To further investigate the stability switches in model (3.1), Figure 3.4(a) illustrates the bifurcation diagrams of the model in the $\rho - \tau$ plane for $\alpha = 0.45$ (see Figure 3.4(a)) and $\alpha = 0.35$. The figures depict that stability switches exist in the model before ρ enters the green zone. In the green zone, i.e., region I, stability switches do not emerge, and the positive equilibrium remains stable regardless of the value of time delay. However, the positive equilibrium disappears

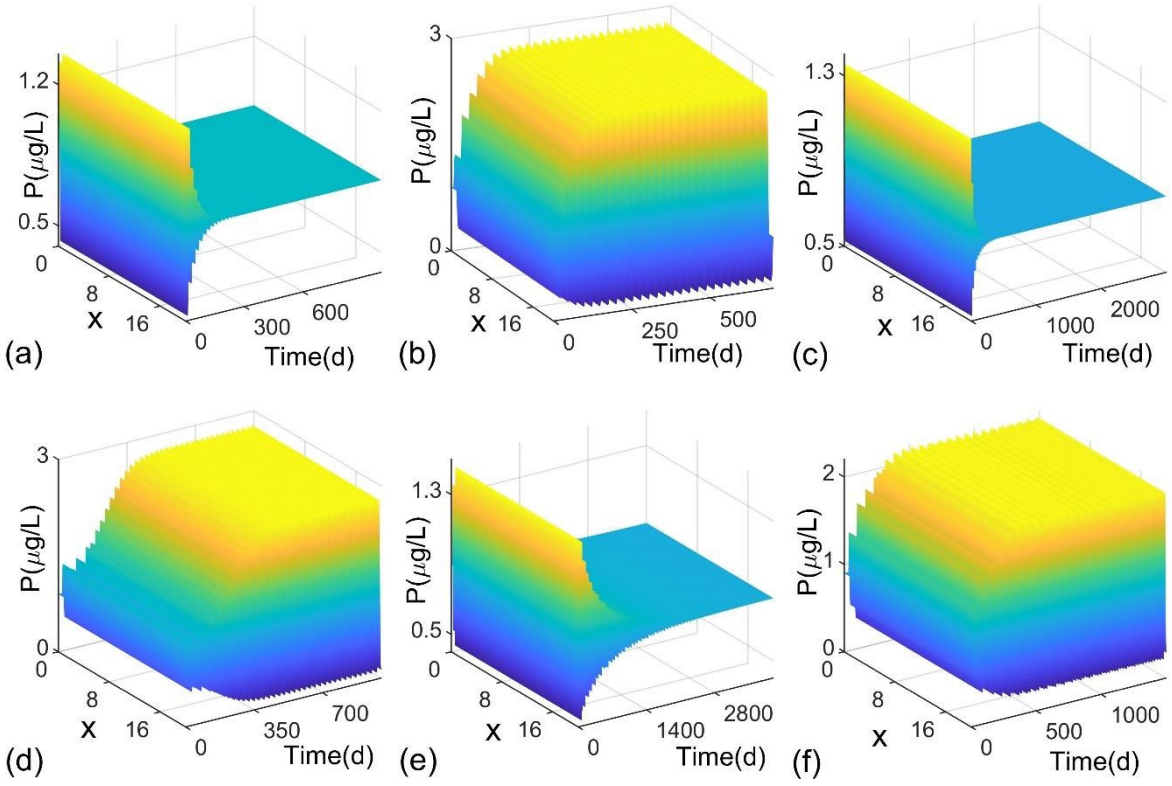

Figure 3.7. Biomass distribution of phytoplankton population in model (3.1) over time and space for $\alpha = 0.35, \rho = 0.05$ and different values of τ: (a) $\tau = 3$, (b) $\tau = 10$, (c) $\tau = 18$, (d) $\tau = 36$, (e) $\tau = 42$ and (f) $\tau = 50$.

from the model for all values of τ if the value of ρ falls within region II. Corresponding to Figure 3.4, the bifurcation diagram of model (3.1) with respect to the delay parameter τ is given in Figure 3.5. The figures only show the biomass of the phytoplankton population by varying the time delay along the $x-$axis. For $\alpha = 0.45$, Figure 3.5(a) shows that a stability switch occurs once, and periodic-2 solutions emerge as the value of time delay increases. Figure 3.6 shows the biomass distribution of phytoplankton over time and space at $\tau = 2, 10$, and 18. It is apparent from Figure 3.6 that the positive equilibrium is stable at $\tau = 2$ and 18 but unstable at $\tau = 10$. For $\alpha = 0.35$, Figure 3.5(b) shows that the model (3.1) goes through three transitions from stable to unstable via Hopf bifurcation as the value of time delay τ gradually increase. That is, stability switches occur twice in the model. The biomass distribution of phytoplankton over time and space is presented in

Figure 3.7. One can easily see in the figure that the positive equilibrium is stable at $\tau = 3, 18$, and 42, but unstable at $\tau = 10, 36$, and 50. Figures. 3.4 & 3.5 indicate that the nonlinear analysis is in agreement with the results predicted by the linear analysis. Note that all the parameters in these results indicate that delay in the growth of phytoplankton is the only reason for the rise in the instability of the positive equilibrium.

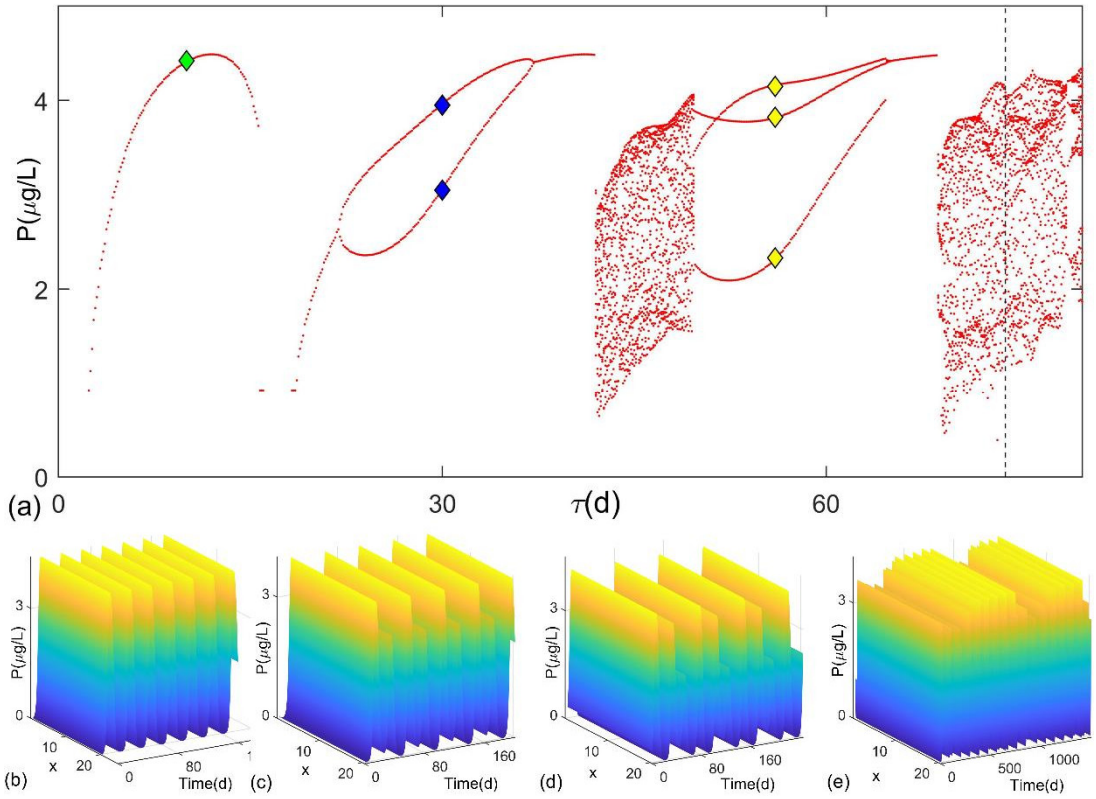

Figure 3.8. (a) Bifurcation diagram of model (3.1) with respect to τ for $\alpha = 0.6$ and $\rho = 0.1$. In the figure, the green, blue and yellow solid diamonds respectively represent the periodic-1, 2 & 3 solutions at $\tau = 10$, 30 and 56; the black dashed line denotes chaotic solution at $\tau = 74$. Figure (b)-(e) show the biomass distributions of phytoplankton in model (3.1) over time and space at $\tau = 10$, $\tau = 30$, $\tau = 56$ and $\tau = 74$, respectively.

Figure 3.8(a) shows a bifurcation diagram of model (3.1) for a wide range of the delay parameter τ. The figure only shows the biomass of the phytoplankton as the model exhibits the same dynamical behaviors of the zooplankton population. The figure clearly shows that the model

exhibits periodic-1, 2, and 3 solutions with a gradual increment in the value of time delay. Moreover, for a very large value of time delay, the model shows chaotic dynamics. In the figure, the periodic-1, 2, and 3 solutions are marked at $\tau = 10$, 30, and 56 with green, blue, and yellow solid diamonds, respectively. Also, there exists a vertical black dashed line at $\tau = 74$, where the model enters the chaotic regime. Furthermore, Figures 3.8(b)-3.8(e) illustrate the biomass distributions of the phytoplankton population in model (3.1) over time and space at these critical values of time delay.

3.5. Conclusions

Planktonic blooms have gained significant attention from ecologists and mathematicians in recent decades (Mukhopadhyay and Bhattacharyya, 2006). Mathematical models have been widely used by researchers as an important tool to explain these bloom phenomena. Huppert et al. (2002) investigated a simple mathematical model and found that high nutrient concentrations can trigger planktonic blooms in aquatic reservoirs. Furthermore, Steele and Henderson (1992) explored the role of predation in plankton models. The influence of time delay in aquatic environments is also inevitable. Researchers have noted that the diffusion of nutrients and plankton plays a crucial role in the spatial distribution of phytoplankton in aquatic ecosystems (Tian, 2012). However, the dynamics induced by time delay, such as oscillation, chaotic behavior, and stability switches in phytoplankton growth models with diffusion, need to be further explored.

In this chapter, a nutrient-plankton model was investigated to reveal the effects of time delay on the growth of phytoplankton and the interplay between nutrient and plankton populations. The proposed model also considers the effect of diffusion to incorporate the spatial movements of nutrient and plankton populations in the aquatic ecosystem. The theoretical results for the model without delay and diffusion showed that the positive equilibrium was locally asymptotically stable

under certain conditions on the model parameters, implying the persistence of nutrient and plankton populations in the ecosystem. However, the positive equilibrium may lose stability when the time lag involved in the growth of phytoplankton exceeded the critical values. In this case, periodic solutions emerge, and the model exhibited oscillatory dynamics of nutrient and plankton populations, indicating that the biomass of plankton populations cannot maintain a certain level. Thus, time delay plays a significant role in inducing oscillations in the nutrient-plankton model. Moreover, the direction of Hopf bifurcation around the positive equilibrium and the stability of the bifurcating periodic solutions were tracked using the center manifold theorem and the normal form theory. Several studies have demonstrated that ecosystems exhibit unstable coexistence of species when the time delay exceeds a critical value (Li and Liu, 2010; Meng and Li, 2020; Rehim et al., 2016). However, simulation results showed that time delay could generate and suppress oscillations in the model. This phenomenon is called stability switches of species coexistence in ecosystems (Song et al., 2014). These results contribute to the control of plankton biomass in aquatic reservoirs when the model exhibits stable coexistence of nutrient and plankton populations.

Furthermore, the effects of time delay on the model's dynamics were also explored through bifurcation diagrams. Figures 3.4 and 3.5 showed the number of stability switches that occur in the model around the positive equilibrium. Unlike other nutrient-plankton models that only show destabilizing role of time delay, the model demonstrated both destabilizing and stabilizing effects of delay on the model's dynamics. Specifically, the model showed the occurrence of multiple stability switches around the positive equilibrium as the delay involved in the growth of phytoplankton. Clearly, the model exhibited periodic-2 & 3 solutions and ultimately became chaotic for larger values of time delay. Therefore, delay can be considered as the main factor in the chaotic behavior of the model. It is worth noting that the emergence of chaos may signify the unpredictability of plankton population biomass distributions over time and space.

The size of an organism affects virtually all aspects of its physiology and ecology (Lebedeva, 1972). The body size of zooplankton gradually decreases during equilibrium conditions compared to chaos (Peters, 1983). Jorgensen et al. (2002) have demonstrated that the size combinations between phytoplankton and zooplankton are crucial for the model's self-organization. The model cannot adapt to the gradual decrease in zooplankton size, resulting in a transition from an equilibrium state to a chaotic condition. Low zooplankton populations benefit from rapid growth. If rapid growth continues, phytoplankton will be rapidly exhausted, causing the zooplankton population to plummet. As a result, the system undergoes violent oscillations and ultimately reaches chaos. However, this behavior is not prevalent in many ecosystems because they are self-organizing and self-adapting (Odum, 1988). They tune themselves to a critical state (Kauffman, 1991) and exhibit a high extent of self-organization based on a hierarchy of feedback mechanisms. The present study also showed that the plankton model may become chaotic if there is a large time delay in the growth of phytoplankton after nutrient uptake. These results indicate that the investigated nutrient-plankton model cannot accurately predict bloom events but it contributes to enhancing our understanding of the influences of time delay and diffusion on the interplay between nutrient and plankton populations in aquatic reservoirs. Overall, these findings may not provide insights into the sustainability of biodiversity by explaining the emergence of chaos in the plankton model, but they can be employed to develop management strategies to preserve and restore the integrity of aquatic habitats.

Chapter 4

DYNAMICS OF A STOCHASTIC LESLIE-GOWER PHYTOPLANKTON-ZOOPLANKTON MODEL WITH PREY REFUGE[2]

Abstract

In this chapter, the interaction dynamics of a Leslie-Gower phytoplankton-zooplankton model under stochastic environment were investigated. The theoretical analysis explored the sufficient conditions for the existence of a global positive solution of the model. The results concluded that noise intensity and prey refuge play a significant role in the coexistence of plankton, and the model exhibited an ergodic stationary distribution. The numerical results further indicated that refuge of phytoplankton could significantly influence the intensity of planktonic oscillations, and prey refuge that is too large or too small is detrimental to plankton coexistence. These findings provide insights into the dynamics of phytoplankton-zooplankton models.

Keywords: Prey refuge, stable in mean, stationary distribution, ergodicity

[2] Guo, Q., Dai, C.J., Wang, L.J., Liu, H., Wang, Y., Li, J., Zhao, M., 2021. Dynamics of a stochastic Leslie-Gower phytoplankton-zooplankton model with prey refuge. (prepared).

4.1. Introduction

The rapid change in plankton populations has drawn considerable attention in recent years as planktonic blooms can significantly affect aquatic ecosystems and pose a human health risk through the food web (Javidi and Ahmad, 2015). Experimental evidence has identified several factors that affect plankton growth dynamics, including nutrient availability (Sandrini et al., 2020), light intensity (Burson et al., 2019), and intraspecific competition (Passarge et al., 2006). Among these factors, the interaction between phytoplankton and zooplankton has become an important research area in aquatic ecosystems, as the effects of zooplankton grazers often extend well beyond the phytoplankton community and influence the diversity of multiple trophic levels (Birtel and Matthews, 2016; Duffy, 2002).

Recent experimental and field studies have successfully explored these interaction dynamics (Landry and Hassett, 1982). For example, a grazing experiment supports that *Daphnia*, a filter feeding cladoceran, can directly affect phytoplankton diversity (Berga et al., 2015; Verreydt et al., 2012). In addition, the role of zooplankton grazing selection on phytoplankton dynamics has been experimentally studied by Ger et al. (2018). However, the extent to which such interaction dynamics are not well established. One potential reason is that nonlinear interactions between plankton species widely exist in aquatic ecosystems, thereby leading to the growth process of plankton considerably more complex. Consequently, studies on the dynamics of plankton growth remain a challenge.

Mathematical modeling of plankton populations has been successfully developed and has become an important field of investigation for providing quantitative insights into the dynamics of plankton growth (Dai et al., 2016; Dai et al., 2019; Ojha and Thakur., 2020). Over the recent years, extensive plankton growth models have been developed (Camara et al., 2019; Chen et al., 2019;

Guo et al., 2020; Kaur et al., 2021; Sarkar et al., 2005; Tian and Ruan., 2019; Zhao and Wei., 2015). Moreover, a growing body of evidence suggests that refuge for plankton is a common phenomenon in some aquatic ecosystems (Li et al., 2017). For example, submerged plants provide a refuge for daphnids against predation (Beklioglu and Moss, 1998; Lauridsen and Lodge, 1996). Additionally, phytoplankton also use benthic sediments as a refuge through the production of cysts. (Schindler and Scheuerell, 2002). Wiles et al. (2006) claimed that stratification of the water column could provide a temporary refuge for phytoplankton to recover. Therefore, considering prey refuge is crucial in studying the dynamics of planktonic interactions.

Furthermore, there is growing evidence that aquatic ecosystems are inevitably affected by environment fluctuations, as they are generally complex and open systems (Zhao et al., 2017b). In fact, blooms occur in response to a combination of climatic and hydrographic events, resulting in the stochastic scaling and timing of blooms (Anderson, 1997; Anderson et al., 2002; Bruno et al., 1989; McGowan et al., 2017), which has led to an increasing interest in understanding how plankton growth responds to environmental fluctuations (Anderies and Beisner, 2000; Liu et al., 2021a; Majumder et al., 2021; Møller et al., 2011; Wang and Liu, 2020; Wei and Fu, 2020). Wang and Liu (2020) improved the stochastic hybrid phytoplankton-zooplankton model proposed by Yu et al. (2019b), in which a unique ergodic stationary distribution existed. Furthermore, the nontrivial positive stochastically periodic solution was studied in a non-autonomous toxic-producing phytoplankton allelopathy model with environmental fluctuation (Zhao et al., 2017a). Yu et al. (2019a) developed a nutrient-plankton model with the effect of regime switching, and the results showed that the Markov chain was beneficial for the survival of plankton. Although stochastic population dynamic models have been widely explored in recent years, the investigation of the related dynamics is still ongoing.

The aim of this chapter is to provide insights into the dynamics of phytoplankton-zooplankton

interactions. This research is organized as follows: in Chapter 4.2, the mathematical model is proposed. Chapter 4.3 discusses the existence of a global positive solution of model (4.1), as well as the persistence and extinction of plankton species. Chapter 4.4 derives the sufficient conditions for the existence of a stationary distribution of model (4.1). Chapter 4.5 presents some numerical results that provide an intuitive view of the effect of white noise and refuge on the interaction between phytoplankton and zooplankton. Finally, the research ends with some conclusions in Chapter 4.6.

4.2. The methods and results

4.2.1. Mathematical model

In this chapter, the noise effect and the refuge of phytoplankton are taken into account in a Leslie-Gower Holling-type II plankton model. The model is formulated based on the following assumptions.

(1) The growth of phytoplankton (x_1) depends on zooplankton (x_2) predation.

(2) The growth of plankton follows a logistic law, denoted by r_1 and r_2, respectively. b_1 denotes the strength of competition among individuals of phytoplankton.

(3) The capture rate of zooplankton on phytoplankton is denoted by α, and c is the maximum value of the per capita reduction rate of zooplankton.

(4) Similar to Mandal et al. (2021a)'s research, a constant proportion m of phytoplankton taking refuge is considered, leaving $(1-m)x_1$ of unprotected phytoplankton available for zooplankton grazing, which follows by Holling type II functional response, $\frac{\alpha(1-m)x_1(t)}{n+(1-m)x_1(t)}$.

Regarding these assumptions, a model schematic that expresses the interactions of nutrient and plankton is depicted in Figure 4.1. The following stochastic nutrient-plankton model is obtained:

$$\begin{cases} dx_1(t) = x_1(t)\left[\left(r_1 - b_1 x_1(t) - \frac{\alpha(1-m)x_2(t)}{n+(1-m)x_1(t)}\right)dt + \sigma_1 dB_1(t)\right], \\ dx_2(t) = x_2(t)\left[\left(r_2 - \frac{c\alpha x_2(t)}{n+(1-m)x_1(t)}\right)dt + \sigma_2 dB_2(t)\right], \end{cases} \tag{4.1}$$

where $B_i(t)$ represents independent standard Brownian motions, and σ_i is the intensities of the white noise for $i = 1, 2$, which is assumed to be a positive, bounded. $x_1(t)$ and $x_2(t)$ denotes population density of phytoplankton and zooplankton population with time t, respectively. All the parameters are positive and have biological meanings as listed in Table 4.1.

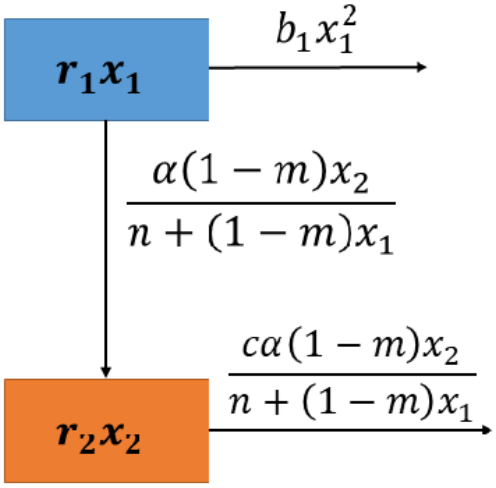

Figure 4.1. The scheme representation of the model (4.1).

For simplicity, the following notations are introduced:

$$\beta_i = 0.5\sigma_i^2, i = 1, 2; R_+^2 = \{\sigma_i \in R^2 | \sigma_i > 0, i = 1, 2\}.$$

Moreover, to derive the dynamical properties of model (4.1), some auxiliary lemmas are presented in Appendix E.

4.2.2. Global positive solutions and persistence and extinction

In this subchapter, the results imply that model (4.1) exists a unique positive solution for any positive initial value.

Lemma 4.1. *For any given initial value* $(x_1(0), x_2(0)) \in R_+^2$, *model (4.1) has a unique global*

solution $(x_1(t), x_2(t)) \in R_+^2$ *for any* $t \geq 0$ *almost surely.*

The proof is given in Appendix F. Lemma 4.1 indicates that the solution of model (4.1) is remain in R_+^2. Then, one can obtain the following Lemma:

Lemma 4.2. *If* $r_1 > \beta_1$, $r_2 > \beta_2$, *then*

$$\lim_{t\to\infty} t^{-1} \ln x_2(t) = 0, \text{ a.s.}$$

The proof is given in Appendix G. Then the extinction and persistence of model (4.1) are explored. Thus, the following results are obtained.

Theorem 4.1. (i) If $r_1 < \beta_1$ and $r_2 < \beta_2$, then both phytoplankton population $x_1(t)$ and zooplankton population $x_2(t)$ are extinct, i.e., $\lim_{t\to+\infty} x_1(t) = 0$, $\lim_{t\to+\infty} x_2(t) = 0$, almost surely (a.s.);

(ii) If $r_1 < \beta_1$ and $r_2 > \beta_2$, then phytoplankton population $x_1(t)$ is extinct and zooplankton population $x_2(t)$ is stable in mean, i.e.,

$$\lim_{t\to+\infty} t^{-1} \int_0^t x_2(s)\, ds = \frac{(r_2-\beta_2)n}{c\alpha}. \text{ a.s.;}$$

(iii) If $r_1 > \beta_1$ and $r_2 < \beta_2$, then zooplankton population $x_2(t)$ is extinct and phytoplankton population $x_1(t)$ is stable in mean, i.e.,

$$\lim_{t\to+\infty} t^{-1} \int_0^t x_2(s)\, ds = \frac{r_1-\beta_1}{b_1}. \text{ a.s.;}$$

(iv) If $r_1 > \beta_1$, $r_2 > \beta_2$ and $m < 1 - \frac{(r_1-\beta_1)c}{r_2-\beta_2}$ then phytoplankton population $x_1(t)$ is extinct and zooplankton population $x_2(t)$ is stable in mean, i.e.,

$$\lim_{t\to+\infty} t^{-1} \int_0^t x_2(s)\, ds = \frac{(r_2-\beta_2)n}{c\alpha}. \text{ a.s.;}$$

(v) If $r_1 > \beta_1$, $r_2 > \beta_2$ and $1 > m > 1 - \frac{(r_1-\beta_1)c}{r_2-\beta_2}$ then both phytoplankton population $x_1(t)$ and the Leslie-Gower term are stable in mean:

$$\lim_{t\to+\infty} t^{-1}\int_0^t x_1(s)\,ds = \frac{r_1-\beta_1}{b_1} - \frac{(1-m)(r_2-\beta_2)}{b_1 c},$$

$$\lim_{t\to+\infty} t^{-1}\int_0^t \frac{x_2(s)}{n+(1-m)x_1(s)}\,ds = \frac{r_2-\beta_2}{c\alpha}.$$

The proof is given in Appendix H. From the previous theorem, one can conclude that the extinction of population can be induced by high-intensity noise, indicating that excessive noise intensity can threaten the survival of populations. Additionally, Theorem 4.1 implies that refuge of phytoplankton plays an important role in extinction and coexistence of plankton.

4.2.3. Stationary distribution and ergodicity

In this subchapter, the existence of stationary distribution is investigated, and the following results are obtained.

Theorem 4.2. If $c > max\left\{\frac{r_2(1-m)^2}{bn}, \frac{r_2(1-m)}{r_1}\right\}$ and $\sigma_i > 0, i = 1, 2$ such that

$$\chi < \min\left\{\frac{bcn-r_2(1-m)^2}{c}\left[x_1^* + \frac{c}{4(bcn-r_2(1-m)^2)}\left(\sigma_1^2 x_1^* + \frac{\alpha}{r_2}\sigma_2^2 x_2^*\right)\right]^2,\ \frac{c\alpha^2}{r_2}(x_2^*)^2\right\}.$$

Then the stochastic process $(x_1(t), x_2(t))$ is ergodic and has a stationary distribution $\mu(\cdot)$ in R_+^2. (x_1^*, x_2^*) is defined as in (I1) and

$$\chi = \frac{c}{16(bcn - r_2(1-m)^2)}\left(\sigma_1^2 x_1^* + \frac{\alpha}{r_2}\sigma_2^2 x_2^*\right)^2 + \frac{1}{2}\left[n + \left(1 - m\frac{x_1}{x_1^*}\right)x_1^*\right]\left(\sigma_1^2 x_1^* + \frac{\alpha}{r_2}\sigma_2^2 x_2^*\right).$$

The proof is given is Appendix I. The results in Theorem 4.2 show that model (4.1) exists an ergodic stationary distribution, implying the stability in stochastic sense.

4.3. Numerical simulation

In this chapter, the effects of prey refuge on the plankton dynamics are further investigated. Unless otherwise mentioned, the parameter values used for numerical results are the same as in Table 4.1. The parameters m, σ_1, and σ_2 are chosen as control parameters.

Table 4.1. Biological explanations of variables and parameters in model (4.1), and numerical values used for simulation results

Parameter	Description	Unit	Value	Source
x_1	Phytoplankton biomass	$\mu g/L$		
x_2	Zooplankton biomass	$\mu g/L$		
r_1	Intrinsic growth rate of phytoplankton	day^{-1}	0.2	0.2[(a)]
r_2	Intrinsic growth rate of zooplankton	day-1	0.1	[0.05,0.25][(b)]
b_1	Phytoplankton death rate due to intraspecific competition	$L/\mu g/day$	0.05	0.08/0.1[(c)]
n	Saturation constant for the uptake of phytoplankton by zooplankton	$\mu g/L$	0.3	0.2/1[(d)]
m	Refuge protection to phytoplankton population	-	[0,1]	Assumed
α	Phytoplankton uptake rate by zooplankton	day^{-1}	0.1	0.1[(e)]
c	Phytoplankton toxin release rate	-	0.3	0.3[(d)]

(a) Kartal et al. (2016); (b) Hopcroft et al. (2005); (c) Sajan and Dubey (2021); (d) Lv et al. (2010); (e) Wang et al. (2016).

Theorem 4.1 demonstrates the critical role of prey refuge and noise density in the persistence of plankton. It is clear from Figure 4.2 that there exist five spaces in $(m - \sigma_1 - \sigma_2)$ plane. Space I correspond to Theorem 4.1 (i), indicating that both phytoplankton and zooplankton are tended to go extinct (see Figure 4.3(a)). In space II, $r_1 < \beta_1$ and $r_2 > \beta_2$ hold, showing that the phytoplankton is extinct while the zooplankton is stable in mean (see Figure 4.3(b)), and the space III represents the opposite scenario to space II (see Figure 4.3(c)). In space IV, the phytoplankton is extinct while the zooplankton is stable in mean (see Figure 4.3(d)). In space V, both phytoplankton population and the Leslie-Gower term are stable in mean (see Figure 4.3(e)).

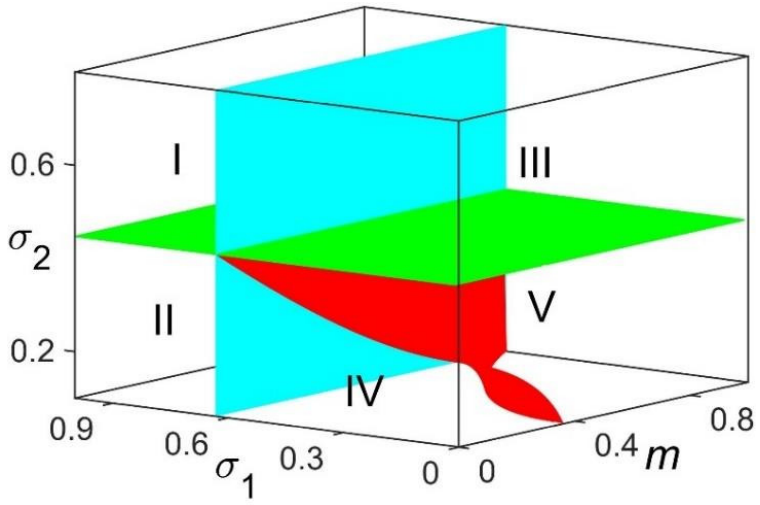

Figure 4.2. The analysis of the threshold for the extinction and persistent of model (4.1) in $(m - \sigma_1 - \sigma_2)$ space. The space I corresponds to Theorem 4.1 (i); the space II corresponds to Theorem 4.1 (ii); the space III corresponds to Theorem 4.1 (iii); the space IV corresponds to Theorem 4.1 (iv); the space V corresponds to Theorem 4.1 (v).

Moreover, by choosing $\sigma_1 = \sigma_2 = 0.2$, the distribution of x_1 and x_2 are presented in Figure 4.4(a) and Figure 4.4(b), respectively. Figure 4.4(a) clearly shows an increase in variance of phytoplankton population density, while Figure 4.4(b) displays an increasing trend followed by a decreasing trend in the variance of zooplankton population density. In addition, the boxplot of x_1 and x_2 under $\sigma_1 = \sigma_2 = 0.2$ are shown in Figure 4.5(a), revealing that the maximum and minimum value of x_1 increase with increasing prey refuge, and x_2 shows an increasing trend followed by a decreasing trend in the maximum and minimum value. Figure 4.5(b) displays the mean and variance of plankton population density, and the results reveal that increasing prey refuge leads to an increase in the mean and variance of x_1, which indicates increasing prey refuge can enhance phytoplankton population oscillation. Meanwhile, the results in Figure 4.5(b) further indicate that the mean and variance of x_2 show an increasing trend followed by a decreasing trend, suggesting that prey refuge can enhance the zooplankton population oscillation within the threshold, but oscillation tends to recede after exceeding the threshold. Furthermore, Figure 4.6 illustrates the

sample path of plankton with respect to m =0.3, 0.5, 0.7, and 0.9. Clearly, the results in Figure 4.6 are consistent with those in Figure 4.4 and 4.5.

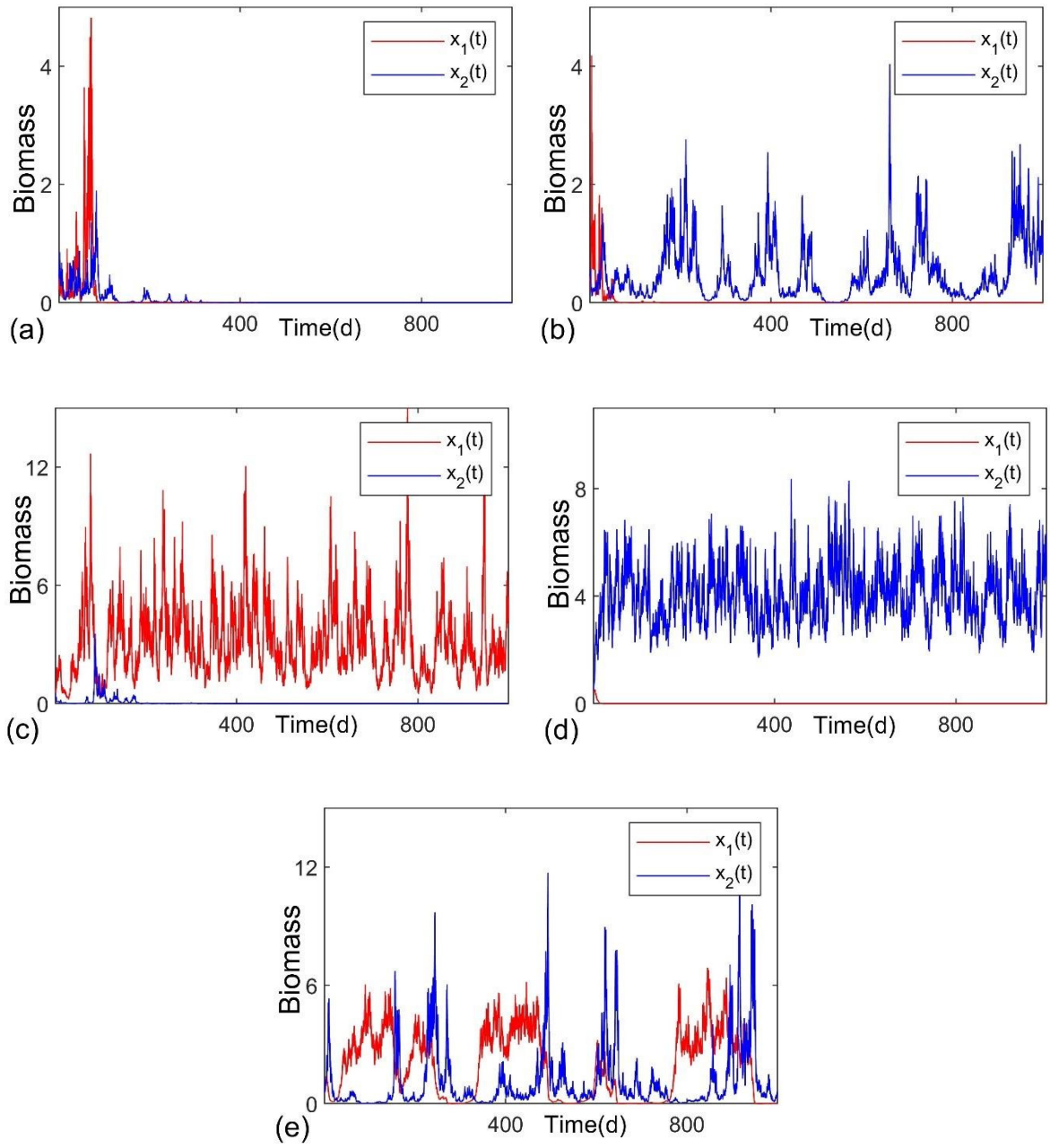

Figure 4.3. Solutions of model (4.1) for $m = 0.2$ with (a) $\sigma_1 = 0.7, \sigma_2 = 0.5$; (b) $\sigma_1 = 0.7, \sigma_2 = 0.3$; (c) $\sigma_1 = 0.3, \sigma_2 = 0.5$; (d) $\sigma_1 = 0.5, \sigma_2 = 0.3$; (e) $\sigma_1 = 0.15, \sigma_2 = 0.35$.

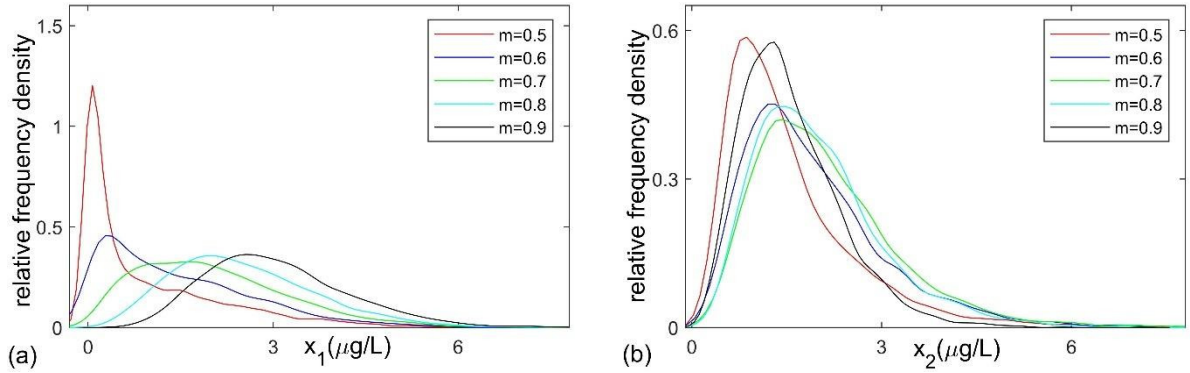

Figure 4.4. For model (4.1) with $\sigma_1 = \sigma_2 = 0.2$, (a) the distribution of x_1 and (b) the distribution of x_2 with respect to m.

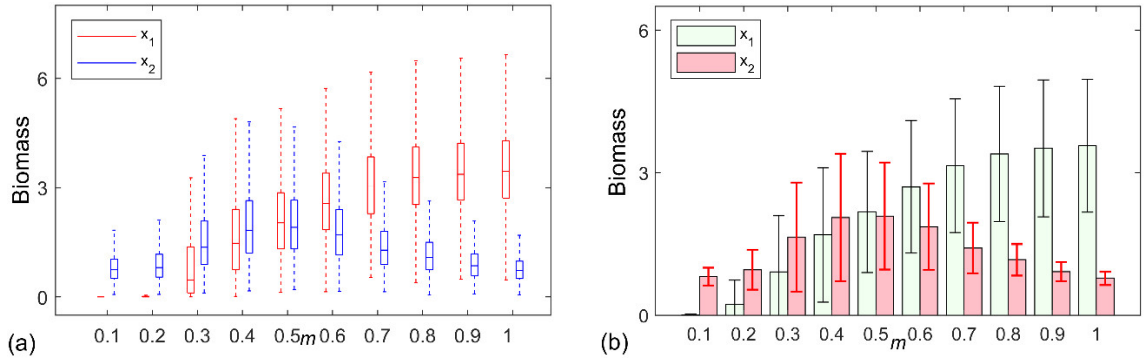

Figure 4.5. For model (4.1) with $\sigma_1 = \sigma_2 = 0.2$, (a) the boxplot of x_1 and x_2 with respect to m; (b) the mean and variance of x_1 and x_2 with respect to m.

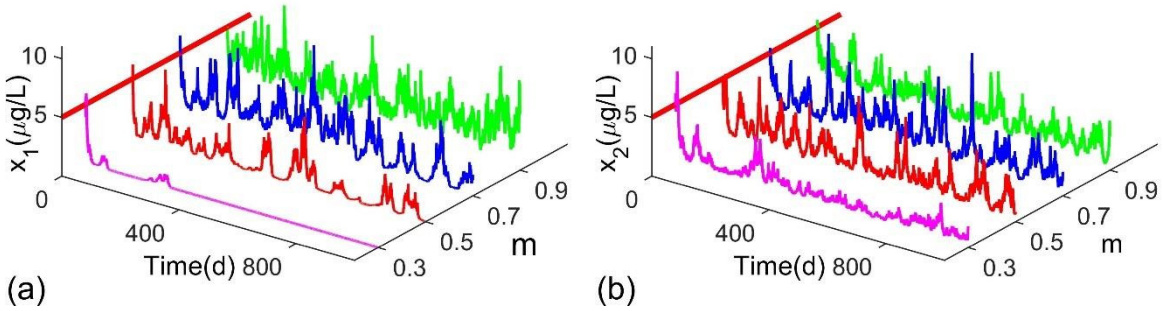

Figure 4.6. For model (4.1) with $\sigma_1 = \sigma_2 = 0.2$, (a) the sample path of x_1 with respect to $m = 0.3, 0.5, 0.7, 0.9$; (b) the sample path of x_2 with respect to $m = 0.3, 0.5, 0.7, 0.9$.

4.4. Conclusions

Previous studies have suggested that environmental fluctuations have a considerable impact on the dynamics of plankton populations. Furthermore, growing evidence suggests that different species respond differently to these fluctuations, resulting in phytoplankton-zooplankton interactions becomes more complex and not well understood. Therefore, it is crucial to investigate the collective response of plankton to environmental changes (Lee et al., 2020). Moreover, due to the prevalence of prey refuge as a common phenomenon in aquatic ecosystems, it is essential to account for prey refuge in modeling studies.

In this chapter, a stochastic Leslie-Gower plankton model incorporating prey refuge was developed. Firstly, the theoretical results concluded that model (4.1) existed a global positive solution for any positive initial values. Then, the sufficient conditions for the persistence and extinction of plankton were derived. The results implied that noise intensity and prey refuge played a crucial role in determining the coexistence of plankton. Specifically, when the noise intensity was within a critical value and the prey refuge was beyond a threshold, phytoplankton and zooplankton could coexist indefinitely. Furthermore, the analysis revealed that model (4.1) has an ergodic stationary distribution, which improves the understanding of how environmental noise affects plankton interaction dynamics by not only indicating random weak stability but also providing a better description of persistence (Gao et al., 2019; Liu et al., 2013).

The numerical results further showed how environmental noise and prey refuge affected the interaction dynamics of model (4.1). As shown in Figure 4.2, the $(m - \sigma_1 - \sigma_2)$ plane could be divided into five spaces, each corresponding to one of the cases in Theorem 4.1. Particularly, space V indicated that plankton populations can coexist. Figure 4.4 illustrated the distribution of the plankton population, revealing that increasing prey refuge leads to an increase in the variance of phytoplankton, which indicates that prey refuge can enhance the oscillation range of the phytoplankton population. However, the variance of zooplankton tended to increase and then

decrease as prey refuge increased, suggesting that excessive prey refuge may be detrimental to zooplankton populations. Figure 4.5(a) showed the boxplot of plankton with respect to prey refuge, and the mean and variance of the plankton were shown in Figure 4.5(b). The numerical results from Figure 4.5 were consistent with Figure 4.4. Clearly, when the refuge of phytoplankton was too small, the phytoplankton population went extinct. When the prey refuge increased within the threshold, both phytoplankton and zooplankton populations showed an increasing trend. However, when the prey refuge exceeded the threshold, the phytoplankton population showed a slower rate of increase in oscillation intensity, whereas the zooplankton population showed a decreasing trend, indicating that excessive refuge of phytoplankton may lead to a decrease in zooplankton populations. Obviously, phytoplankton refuge that is too large or too small is not conducive to plankton coexistence. The present study provides insights into how phytoplankton refuge affects plankton interaction dynamics under environmental fluctuations.

Chapter 5

STOCHASTIC PERIODIC SOLUTION OF A NUTRIENT-PLANKTON MODEL WITH SEASONAL FLUCTUATION[3]

Abstract

In this chapter, a stochastic nutrient–plankton model with seasonal fluctuation was developed to investigate how seasonality and environmental noise affect the dynamics of aquatic ecosystems. Firstly, the survival analysis of plankton was proposed. Then, by using Lyapunov function and Khasminskii's theory for periodic Markov processes, the sufficient conditions for the existence of positive periodic solution were derived. Numerical simulations were carried out to provide a better understanding of the model, and the results indicated that seasonal fluctuation was beneficial to the coexistence of plankton species.

Keywords: Extinction and persistence, survival analysis, periodic solution, white noise

[3]Guo, Q., Dai, C.J., Wang, L.J., Liu, H., Wang, Y., Li, J., Zhao, M., 2022. Stochastic periodic solution of a nutrient-plankton model with seasonal fluctuation. Journal of Biological Systems. 30, 695-720. DOI: 10.1142/S0218339022500255.

5.1. Introduction

Phytoplankton is the basis of aquatic food webs and can directly affect large-scale global processes by absorbing carbon dioxide from the atmosphere (Huppert et al., 2002). However, excessive growth of phytoplankton may disrupt food webs and create large hypoxic zones leading to fish deaths. Furthermore, excessive growth of phytoplankton can disturb the balance of ecological structure and function (Otten and Paerl, 2011). Experimental and mathematical studies have revealed an important fact that temperature (Paerl and Huisman, 2008), light (Anderson et al., 1994), and nutrient supply (Conley et al., 2009) are all responsible for the algae growth. However, due to the complexity and high nonlinearity of aquatic ecosystems, the dynamics of phytoplankton growth are not well understood (Dai et al., 2016).

Mathematical modeling is regarded as an efficient method to explain the complex dynamical behaviors of phytoplankton growth because mathematical models can provide quantitative insights into the dynamics of phytoplankton growth (Dai et al., 2019; Guo et al., 2020). Additionally, the two classical ways to study phytoplankton growth dynamics are the bottom-up control and top-down control approaches, which have been widely explored in recent years (Dai et al., 2015; Sekerci and Ozarslan, 2020; Tian and Ruan, 2019; Zhao and Wei, 2015). For example, a simple nutrient-phytoplankton model was proposed and studied theoretically and numerically in Huppert et al. (2002), and the results revealed that a bloom can only be triggered by nutrients. Furthermore, the effect of spatial heterogeneity on phytoplankton allelopathy was studied in a nutrient-plankton model by Mukhopadhyay and Bhattacharyya (2006).

All the forementioned literatures assumed an unvarying deterministic environment, where all the biological parameters were constants. However, it has been observed that environmental fluctuations underlie key processes of the structure and function of ecosystems (Vellend et al., 2014), such as carrying capacities, birth rates, and other parameters, to some extent, exhibit random fluctuations

(Black and McKane, 2012; May, 1973). Since the pioneering work of Haminskii (1980), many explanations relying on stochastic population dynamics have been proposed (Cai et al., 2020; Dean and Shnerb, 2020; Dobramysl et al., 2018; Liu and Deng, 2020). Importantly, Mao et al. (2002) revealed an important fact that stochastic noise can suppress potential explosions in population dynamics, while Deng et al. (2008) pointed out that noise can suppress or express exponential growth.

In fact, blooms occur in response to a combination of physical, chemical, and biological processes. In addition, the climatic and hydrographic events contribute to the unpredictability of algal blooms (Anderson et al., 2002; Bruno et al., 1989; McGowan et al., 2017). Some blooms occur in spring (Hunter-Cevera et al., 2016), others in summer (Kahrua et al., 2020), and even in winter (Ma et al., 2016). Moreover, the high degree of variability in the scale and timing of blooms results in the occurrence of blooms characterized as ultimately random phenomena, which makes understanding the growth of phytoplankton challenging. In recent years, numerous stochastic phytoplankton growth models have been proposed to investigate the bloom phenomenon (Chen et al., 2020c; Song et al., 2020a; Wang and Liu, 2020; Yu et al., 2019b; Zhao et al., 2016). Imhof and Walcher (2005) constructed a stochastic single-substrate chemostat model and demonstrated that white noise may lead to extinction in certain scenarios while the deterministic model predicts persistence. Yu et al. (2019a) investigated a nutrient-plankton model involving regime switching effects, and the results suggested that the Markov chain was beneficial for the survival of plankton.

Moreover, one of the interesting problems in phytoplankton growth studies is the seasonal fluctuation in the plankton community. Extensive research has been conducted on the mechanistic principles underlying the real-world randomness caused by external perturbations like seasonal differences in water temperature, nutrient supply, etc. (Yuan and Zhang, 2012a), resulting in changes in population density exhibiting a more or less periodicity. Smayda (1998) demonstrated that irrespective of highly variable planktonic habitats, there are impressive, quasiregular, predictable

annual occurrences of major blooms, in seasonal cycles. For example, the seasonal changes in water temperature result in seasonal blooms of *Microcystis* spp. in Lake Taihu, China, lasting from May to October (Otten and Paerl, 2011). Additionally, Wu et al. (2013) analyzed harmful algal blooms (HABs) data for over 11 years in the southwest Bohai Sea and found that the occurrences of HABs exhibit significant seasonality. Due to its evident importance, the effect of seasonal fluctuation on plankton dynamics under stochastic environments has been extensively studied in recent years (Jang and Allen, 2015; Yuan and Zhang, 2012b; Zhao et al., 2017a).

This chapter aims to improve the understanding of phytoplankton growth dynamics under periodic environmental and stochastic effects. The rest of the chapter is arranged as follows: The mathematical model is presented in Chapter 5.2, the survival analysis and conditions for the existence of nontrivial periodic solutions of model (5.2) are proposed in Chapter 5.3. In Chapter 5.4, some numerical simulations are performed to illustrate the analysis results. In the end, the conclusion is provided in Chapter 5.5.

5.2. The mathematical model

In this chapter, the interactions among nutrients, phytoplankton, and zooplankton are considered. Motivated by the mathematical models of Ruan (1993) and Yu et al. (2019a), a phytoplankton growth model consisting of nutrient (N), phytoplankton (P) and zooplankton (Z) is developed. The model is formulated based on the following assumptions.

(1) Zooplankton graze on phytoplankton and the growth of phytoplankton depends on nutrient.

(2) The nutrient uptake of phytoplankton follows a logistic law, and the zooplankton predation function is described by the Beddington-DeAngelis form (Beddington, 1975; DeAngelis et al., 1975), $\frac{\beta PZ}{1+mZ+nP}$, where β represents the consumption rate, and m and n denote the mutual interference between the zooplankton and phytoplankton saturation constant, respectively.

(3) S_0 and D denote the constant nutrient input and washout rate of nutrient, respectively. In addition, the constant α describes the maximal nutrient uptake.

(4) Referring to the model of Ruan (1993), nutrient recycling is considered as an instantaneous term, where the nutrient recycling rate from the dead phytoplankton and zooplankton is denoted as h and δ, respectively.

(5) Parameters c and b represent the mortality of phytoplankton and zooplankton, respectively.

(6) Furthermore, white noise is incorporated into the model to describe the random fluctuations in the real world, as environmental noise is ubiquitous in aquatic ecosystems (Liu and Wang, 2010).

Based on the above assumptions, a model schematic diagram is shown in Figure 5.1. Following the approach used in Liu and Bai (2016), Li and Mao (2009), and Zhu and Yin (2009), i.e., the white noise is assumed to mainly affect the growth rates of the plankton. This approach has been claimed to be reasonable and well justified biologically (Braumann, 2002; Liu and Bai, 2016). Thus, the following nutrient-plankton model, which accounts for white noise:

$$\begin{cases} dN(t) = [D\big(S_0 - N(t)\big) - \alpha P(t)N(t) + h)P(t) + \delta Z(t)]dt + \sigma_1 N(t)dB_1(t), \\ dP(t) = \left[\alpha P(t)N(t) - cP(t) - \frac{\beta P(t)Z(t)}{1+mZ(t)+nP(t)}\right]dt + \sigma_2 P(t)dB_2(t), \\ dZ(t) = \left[\frac{\beta P(t)Z(t)}{1+mZ(t)+nP(t)} - bZ(t)\right]dt + \sigma_3 Z(t)dB_3(t), \end{cases} \tag{5.1}$$

where $B_i(t)$ are independent standard Brownian motions, and σ_i^2 are the intensities of the white noise for $i = 1, 2, 3$. Throughout this chapter, the processes $B_i(t), i = 1, 2, 3$ are defined on a complete probability space $(\Omega, \mathfrak{F}, \{\mathfrak{F}_t\}_{t\geq 0}, \mathbb{P})$. In addition, the biological meanings of the variables and parameters involved in model (5.1) are listed in Table 5.1.

Additionally, it is widely recognized that the growth of plankton is evidently affected by seasonal fluctuations (e.g., periodic fluctuation with the seasons (Zhao et al., 2017a)). Thus,

seasonal fluctuations are incorporated into model (5.1), yielding the following model:

$$\begin{cases} dN(t) = [D(t)\big(S_0(t) - N(t)\big) - \alpha(t)P(t)N(t) + h(t))P(t) + \delta(t)Z(t)]dt \\ \qquad\qquad +\sigma_1(t)N(t)dB_1(t), \\ dP(t) = \left[\alpha(t)P(t)N(t) - c(t)P(t) - \frac{\beta(t)P(t)Z(t)}{1+m(t)Z(t)+n(t)P(t)}\right]dt + \sigma_2(t)P(t)dB_2(t), \\ dZ(t) = \left[\frac{\beta(t)P(t)Z(t)}{1+m(t)Z(t)+n(t)P(t)} - b(t)Z(t)\right]dt + \sigma_3(t)Z(t)dB_3(t), \end{cases} \tag{5.2}$$

where all the parameters are positive, bounded, continuous θ-periodic functions.

By now, a stochastic nutrient–plankton model is developed focusing on the effects of seasonal fluctuation and the stochastic environment on phytoplankton growth dynamics.

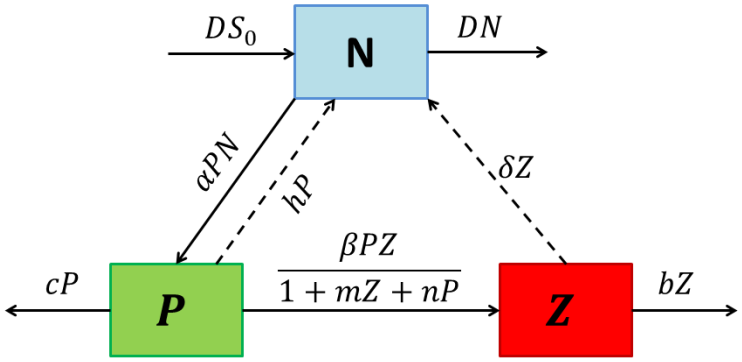

Figure 5.1. The scheme representation of the model (5.1).

Denote

$$f^u = \sup_{t\in[0,+\infty)} f(t) \quad and \quad f^l = \inf_{t\in[0,+\infty)} f(t),$$

where $f(t)$ is a bounded function on $[0,+\infty)$. In addition, in view of Gray et al. (2011)'s research, the existence of the global positive solution of model (5.2) is obtained. Furthermore, according to Lemma 2.3 in Zhao (2016), the following relations obtained:

$$\lim_{t\to+\infty} \sup[N(t) + P(t) + Z(t)] < \infty, \lim_{t\to+\infty} \frac{1}{t}\int_0^t \sigma_1\big(r(s)\big)N(s)dB_1(s) = 0, \tag{5.3}$$

$$\lim_{t\to+\infty} \frac{1}{t}\int_0^t \sigma_2\big(r(s)\big)P(s)dB_2(s) = 0, \lim_{t\to+\infty} \frac{1}{t}\int_0^t \sigma_3\big(r(s)\big)Z(s)dB_3(s) = 0, \tag{5.4}$$

hold almost surely. For convenience, the following function is defined:

$$u(t) = \frac{\int_t^{t+\theta} \exp\left\{\int_s^t D(\tau)\, dt\right\} \alpha(s) ds}{1 - \exp\left\{-\int_0^\theta D(\tau)\, d\tau\right\}}.$$

It is easy to check that $u(t)$ is the unique θ −periodic solution of equation $u'(t) = D(t)u(t) - \alpha(t)$. In addition, the following notations are introduced:

$$\vartheta(t) = \alpha(t) + [c(t) - h(t) - D(t)]u(t),$$
$$\eta(t) = \alpha(t) + [b(t) - \delta(t) - D(t)]u(t),$$
$$\Re_0^\theta = \frac{1}{\theta}\int_0^\theta \left[u(s)D(s)S_0(s) - \left(c(s) + \frac{1}{2}\sigma_2^2(s)\right)\right] ds,$$
$$\Re_1^\theta = -\frac{1}{\theta}\int_0^\theta \left[b(s) + \frac{1}{2}\sigma_3^2(s) - \frac{\beta(s)}{n(s)}\right] ds,$$
$$\Re_2^\theta = \beta^l \Re_0^\theta - \vartheta^u \frac{1}{\theta}\int_0^\theta \left[\left(b(s) + \tfrac{1}{2}\sigma_3^2(s)\right)\right] ds,$$

and two lemmas are presented in Appendix E.

5.3. The main results

In this chapter, the dynamical behaviors of the model are investigated. First, the survival analysis of model (5.2) is investigated, and then sufficient conditions for the existence of nontrivial periodic solution are derived.

5.3.1. Survival analysis of model (5.2)

In this chapter, the survival analysis of model (5.2) is given. First, one can get the following lemma.

Lemma 5.1. *For model (5.2), if* $\lim_{t\to+\infty} P(t) = 0$ *a.s., then* $\lim_{t\to+\infty} Z(t) = 0$ *a.s.*

The proof is given in Appendix J. The result in Lemma 5.1 suggests that if phytoplankton species are extinct with sufficient large time, then the zooplankton population follows.

Then, the following assumptions are presented:

Assumption 1. For arbitrary $0 < \iota < 1$, there exists a set $\Omega_\iota \subset \Omega$ with $\mathbb{P}(\Omega_\iota) \geq 1 - \iota$ and a

constant $\mathfrak{F} = \mathfrak{F}(\iota)$ such that $\lim_{t\to\infty} sup\frac{1}{t}\int_0^t \beta^l P(s)ds - \lim_{t\to\infty}\frac{1}{t}\int_0^t \left[b(t) + \frac{1}{2}\sigma_3^2(t)\right] ds \leq \iota$, for $\omega \in \Omega_\iota$ and $t > \mathfrak{F}$.

Thus, the following theorem is obtained.

Theorem 5.1. Denote $(N(t), P(t), Z(t))$ to be the solution of model (5.2) with initial values $(N(0), P(0), Z(0)) \in \mathbb{R}_+^3$. If $\underset{t\geq 0}{inf}\{c(t) - h(t) - D(t)\} \geq 0, \underset{t\geq 0}{inf}\{b(t) - \delta(t) - D(t)\} \geq 0$ holds, then one can obtain

(i) If $\mathfrak{R}_0^\theta < 0$, then $\underset{t\to\infty}{lim} P(t) = \underset{t\to\infty}{lim} Z(t) = 0$ almost surely;

(ii) If $\mathfrak{R}_0^\theta > 0$ and $\mathfrak{R}_1^\theta < 0$, then

$$\frac{\mathfrak{R}_0^\theta}{\vartheta^u} \leq \underset{t\to\infty}{lim\ inf}\frac{1}{t}\int_0^t P(s)\,ds \leq \underset{t\to\infty}{lim\ sup}\frac{1}{t}\int_0^t P(s)\,ds \leq \frac{\mathfrak{R}_0^\theta}{\vartheta^l}$$

and $\underset{t\to\infty}{lim} Z(t) = 0$ almost surely;

(iii) Under Assumption 1, if $\min\{D^l, (c-h)^l, (b-\delta)^l\} > \frac{1}{2}\max\{(\sigma_1^u)^2, (\sigma_2^u)^2, (\sigma_3^u)^2\}$ and $\mathfrak{R}_2^\theta > \frac{\beta^l\beta^u}{m^l} > 0$ hold, there exist a constant $\zeta > 0$ such that

$$min\left\{\underset{t\to\infty}{lim\ inf}\frac{1}{t}\int_0^t P(s)\,ds,\ \underset{t\to\infty}{lim\ inf}\frac{1}{t}\int_0^t Z(s)\,ds\right\} \geq \zeta > 0$$

almost surely.

The proof is given in Appendix K. Theorem 5.1 provides the information about the survival analysis of plankton in periodic environment, that is, when noise intensity is small, the plankton populations can coexist under certain conditions.

5.3.2. Existence of the nontrivial periodic solution of model (5.2)

In this subchapter, the existence of positive θ −periodic solution is studied. The result is given in Theorem 5.2.

Theorem 5.2. If $\min\{D^l, (c-h)^l, (b-\delta)^l\} > \frac{1}{2}\max\{(\sigma_1^u)^2, (\sigma_2^u)^2, (\sigma_3^u)^2\}$ and $\Re_2^\theta > 0$ hold. Then model (5.2) has at least one positive θ −periodic solution.

The proof is given is Appendix L. The results in Theorem 5.2 suggest that if the model has low noise intensity, the model admits a positive θ −periodic solution when $\Re_2^\theta > 0$, which reveals that periodic blooms of phytoplankton can be triggered.

Table 5.1. Biological explanations of variables and parameters in model (5.1), and numerical values used for simulation results

Parameter	Description	Unit	Value	Source
N	Nutrient concentration	$\mu g/L$		
P	Phytoplankton biomass	$\mu g/L$		
Z	Zooplankton biomass	$\mu g/L$		
α	Maximal nutrient uptake rate of phytoplankton	$L/\mu g/day$	0.8	0.6[(a)]
h	Nutrient recycling rate from dead phytoplankton	day^{-1}	0.08	0.08[(b)]
δ	Nutrient recycling rate from dead zooplankton	day^{-1}	0.01	0.01[(f)]
c	Death rate for phytoplankton	day^{-1}	0.6	[0.2,0.65][(c)]
b	Death rate for zooplankton	day^{-1}	0.5	[0.08,0.6][(d)]
β	Consumption rate of phytoplankton by zooplankton	day^{-1}	0.4	0.5[(e)]
n	Phytoplankton saturation constant	$L/\mu g$	0.5	Assumed
m	Mutual interference between the zooplankton	$L/\mu g$	[0,5]	Assumed
D	Washout rate for nutrient	day^{-1}	0.5	0.4[(g)]
S_0	Input concentration of nutrient	$\mu g/L$	[0,10]	[0,12.5][(b)]

(a) Jang and Baglama (2005); (b) Ruan (2001); (c) Garcés et al. (2005); (d) Turner et al. (2014); (e) Jang and Allen (2015); (f) Yu et al. (2019a); (g) Rehim et al. (2016).

5.4. Numerical simulation

In this chapter, some numerical results are presented to further investigate how seasonal

fluctuation affects model (5.2). For the stochastic model (5.2), it is assumed that all the parameters are periodic and have a common period of 50 days. The parameter set in the periodic environment is chosen as follows:

$$D = 0.5 + 0.01\sin(t/25),\ \alpha = 0.8 + 0.1\sin(t/25), h = 0.08 + 0.1\sin(t/25),$$

$$\delta = 0.01 + 0.1\sin(t/25), \beta = 0.4 + 0.1\sin(t/25), c = 0.6 + 0.01\sin(t/25),$$

$$n = 0.5 + 0.01\sin(t/25), b = 0.5 + 0.1\sin(t/25), \sigma_1 = 0.15 + 0.01\sin(t/25),$$

$$\sigma_2 = 0.15 + 0.01\sin(t/25), \sigma_3 = 0.15 + 0.01\sin(t/25).$$

The parameters m and S_0 are selected as control parameters.

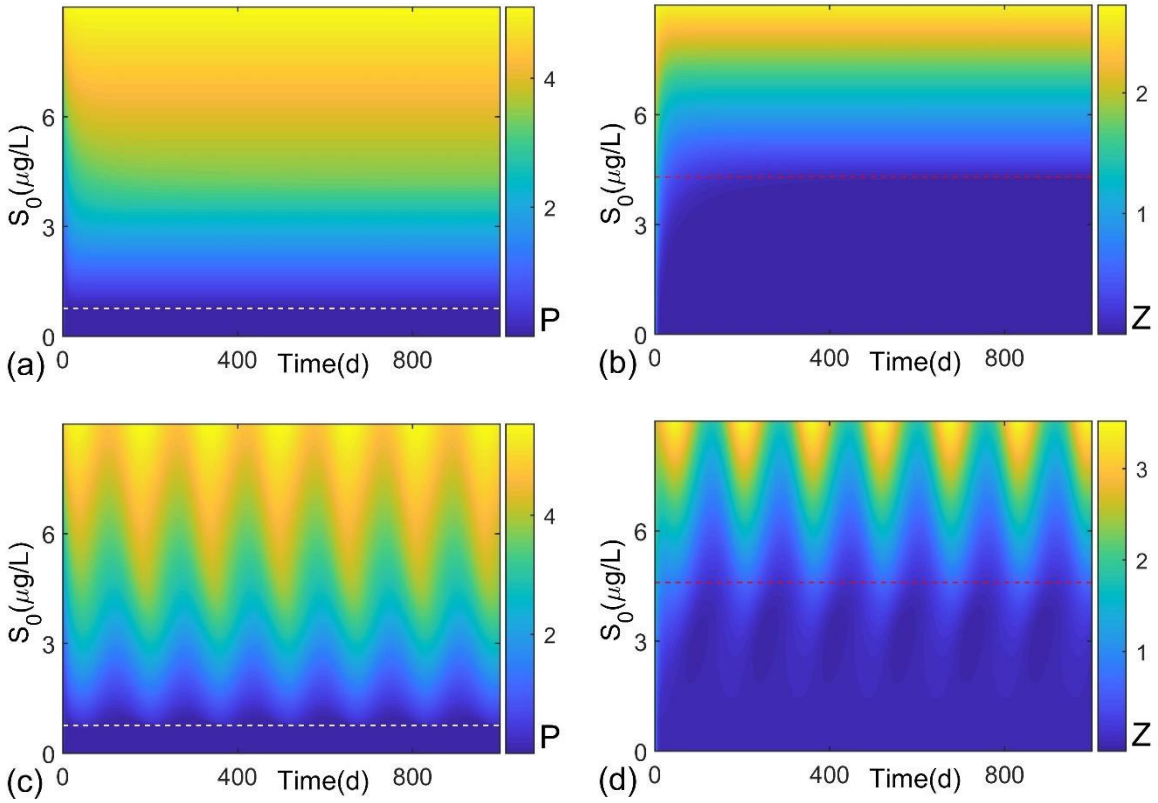

Figure 5.2. For model (5.1) without noise, (a) the solutions of P in the (S_0, t) plane and (b) the solutions of Z in the (S_0, t) plane. For model (5.2) without noise, (c) the solutions of P in the (S_0, t) plane and (d) the solutions of Z in the (S_0, t) plane. The white dash line and the red dash line represents the critical value of $\Re_0^\theta = 0$ and $\Re_2^\theta = \beta^u\beta^l/m^l$, respectively.

First, under $m = 0.2 + 0.01\sin(t/25)$, Figure 5.2 displays the solution of phytoplankton and zooplankton populations for the deterministic model with respect to nutrient input S_0. The results from Figure 5.2 show that the phytoplankton and zooplankton species can coexist after the nutrient input exceeds the threshold. Different from the deterministic model, the periodic environment can cause periodic bloom events of phytoplankton, and the zooplankton biomass changes periodically over time. Additionally, the sample paths of plankton populations for the deterministic model are given in Figure 5.3, which reveal that the increase in nutrient input level leads to a marked increase in the amplitude of planktonic oscillation.

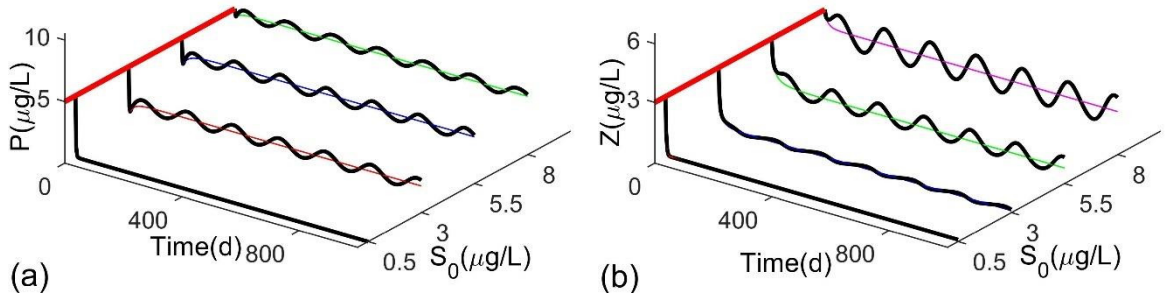

Figure 5.3. For model (5.1) without noise, (a) The sample paths of phytoplankton and (b) zooplankton corresponding to $S_0 = 0.5 + 0.1\sin(t/25)$, $3 + 0.1\sin(t/25)$, $5.5 + 0.1\sin(t/25)$ and $8 + 0.1\sin(t/25)$, respectively. The black line represents the solutions for model (5.2) without noise.

For model (5.2), the theoretical analysis reveals that there exists a nontrivial periodic solution under certain conditions. Thus, the solutions of model (5.1) and (5.2) with respect to nutrient input are presented, respectively (see Figure 5.4). Figure 5.4 shows that when the parameters are periodic functions, periodic coexistence of phytoplankton and zooplankton exists after the nutrient input exceeds the critical value. Furthermore, the results imply that the patterns in Figure 5.4 are in agreement with those obtained in Figure 5.2. However, it is worth mentioning that the plankton density for the stochastic model is always oscillating over time instead of maintaining a certain level (see Figure 5.4). More importantly, the results obtained in Figure 5.4 imply that

environmental fluctuation and nutrient input can significantly increase the distribution and oscillation intensity of plankton biomass.

Furthermore, the sample paths with respect to nutrient input are given in Figure 5.5 by choosing $S_0 = 0.5 + 0.1\sin(t/25)$, $3 + 0.1\sin(t/25)$, $5.5 + 0.1\sin(t/25)$, and $8 + 0.1\sin(t/25)$. Additionally, for model (5.2), by choosing $S_0 = 8 + 0.1\sin(t/25)$, the probability histograms for phytoplankton and zooplankton species are illustrated in Figures 5.5(b) and 5.5(d), which can be regarded as approximate probability density functions of the stationary distribution. From Figure 5.5, it is obvious that nutrient input can enhance the oscillation intensity of plankton biomass, and the results show that the overall trend of stochastic periodic solutions of model (5.2) exhibits obvious periodicity.

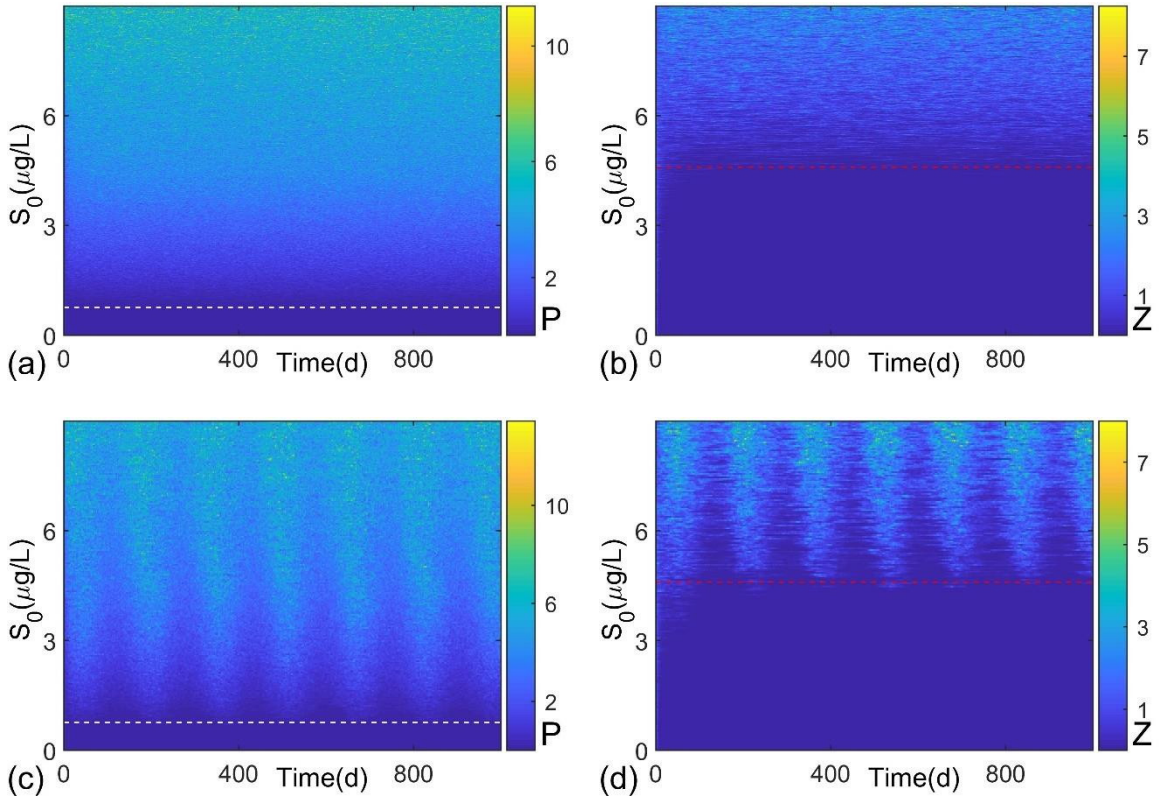

Figure 5.4. For model (5.1), (a) the solutions of P in the (S_0, t) plane and (b) the solutions of Z in the (S_0, t) plane. For model (5.2), (c) the solutions of P in the (S_0, t) plane and (d) the solutions of Z in the (S_0, t) plane. The white dash line and the red dash line represent the critical value of $\Re_0^\theta = 0$ and $\Re_2^\theta = \beta^u\beta^l/m^l$, respectively.

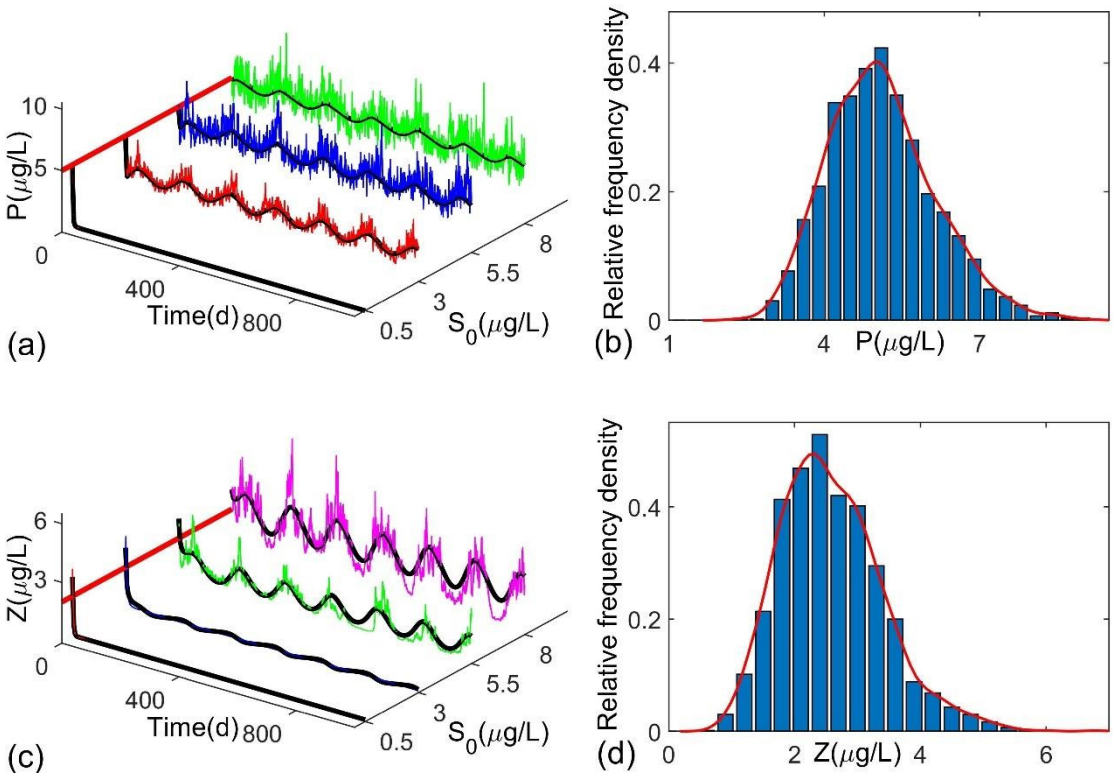

Figure 5.5. For model (5.2), (a) the sample paths of phytoplankton and (c) zooplankton corresponding to $S_0 = 0.5 + 0.1\sin(t/25)$, $3 + 0.1\sin(t/25)$, $5.5 + 0.1\sin(t/25)$ and $8 + 0.1\sin(t/25)$, respectively. The black line represents the solutions for the deterministic model. (b) Probability histograms for phytoplankton and (d) zooplankton with $S_0 = 8 + 0.1\sin(t/25)$.

To further investigate the effect of seasonal fluctuations on the distribution of plankton, Figure 5.6 is given, which describes the changes in the mean and variance of plankton biomass. Clearly, with the increase in nutrient input, phytoplankton biomass shows a steady increasing trend, but there is no significant difference between model (5.2) and (5.1) in the mean and variance of phytoplankton biomass (see Figure 5.6(a)). Actually, in contrast to seasonal fluctuation, the concentration of available nutrients is one of the decisive factors controlling phytoplankton productivity because nutrient limitation is directly related to phytoplankton growth (Hder and Gao, 2015). This is consistent with the results in Figure 5.6(a) that seasonal fluctuation shows less impact than nutrient input on phytoplankton growth. By contrast, zooplankton growth does not depend directly on nutrients (Gajbhiye, 2002), but is directly affected by phytoplankton and higher-

level predators. In addition, the effect of seasonal fluctuation on the zooplankton community is both intense and prolonged compared to their life spans (Mackas et al., 2012), which results in zooplankton populations being more easily affected by seasonal fluctuation than phytoplankton. The results from Figure 5.6(b) suggest that seasonal fluctuation significantly increases the distribution and oscillation intensity of zooplankton biomass. From an ecological point of view, the periodic environment is beneficial to the survival of zooplankton and the coexistence of plankton. Furthermore, under $S_0 = 8 + 0.1\sin(t/25)$, the distribution of plankton of model (5.2) in different periods is given in Figure 5.7, which shows that the distribution of phytoplankton of model (5.2) is almost identical in different periods (see Figure 5.7(a)). In contrast, the results from Figure 5.7(b) show that there is a significant change in the distribution of zooplankton with respect to periods.

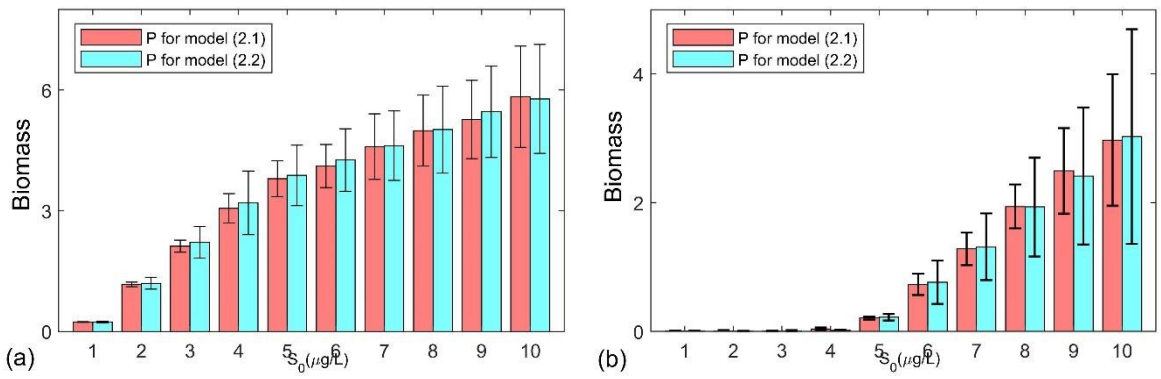

Figure 5.6. For model (5.1) and (5.2), (a) the mean and variance of phytoplankton biomass with respect to nutrient input S_0; (b) The mean and variance of zooplankton biomass with respect to nutrient input S_0.

In recent years, the effect of mutual interference of zooplankton on the dynamics of plankton growth models has been explored. For example, it has been reported that the mutual interference of zooplankton can stabilize the population interactions (De Silva and Jang, 2017; De Silva and Jang, 2018). Thus, the plankton biomass distribution with respect to the mutual interference of zooplankton is given in Figure 5.8. Under $S_0 = 2 + 0.1\sin(t/25)$, the solutions of plankton in

model (5.2) are given in Figures 5.8(a) and 5.8(b), respectively. Clearly, there is an obvious periodic motion for phytoplankton biomass, but the zooplankton population tends to go extinct. Then, by fixing nutrient input $S_0 = 5 + 0.1\sin(t/25)$, Figures 5.8(c) and 5.8(d) show the solutions of phytoplankton and zooplankton, respectively. Obviously, both phytoplankton and zooplankton show periodic trends over time, and the increase in the mutual interference of zooplankton causes a decreasing trend in the oscillation intensity of zooplankton biomass. In the end, under nutrient input $S_0 = 5 + 0.1\sin(t/25)$, the solutions of phytoplankton and zooplankton are given in Figures 5.8(e) and 5.8(f), respectively. Figures 5.8(e) and 5.8(f) show similar results to Figures 5.8(c) and 5.8(d).

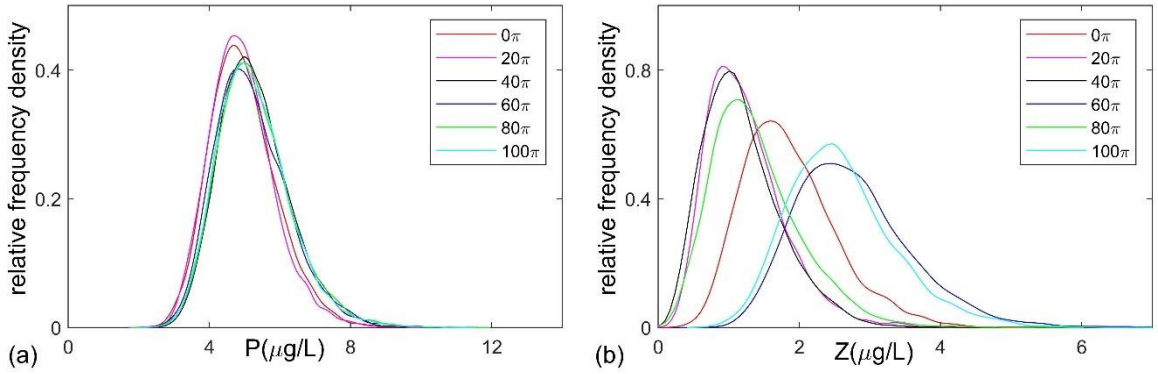

Figure 5.7. For model (5.2), (a) the distribution of phytoplankton biomass in different periods; (b) the distribution of zooplankton biomass in different periods.

The results from Figure 5.8 imply that excessive mutual interference of zooplankton may not be beneficial to the survival of the zooplankton population. Furthermore, Figure 5.8 reveals a point that the distribution of phytoplankton biomass is more sensitive to nutrient input than the mutual interference of zooplankton because nutrient limitation is directly related to phytoplankton growth (Hder and Gao, 2015). Notably, although the mutual interference of zooplankton can affect the oscillation intensity of zooplankton biomass, increasing the mutual interference of zooplankton does not really influence the dynamic properties of the model under this condition.

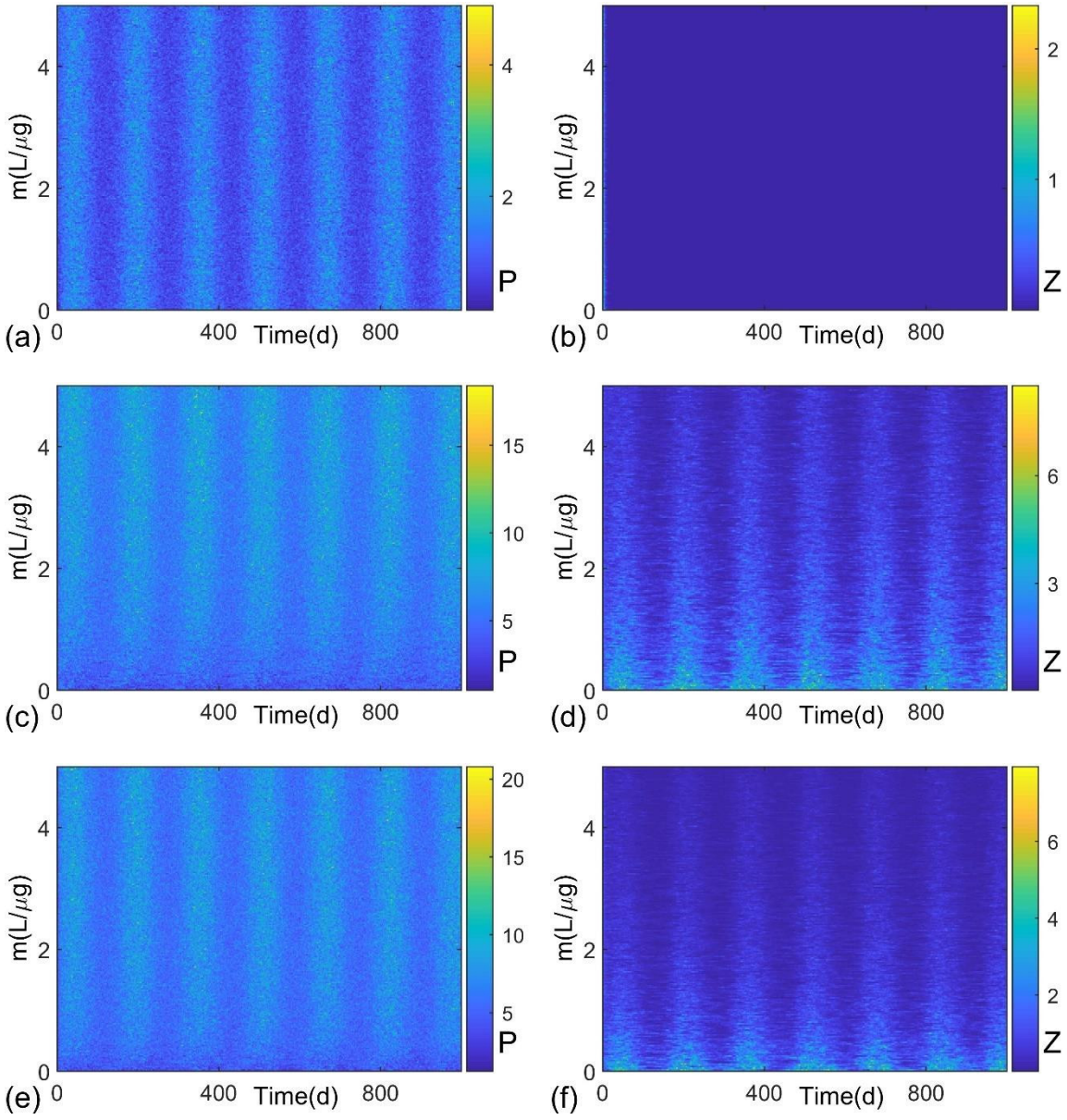

Figure 5.8. For model (5.2), (a) the solutions of P in the (m,t) plane and (b) the solutions of Z in the (m,t) plane with $S_0 = 2 + 0.1\sin(t/25)$; (c) The solutions of P in the (m,t) plane and (d) the solutions of Z in the (m,t) plane with $S_0 = 5 + 0.1\sin(t/25)$; (e) The solutions of P in the (m,t) plane and (f) The solutions of Z in the (m,t) plane with $S_0 = 8 + 0.1\sin(t/25)$.

5.5. Conclusion

Understanding the dynamics of plankton growth is one of the major goals for ecologists and mathematicians, as phytoplankton communities are known to have a significant impact on aquatic

ecosystems (Huppert et al., 2002). It is now well established that both seasonality and stochasticity are important factors influencing the dynamics of phytoplankton growth (Freund et al., 2006). In recent years, there has been increasing interest in stochastic phytoplankton growth models incorporating seasonal fluctuation (Ghosh et al., 2019; Wei and Fu, 2020).

In this chapter, a stochastic nutrient–plankton model with seasonal fluctuation was developed. The theoretical analysis derived the sufficient condition for the survival of plankton populations. The results implied that if the mortality rate of plankton was large and the noise intensity was small enough, the extinction and persistence in mean of plankton depend on $\mathfrak{R}_0^\theta$ and $\mathfrak{R}_1^\theta$. Then, the sufficient condition for the existence of a stochastic positive periodic solution was carried out using Khasminskii's theory for periodic Markov processes.

The numerical simulation further showed the effect of white noise and seasonal fluctuations on the distribution of plankton biomass. Figures 5.2 and 5.4 displayed the changes in plankton biomass for the deterministic model and the stochastic model with respect to nutrient input, respectively. Comparing the patterns of phytoplankton and zooplankton species in the stochastic model (see Figure 5.4) with their corresponding deterministic model in Figure 5.2, it is obvious that the oscillation phenomenon in the stochastic model became pronounced, demonstrating that environmental fluctuations significantly increase the oscillation intensity of plankton populations. Figure 5.4 showed that under seasonal fluctuations, the model (5.2) was persistent in mean and existed a positive periodic solution within certain conditions, which implies that seasonality and stochasticity may cause the periodic bloom of phytoplankton. Additionally, the sample paths of plankton with respect to nutrient input implied that a high nutrient input level could enhance the oscillation intensity of plankton biomass, and the overall trend of stochastic periodic solutions of model (5.2) presented obvious periodicity after the nutrient input went beyond a certain level.

It would also important to note that with an increase in nutrient input, the mean and variance

of phytoplankton biomass did not constitute a visible difference between constant parameters and periodic parameters. However, the variance of zooplankton biomass in model (5.2) with periodic parameters was much higher than that in model (5.2) with constant parameters, while the mean remained at the same level. One possible explanation is that the phytoplankton population is more sensitive to nutrient availability than seasonal fluctuation, while the zooplankton population is more easily affected by seasonal fluctuation. Figure 5.6 suggested that seasonal fluctuations may contribute to the survival of zooplankton and further promoted the coexistence of plankton. Furthermore, the distribution of plankton biomass of model (5.2) with respect to the period was carried out, and the results demonstrated that there was no significant difference in the distribution of phytoplankton biomass at various periods from 0π to 100π, but the distribution of zooplankton biomass was sensitive to changes in periodicity (see Figure 5.7). This study provides insights into how seasonal fluctuations influence phytoplankton growth dynamics under stochastic environment.

Additionally, it is generally accepted that the mutual interference of zooplankton may affect the stability of population interactions (De Silva and Jang, 2017; De Silva and Jang, 2018). The changes in plankton biomass with respect to the mutual interference of zooplankton were presented in Figure 5.8. The results from Figure 5.8 revealed that with mutual interference of zooplankton, the oscillation intensity of zooplankton biomass showed a decreasing trend, but there was no significant change in the dynamic properties of the model. However, it is evident from Figure 5.8 that increased nutrient input could have a significant impact on phytoplankton biomass distribution. From a biological point of view, the changes in phytoplankton biomass are more sensitive to nutrient input in contrast to the mutual interference of zooplankton. This study may provide a better understanding of the role of seasonal fluctuation and nutrient input for phytoplankton growth under environmental fluctuation, and the results provide insights into the dynamics of phytoplankton growth.

Chapter 6

DYNAMICS OF A STOCHASTIC NUTRIENT-PLANKTON MODEL WITH REGIME-SWITCHING[4]

Abstract

In this chapter, a stochastic nutrient–plankton model with regime switching was proposed, where the regime-switching plankton mortality was described by a continuous time Markov chain with different states. Firstly, the effects of regime-switching plankton mortality on the distribution of plankton biomass, as well as the persistence and extinction of plankton populations, were examined. Moreover, theoretical analysis showed that the model existed a unique stationary distribution, which is ergodic, indicating that the plankton populations will survive forever. By applying a sophisticated sensitivity analysis technique, it was observed that the phytoplankton biomass was highly sensitive to the grazing rate by zooplankton and least sensitive to the re-mineralization of dead biomass of plankton into nutrients concentration. The numerical results showed that the persistence and extinction of plankton populations were sensitive to variations in nutrient input. Additionally, the numerical analysis showed that noise can enhance the oscillations of plankton biomass, and the regime-switching plankton mortality has the capacity to decrease the amplitudes of the oscillations in the bloom phase. The results emphasized that regime-switching plankton mortality contributes to the survival of plankton populations in the aquatic system.

Keywords: Nutrient input, regime-switching plankton mortality, stochastic permanence, stationary distribution, sensitivity

[4]Guo, Q., Wang, Y., Dai, C.J., Wang, L.J., Liu, H., Li, J., Tiwari, P.K., Zhao, M., 2023. Dynamics of stochastic nutrient-plankton model with regime-switching. Ecological Modelling. 477, 110249. DOI: 10.1016/j.ecolmodel.2022.110249.

6.1. Introduction

Phytoplankton blooms are the rapid accumulation of algae to sufficient numbers, sometimes reaching millions of cells per liter, resulting in severe negative consequences such as oxygen depletion, fish mortality, and human illness (Anderson,1997). Results from both experimental and field observations have demonstrated that planktonic ecosystems are affected by many factors, such as light (Burson et al., 2019), temperature (Righetti et al., 2019), nutrients (Burson et al., 2018), and zooplankton (Huisman et al., 2018). The complexity of planktonic ecosystems contributes to the difficulty in preventing the occurrence of massive phytoplankton blooms (Dai et al., 2019). For instance, the results reported by Jiang et al. (2015) suggested that the phytoplankton community in different areas of Lake Erie shows different sensitivities to nitrogen and phosphorus concentrations. In fact, blooms are likely to occur in response to a combination of climatic and hydrographic events, and the nonlinearity of ecological dynamics results in unpredictable algal blooms (Anderson et al., 2002; Bruno et al., 1989; McGowan et al., 2017). Actually, the growth responses of plankton are inevitably affected by random fluctuations (Freund et al., 2006), which result in the stochastic scale and timing of blooms. For example, blooms may occur in bays or estuaries covering thousands of square kilometers, and last for a few weeks to years (Anderson, 1997).

The appearance of algal blooms is often considered one of the key signals of eutrophication (Huppert et al., 2002), indicating the balance between the processes of algae production and consumption is broken (Cloern, 2001). Growing evidence supports that the phytoplankton blooms are generally followed by a sudden termination within a few days (Abada et al., 2021; Aberle et al., 2007), demonstrating that mortality rates are higher during the decline phase compared to the development phase of blooms (Garcés et al., 2005), and the underlying cause remains a mystery. In recent years, the sudden collapse of phytoplankton blooms has drawn increasing attention

among research scientists. Abada et al. (2021) reported that the secretion of NO by algae and the dramatic decrease in dissolved oxygen levels contributes to higher phytoplankton mortality and further promote the collapse of the entire algal population. Specifically, Børsheim et al. (2005) demonstrated that phytoplankton mortality varies between 8 to 18% of present biomass per day in the development phase and reaches 45% in the bloom phase, followed by a collapse of the bloom, indicating that phytoplankton mortality is an important factor regulating bloom termination.

Phytoplankton mortality has been measured in several experimental studies. The mortality of natural single *Alexandrium* spp. cells during the development, maintenance, and decline phases of blooms was studied by Garcés et al. (2005), using a dilution experiment. Their results indicated that the mortality rates of *Alexandrium taylori*, one of the single *Alexandrium* spp., ranged from 0.2 to 0.65 d^{-1}, with the highest mortality rates during the decline phase. This may be attributed to the fast-growing algae causing a dramatic decrease in dissolved oxygen levels due to the metabolism of algae (Cloern, 2001). Additionally, decreased light penetration in the bottom of the water also results in a decrease in oxygen production (Møhlenberg, 1999). Furthermore, the rapid decomposition of dead algae leads to the depletion of dissolved oxygen and creates a hypoxic or anoxic 'dead zone' lacking sufficient oxygen to support aquatic organisms (Anderson, 1997; Chislock et al., 2013). Zooplankton mortality varies substantially in the decline phase of bloom events after the massive death of algae (Lin et al., 2014). Boyd et al. (1975) measured the average density of Anabaena variabilis filaments and the concentration of dissolved oxygen before and after the phytoplankton die-off. Their findings showed that the average density of Anabaena variabilis filaments increased from 2440 cells ml^{-1} to 3600 cells ml^{-1} in the development phase, with the peaks reaching 37300 cells ml^{-1}, and then suddenly decreased to less than 1000 cells ml^{-1} in the following days, while the concentration of dissolved oxygen dramatically decreased from 9 mg/L to 0.15 mg/L.

The sharp increase in plankton mortality during the decline phase can be described by the so-called colored noise, specifically the telegraph noise that can be represented by a finite-state Markov chain switching between two or more environmental regimes (Du et al., 2004; Liu and Wang, 2010). Usually, the switching among different environments is memoryless, and the waiting time for the next switch follows an exponential distribution (Li et al., 2009; Luo and Mao, 2007; Zou and Wang, 2014). Over the last few decades, a number of stochastic models have been used to explore the dynamics of phytoplankton growth. Additionally, stochastic noise has been proven to suppress or express exponential growth in population dynamics (Deng et al., 2008; Mao et al., 2002). In addition to white noise, aquatic ecosystems are greatly affected by colored noise. For example, the growth environment in winter is much different from that in summer, resulting in seasonal changes in the diversity of phytoplankton. In fact, the changes between different regimes can be described by the Markov chain and their effects on population dynamics have been extensively explored. Yu et al. (2019a) studied a nutrient–plankton food chain model with regime switching, and found that the Markov chain is beneficial for the survival of plankton. The study by Chen et al. (2020) demonstrated that the Markov chain could balance the density of the population under different regimes. Although considerable efforts have been devoted to understanding the factors regulating the development of phytoplankton blooms, the dynamical behaviors induced by regime-switching plankton mortality remain largely unexplored.

In the study of plankton dynamics, constant phytoplankton mortality is commonly used. However, constant phytoplankton mortality cannot explain the sudden decline of phytoplankton blooms. Considering the variability in the mortality of phytoplankton as observed in previous experimental studies, it is unrealistic to represent phytoplankton mortality with a constant. In this chapter, regime-switching plankton mortality is described using a continuous time Markov chain with different states, and a stochastic nutrient–plankton model is developed to investigate the

effects of regime-switching plankton mortality on the phytoplankton growth dynamics. The present chapter applies colored noise to describe the changes in the mortality of plankton over different phases of blooms. The objectives of the present work are to provide insight into phytoplankton responses to stochastic environment under regime switching by using a nutrient-phytoplankton zooplankton model.

The rest of the chapter is organized as follows. The mathematical model is presented in the next chapter. In Chapter 6.3, the dynamical behaviors of the proposed model are investigated. Some numerical simulations are performed in Chapter 6.4 to explore the model's dynamics and complexity in the aquatic system. Sensitivity analyses are also presented to help us identify the crucial parameters causing/terminating the planktonic bloom. In Chapter 6.5, a discussion about the implications of the results obtained in this study is presented. Lastly, some conclusions are provided in Chapter 6.6.

6.2. The mathematical model

In recent years, nutrient-phytoplankton-zooplankton type food web models have been widely employed in aquatic ecosystem studies, with the basic assumption that phytoplankton absorbs nutrients and is grazed upon by herbivorous zooplankton (Jang et al., 2006; Mitra, 2009). In aquatic ecosystems, a number of factors such as light and temperature are responsible for the growth of phytoplankton. To avoid model complexity, this research does not consider the effects of light and temperature on phytoplankton growth and assumes that the growth of phytoplankton fully depends on the availability of nutrients. Meanwhile, all other environmental factors (e.g., light, temperature, etc.) are assumed to be sufficiently abundant. The model is developed by modifying the aquatic planktonic ecosystem model presented by Ruan (2001), which has been widely implemented. The model is composed of nutrients, phytoplankton, and zooplankton. The nutrient concentration

consists of nutrient input, nutrient washout, and its uptake by phytoplankton. Furthermore, the process of nutrient regeneration due to bacterial decomposition of the dead biomass of plankton is involved, which has been widely reported (Guo et al., 2020; Ruan, 1993; Zhuang et al., 2021). The phytoplankton biomass is determined by two factors: the growth caused by the conversion of nutrients, and the loss caused by predation and natural death. In addition, the predation is described by the Beddington-DeAngelis functional response (Beddington, 1975; DeAngelis et al., 1975). The zooplankton biomass is determined by the growth caused by the conversion of phytoplankton and the loss caused by natural death.

At any time $t > 0$, $N(t)$, $P(t)$, and $Z(t)$ represent the nutrient concentration, phytoplankton density, and zooplankton density, respectively. The model is formulated based on the following assumptions.

(1) Phytoplankton growth depends on nutrient concentration and zooplankton predation.

(2) The nutrient uptake by phytoplankton follows a logistic law, and predation is described by the Beddington-DeAngelis form (Beddington, 1975; DeAngelis et al., 1975), $\frac{\beta PZ}{(1+mZ+nP)}$, where β represents the consumption rate, and m and n denote the mutual interference between zooplankton and the phytoplankton saturation constant, respectively.

(3) Following Ruan (1993), the constant nutrient input and washout rates to the lake ecosystem are denoted by S_0 and D, respectively. Let α stand for the maximal nutrient uptake by the phytoplankton.

(4) Both phytoplankton and zooplankton die naturally in the aquatic ecosystem at constant rates c and b, respectively.

(5) The dead biomass of phytoplankton/zooplankton is termed as detritus by ecologists worldwide. Indeed, the dead biomass of phytoplankton and zooplankton is first converted into detritus. Then, they are decomposed by micro-organisms and at the end of the process, nutrients

are regenerated. To avoid any model complexity, this research does not consider an explicit dynamic of detritus in the nutrient-plankton model (Thakur et al., 2021).

(6) The nutrients are partially recycled from the dead biomass of plankton by bacterial decomposition. For simplicity, the time required to regenerate nutrients is neglected, and nutrient recycling is considered an instantaneous term. The nutrient recycling rates from the dead biomass of phytoplankton and zooplankton are denoted by h and δ, respectively.

(7) Aquatic ecosystems are inevitably affected by random perturbations coming from the environment. In this research, environmental variables can act as noise sources because of their random fluctuations, resulting in a stochastic dynamic to the plankton model (Denaro et al., 2013; Valenti et al., 2016). Following previous studies (Luo and Mao, 2007; Zhao, 2016; Zou and Wang, 2014), white noise is considered to represent the random fluctuations in the natural world.

Based on the above assumptions, a model schematic diagram is shown in Figure 6.1. In the figure, the dashed lines reflect the fact that the dead biomass of phytoplankton and zooplankton does not directly convert into nutrients. Instead, they are first converted into an intermediate substance, detritus, and then into nutrient concentration. The following stochastic nutrient–plankton model is developed:

$$\begin{cases} dN(t) = \left[D\left(S_0 - N(t)\right) - \alpha P(t)N(t) + hP(t) + \delta Z(t)\right]dt + \sigma_1 N(t)dB_1(t), \\ dP(t) = \left[\alpha P(t)N(t) - cP(t) - \frac{\beta P(t)Z(t)}{1+mZ(t)+nP(t)}\right]dt + \sigma_2 P(t)dB_2(t), \\ dZ(t) = \left[\frac{\beta P(t)Z(t)}{1+mZ(t)+nP(t)} - bZ(t)\right]dt + \sigma_3 Z(t)dB_3(t), \end{cases} \tag{6.1}$$

where $B_i(t)$ are the independent standard Brownian motions and σ_i^2 are the intensities of the white noise for $i = 1, 2, 3$. In addition, model (6.1) shares the common biological meaning with other phytoplankton growth models. The biological meanings of variables and parameters involved in the model (6.1) are listed in Table 6.1.

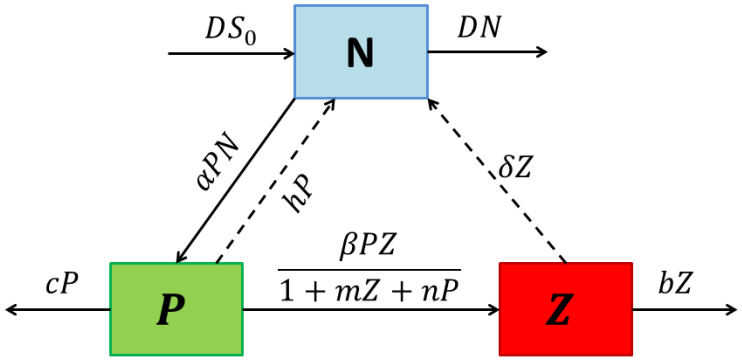

Figure 6.1. Schematic diagram representing the dynamics of the considered nutrient–phytoplankton–zooplankton model. In the figure, the black dashed lines represent the re-mineralization of the dead biomasses of phytoplankton and zooplankton into the nutrient concentration.

The constant plankton mortality is widely accepted in most aquatic ecosystem models. However, in natural aquatic ecosystems, the peak of phytoplankton biomass is generally followed by a sudden decline within a few days, and then it moves to the next bloom cycle. More importantly, several empirical evidences support the fact that plankton mortality varies in different phases of algal blooms. For example, Choi et al. (2017) measured the loss of biomass of *Alexandrium fundyense* in the bloom and decline phases. The results showed that the peak concentrations of *Alexandrium fundyense* reached 1×10^6 cells L^{-1} in the bloom phase and then dramatically decreased in the decline phase, eventually dropped to less than 1000 cells L^{-1}. Furthermore, Boyd et al. (1975) measured the average density of *Anabaena variabilis* filaments and the concentration of dissolved oxygen in different phases of a bloom. The experimental evidence showed that the average density of *Anabaena variabilis* filaments increased from 3600 cells ml^{-1} to 37300 cells ml^{-1} in the bloom phase and then sharply decreased to less than 1000 cells ml^{-1} in the decline phase of the bloom, while the concentration of dissolved oxygen dramatically decreased from 9 mg/L to 0.15 mg/L, resulting in the massive death of aerobic organisms.

Obviously, plankton mortality shows significant differences between the bloom and decline

phases of bloom events. Thus, shifting plankton mortality can be described as a random switching between two or more environmental regimes (Du et al., 2004; Liu and Wang, 2010). Considering the experimental evidence (Børsheim et al., 2005; Boyd et al., 1975), regime-switching plankton mortality is described as a continuous time Markov chain with different states, and the mortality of phytoplankton and zooplankton is denoted as $(c(1), c(2))$ and $(b(1), b(2))$, respectively. Therefore, the presented model, which accounts for both colored and white noise, is shown as follows:

$$\begin{cases} dN(t) = [D(r(t))\left(S_0(r(t)) - N(t)\right) - \alpha(r(t))P(t)N(t) + h(r(t))P(t) \\ \qquad\qquad +\delta(r(t))Z(t)]dt + \sigma_1(r(t))N(t)dB_1(t) \\ dP(t) = \left[\alpha(r(t))P(t)N(t) - c(r(t))P(t) - \frac{\beta(r(t))P(t)Z(t)}{1+m(r(t))Z(t)+n(r(t))P(t)}\right]dt \\ \qquad\qquad +\sigma_2(r(t))P(t)dB_2(t) \\ dZ(t) = \left[\frac{\beta(r(t))P(t)Z(t)}{1+m(r(t))Z(t)+n(r(t))P(t)} - b(r(t))Z(t)\right]dt \\ \qquad\qquad +\sigma_3(r(t))Z(t)dB_3(t) \end{cases} \tag{6.2}$$

where $r(t)$ represents a continuous time Markov chain with state space $\mathbb{S} = \{1, 2, \cdots, \mathbb{m}\}, 1 \leq \mathbb{m} < \infty$. Throughout this chapter, the process $B_i(t)$ and $r(t)$ are defined on a complete probability space $(\Omega, \mathfrak{F}, \{\mathfrak{F}_t\}_{t\geq 0}, \mathbb{P})$, and $r(t)$ is independent of $B_i(t), i = 1, 2, 3$. From a biological point of view, the initial value $(N(0), P(0), Z(0)) \in \mathbb{R}^3_+$, and all parameters are assumed to be positive. The model (6.2) shares the same biological meaning as the previous model (6.1).

$\mathbb{R}^n_+$ is denoted as the positive cone in $\mathbb{R}^n$. For a vector $f = (f(1),\ f(2),\ \cdots,\ f(\mathbb{m}))$, denote $\hat{f} = \min_{k\in\mathbb{S}}\{f(k)\}$, $\check{f} = \max_{k\in\mathbb{S}}\{f(k)\}$. Let $r(t)$ be a right-continuous Markov chain with state space $\mathbb{S} = \{1, 2, \cdots, \mathbb{m}\}, 1 \leq \mathbb{m} < \infty$, and $(q_{ij})_{\mathbb{m}\times\mathbb{m}}$ is the Q-matrix of $r(t)$ satisfying the following for a sufficiently small $\Delta t > 0$:

$$\mathbb{P}\{r(t+\Delta t) = j | r(t) = i\} = \begin{cases} q_{ij}\Delta t + o(\Delta t), & if\ \ i \neq j, \\ 1 + q_{ii}\Delta t + o(\Delta t), & if\ \ i = j, \end{cases}$$

where q_{ij} is the transition rate from state i to state j, $i, j \in \mathbb{S}$, $q_{ij} \geq 0$ if $i \neq j$, and $q_{ii} = -\sum_{i \neq j} q_{ij}$. In addition, the Markov chain $r(t)$ is assumed to be irreducible and independent of the Brownian motion $B_l(t)$ $(l = 1, 2, 3)$. Hence, the Markov chain $r(t)$ is ergodic and has a unique stationary distribution $\pi = (\pi_1, \pi_2, \cdots, \pi_{\mathbb{m}})$, which is the solution of the following equation:

$$\pi\, Q = 0, \sum_{i \in \mathbb{S}} \pi_i = 1 \text{ and } \pi_i > 0, \forall i \in \mathbb{S}.$$

By now, a nutrient-plankton model has been developed to investigate the effects of regime-switching plankton mortality on phytoplankton growth dynamics.

6.3. The main results

In view of Gray et al. (2011), for any given initial value $(N(0),\ P(0),\ Z(0),\ r(0)) \in \mathbb{R}_+^3 \times \mathbb{S}$, the stochastic model (6.2) has a unique positive solution $(N(t),\ P(t),\ Z(t),\ r(t))$ for all $t \geq 0$. Furthermore, according to Lemma 2.3 in Zhao (2016), the following relations hold almost surely:

$$\lim_{t \to +\infty} \sup[N(t) + P(t) + Z(t)] < \infty\,, \lim_{t \to +\infty} \frac{1}{t} \int_0^t \sigma_1\big(r(s)\big) N(s) dB_1(s) = 0\,, \tag{6.3}$$

$$\lim_{t \to +\infty} \frac{1}{t} \int_0^t \sigma_2\big(r(s)\big) P(s) dB_2(s) = 0\,,\ \lim_{t \to +\infty} \frac{1}{t} \int_0^t \sigma_3\big(r(s)\big) Z(s) dB_3(s) = 0\,. \tag{6.4}$$

6.3.1 Stochastically ultimately boundness

Regarding the stochastically ultimate boundedness of the solution of model (6.2), the following theorem is presented.

Theorem 6.1. For any initial value $(N(0), P(0), Z(0)) \in \mathbb{R}_+^3$, there exist $\chi > 0$ and $\varepsilon \in (0, 1)$ such that

$$\lim_{t \to +\infty} \sup \mathbb{P}\left\{|(\mathrm{N(t)}, \mathrm{P(t)}, \mathrm{Z(t)})| = \sqrt{\mathrm{N^2(t) + P^2(t) + Z^2(t)}} > \chi\right\} < \varepsilon.$$

Thus, the solution of model (6.2) is stochastic ultimately bounded.

The proof is given in Appendix M. Theorem 6.1 shows that the solutions of model (6.2) is

stochastically ultimately bounded.

6.3.2 Stochastic permanence

Denote $h = \max\{\check{D}, \check{c} - \hat{h}, \check{b} - \hat{\delta}\}$. For the stochastic permanence of the model (6.2), the following result is obtained.

Lemma 6.1. *If κ is a positive constant such that*

$$0 < \frac{\kappa+1}{2} max\ \{\check{\sigma}_1^2, \check{\sigma}_2^2, \check{\sigma}_3^2\} < \hat{D}\hat{S}_0 - h,$$

then the solution of model (6.2) has the following property:

$$\lim_{t\to+\infty} \sup \mathbb{E}\,|X(t)|^{-\kappa} \leq \Pi,$$

where

$$\Pi = \frac{3^\kappa(4\rho F_1 + F_2^2)}{4\rho F_1} \max\left\{1, \left(\frac{2F_1 + F_2 + \sqrt{F_2^2 + 4F_1\rho}}{2F_1}\right)^{\kappa-2}\right\}.$$

$$F_1 = \kappa\left[\hat{D}\hat{S}_0 - h - \frac{\kappa+1}{2}\max\{\check{\sigma}_1^2, \check{\sigma}_2^2, \check{\sigma}_3^2\}\right] - \rho > 0,$$

$$F_2 = \kappa[h + \max\{\check{\sigma}_1^2, \check{\sigma}_2^2, \check{\sigma}_3^2\}] + 2\rho > 0.$$

The prove of Lemma 6.1 is given in Appendix N. Applying the Chebyshev's inequality, one can derive the following result from Theorem 6.1 and Lemma 6.1.

Theorem 6.2. if

$$\max\{\check{\sigma}_1^2, \check{\sigma}_2^2, \check{\sigma}_3^2\} < 2\big(\hat{D}\hat{S}_0 - h\big),$$

then the solution of model (6.2) is stochastically permanent.

The proof is given in Appendix O. Theorem 6.2 indicates that model (6.2) is stochastic permanent if the environment fluctuation is less than the threshold. The results from Theorem 6.2 imply that the stochastic permanence can be obtained by controlling noise intensity.

6.3.3 The persistence and extinction of plankton

In this subchapter, the extinction and persistence of plankton in the aquatic system is investigated. For the sake of convenience, the following notations for all $k \in \mathbb{S}$ are introduced:

$$\gamma(k) = \alpha(k) + [c(k) - h(k) - D(k)]v(k),$$

$$\eta(k) = \alpha(k) + [b(k) - \delta(k) - D(k)]v(k),$$

$$\mathfrak{R}_0^S = \sum_{k\in\mathbb{S}} \pi_k \left[v(k)D(k)S_0(k) - \left(c(k) + \frac{1}{2}\sigma_2^2(k) \right) \right],$$

$$\mathfrak{R}_1^S = -\sum_{k\in\mathbb{S}} \pi_k \left[b(k) + \frac{1}{2}\sigma_3^2(k) - \frac{\beta(k)}{n(k)} \right],$$

where $v(k)$ is the solution of Eq. (6.5). Furthermore, the following assumption is carried out.

Assumption 1. $q_{ij} > 0,\ i \neq j,\ i,j \in \mathbb{S}$.

To begin with, two lemmas are presented as follows.

Lemma 6.2. *The linear system*

$$D(K)v(k) - \sum_{l\in\mathbb{S}} q_{kl}\, v(l) - \alpha(k) = 0, k \in \mathbb{S}, \tag{6.5}$$

admits a unique solution $V \equiv (v(1),\ v(2),\ \cdots,\ v(\mathbb{m}))^T$.

The proof is given in Appendix P. Then, the following lemma is given by using two auxiliary results in Appendix E.

Lemma 6.3. *For model (6.2), if* $\lim_{t\to+\infty} P(t) = 0$ *a.s., then* $\lim_{t\to+\infty} Z(t) = 0$ *a.s.*

The proof is given in Appendix Q. From the above auxiliary results, one can derive the following theorem regarding the persistence and extinction of plankton:

Theorem 6.3. If $min_{k\in\mathbb{S}}\{c(k) - h(k) - D(k)\} \geq 0$ and $min_{k\in\mathbb{S}}\{b(k) - \delta(k) - D(k)\} \geq 0$, then the solution $(N(t),\ P(t),\ Z(t),\ r(t))$ of model (6.2) has the following properties:

(i) If $\mathfrak{R}_0^S < 0$, then

$$\lim_{t\to+\infty} P(t) = 0 \text{ and } \lim_{t\to+\infty} Z(t) = 0 \text{ a.s,}$$

Both phytoplankton and zooplankton are extinct from the aquatic system.

(ii) If $\mathfrak{R}_0^S > 0$ and $\mathfrak{R}_1^S < 0$, then

$$\frac{\mathfrak{R}_0^S}{\check{\gamma}} \leq \lim_{t\to\infty} \inf \frac{1}{t}\int_0^t P(s)ds \leq \lim_{t\to+\infty} \sup \frac{1}{t}\int_0^t P(s)ds \leq \frac{\mathfrak{R}_0^S}{\hat{\gamma}} \textit{ and } \lim_{t\to+\infty} Z(t) = 0 \textit{ a.s.,}$$

Phytoplankton is persistent in mean and zooplankton is extinct from the aquatic system.

The proof is given in Appendix R. Theorem 6.3 indicates that the extinction and persistence in mean of plankton depend on $\mathfrak{R}_0^S$ and $\mathfrak{R}_1^S$. For $\mathfrak{R}_0^S < 0$, both phytoplankton and zooplankton are extinct for sufficiently large time. Meanwhile, when $\mathfrak{R}_0^S < 0$ and $\mathfrak{R}_1^S > 0$, the phytoplankton is persistent in mean and zooplankton is extinct from the aquatic system.

6.3.4 Ergodicity of model (6.2)

In this subchapter, the sufficient conditions for the existence and uniqueness of the stationary distribution of model (6.2) is derived. Following Yu et al. (2019a) and Zhu and Yin (2007), one can get the following theorem.

Theorem 6.4. Under Assumption 1, if for given initial condition $(N(0), P(0), Z(0), r(0)) \in \mathbb{R}_+^3 \times \mathbb{S}$, $min_{k\in\mathbb{S}}\{c(k) - h(k) - D(k)\} > \frac{1}{2}max\{(\hat{\sigma}_1)^2, (\hat{\sigma}_2)^2, (\hat{\sigma}_3)^2\}$ and $\mathfrak{R}_2^S > 0$, then the stochastic process $(N(t), P(t), Z(t), r(t))$ defined by the solution of model (6.2) is ergodic and has a unique stationary distribution in $\mathbb{R}_+^3 \times \mathbb{S}$.

The proof is given in Appendix S. Theorem 6.4 provides the sufficient conditions for the existence of ergodic stationary distribution. It shows that if the intensities of the white noise are within the threshold and $\mathfrak{R}_2^S > 0$, the stochastic process $(N(t), P(t), Z(t), r(t))$ is ergodic and admits a unique stationary distribution. Next, the explicit lower bound for phytoplankton is studied. The following assumption from Eq. (6.4) is carried out.

Assumption 2. For arbitrary $0 < \iota < 1$, there exist a set $\Omega_\iota \subset \Omega$ with $\mathbb{P}(\Omega_\iota) \geq 1 - \iota$ and a constant $\mathcal{F} = \mathcal{F}(\iota)$ such that for $\omega \in \Omega_\iota$ and $t > \mathcal{F}$

$$\lim_{t\to\infty} sup \frac{1}{t}\int_0^t \hat{\beta}P(s)ds - \lim_{t\to\infty}\frac{1}{t}\int_0^t \left[b\big(r(s)\big) + \frac{1}{2}\sigma_3^2(r(s))\right] ds \leq \iota.$$

Now, one can obtain the following theorem.

Theorem 6.5. Let Assumptions 1 and 2 hold. If

$$min\{\widehat{D}, \hat{c} - \check{h}, \hat{b} - \check{\delta}\} > \frac{1}{2} max\{(\hat{\sigma}_1)^2, (\hat{\sigma}_2)^2, (\hat{\sigma}_3)^2\},$$

then for model (6.2) whenever $\mathfrak{R}_2^S > \check{\beta}\hat{\beta}/\widehat{m}$ there exists a constant ς such that

$$\lim_{t\to\infty} inf \frac{1}{t}\int_0^t P(s)\, ds \geq \varsigma > 0 \text{ and } \lim_{t\to\infty} inf \frac{1}{t}\int_0^t Z(s)\, ds \geq \mathfrak{R}_2^S - \frac{\check{\beta}\hat{\beta}}{\widehat{m}} > 0 \text{ a.s.},$$

Thus, both phytoplankton and zooplankton are persistent in mean.

The proof is given in Appendix T. Biologically, Theorem 6.5 tells that if the environmental noise is within the threshold and $\mathfrak{R}_2^S > \check{\beta}\hat{\beta}/\widehat{m}$, then both phytoplankton and zooplankton can survive forever.

6.4. Numerical simulation

In this chapter, some numerical results are presented to further investigate how regime-switching plankton mortality affects the distribution of plankton biomass in the aquatic system. Unless otherwise mentioned, the parameter values used for numerical results are the same as those listed in Table 6.1. Let the transition rate from state 1 to state 2 be the same as the transition rate from state 2 to state 1, that is, $Q = (-1/2, 1/2; 1/2, -1/2)$. The nutrient input S_0, consumption rate β, phytoplankton mortality c, and zooplankton mortality b are the main control parameters.

6.4.1. Sensitivity analysis

In comparison with simply varying the parameters to observe the outcome of the model, the techniques of sensitivity analysis are mathematically more sophisticated. Thus, a basic differential

Table 6.1. Biological explanations of variables and parameters in model (6.1), and numerical values used for simulation results

Parameter	Description	Unit	Value	Source
N	Nutrient concentration	$\mu g/L$		
P	Phytoplankton biomass	$\mu g/L$		
Z	Zooplankton biomass	$\mu g/L$		
α	Maximal nutrient uptake rate by phytoplankton	$L/\mu g/day$	0.8	0.6[(a)]
h	Nutrient recycle rate from the dead biomass of phytoplankton	day^{-1}	0.08	0.08[(b)]
δ	Nutrient recycle rate from the dead biomass of zooplankton	day^{-1}	0.01	0.01[(f)]
c	Death rate for phytoplankton	day^{-1}	[0.4,0.7]	[0.2,0.65][(c)]
b	Death rate for zooplankton	day^{-1}	[0.4,0.7]	[0.08,0.6][(d)]
β	Consumption rate of phytoplankton by zooplankton	day^{-1}	0.2/0.5	0.5[(e)]
n	Phytoplankton saturation constant	$\mu g/L$	0.5	Assumed
m	Mutual interference between the zooplankton	$\mu g/L$	0.2	Assumed
D	Washout rate for nutrient	day^{-1}	0.25	0.2/0.3[(f)]
S_0	Input concentration of nutrient	$\mu g/L$	[0,12]	[0,12.5][(b)]

(a) Jang and Baglama (2005); (b) Ruan (2001); (c) Garcés et al. (2005); (d) Turner et al. (2014); (e) Jang and Allen (2015); (f) Yu et al. (2019a).

analysis approach is adopted to determine the semi-relative and logarithmic sensitivity solutions of model (6.1) for the plankton populations in the absence of environmental noise (Bortz and Nelson, 2004, Misra et al., 2016). The semi-relative sensitivity of the model solutions for a variable X to a parameter y is given by $y\frac{\partial X(t,y)}{\partial y}$ and is computed by formally differentiating model (6.1) with respect to y and interchanging the order of time and parameter derivative. Since model (6.1) has 3 state variables, one can obtain a system of 3 equations for the sensitivity functions $X_y(t,y) = \frac{\partial X}{\partial y}(t,y)$

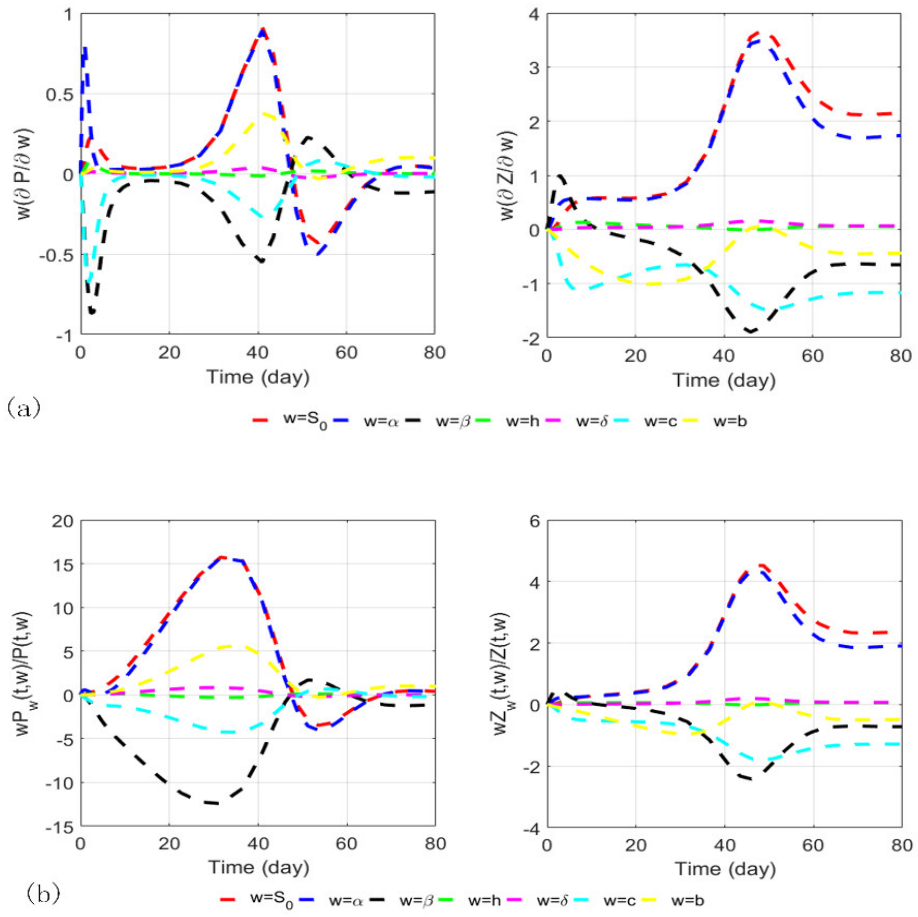

Figure 6.2. (a) Semi-relative sensitivity and (b) logarithmic sensitivity solutions of the model (6.2) in the absence of environmental noise with respect to S_0, α, β, h, δ, c and b. Parameters are at the same values as in Table 6.1 except S_0=1.2, β=0.5, c=0.4 and b=0.04.

$$\frac{d}{dt}\left(\frac{\partial X(t)}{\partial y}\right) = \frac{\partial f}{\partial X}\frac{\partial X(t)}{\partial y} + \frac{\partial f}{\partial y}, \tag{6.6}$$

with initial conditions $\partial X(0)/\partial y = 0$, where $\partial f/\partial x$ represents the Jacobian of model (6.1) without environmental noise and $\partial f/\partial y$ is the derivative of the right side of model (6.1) (represented by $f(t, X, y)$) with respect to y. To obtain the sensitivity functions, first, model (6.6) is solved for $X_y(t, y)$ by coupling it with the original model (6.1) without environmental noise (total 3+3 equations). The values of the sensitivity functions provide the rates of change of the variables with respect to the change in the chosen parameter (y) as time flows. For example,

$P_\beta(80, 0.5) = -0.112$ means that the derivative of P with respect to β at $t = 80$ days and $\beta = 0.5$ per day is $-0.112\ \mu g$ day/L. Finally, the semi-relative sensitivity solutions are calculated by multiplying the unmodified sensitivity functions with respect to the parameter y, i.e., $yX_y(t, y)$, which provides the amount the state will change when the parameter y is doubled (i.e., a perturbation on the order of y).

The sensitivities of plankton densities are plotted for the seven most sensitive relevant parameters (S_0, α, β, h, δ, c and b) in Figure 6.2. Among these parameters, only S_0 can be influenced by human activities. From the graph, it is clear that the perturbations of the parameters exhibit their greatest influences early in the simulation, with a large initial expected variation in the plankton densities. It is clear that the doubling of S_0 and α can yield a sudden increase in plankton densities around $t = 43$ days. There is a huge increase in the density of phytoplankton at 43 days, followed by a sudden huge decrease just a few days later. This decrease in the density of phytoplankton is due to the less availability of nutrients as they are taken up by the phytoplankton. On the other hand, on doubling the uptake rate of phytoplankton by zooplankton (β), the biomass of phytoplankton decreases whereas that of zooplankton increases in the initial phase of time. But as time flows, the biomass of zooplankton decreases and that of phytoplankton increases. Again, there is an increment in zooplankton and a decrement in phytoplankton biomass as time flows. Doubling the mortality rate of phytoplankton (c), the biomasses of both the plankton significantly changes in the aquatic system. The densities of phytoplankton increase while the zooplankton densities decrease significantly in the initial stage on doubling the mortality rate of the latter. The plankton densities in the aquatic system are least sensitive to the re-mineralization of dead biomasses of phytoplankton and zooplankton. However, different parameters have different strengths of influences, S_0 has the greatest influence on phytoplankton as well as zooplankton densities. It is worth noting that these outcomes greatly depend on the parameterization of the model.

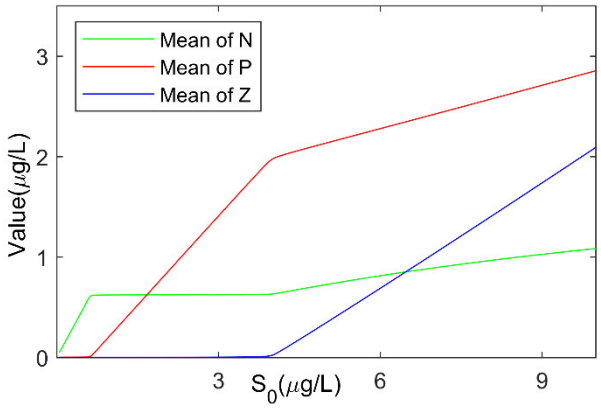

Figure 6.3. For model (6.2) without noise and regime switching, the mean values of the solutions with respect to nutrient input.

Next, the logarithmic sensitivity solutions

$$\left(\frac{\partial \log(X)}{\partial \log(y)}(t) = \frac{y}{X(t,y)} X_y(t,y)\right)$$

with respect to all of the previously mentioned parameters are presented in Figure 6.2(b). These quantities are dimensionless and indicate what percentage change in the variables can be expected from a doubling of a parameter y. Thus, to get a complete idea about the sensitivity of the solutions to a particular parameter, it is best to calculate both semi-relative and logarithmic sensitivity solutions. Figure 6.2(b) shows that doubling the parameters S_0, α, h, δ, and b results in a 34.62%, 34.62%, 1.42%, 1.42% and 98.01% increment in the density of phytoplankton, respectively at the end of 80 days. On the other hand, the density of phytoplankton reduces by 112.7% and 19.22% on doubling the parameters β and c, respectively at 80 days. Similarly, the figure displays that at the end of 80 days, the zooplankton density reduces by 71.46%, 128.1% and 48.06% on doubling the parameters β, c, and b, respectively. Furthermore, it is apparent from the figure that the zooplankton density boosts up by 235.7%, 190.4%, 7.275% and 7.275% at the end of 80 days on doubling the values of model parameters S_0, α, h, and δ. In addition, the mean value of the solution of the deterministic model is presented by choosing constant plankton mortality rate and fixing

$\beta = c = b = 0.5$, with respect to nutrient input in Figure 6.3. Obviously, the mean of plankton biomass increases with an increase in the nutrient input level. As the nutrient input exceeds a threshold value, the plankton populations can coexist in the aquatic system.

6.4.2. Effects of regime shifting plankton mortality

Figure 6.4 shows three different types of the model (model (6.1), model (6.2) without noise, and model (6.2)) for their sensitivity to changes in the nutrient input, since the concentration of available nutrient is one of the decisive factors controlling phytoplankton productivity (Häder and Gao, 2015). Instead of increasing and decreasing parameter values by a defined percentage, the entire range of possible nutrient input values is determined by previous studies. The other parameter values used for the model analysis are the same as those in Table 6.1. The sensitivity analysis involves changing the nutrient input to observe its effects on the biomass of plankton populations. The analysis shows that the persistence and extinction of plankton populations can be divided into three stages (see Figure 6.4). When the nutrient input is low (below the white dashed line), both phytoplankton and zooplankton populations eventually die out. With an increase in the nutrient input, the phytoplankton population persists, while the zooplankton population tends to go extinct (above the white dashed line and below the red dashed line). Once the nutrient input exceeds the critical value (above the red dashed line), both phytoplankton and zooplankton populations can coexist indefinitely. Moreover, it is worthy to note that nutrient input enhances the amplitude of oscillation because higher plankton biomass is achieved with increased nutrient input. The results from Figure 6.4 imply that the persistence and extinction of plankton populations are sensitive to variations in nutrient inputs.

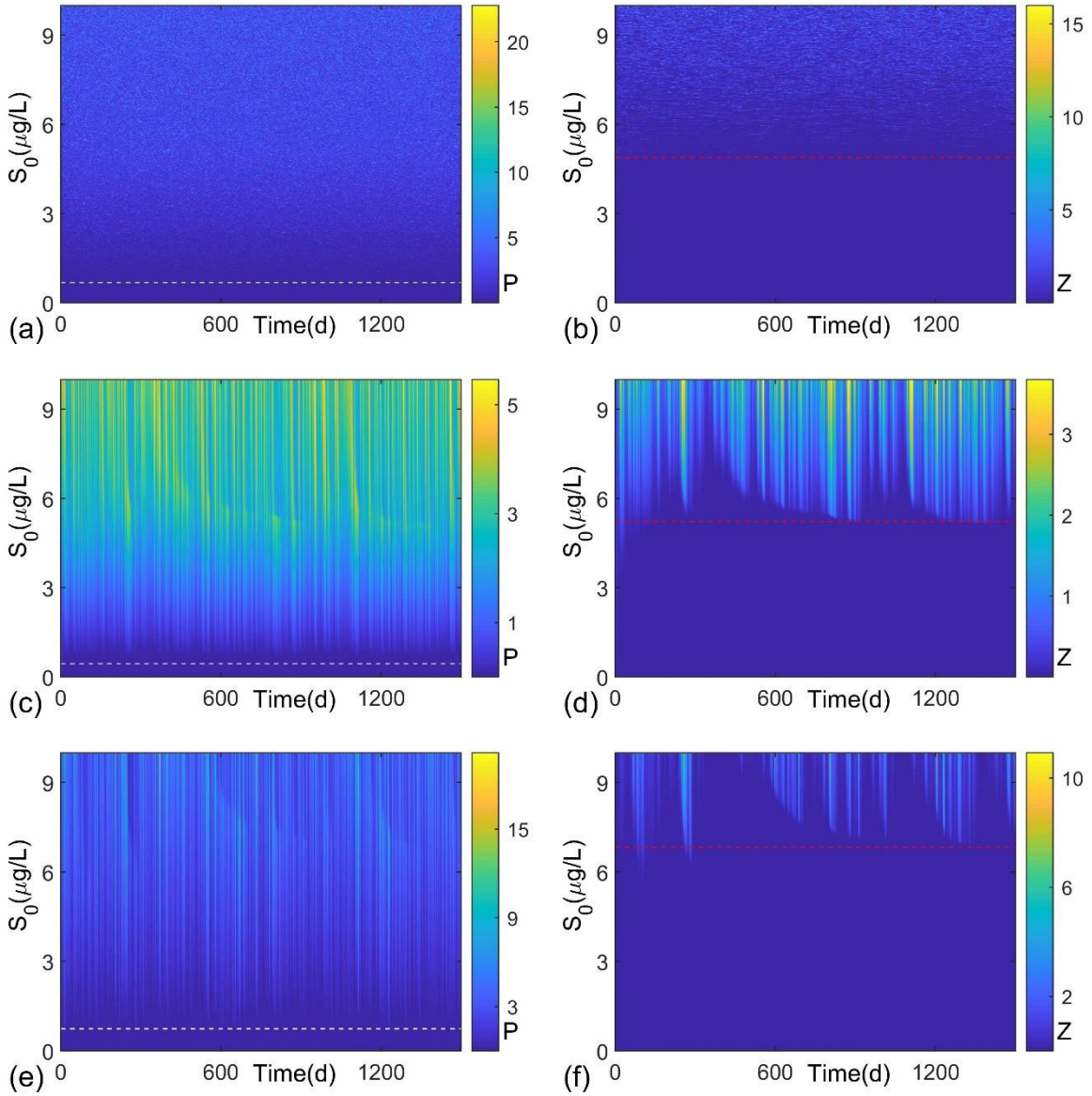

Figure 6.4. The solutions of model (6.1) in the (S_0, t) plane for (a) P and (b) Z; the solutions of model (6.2) without environmental noise in the (S_0, t) plane for (c) P and (d) Z; the solutions of model (6.2) in the (S_0, t) plane for (e) P and (f) Z. The white and the red dashed line respectively represent the critical value of $\mathfrak{R}_0^S = 0$ and $\mathfrak{R}_2^S = \check{\beta}\hat{\beta}/\widehat{m}$.

Additionally, Figure 6.4 presents another important result. When white noise is applied to the deterministic model, Figures 6.4(a) and 6.4(b) show that the plankton density always oscillates instead of maintaining a constant level. Furthermore, the shifting plankton mortality is described by the right continuous Markov chain $r(t)$ on state space $\mathbb{S} = \{1, 2\}$, and the low mortality of plankton is set at 0.4 d^{-1} while the high mortality of plankton is set at 0.7 d^{-1}. Figures 6.4(c) and

6.4(d) display the solutions of model (6.2) without noise, and the results indicate that the plankton biomass oscillates within a smaller range but shows obvious switching between different states. Clearly, the switching phenomenon is induced by shifting plankton mortality. In addition, Figures 6.4(e) and 6.4(f) show the effect of regime-switching plankton mortality on the distribution of plankton biomass in a stochastic environment. It is evident from Figures 6.4(e) and 6.4(f) that the oscillation range of plankton biomass becomes larger, and the switching between different states also becomes more pronounced. Apparently, the regime-switching plankton mortality significantly affects the planktonic ecosystem in a stochastic environment.

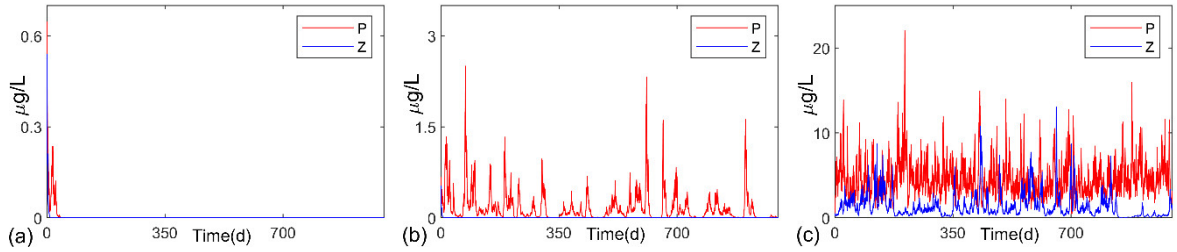

Figure 6.5. The paths of phytoplankton and zooplankton in the model (6.2) for (a) $\beta = S_0 = 0.5$, (b) $\beta = 0.2, S_0 = 1$ and (c) $\beta = 0.5, S_0 = 12$.

In the study of stochastic population dynamics, persistence and extinction are important topics. From Theorem 3.3, it is obvious that the extinction and persistence in mean of plankton depend on $\mathfrak{R}_0^S$ and $\mathfrak{R}_1^S$. For $\beta = S_0 = 0.5$, one can get $\mathfrak{R}_0^S = -0.195 < 0$, which means that both phytoplankton and zooplankton become extinct according to Theorem 6.3(i) (see Figure 6.5(a)). Next, by fixing $\beta = 0.2, S_0 = 1$, one can find that $\mathfrak{R}_0^S = 0.2050 > 0, \mathfrak{R}_1^S = -0.195 < 0$, which indicates that phytoplankton is persistent in mean while zooplankton becomes extinct according to Theorem 6.3(ii) (see Figure 6.5(b)). The results from Figures 6.5(a) and 6.5(b) reveal that a higher nutrient input and less consumption of phytoplankton by zooplankton contribute to the survival of the phytoplankton population in the aquatic system. Similarly, by selecting $\beta = 0.5, S_0 = 12$, one can get $\mathfrak{R}_2^S = 3.32202 > \hat{\beta}\check{\beta}/\widehat{m} = 1.25 > 0$. According to Theorems 6.4 and 6.5, the model (6.2)

is persistent in mean and exhibits a unique stationary distribution, i.e., the plankton species can survive forever (see Figure 6.5(c)).

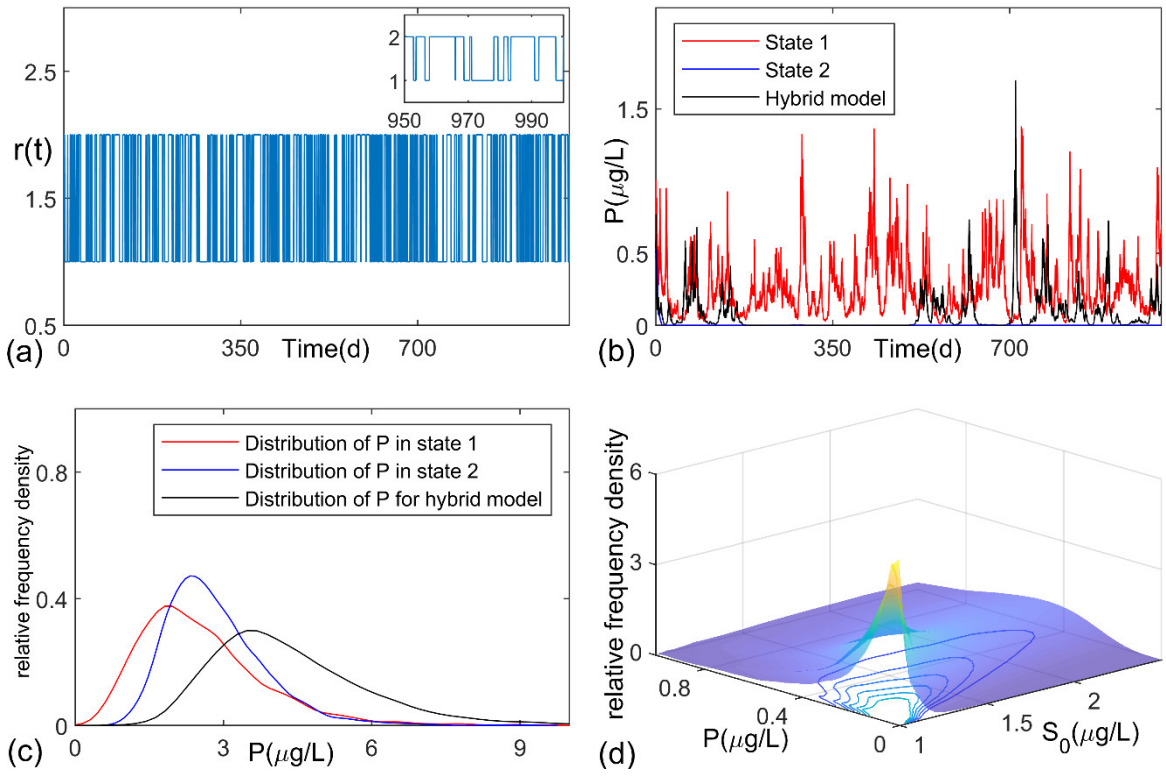

Figure 6.6. For model (6.2) with $\beta = 0.5$, (a) the Markov chain with respect to $S_0 = 8$; (b) the sample path of phytoplankton; (c) the distribution of phytoplankton population with respect to state 1, state 2 and hybrid system, respectively; (d) the distribution of phytoplankton population at $t = 1000$ with respect to nutrient input S_0.

In order to investigate the distributions of phytoplankton biomass in different states, Figure 6.6(a) illustrates the path of the Markov chain by choosing $S_0 = 8$, $\beta = 0.5$ in model (6.2). Additionally, Figure 6.6(b) displays the sample paths for the phytoplankton population in state 1, state 2, and the hybrid model, respectively. It is apparent that the phytoplankton population becomes extinct in state 1 but persists in state 2 as well as in the hybrid model. Moreover, the distributions of phytoplankton biomass in state 1, state 2, and the hybrid model demonstrate that the Markov chain has the potential to enhance the oscillation cycles of the plankton (see Figure

6.6(c)). Figure 6.6(d) displays the distribution of phytoplankton biomass with respect to the nutrient input S_0, which indicates that an increasing nutrient input leads to a significant increase in the variance of phytoplankton biomass.

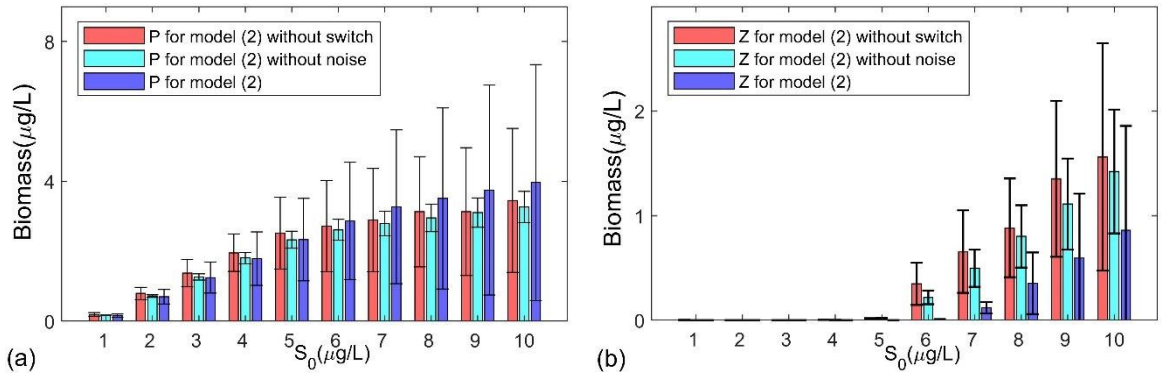

Figure 6.7. (a) The mean and the variance for phytoplankton biomass with respect to nutrient input S_0; (b) The mean and the variance for zooplankton biomass with respect to nutrient input S_0.

Figure 6.7 shows the mean and variance of plankton biomass under three conditions for $S_0 = 1, 2, \dots, 10$. The results imply that both the variance and the mean of plankton biomass show an overall increasing trend as nutrient inputs increase. When the plankton community suffers from nutrient deficiency, the mean and variance of phytoplankton biomass are lower for shifting plankton mortality than for constant plankton mortality. However, the variance of phytoplankton biomass in model (6.2) shows a comparatively large increasing trend. In contrast, the zooplankton tends to become extinct when the nutrient input is low. Moreover, with an increase in the nutrient input, the variances of plankton biomass with shifting plankton mortality show a faster increasing trend. Obviously, regime-switching plankton mortality significantly increases the ranges of distribution and oscillation intensity of phytoplankton biomass, suggesting that such plankton mortality is beneficial for the survival of phytoplankton under high nutrient levels.

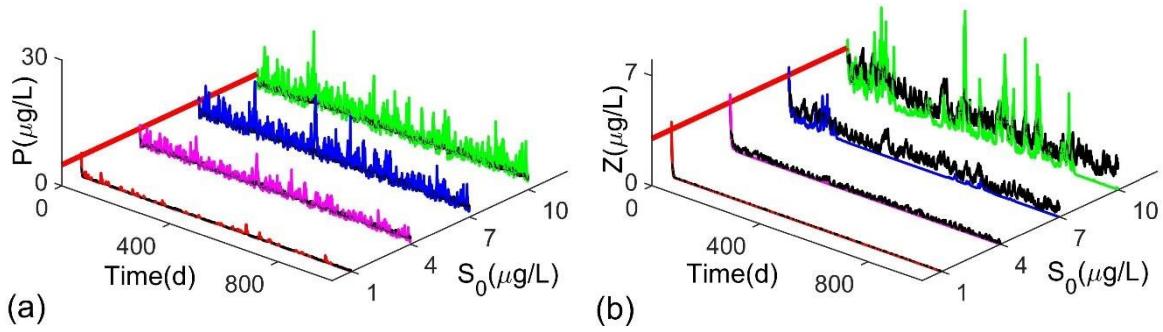

Figure 6.8. For model (6.2), the sample paths of (a) phytoplankton and (b) zooplankton for $S_0 = 1, 4, 7$ and 10, respectively. The black line represents the solutions for determined model.

Numerous research studies support the fact that the growth rate of phytoplankton may not be able to maintain a high level of plankton in the aquatic system due to zooplankton grazing and intraspecific competition among the plankton for available resources such as light and nutrients (Sommer, 1991; Sommer, 2012). The results from Figure 6.7 imply that when the nutrient input exceeds a critical level, zooplankton appear in the aquatic system, and the mean and variance of phytoplankton biomass show relatively slower increasing trends, while the mean of zooplankton biomass has a larger increasing trend. A possible explanation behind this behavior of plankton might be the predation by zooplankton and the intraspecific competition of phytoplankton for resources. Finally, the sample paths of model (6.2) for plankton are shown in Figure 6.8, revealing that an increasing input of nutrients leads to a marked increase in the amplitude of planktonic oscillations.

6.5. Discussion

The sudden changes in plankton mortality have been observed in several experimental studies. Thus, considering the impact of shifting plankton mortality on the population growth of planktonic algae is crucial. In this study, a nutrient-plankton model considering shifting plankton mortality is developed. The theoretical results imply that when the minimum plankton mortality is beyond a

threshold value, the extinction and persistence in the mean of plankton depend on $\mathfrak{R}_0^S$ and $\mathfrak{R}_1^S$. It is observed that model (6.2) possesses an ergodic stationary distribution, indicating that the plankton populations can survive forever. Moving beyond the theoretical analysis, several numerical simulations have been carried out to explore plankton dynamics. The sensitivity results indicate that the biomasses of plankton in the aquatic system are highly sensitive to the input rates of nutrients, the grazing rate of phytoplankton by zooplankton, and the mortality rates of planktons. These results emphasize the need to focus on controlling the input rate of nutrients coming into the lakes from outside during the bloom phase.

Furthermore, three different types of the models (model (6.1), model (6.2) without noise, and model (6.2)) for their sensitivity to changes in the nutrient input is shown in Figure 6.4. It has been well documented that nutrient availability is directly related to phytoplankton growth (Häder and Gao, 2015; Elliott et al., 2006), and the distribution of phytoplankton biomass is sensitive to nutrient input (Elliott et al., 2006). Figure 6.4 clearly shows that when the nutrient input is less than a certain level, both phytoplankton and zooplankton populations tend to go extinct. If the nutrient input is between the white and red dashed lines, the phytoplankton population is persistent, and the zooplankton population disappears from the aquatic system. As the nutrient input exceeds the red dashed line, both phytoplankton and zooplankton populations can coexist forever. Figure 6.4 suggests that nutrient input plays an important role in determining the survival of plankton; the persistence and extinction of plankton populations are sensitive to variations in nutrient input. These findings are consistent with the results reported by Elliott et al. (2006).

Additionally, Figure 6.4 shows a comparison of the plankton biomass in three different models. The differences in the dynamics of the models are governed by nutrient input. The results from Sherratt and Smith (2008) support the idea that population density always exhibits oscillatory behavior due to the existence of noise and other factors. As shown in Figures 6.4(a) and 6.4(b), the

plankton population density always oscillates instead of maintaining a certain level owing to the presence of environmental noise, which is consistent with the findings of Sherratt and Smith (2008). By contrast, for the model (6.2) without noise (see Figures 6.4(c) and 6.4(d)), the oscillation intensity of plankton biomass remains lower than that in Figures 6.4(a) and 6.4(b) due to the lack of environmental noise. However, the distribution of plankton biomass switches between different states, which is not observed in Figures 6.4(a) and 6.4(b). One possible explanation is that the increasing plankton mortality leads to a sudden collapse of plankton populations. Figures 6.4(e) and 6.4(f) show that the switching becomes more pronounced due to the coupling between noise and shifting plankton mortality, and the oscillation intensity of plankton biomass is significantly stronger than in Figures 6.4(c) and 6.4(d). These results further indicate that noise can enhance the oscillation of plankton biomass, and the high plankton mortality in the decline phase results in a dramatic collapse in the phytoplankton population, which agrees with the experimental results mentioned in Børsheim et al. (2005), Boyd et al. (1975), and Choi et al. (2017).

In the study of stochastic population dynamics, the persistence and extinction of interacting populations are the most important topics (de la Hoz and Vadillo, 2012; Liu and Wang, 2010). From the biological points of view, the stochastic persistence means that the population will survive forever. Figure 6.5 displays the persistence and extinction of the plankton populations in model (6.2). Apparently, the plankton populations can survive forever under certain conditions (see Figure 6.5(c)). Besides the stochastic persistence of the model, the numerical analysis has shown how shifting plankton mortality affects the survival of the phytoplankton population in the aquatic habitat (see Figure 6.6). Figure 6.6(b) depicts that the phytoplankton population goes extinct in state 1 but is persistent in state 2 when the nutrient input is low; the phytoplankton population in the hybrid model is persistent. It is inferred from Figure 6.6(b) that under the influence of the Markov chain, although the phytoplankton population tends to go extinct in one

state, it still has a chance to persist. Under high nutrient input, regime-switching plankton mortality can enhance the oscillation intensity of phytoplankton density, which means the model with regime-switching plankton mortality is more beneficial for the survival of plankton populations compared to the case when plankton mortality is constant (see Figure 6.6(c)). When compared with regime-switching plankton mortality, nutrients have been proven to be an important factor influencing the growth of phytoplankton in the aquatic system. The distribution of phytoplankton biomass with respect to nutrient input suggests that increasing nutrient levels enhance the biomass of phytoplankton in the model (see Figure 6.6(d)). The capability of nutrient loading to stimulate the growth of phytoplankton is well demonstrated in Ramin et al. (2012).

Indeed, extensive research has established that total phytoplankton biomass may ultimately respond to changes in nutrient availability (Carpenter et al., 2016; Salmaso, 2010), and that external nutrient loading is a significant factor positively related to the total phytoplankton biomass (Ramin et al., 2012). The simulation results reveal that nutrient input shows a positive control on the mean as well as variance of phytoplankton biomass (see Figure 6.7). Additionally, nutrient input can significantly increase zooplankton biomass as the increased phytoplankton biomass due to nutrient input provides sufficient food for grazing zooplankton. However, the growth rate of phytoplankton shows a decreasing trend after the nutrient input exceeds a threshold value. It is well documented that phytoplankton abundance moderately increases rather than being maintained at a high level, following nutrient enrichment in the aquatic system (Ramin et al., 2012). Moreover, Figure 6.7 shows that the plankton biomass in model (6.2) has the highest mean and variance values in contrast to model (6.1) and the model (6.2) without noise. This suggests that shifting plankton mortality is more beneficial for the survival of plankton populations in the aquatic system compared to when plankton experiences constant mortality. This might be due to the sudden collapse of the algal population, which creates a suitable environment for plankton to grow and

provides chances for their survival.

6.6. Conclusions

A stochastic nutrient-plankton model incorporating regime-switching plankton mortality was implemented in this chapter. Several theoretical and numerical analyses were presented aiming to understand how shifting plankton mortality affects phytoplankton growth dynamics. Analytically, the threshold value for the survival of plankton species was derived, and the theoretical analysis provided conditions under which the model was persistent or one of the plankton populations went extinct. Furthermore, the results showed that model (6.2) admitted an ergodic stationary distribution. In addition, the numerical results revealed that the coupling between noise and regime-switching plankton mortality was not only capable of enhancing the oscillatory behavior of plankton populations, but also decreasing the amplitude of the plankton oscillations in the bloom phase. The simulation results indicated that nutrient loading in the aquatic system was an important factor in controlling phytoplankton biomass, while regime-switching plankton mortality provided a higher survival chance for plankton populations. It is worth noting that the importance of the proposed model lies not in the precision with which it predicts specific events within a particular lake/ocean, but in its contribution to the studies on how regime-switching plankton mortality influences phytoplankton growth in lakes and oceans. Additionally, the results obtained in this study may provide a reasonable explanation for the observed sharp collapse of a phytoplankton bloom in experiments. Furthermore, it is worth noting that considering the explicit role of detritus, the dead biomasses of phytoplankton and zooplankton, in model (6.2) will mimic a more realistic situation in the nutrient-plankton model.

Chapter 7

DYNAMICS OF A STOCHASTIC NUTRIENT-PLANKTON MODEL WITH IMPULSIVE CONTROL STRATEGY[5]

Abstract

In this paper, an impulsive nutrient-plankton model in a stochastic environment is investigated. The model dynamics have been studied by using theoretical and numerical approaches. The results show the existence of a global positive solution, indicating that the population size will remain non-negative for a sufficiently large time. By employing a Lyapunov function, sufficient conditions for the existence of a positive T-periodic solution are derived. The numerical results indicate that the coupling between environmental stochasticity and impulsive control plays an important role in regulating the interplay between nutrients concentration and plankton densities in aquatic ecosystems. Overall, the results obtained in this study may provide insight into how plankton dynamics respond to impulsive perturbations under environmental fluctuations.

Keywords: Nutrient-plankton model, Stochastic periodic solutions, Impulsive control, Environmental fluctuation

[5]Guo, Q., Liu, H., Wang, Y., Li, J., Zhao, M., Tiwari, P.K., Jin, Z., Dai, C.J., 2023. Dynamics of a stochastic nutrient-plankton model with impulsive control strategy. European Physical Journal Plus. 138, 470. DOI: 10.1140/epjp/s13360-023-04111-0.

7.1. Introduction

Investigating the dynamics of phytoplankton in aquatic systems has become an essential topic of research among scientists around the globe. Although phytoplankton is a vital component of the aquatic ecosystem (Song et al., 2020a), the excessive growth of phytoplankton can cause decay and death of many aquatic plants. The decomposition of dead algae may lead to a consumption of dissolved oxygen by the bacterial pool, resulting in massive mortality events in fish populations (Boyd et al., 1975; Leng, 2009; Mishra et al., 2022). Moreover, certain species of phytoplankton produce toxins, thereby killing the marine life and also affecting the health of people through the food web (Hallegraeff, 2010). Significant research attention has been devoted to investigating the controlling factors responsible for the rise or decline of phytoplankton populations in aquatic systems (Dai et al., 2016; Huisman et al., 1999; Tiwari et al., 2019). It has been well documented that high nutrient load is one of the major triggers for algal blooms (e.g., cyanobacteria) (Downing et al., 2001; McCarthy et al., 2009). Experimental studies have demonstrated that both nutrients and zooplankton can significantly affect the phytoplankton community (Vanni, 1987). However, the actual mechanism by which phytoplankton form blooms is far more complex than expected. Thus, understanding the factors that contribute to algal blooms has attracted considerable scientific attention in recent years (Anderson et al., 2012; Li et al., 2020).

Several studies have supported the fact that algal blooms are consequences of the interplay of various hydrodynamical, chemical processes, and biological processes in aquatic systems (Chen and Mynett, 2006). However, the mechanisms regulating plankton dynamics and diversity are still not well understood by researchers (Dai et al., 2019; Guo et al., 2020). Moreover, the nonlinearity and complexity of aquatic ecosystems make it challenging to gain insight into plankton dynamics solely depended on experiments or field observations. Thus, mathematical models of ecological population dynamics have been developed in the study of plankton dynamics as it not only captures

the ubiquitous stoichiometric constraints for the growth and interactions of species (Alijani et al., 2015), but also provide quantitative insights into population growth dynamics (Dai et al., 2016). Following the pioneering works of Volterra (1926) and Lotka (1925), numerous plankton models have been developed by introducing various types of functional responses into classical predator-prey models, with the aim of understanding the triggering mechanisms of phytoplankton blooms in aquatic ecosystems (Chakraborty et al., 2015; Liu et al., 2023; Ruan and He, 1998; Yu et al., 2019a).

Although a number of studies have focused on the dynamic interactions of prey and predator populations in constant environments (Das et al., 2022; Paul et al., 2021; Nie et al., 2011), real ecological communities are inherently random, and biological phenomena in real ecosystems are inevitably affected by environmental fluctuations (May, 2019; Guo et al., 2023), such as white noise. White noise is characterized by many small, independent random fluctuations, such as rainfall, wind, or day-to-night variations. Despite the existence of environmental fluctuations in aquatic ecosystems, algal blooms are highly correlated with complex interactions of climatic factors and hydrographic processes (McGowan et al., 2017), which can cause stochastic scaling and timing of algal blooms (Chen et al., 2014). Moreover, stochastic population models have attracted a great deal of attention as they can capture evolutionary trend of populations in a randomly varying environment (Dobramysl et al., 2018; Meerson and Sasorov, 2008; Zhou et al., 2022). In Mao et al., (2002) and Deng et al., (2008), the authors concluded that stochastic noise has the potential to suppress or boost the exponential growth of populations in ecological systems.

In addition to environmental fluctuations, natural aquatic ecosystems are inevitably subject to pulse perturbations (Stelzer et al., 2022), which result in an abrupt change in nutrient concentrations and the abundances of phytoplankton populations. For instance, heavy rainfalls trigger nutrient input through river discharge, resulting in algal blooms in coastal areas (Han et al.,

2023). In Tang et al. (2020), the authors reported that sediment resuspension caused by wind-induced wave shear stress and the stochastic nature of turbulence may also contribute to the release of internal nutrients, thereby maintaining a significant potential for obstinate eutrophication and algal blooms. The findings of Cui et al. (2016) demonstrated that wind can mix floating phytoplankton cells away from the water surface when the wind speed exceeds a critical value. These phenomena can instantaneously change the status of the system and are commonly described as pulsed instantaneous behavior, which cannot be considered continuous (Li et al., 2019). Impulsive differential equations can accurately capture the instantaneous state of a system, and have been widely used to describe such instantaneous perturbations in the plankton system. The effects of impulsive perturbations have gained considerable interest among mathematicians as well as ecologists in recent years (Liu and Rohlf, 1998; Zhao et al., 2017b). Authors such as Li et al. (2019), Guo et al. (2015), and Yang and Zhao (2012) have concluded that impulsive perturbations may alter the dynamical behavior of an ecosystem; however, some proper impulsive perturbations can maintain the rhythm of the ecosystem.

The synergistic effects of stochasticity and impulsive perturbations on the interacting dynamics of predator-prey systems in ecological communities have received considerable attention among research scientists (Liu et al., 2018; Liu and Liu, 2019; Yu et al., 2019b). A stochastic non-autonomous Lotka–Volterra predator–prey model with impulsive effects was analyzed in Zhang et al. (2017a). The results indicate that both stochastic noises and impulsive perturbations play crucial roles in the persistence as well as the extinction of species. Zuo and Jiang (2016) investigated the dynamics of a stochastic non-autonomous Holling-Tanner predator-prey model involving impulsive effects and reported that the model can experience the extinction of predator populations due to the presence of environmental fluctuations (impulses). Despite numerous advancements in understanding plankton dynamics, the responses of plankton populations to

impulsive perturbation under environmental fluctuation have not been established yet.

In view of the importance of impulsive control and environmental fluctuation, this chapter aims to develop a stochastic model for the nutrient-plankton system with impulsive control in order to investigate and understand the effects of impulsive perturbation on plankton dynamics in a random environment. The remainder of this article is organized as follows: a stochastic nutrient-plankton model with impulsive control is constructed in the next chapter and all the main results are presented in Chapter 7.3. In Chapter 7.4, numerical simulations are conducted to test the sensitivity of the model parameters and comprehend the effects of environmental noise and impulsive control on plankton dynamics. Finally, a comprehensive discussion and conclusion on the dynamics of plankton populations is provided, and their responses to the environmental fluctuations and impulsive effects are shown at the end of the paper.

7.2. The mathematical model

Mathematical models have been widely implemented in the study of plankton dynamics over the decades as they allow for qualitative capture of the field observed instantaneous dynamics of ecosystems. Here, a nutrient-plankton model with the effects of impulsive control and stochastic fluctuation on the phytoplankton growth dynamics is developed. Previously, mathematical models of food web types have been widely used to describe the dynamics of nutrient-phytoplankton-zooplankton interactions in aquatic habitats (Mukhopadhyay and Bhattacharyya, 2006; Ruan, 2001; Thakur et al., 2021). For the model formulation, I consider an aquatic system and assume that the growth of the phytoplankton population fully depends on the availability of nutrients, with other environmental factors such as light, temperature, etc., being sufficiently abundant for their growth. Indeed, the proposed model is a modification of the plankton model proposed in Ruan (2001), where the authors considered nutrient, phytoplankton, and zooplankton as dynamic variables. It

should be noted that the nutrient concentration in the aquatic ecosystem includes nutrients washout and its uptake by phytoplankton. In addition, the phytoplankton biomass is determined by its growth through nutrient conversion, and loss due to predation by zooplankton species and natural death (Holling, 1959b). The zooplankton biomass is determined by its growth through phytoplankton consumption, and loss due to natural death and intraspecific competition due to the limitation of resources in the aquatic system.

At any instant of time $t > 0$, $N(t)$, $P(t)$, and $Z(t)$ denote the concentration of nutrients, phytoplankton population, and zooplankton population, respectively. The model is formulated based on the following ecological assumptions.

(1) There is washout of nutrients in the aquatic system at the rate D. The uptake of nutrients by phytoplankton follows the Holling type II functional response described by $\frac{mNP}{a+P}$, where a represents the half-saturation constant and m denotes the rate of consumption. I denote by n a constant that represents the conversion of nutrients into phytoplankton biomass.

(2) The phytoplankton population faces natural mortality at a constant rate c. The predation function of phytoplankton by zooplankton follows the Holling type II form Holling (1959b), which is by $\frac{\beta PZ}{a+P}$. Here, β represents the grazing rate of phytoplankton by zooplankton.

(3) I denote η as the biomass conversion rate of phytoplankton into zooplankton. The zooplankton population die naturally at a constant rate b, and also face intraspecific competition for the available food sources in the aquatic system. Let ρ be the strength of such competition among the zooplankton species.

(4) Considering the ubiquitous presence of stochastic fluctuations in the natural world (May, 1973), I employ white noise to represent random fluctuations in the aquatic ecosystem.

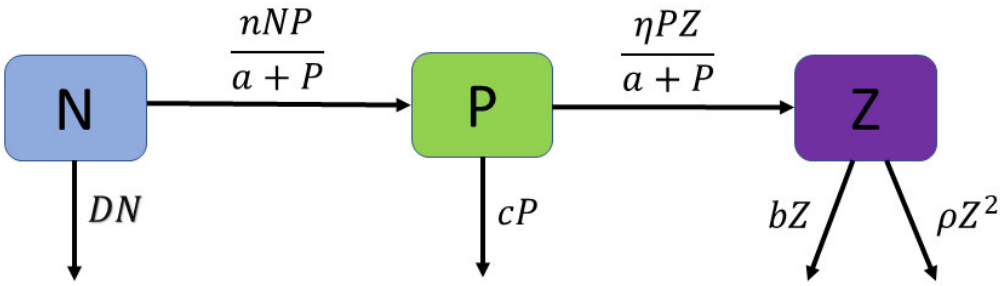

Figure 7.1. Schematic diagram depicting the interplay among nutrients, phytoplankton, and zooplankton in an aquatic ecosystem.

In view of the above assumptions, a schematic diagram is presented in Figure 7.1, and I come up with the following nutrient-plankton model with stochastic fluctuations (Luo and Mao, 2007; Zou and Wang, 2014):

$$\begin{cases} dN(t) = \left[-D(t)N(t) - \frac{m(t)P(t)N(t)}{a(t)+P(t)}\right]dt + \sigma_1(t)N(t)dB_1(t), \\ dP(t) = \left[\frac{n(t)P(t)N(t)}{a(t)+P(t)} - c(t)P(t) - \frac{\beta(t)P(t)Z(t)}{a(t)+P(t)}\right]dt + \sigma_2(t)P(t)dB_2(t), \\ dZ(t) = \left[\frac{\eta(t)P(t)Z(t)}{a(t)+P(t)} - b(t)Z(t) - \rho(t)Z(t)^2\right]dt + \sigma_3(t)Z(t)dB_3(t). \end{cases} \tag{7.1}$$

In model (7.1), $B_i(t)$ represents the independent standard Brownian motions and σ_i^2 stands for the intensities of the white noise for $i = 1, 2, 3$. Model (7.1) shares the common biological meaning with the usual phytoplankton growth models. All the parameters involved in model (7.1) are positive, bounded and continuous θ −periodic functions. The biological meanings of variables and parameters describing model (7.1) are provided in Table 7.1.

Moreover, natural aquatic ecosystems are inevitably affected by pulse perturbations (Stelzer et al., 2022). For instance, wind-induced wave motion can trigger internal nutrient release and vertical migration of phytoplankton populations (Tang et al., 2020; Cui et al., 2016), leading to an abrupt change in nutrient concentration and phytoplankton biomass in the aquatic ecosystem experiences. To encapsulate the impact of pulse perturbations, the stochastic model (7.1) is extended to the following form:

$$\begin{cases} dN(t) = \left[-D(t)N(t) - \frac{m(t)P(t)N(t)}{a(t)+P(t)}\right]dt + \sigma_1(t)N(t)dB_1(t), \\ dP(t) = \left[\frac{n(t)P(t)N(t)}{a(t)+P(t)} - c(t)P(t) - \frac{\beta(t)P(t)Z(t)}{a(t)+P(t)}\right]dt + \sigma_2(t)P(t)dB_2(t), \\ dZ(t) = \left[\frac{\eta(t)P(t)Z(t)}{a(t)+P(t)} - b(t)Z(t) - \rho(t)Z(t)^2\right]dt + \sigma_3(t)Z(t)dB_3(t). \end{cases} \Bigg\} t \neq t_k, k \in \mathbb{N}, \\ \begin{cases} N(t_k^+) = (1+\alpha_{1k})N(t_k), \\ P(t_k^+) = (1+\alpha_{2k})P(t_k), \\ Z(t_k^+) = Z(t_k), \end{cases} \Bigg\} t = t_k, k \in \mathbb{N}. \tag{7.2}$$

Note that model (7.2) shares a common biological meaning with model (7.1), and comprises a sequence of real numbers, $0 < t_1 < t_2 < \cdots < t_k < \cdots$, $\lim_{t\to\infty} t_k = +\infty$. For biological reasons, it is assumed that $1 + \alpha_{ik} > 0$ for $i = 1, 2$ and $k = 1, 2, \cdots$. For $\alpha_{ik} > 0$ $(i = 1, 2)$, the impulsive effects represent the process of species introductions. However, $\alpha_{ik} < 0$ $(i = 1, 2)$ denote the harvesting of species. In this research, only the former case is considered. Additionally, throughout this research, it is always assumed that there exists a positive integer p such that $t_{k+p} = t_k + T$, $\alpha_{i(k+p)} = \alpha_{ik}$, $i = 1, 2$, $k \in Z^+$, and $[0, T) \cap \{t_k, k \in Z^+\} = \{t_1, t_2, \cdots, t_p\}$.

7.3. The main results

For the proposed model, some analytical results are presented in this chapter. Throughout this chapter, $(\Omega, \mathcal{F}, \{\mathcal{F}_t\}_{t\geq 0}, \mathbf{P})$ is considered as a complete probability space with a filtration $\mathcal{F}_{t(t\geq 0)}$ satisfying the usual normal conditions (i.e., it is right continuous and $\mathcal{F}_0$ contains all **P**-null sets). To deduce the following results, some notations and auxiliary results are presented in Appendix U.

7.3.1 Existence and uniqueness of the global positive solution

In this subchapter, the existence and uniqueness of the global positive solution is investigated. At first, the following model without impulses is presented:

$$\begin{cases} dy_1(t) = y_1(t)\left[-D(t) + \frac{1}{T}\sum_{j=1}^{p}\log\left(1+\alpha_{1j}\right) - \frac{m(t)A_2(t)y_2(t)}{a(t)+A_2(t)y_2(t)}\right]dt \\ \qquad\qquad +\sigma_1(t)y_1(t)dB_1(t), \\ dy_2(t) = y_2(t)\left[\frac{n(t)A_1(t)y_1(t)}{a(t)+A_2(t)y_2(t)} + \frac{1}{T}\sum_{j=1}^{p}\log\left(1+\alpha_{2j}\right) - c(t) - \frac{\beta(t)y_3(t)}{a(t)+A_2(t)y_2(t)}\right]dt \\ \qquad\qquad +\sigma_2(t)y_2(t)dB_2(t), \\ dy_3(t) = y_3(t)\left[\frac{\eta(t)A_2(t)y_2(t)}{a(t)+A_2(t)y_2(t)} - b(t) - \rho(t)y_3(t)\right]dt + \sigma_3(t)y_3(t)dB_3(t), \end{cases} \quad (7.3)$$

with

$$A_1(t) = \left[\prod_{j=1}^{p}\left(1+\alpha_{1j}\right)\right]^{-\left(\frac{t}{T}\right)}\prod_{0\le t_k<t}(1+\alpha_{1k}),$$

$$A_2(t) = \left[\prod_{j=1}^{p}\left(1+\alpha_{2j}\right)\right]^{-\left(\frac{t}{T}\right)}\prod_{0\le t_k<t}(1+\alpha_{2k}).$$

where both $A_1(t)$ and $A_2(t)$ are periodic functions with period T (Zhang et al., 2017b). It is assumed that the product is equal to unity if the number of factors is zero. Next, the following lemma is presented.

Lemma 7.1. *Let* $N(t) = A_1(t)y_1(t)$, $P(t) = A_2(t)y_2(t)$, *and* $Z(t) = y3(t)$.

(i) If $(N(t), P(t), Z(t))$ *is a solution of model (7.2), then* $(y_1(t), y_2(t), y_3(t))$ *is a solution of model (7.3).*

(ii) If $(y_1(t), y_2(t), y_3(t))$ *is a solution of model (7.3), then* $(N(t), P(t), Z(t))$ *is a solution of model (7.2).*

The proof of above lemma follows Zhang and Tan (2015), and hence is omitted.

Next, the following theorem is presented and the proof is given in Appendix V.

Theorem 7.1. For any initial values $\left(N(0), P(0), Z(0)\right) \in R_+^3$, model (7.2) exhibits a unique positive solution $(N(t), P(t), Z(t))$ that is remain in R_+^3 with probability one.

The results from Theorem 7.1 indicate that the population size is remain nonnegative for sufficiently large time t.

7.3.2 Existence of positive *T*-periodic solution

In this subchapter, the existence and uniqueness of positive periodic solutions of model (7.2) is investigated.

Lemma 7.2. *(Yu et al., 2019a). For any initial values* $\left(y_1(0), y_2(0), y_3(0)\right) \in R_+^3$*, all the solutions* $(y_1(t),\ y_2(t),\ y_3(t))$ *of model (7.3) satisfy:*

$$\lim_{t\to\infty} sup\, y_1(t) < \infty,\ a.s.,\ \lim_{t\to\infty} sup\, y_2(t) < \infty,\ a.s., \lim_{t\to\infty} sup\, y_3(t) < \infty,\ a.s.$$

Thus, there exist positive constants M_1*,* M_2*, and* M_3 *such that*

$$y_1(t) \le M_1, y_2(t) \le M_2, y_3(t) \le M_3\ for\ all\ t \ge 0\ a.s.$$

Define

$$\phi_1 \triangleq \frac{1}{T}\sum_{j=1}^{p} \log\left(1+\alpha_{1j}\right) - \langle D(t) + \sigma_1^2(t)\rangle_T - \frac{m^u A_2^u}{A_2^l},$$

$$\phi_2 \triangleq \frac{1}{T}\sum_{j=1}^{p} \log\left(1+\alpha_{2j}\right) - \langle c(t) + \sigma_2^2(t)\rangle_T - \frac{\beta^u M_3}{a^l}.$$

Now, one can have the following theorem.

Theorem 7.2. If $\phi_1 > 0$ and ϕ_2>0, then model (7.2) possesses a positive T-periodic solution.

The proof of the above theorem is given in Appendix W. Biologically, Theorem 7.2 tells that if the environmental noise is small, $\phi_1 > 0$, and ϕ_2>0, then model (7.2) exhibits a positive T-periodic solution, indicating that the phytoplankton blooms exhibit more or less periodicity.

7.4. Numerical simulation

Although some theoretical analyses of model (7.2) were conducted in the previous chapter, obtaining detailed information on the combined actions of stochastic and impulse effects on plankton dynamics is challenging due to the model's complexity. Thus, this chapter presents some numerical analyses to further explore the combined actions of stochastic and impulsive effects on the biomass distributions of populations in the aquatic ecosystem. Unless otherwise mentioned in

Table 7.1. Biological explanations of parameters in model (7.1), and their numerical values used for simulation results

Parameter	Description	Unit	Value	Source
N	Nutrient concentration	$\mu g/L$		
P	Phytoplankton biomass	$\mu g/L$		
Z	Zooplankton biomass	$\mu g/L$		
m	Maximal nutrient uptake rate by phytoplankton	day^{-1}	0.5	[0.2,1][(a)]
n	Conversion rate of nutrient into the biomass of phytoplankton	day^{-1}	0.2	0.2[(b)]
η	Conversion rate of phytoplankton biomass into the biomass of zooplankton	day^{-1}	0.5	0.6[(b)]
c	Natural death rate of phytoplankton	day^{-1}	0.5	0.58[(f)]
b	Natural death rate of zooplankton	day^{-1}	0.03	0.03[(c)]
β	Consumption rate of phytoplankton by zooplankton	day^{-1}	0.01	0.021[(e)]
a	Phytoplankton saturation constant	$\mu g/L$	0.2	Assumed
ρ	Strength of competition among the zooplankton population	$L/\mu g/$day	0.3	Assumed
D	Washout rate for nutrient	day^{-1}	0.01	0.01[(d)]

(a) Alijani et al. (2015); (b) Kartal et al. (2016); (c) Gao et al. (2008); (d) Tiwari et al. (2019); (e) Das et al. (2018); (f) Gourley and Ruan (2003);

the text, the parameter values used for the numerical results are the same as in Table 7.1. The impulsive perturbation and noise intensity are chosen as control parameters. It is well documented that biological and environmental parameters are subject to fluctuation over time (Fan and Wang, 2000), and can induce more or less periodicity in population density, such as the seasonal blooms of *Microcystis* spp. in Lake Taihu, China (Otten and Paerl, 2011). Thus, we assume that all the parameters in model (7.2) are periodic and have a common period of 40 days. The parameter set in the periodic environment is chosen as follows:

$$D = 0.01 + 0.01\sin(\pi t/20),\ m = 0.5 + 0.01\sin(\pi t/20),\ n = 0.2 + 0.01\sin(\pi t/20),$$

$$\eta = 0.5 + 0.01\sin(\pi t/20),\ c = 0.5 + 0.01\sin(\pi t/20),\ b = 0.03 + 0.01\sin(\pi t/20),$$

$$\beta = 0.01 + 0.01\sin(\pi t/20),\ a = 0.2 + 0.01\sin(\pi t/20),\ \rho = 0.3 + 0.01\sin(\pi t/20).$$

7.4.1 Effects of impulsive control

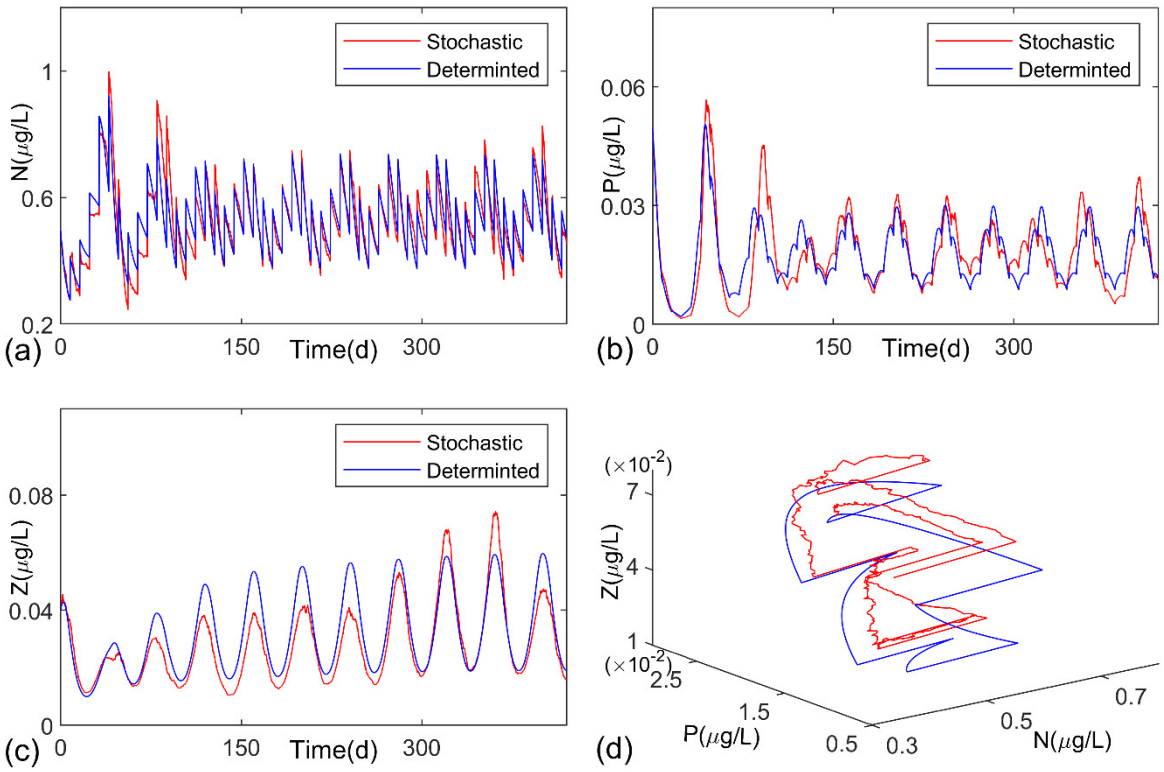

Figure 7.2. The evolution of a single path of solutions for model (7.2) and the corresponding impulsive model without random noise. The figures depict the paths of (a) nutrient, (b) phytoplankton, (c) zooplankton, and the (d) phase diagram.

According to Theorem 7.2, model (7.2) exhibits a positive T-periodic solution under certain conditions. The noise intensity is chosen as $\sigma_1 = \sigma_2 = \sigma_3 = 0.02 + 0.01\sin(\pi t/20)$, and the pulse intensity is set as $\alpha_1 = 0.5$, $\alpha_2 = 0.1$. The impulse frequency is selected as $p = 5$. Then, the evolution of a single path of solutions for model (7.2) is presented in Figure 7.2. It is apparent from the figure that the stochastic periodic solutions of model (7.2) fluctuate around the periodic solutions of its corresponding deterministic model, but the overall trend is periodicity. The results from Figure 7.2 indicate that the plankton density will exhibit periodicity, which is consistent with the periodic bloom events observed in real aquatic ecosystems (Otten and Paerl, 2011).

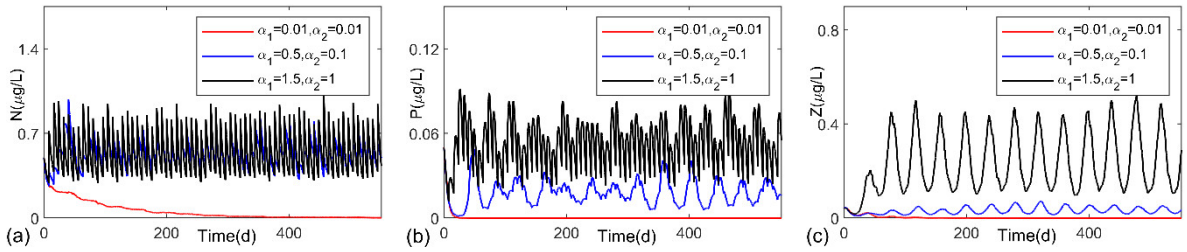

Figure 7.3. Under $\sigma_1 = \sigma_2 = \sigma_3 = 0.02 + 0.01\sin(\pi t/20)$, the evolution of a single path of (a) nutrient, (b) phytoplankton and (c) zooplankton in model (7.2) with respect to time for three different sets of pulse intensity.

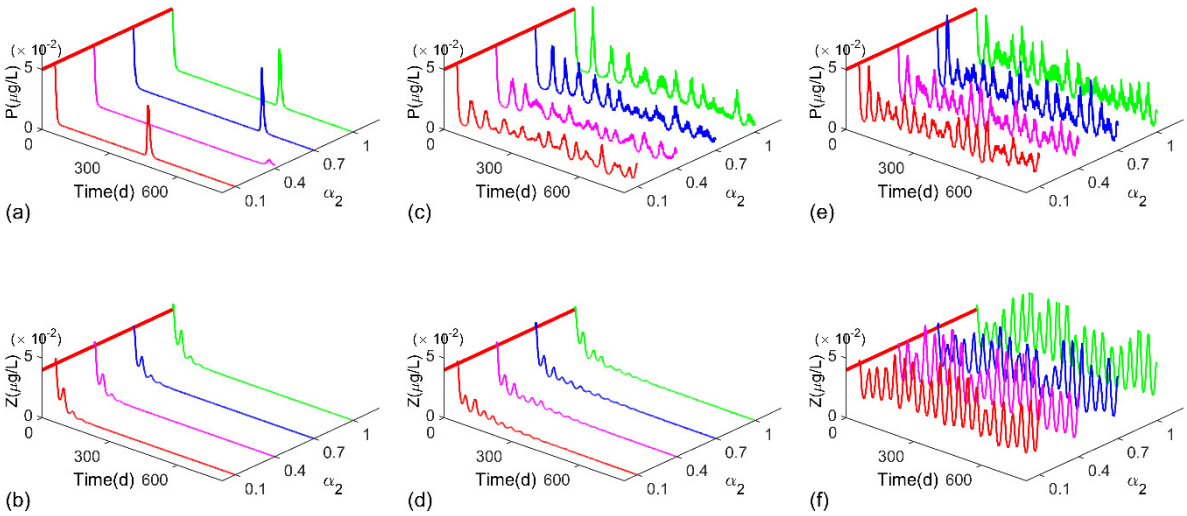

Figure 7.4. The evolutions of a single path of phytoplankton (first row) and zooplankton (second row) in model (7.2) with respect to time for $\alpha_2 = 0.1$, 0.4, 0.7, and 1. In this figure, $\sigma_1 = \sigma_2 = \sigma_3 = 0.02 + 0.01\sin(\pi t/20)$, and $\alpha_1 = 0.1$ (first column), $\alpha_1 = 0.3$ (second column) and $\alpha_1 = 0.5$ (third column).

Next, the numerical analysis presents the effect of impulsive control on the distributions of plankton populations. To do this, by fixing the noise intensity and the value of p, Figure 7.3 shows the evolution of a single path of nutrient concentration and plankton populations with respect to three different sets of pulse intensity. The figure shows that for a low pulse intensity, i.e., $\alpha_1 = \alpha_2 = 0.01$, the nutrient concentration becomes zero and the plankton populations tend to go extinct. It is evident from the figure that when the pulse intensity increases to $\alpha_1 = 0.5$ and $\alpha_2 = 0.1$, the nutrient concentration and the plankton populations remain in the aquatic system. However, when

increasing the pulse intensity to $\alpha_1 = 1.5$ and $\alpha_2 = 1$, the nutrient concentration and the plankton populations show stronger oscillatory behaviors. The results from Figure 7.3 suggest that the pulse intensity has the potential to alter plankton dynamics. For instance, heavy rainfall can lead to high nutrient input into the water bodies due to river discharge or massive erosion, subsequently, accelerating the growth of algae.

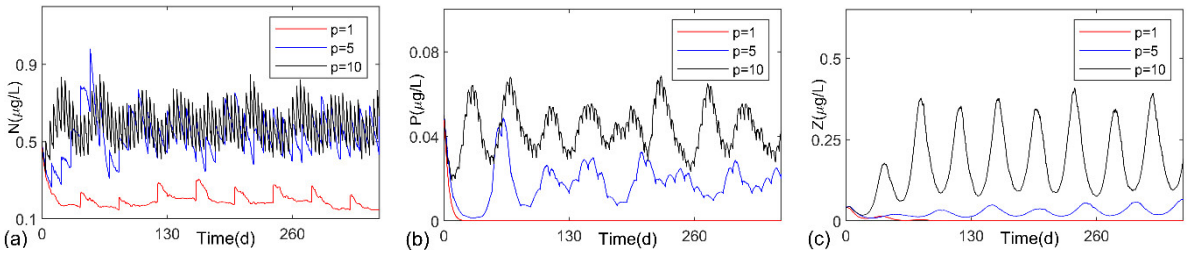

Figure 7.5. Under $\sigma_1 = \sigma_2 = \sigma_3 = 0.02 + 0.01\sin(\pi t/20)$, $\alpha_1 = 0.5$ and $\alpha_2 = 0.1$, the evolution of a single path of (a) nutrient, (b) phytoplankton and (c) zooplankton in model (7.2) with respect to time for three different values of p.

Furthermore, the impact of pulse intensity on the plankton population is illustrated in Figure 7.4. Figures 7.4(a) & 7.4(b) show that if the nutrient pulse is equal to 0.1, both phytoplankton and zooplankton populations disappear from the ecosystem, even if the pulse intensity of phytoplankton is high. One possible reason behind this behavior of the ecosystem is that a small nutrient pulse could not provide sufficient nutrients for the survival of the phytoplankton population. Consequently, the aquatic system faces a lack of food to meet the requirements of the zooplankton population, resulting in the extinction of both phytoplankton and zooplankton populations. Additionally, it is clear that when the nutrient pulse intensity reaches 0.3, the phytoplankton population becomes persistent, whereas the zooplankton population is doomed to go extinct despite the high pulse intensity of the phytoplankton population (see Figures 7.4(c) & 7.4(d)). This may happen in the aquatic system as the nutrient concentration and phytoplankton biomass are not enough to support the life of the zooplankton population. Furthermore, Figures

7.4(e) and 7.4(f) show that if the nutrient pulse intensity increases to 0.5, then both the phytoplankton and zooplankton populations persist in the ecosystem, irrespective of the small pulse intensity of the phytoplankton population. Thus, the results from Figure 7.4 indicate that the survival, as well as the coexistence of plankton populations, are strongly correlated with the nutrient pulse. Actually, in aquatic ecosystems, multiple external disturbances have been reported to have the potential to increase phytoplankton abundance in the water bodies. For example, wind-induced mixing may affect the migration of phytoplankton species, leading to an increment in the abundance of phytoplankton at a particular location.

Apart from pulse intensity, pulse frequency also plays a significant role in the survival of plankton populations (Liu et al., 2023). Figure 7.5 depicts the paths of nutrient concentration and plankton populations for different values of p. Obviously, when the pulse frequency is 1, i.e., $p = 1$, the nutrient concentration does not vanish while the plankton populations go extinct. However, as the pulse frequency increases to 5, the nutrient concentration and plankton populations persist in the ecosystem. However, on further increasing the pulse frequency, the nutrient concentration and plankton populations show stronger oscillatory behaviors. Biologically, a small nutrient pulse frequency may not be able to provide sufficient nutrients for the survival of the phytoplankton population, and the lack of phytoplankton reserves might not be sufficient to support the survival of the zooplankton population in the aquatic ecosystem.

7.4.2 Effects of stochastic fluctuation

In real aquatic ecosystems, environmental stochasticity plays an important role in influencing plankton dynamics (Yu et al., 2019a). Excessive noise intensity may threaten aquatic species, leading to undesirable and potentially irrevocable changes in ecosystem functioning. For example, a dramatic drop in temperature resulted in the complete disappearance of the *Cylindrospermopsis*

filaments (Borics et al., 2000). By fixing the pulse intensity as $\alpha_1 = 0.5$ and $\alpha_2 = 0.1$, Figure 7.6 shows the impact of environmental fluctuations on nutrient concentration and plankton populations for $p = 5$,. Apparently, when the noise intensity is too low, i.e., $\sigma_1 = \sigma_2 = \sigma_3 = 0.02 + 0.01\sin(\pi t/20)$, the plankton populations persist in the ecosystem. However, when the noise intensity increases to $\sigma_1 = \sigma_2 = \sigma_3 = 0.1 + 0.01\sin(\pi t/20)$, the nutrient concentration and plankton populations exhibit a stronger oscillatory behavior, indicating a comparatively higher chance of survival for the plankton populations. An interesting observation is that with an increase in noise intensity to $\sigma_1 = \sigma_2 = \sigma_3 = 0.5 + 0.01\sin(\pi t/20)$, the nutrient concentration becomes zero and the plankton populations tend to go extinct, whereas the deterministic model shows a periodic solution. This implies that excessive noise intensity may accelerate the extinction of plankton populations in the aquatic zone.

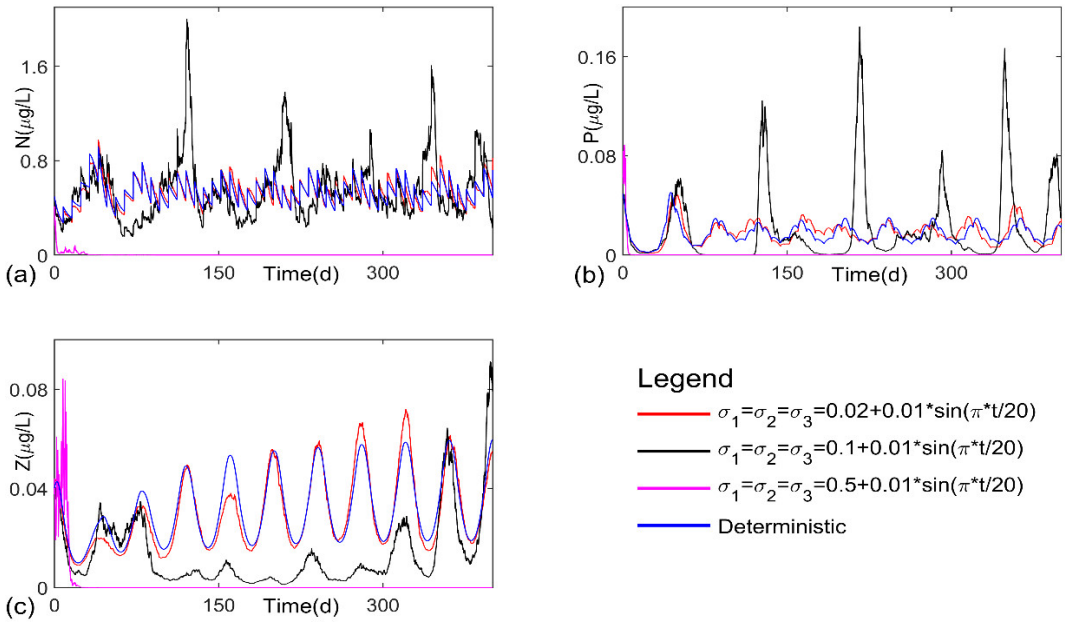

Figure 7.6. The evolution of a single path of (a) nutrient, (b) phytoplankton and (c) zooplankton in model (7.2) with respect to time for $\alpha_1 = 0.5$ and $\alpha_2 = 0.1$. In the figure, the red, blue and black lines respectively correspond to $\sigma_1 = \sigma_2 = \sigma_3 = 0.02 + 0.01\sin(\pi t/20)$, $\sigma_1 = \sigma_2 = \sigma_3 = 0.1 + 0.01\sin(\pi t/20)$ and $\sigma_1 = \sigma_2 = \sigma_3 = 0.5 + 0.01\sin(\pi t/20)$.

The results from Figure 7.6 indicate that increments in noise intensity up to a certain limit can enhance the amplitude of oscillations in plankton populations. However, if the noise intensity goes beyond a certain range, it may threaten the entire ecosystem. In natural aquatic ecosystems, considering the stochastic nature of turbulence, appropriate turbulent mixing can promote internal nutrient release through sediment resuspension, contributing to the growth of plankton species. However, strong turbulence can disrupt various elements of phytoplankton species' life cycles, such as the mitotic cycle and chromosome separation (Sengupta et al., 2017). Thus, controlling environmental fluctuations can be a key factor in mitigating planktonic blooms.

7.5. Conclusion and discussion

Here, the dynamics of a stochastic nutrient-plankton model with impulsive control were explored. Some theoretical and numerical analyses were presented to investigate how the plankton populations respond to the combined actions of pulse perturbation and environmental fluctuation. Analytically, the results indicated that model (7.2) exists a global positive solution, which suggests that the population size will remain non-negative for all future time. In addition, some sufficient conditions were obtained under which the model exhibits a positive T-periodic solution, implying that changes in plankton populations' density will exhibit more or less periodicity. The results from Theorem 7.2 indicated that both the pulse intensity and the noise intensity play important roles in the existence of positive T-periodic solution. Figure 7.2 showed that environmental noise can change the biomass of nutrient and plankton, and induce fluctuations around the solutions of the corresponding deterministic model. Figure 7.3 depicted that when the pulse intensity is small, the plankton populations tend to go extinct. This happens as the low pulse intensity leads to insufficient nutrient supply in the aquatic ecosystem. Furthermore, the results showed that increased pulse intensity was capable of increasing the oscillatory tendency in the plankton populations, which

indicates that the pulse intensity can increase the maximum plankton population size. Thus, it can be inferred that the pulse intensity can significantly affect the survival of plankton populations in the aquatic habitat.

In natural aquatic ecosystems, some disturbances, such as wind-induced mixing, can lead to an instantaneous increase in the biomass of phytoplankton. However, such phenomenon may not be the primary driver of bloom events. Figure 7.4 showed a detailed view of how nutrient pulse and phytoplankton pulse affect the evolution of plankton populations. It was observed that when the nutrient pulse was small, both phytoplankton and zooplankton populations tended to go extinct, even when a high pulse of the phytoplankton population was applied. One possible explanation is that the growth of phytoplankton is directly correlated with the nutrient concentration, and the low nutrient pulse may lead to nutrient deficiency in the aquatic ecosystem, ultimately causing stagnation in the growth rate of phytoplankton species (Ittekkot et al., 1981). The low nutrient pulse and a lack of phytoplankton in the aquatic reservoir might have impaired the growth, survival, and possibly reproduction of the zooplankton species. The results also noted that with an increment in the nutrient pulse, the phytoplankton population becomes persistent while the zooplankton population goes extinct. This indicates that a high nutrient concentration in the aquatic reservoir will allow the phytoplankton population to survive, but it will not be appropriate to support the coexistence of both the phytoplankton and zooplankton species. Moreover, Figure 7.4 showed that, if the nutrient pulse was 0.5, then both the phytoplankton and zooplankton populations become persistent, even though the phytoplankton pulse was low. The results from Figure 7.4 suggest that in comparison to the phytoplankton pulse, the nutrient pulse is the primary driver in controlling the oscillations, survival, and extinction of both phytoplankton and zooplankton populations. Here, the results are in agreement with the findings of Huang et al. (2018) and Paerl and Barnard (2020).

Owing to the fact that the number of pulses per period plays a significant role in the survival

of plankton populations (Liu et al., 2023), Figure 7.5 showed that when the number of pulses per period is equal to 1, both the phytoplankton and zooplankton populations tend to go extinct in the aquatic system. Biologically, a lower pulse number may result in insufficient nutrient concentration in the aquatic ecosystem, which is unable to support the survival of plankton populations. But, with an increase in the pulse frequency, the persistency of plankton populations increases. The results also showed that the oscillatory tendency in the plankton populations also becomes stronger as the pulse frequency increases. This implies that a high pulse number can increase the survival chances of plankton populations in the aquatic system. The existing research has recognized the critical role played by environmental fluctuations in regulating plankton dynamics (Yu et al., 2019a). The simulation results demonstrated that random fluctuations have significant effects on the survival of plankton populations in the aquatic habitat (see Figure 7.6). Figure 7.6 showed that if the noise intensity was within a certain range, then environmental fluctuations are capable of enhancing the oscillations of plankton populations. This indicates that appropriate noise control may increase the survival chances of plankton populations in the aquatic system. However, excessive noise intensity may result in the collapse of the entire ecosystem. For instance, a dramatic drop in temperature can cause the complete disappearance of the *Cylindrospermopsis* filaments (Borics et al., 2000). The results from Figure 7.6 suggested that environmental noise is another essential factor for phytoplankton growth. Overall, the findings suggest that nutrient pulse and environmental fluctuations play a crucial role in the survival of plankton populations. It is worth noting that the objectives of this research are not the precision with which it predicts specific events within a particular lake/ocean, but its contribution to the studies on how the coupling between environmental stochasticity and impulsive effects influence the growth of plankton populations in lakes/oceans. Moreover, our results may provide some insights into possible management strategies to prevent algal blooms in aquatic ecosystems.

Chapter 8

CONCLUSION AND RECOMMENDATIONS

8.1. Synthesis and conclusion

Phytoplankton offer great potential for exploitation, serving as the base of the trophic chain and playing a crucial role in stabilizing aquatic ecosystems. In recent years, considerable efforts, such as experimental and mathematical studies, have been made to explore the dynamics of phytoplankton growth. However, due to the nonlinear nature and complexity of aquatic ecosystems, the underlying mechanisms that drive changes in phytoplankton dynamics have remained a challenge. Thus, the current study developed five mathematical models to investigate the dynamics of phytoplankton growth, including (i) delayed nutrient-plankton model with diffusion; (ii) stochastic Leslie-Gower phytoplankton-zooplankton model with prey refuge; (iii) stochastic nutrient-plankton model with seasonal fluctuation; (iv) stochastic nutrient-plankton model with regime switching; and (v) stochastic nutrient-plankton model with impulsive control.

It has been recognized that delay effect exists in the phytoplankton growth process, such as nutrient transformation and nutrient recycling related to decomposition. There is growing evidence suggesting that spatial distribution also plays an important role in plankton dynamics, as the abundance of plankton species changes not only in time but also in space. In Chapter 3, a delayed nutrient-plankton model with diffusion was proposed to explore the effect of delay on the modeling dynamics. The results indicated that the delay could destabilize the model via Hopf bifurcation when the delay passed through the critical value. Furthermore, increasing delay could lead to the emergence of stability switches instead of playing only a destabilizing effect in the model. More importantly, numerical results revealed that chaotic behavior could be induced by delay, indicating that delay-induced chaos can appear in a spatiotemporal plankton model. This work may provide

insightful information about how delay affects the dynamics of spatiotemporal plankton growth models. It is important to note that the emergence of chaos indicates the unpredictable feature of the bloom phenomenon. Thus, the current study cannot predict algal bloom events but contributes to the study of how delay affects phytoplankton growth.

In natural ecosystems, phytoplankton growth processes are inevitably influenced by environmental fluctuations, which can be mathematically described by white noise. The noise intensity is more difficult to measure in experimental studies, thus many researchers prefer to use mathematical models to study the stochastic dynamics of aquatic ecosystems. Furthermore, recent evidence supports that the refuge of phytoplankton is a common phenomenon in aquatic ecosystems. For example, water column stratification can be used as a temporary shelter for phytoplankton recovery. Thus, in Chapter 4, a stochastic Leslie-Gower nutrient-phytoplankton model with prey refuge was proposed, in which the effects of random fluctuation and prey refuge on the phytoplankton population were studied. The results showed that excessive noise intensity could result in the extinction of plankton species. Theoretical analysis further indicated that the refuge of phytoplankton played an important role in the coexistence of plankton species. Furthermore, the numerical results revealed that the refuge of phytoplankton could significantly change the mean and the variance of plankton biomass, indicating that prey refuge could enhance the oscillation range of the phytoplankton population. The numerical results further showed that too large or too small phytoplankton refuge was not conducive to plankton coexistence. The present study provides insight into how phytoplankton refuge affects plankton interaction dynamics under environmental fluctuations.

There is evidence that blooms occur periodically due to seasonal changes in the environment. For example, Lake Taihu in China experiences phytoplankton blooms almost every year from May to October. This periodicity is attributed to changes in nutrient supply, water temperature, and light

intensity, which all exhibit a periodic pattern and subsequently lead to periodic blooms. Although extensive studies have focused on the effect of seasonal fluctuation on algal growth, the complexity of the aquatic environment limits our understanding of seasonal phytoplankton blooms. In Chapter 5, a stochastic nutrient-plankton model with seasonal fluctuation was proposed, and the results showed that seasonality and stochasticity may cause the periodic bloom of the phytoplankton population. Additionally, the oscillation intensity of plankton biomass could be influenced by nutrient input, and the overall trend of solutions presents obvious periodicity after nutrient input went beyond a certain level. Importantly, the distribution of phytoplankton under constant and periodic parameters does not show a notable difference, but seasonal fluctuation could considerably alter the distribution of zooplankton. The simulation results further implied that the distribution of zooplankton biomass was sensitive to changes in periodicity. The present study provides insights into how seasonal fluctuations influence plankton dynamics under stochastic environments.

In recent years, constant plankton mortality has been widely used in most aquatic ecosystem models. However, during the decline phase of blooms, the decomposition of dead plankton consumes a large amount of oxygen, resulting in a sharp decrease in dissolved oxygen. Thus, phytoplankton mortality in the decline phase is much higher than that in the development phase. In Chapter 6, colored noise was used to describe the shifting plankton mortality in the model and a stochastic nutrient-plankton model with regime switching was proposed. The theoretical analysis suggested that the plankton population could survive forever under certain conditions. Moreover, sensitivity analysis showed that phytoplankton biomass was highly sensitive to the grazing rate by zooplankton and least sensitive to the re-mineralization of dead biomass into nutrients. Numerical results further revealed an important fact that the Markov chain could significantly enhance plankton population oscillation. From an ecological point of view, regime-switching plankton

mortality is beneficial to the survival of plankton. The present study may not predict the algal bloom phenomenon but provides an understanding of how regime-switching plankton mortality influences plankton dynamics.

In the study of control and prevention of phytoplankton blooms, impulsive control has been widely adopted in phytoplankton growth models. Specifically, growing evidence suggests that proper impulsive control strategies can contribute to the survival of plankton populations. Although extensive research has focused on the effects of impulsive control on phytoplankton growth, little attention has been paid to the coupling between stochastic and impulse effects on plankton dynamics. In Chapter 7, a stochastic nutrient-plankton model with impulsive control was developed to investigate how random fluctuation and impulsive control influence phytoplankton growth. Theoretical analysis obtained sufficient conditions for the existence of a positive T-periodic solution. The numerical analysis revealed that nutrient pulse is the primary strategy for controlling algal blooms, and noise disturbance played an important role in the survival of plankton populations. Moreover, numerical analysis showed that excessive noise intensity could threaten the entire ecosystem. The results may provide insightful information about the possible management of excessive algal growth in aquatic systems.

Field observation and experimental studies offer a qualitative and quantitative analysis, while mathematical models represent more of a mechanistic study. Notably, some dynamical behaviors, such as bifurcation, cannot be obtained experimentally. Therefore, the use of phytoplankton growth models has become a promising way to investigate bloom phenomena and has attracted much attention. The present research provides a better understanding of the dynamics in the planktonic community. For instance, complex dynamics can be induced by delay, indicating that spatiotemporal chaos can appear in a spatiotemporal plankton model. White noise and colored noise are suggested to play a significant role in planktonic communities, and the seasonal

fluctuation is considered an important factor affecting the periodic bloom events of phytoplankton. Specifically, controlling nutrient input is considered as the primary strategy in preventing and controlling algal blooms. It is worth mentioning that the proposed models may not accurately mimic reality, but they can provide a better understanding of the dominant processes determining the phytoplankton growth and offer some general suggestions for the control of bloom events.

8.2. Limitations and future research

Although the proposed models provided some understanding of the dynamics of phytoplankton growth, they cannot explain all the mechanisms behind phytoplankton growth. These models require further revision before they can be applied in the field. In fact, the real aquatic ecosystems are complex. To reduce the complexity of models and computations, it is often necessary to ignore certain aspects of natural aquatic ecosystems and focus only on the aspects most relevant to the problem at hand. For example, during the model building process, I typically assume that temperature and light are adequate. Therefore, the developed models may not fully reflect the complexity of real aquatic ecosystem. Additionally, my research only focuses on the interactions between nutrient concentration, phytoplankton population, and zooplankton population. Thus, my research may only partially describe the nutrient-phytoplankton-zooplankton interactions.

This study investigated delay-induced dynamics, such as periodic solution and chaos, and provided insight into the oscillatory and chaotic behavior that is likely common in population ecosystems. The emergence of chaos is beneficial in promoting phytoplankton biodiversity. However, there is currently little empirical evidence to support the existence of chaos in aquatic ecosystems. A possible explanation might be the limited access to long-term experimental data. While the current studies demonstrate the existence of spatiotemporal chaos in phytoplankton

growth models, the mechanism for the formation of chaos in aquatic ecosystems require further investigation. Additionally, previous studies have demonstrated that the distribution of plankton can differ significantly not only in spatial but also in temporal scales, resulting in the emergence of plankton patterns (such as stationary strips, spots, and strips-spots mixture patterns). Although considerable efforts have been made to understand the principal features and spatiotemporal variability of plankton species, they are still not well understood, especially delay-induced spatiotemporal plankton patterns. Therefore, further research on delay-induced plankton pattern in aquatic ecosystem is needed.

The dynamics of stochastic phytoplankton growth is another interesting problem in aquatic ecosystems. The current study provided four different stochastic phytoplankton growth models and investigated the plankton dynamics under various random disturbances. However, the complexity of aquatic ecosystem limits the studies of stochastic phytoplankton growth dynamics. For instance, aquatic ecosystems are not only affected by regime switching (e.g., plankton mortality, nutrient supply) but are also influenced by abrupt disturbances (e.g., earthquakes, hurricanes). Although extensive research has been carried out on the coupling effect of random fluctuations, it remains unclear how these stochastic fluctuations affect planktonic ecosystems.

Another area of interest for further research is the impact of essential abiotic resources, such as temperature and light intensity, on the structure and succession of phytoplankton. A considerable amount of literature indicates that the temperature and light intensity are highly variable with environmental fluctuations, resulting in changes in phytoplankton biomass. However, the proposed dynamic models in this study have not considered these abiotic factors. To gain a better understanding of how phytoplankton growth responds to temperature and light intensity, further research should incorporate a phytoplankton growth model that takes these factors into account.

Additionally, experimental work is needed to provide validation for the results obtained in

current research, thereby enhancing the reliability and accuracy of the models. In the present research, the models were developed relying on certain assumptions and simplifications, the experiments can be used to validate the validity of these assumptions. By comparing model outputs with experimental results, the scope and limitations of the models can be determined, leading to model improvements and adjustments. Actually, models can be used for optimization, result prediction, and decision-making, while experiments provide real-world validation and application of the models. The integration of models and experiments is able to enhance the reliability, accuracy, and applicability of research, providing a more comprehensive and in-depth understanding of scientific inquiry. Hence, a combined experimental and modeling approach is essential in future research.

References

Abada, A., Sperfeld, M., Carmieli, R., Ben-Dor, S., Zhang, I.H., Babbin, A.R., Segev, E., 2021. Aerobic bacteria produce nitric oxide via denitrification and trigger algal population collapse. BioRxiv Preprint.

Aberle, N., Lengfellner, K., Sommer, U., 2007. Spring bloom succession, grazing impact and herbivore selectivity of ciliate communities in response to winter warming. Oecologia. 150, 668–681.

Adak, D., Bairagi, N., Hakl, R., 2020. Chaos in delay-induced Leslie–Gower prey–predator–parasite model and its control through prey harvesting. Nonlinear Analysis: Real World Applications. 51, 102998.

Agmour, I., Baba, N., Bentounsi, M., Achtaich, N., Foutayeni, Y.E., 2021. Mathematical study and optimal control of bioeconomic model concerning harmful dinoflagellate phytoplankton. Computational and Applied Mathematics. 40, 129.

Agnihotri, K., Kaur, H., 2019. The dynamics of viral infection in toxin producing phytoplankton and zooplankton system with time delay. Chaos, Solitons & Fractals. 118, 122–133.

Akhmet, M.U., Arugaslan, D., Beklioglu, M., 2006. Impulsive control of the population dynamics. In Proceedings of the conference on differential and difference equations, differential & difference equations and applications. Hindawi Publishing Corporation. 2006, 21–30.

Alijani, M.K., Wang, H., Elser, J.J., 2015. Modeling the bacterial contribution to planktonic community respiration in the regulation of solar energy and nutrient availability. Ecological Complexity. 23, 25–33.

Alshahri, A.H., Fortunato, L., Ghaffour, N., Leiknes, T., 2021. Controlling harmful algal blooms (HABs) by coagulation-flocculation-sedimentation using liquid ferrate and clay. Chemosphere. 274, 129676.

Amorim, C.A., Moura, A.D.N., 2021. Ecological impacts of freshwater algal blooms on water quality, plankton biodiversity, structure, and ecosystem functioning. Science of the Total Environment. 758, 143605.

Anderies, J.M., Beisner, B.E., 2000. Fluctuating environments and phytoplankton community structure: a stochastic model. The American Naturalist. 155, 556–569.

Anderson, C.R., Moore, S.K., Tomlinson, M.C., Silke, J., Cusack, C.K., 2015. Living with harmful algal blooms in a changing world: strategies for modeling and mitigating their effects in coastal marine ecosystems. In Coastal and marine hazards, risks, and disasters. 495-561.

Anderson, D.M., 1997. Turning back the harmful red tide. Nature. 388, 513–514.

Anderson, D.M., 2009. Approaches to monitoring, control and management of harmful algal blooms (HABs). Ocean & Coastal Management. 52, 342–347.

Anderson, D.M., Boerlage, S.F., Dixon, M.B., 2017. Harmful Algal Blooms (HABs) and Desalination: a Guide to Impacts, Monitoring and Management.

Anderson, D.M., Cembella, A.D., Hallegraeff, G.M., 2012. Progress in understanding harmful algal blooms: paradigm shifts and new technologies for research, monitoring, and management. Annual Review of Marine Science. 4, 143–176.

Anderson, D.M., Fensin, E., Gobler, C.J., Hoeglund, A.E., Hubbard, K.A., Kulis, D.M., Landsberg, J.H., Lefebvre, K.A., Provoost, P., Richlen, M.L., Smith, J.L., Solow, A.R., Trainer, V.L., 2021. Marine harmful algal blooms (HABs) in the United States: History, current status and future trends. Harmful Algae. 102, 101975.

Anderson, D.M., Glibert, P.M., Burkholder, J.M., 2002. Harmful algal blooms and eutrophication: Nutrient sources, composition, and consequences. Estuaries. 25, 704–726.

Anderson, T.H., Taylor, G.T., 2001. Nutrient pulses, plankton blooms, and seasonal hypoxia in western Long Island Sound. Estuaries. 24, 228-243.

Andersson, A., Haecky, P., Hagström, A., 1994. Effect of temperature and light on the growth of micro-nano-and pico-plankton: impact on algal succession. Marine Biology. 120, 511–520.

Ansari, A.A., Singh, G.S., Lanza, G.R. Rast, W., 2010. Eutrophication: causes, consequences and control. Vol. 1. Springer Science & Business Media.

Aota, Y., Nakajima, H., 2000. Mathematical analysis on coexistence conditions of phytoplankton and bacteria systems with nutrient recycling. Ecological modelling. 135, 17–31.

Araki, M., Okano, K., Ohta, S., Suzuki, E., Fujibayashi, M., Miyata, N., 2018. Characteristics of harmful algal blooms during a low water temperature season in Lake Hachiro. Journal of Water and Environment Technology. 16, 175–183

Baek, S.H., Kim, D., Kim, Y.O., Son, M., Kim, Y.J., Lee, M., Park, B.S., 2019. Seasonal changes in abiotic environmental conditions in the Busan coastal region (South Korea) due to the

Nakdong River in 2013 and effect of these changes on phytoplankton communities. Continental Shelf Research. 175, 116-126.

Balaji-Prasath, B., Wang, Y., Su, Y. P., Hamilton, D.P., Lin, H., Zheng, L., Zhang, Y., 2022. Methods to control harmful algal blooms: a review. Environmental Chemistry Letters. 20, 3133-3152.

Banerjee, M., Petrovskii, S., 2011. Self-organised spatial patterns and chaos in a ratio-dependent predator–prey system. Theoretical Ecology. 4, 37–53

Bao, J.H., Mao, X.R., Yin, G., Yuan, C.G., 2011. Competitive Lotka–Volterra population dynamics with jumps. Nonlinear Analysis: Theory, Methods & Applications. 74, 6601–6616.

Baretta-Bekker, H.J.G, Duursma, E.K., Kuipers, B.R., 1998. Encyclopedia of marine sciences. Springer Science & Business Media.

Beaulieu, M., Pick, F., Gregory-Eaves, I., 2013. Nutrients and water temperature are significant predictors of cyanobacterial biomass in a 1147 lakes data set. Limnol. Oceanogr. 58, 1736–1746.

Beddington, J.R., 1975. Mutual Interference Between Parasites or Predators and its Effect on Searching Efficiency. The Journal of Animal Ecology. 44, 331–340.

Beklioglu, M., Moss, B., 1998. The effects of tench (Tinca tinca (L.)) and sticklebacks (Gasterosteus aculeatus L.) on planktonic and benthic communities in mesocosms in a shallow lake. Aquatic Ecology. 32, 229–240.

Belabbas, M., Ouahab, A., Souna, F., 2021. Rich dynamics in a stochastic predator-prey model with protection zone for the prey and multiplicative noise applied on both species. Nonlinear Dynamics. 106, 2761-2780.Benincà, E., Ballantine, B., Ellner, S.P., Huisman, J., 2015. Species fluctuations sustained by a cyclic succession at the edge of chaos. Proceedings of the National Academy of Sciences. 112, 6389-6394.

Benincà, E., Jöhnk, K.D., Heerkloss, R., Huisman, J., 2009. Coupled predator–prey oscillations in a chaotic food web. Ecology letters. 12, 1367–1378.

Bentounsi, M., Agmour, I., Achtaich, N., Foutayeni, Y.E., 2018. The Hopf bifurcation and stability of delayed predator–prey system. Computational and Applied Mathematics. 37, 5702–5714.

Beretta, E., Bischi, G.I., Solimano, F., 1990. Stability in chemostat equations with delayed nutrient recycling. Journal of Mathematical Biology. 28, 99–111.

Berga, M., Östman, Ö., Lindström, E.S., Langenheder, S., 2015. Combined effects of zooplankton grazing and dispersal on the diversity and assembly mechanisms of bacterial metacommunities. Environmental Microbiology. 17, 2275–2287.

Bhagowati, B., Talukdar, B., Ahamad, K.U., 2020. Lake eutrophication: causes, concerns and remedial measures. Emerging Issues in the Water Environment during Anthropocene: A South East Asian Perspective. 211-222.

Bharathi, M. D., Sarma, V. V. S. S., Ramaneswari, K., 2018. Intra-annual variations in phytoplankton biomass and its composition in the tropical estuary: Influence of river discharge. Marine Pollution Bulletin. 129, 14-25.

Birtel, J., Matthews, B., 2016. Grazers structure the bacterial and algal diversity of aquatic metacommunities. Ecology. 97, 3472–3484.

Biswas, S., Tiwari, P.K., Bona, F., Pal, S., Venturino, E., 2020a. Modeling the avoidance behavior of zooplankton on phytoplankton infected by free viruses. Journal of Biological Physics. 46, 1-31.

Biswas, S., Tiwari, P.K., Kang, Y., Pal, S., 2020b. Effects of zooplankton selectivity on phytoplankton in an ecosystem affected by free-viruses and environmental toxins. Mathematical Biosciences and Engineering. 17, 1272-317.

Biswas, S., Tiwari, P.K., Pal, S., 2022. Effects of toxicity and zooplankton selectivity on plankton dynamics under seasonal patterns of viruses with time delay. Mathematical Methods in the Applied Sciences. 45, 585-617.

Black, A.J., McKane, A.J., 2012. Stochastic formulation of ecological models and their applications. Trends in ecology & evolution. 27, 337–345.

Børsheim, K.Y., Vadstein, O., Myklestad, S.M., Reinertsen, H., Kirkvold, S., Olsen, Y., 2005. Photosynthetic algal production, accumulation and release of phytoplankton storage carbohydrates and bacterial production in a gradient in daily nutrient supply. Journal of Plankton Research. 27, 743–755.

Borics, G., Grigorszky, I., Szab$\acute{o}$, S., Padis$\acute{a}$k, J., 2000. Phytoplankton associations in a small hypertrophic fishpond in East Hungary during a change from bottom-up to top-down control. In: Reynolds, C.S., Dokulil, M., Padis$\acute{a}$k, J. (eds) The Trophic Spectrum Revisited, Developments in Hydrobiology. 150, 79–90.

Bortz, D., Nelson, P., 2004. Sensitivity analysis of a nonlinear lumped parameter model of HIV infection dynamics. Bulletin of Mathematical Biology. 66, 1009–1026.

Boyd, C.E., Prather, E.E., Parks, R.W., 1975. Sudden mortality of a massive phytoplankton bloom. Weed Science. 23, 61–67.

Brandenburg, K.M., de Senerpont Domis, L.N., Wohlrab, S., Krock, B., John, U., van Scheppingen, Y., van Donk, E., Van de Waal, D.B., 2017. Combined physical, chemical and biological factors shape Alexandrium ostenfeldii blooms in the Netherlands. Harmful algae. 63, 146–153.

Braumann, C.A., 2002. Variable effort harvesting models in random environments: Generalization to density-dependent noise intensities. Mathematical Biosciences. 177, 229–245.

Bruno, D.W., Dear, G., Seaton, D.D., 1989. Mortality associated with phytoplankton blooms among farmed Atlantic salmon, Salmo salar L., in Scotland. Aquaculture. 78, 217–222.

Burson, A., Stomp, M., Greenwell, E., Grosse, J., Huisman, J., 2018. Competition for nutrients and light: testing advances in resource competition with a natural phytoplankton community. Ecology. 99, 1108–1118.

Burson, A., Stomp, M., Mekkes, L., Huisman, J., 2019. Stable coexistence of equivalent nutrient competitors through niche differentiation in the light spectrum. Ecology. 100, e02873.

Cael, B.B., Dutkiewicz, S., Henson, S., 2021. Abrupt shifts in 21st-century plankton communities. Science Advances. 7, eabf8593.

Cai, Y.M., Cai, S.Y., Mao, X.R., 2020. Stochastic delay foraging arena predator–prey system with Markov switching. Stochastic Analysis and Applications. 38, 191–212.

Camara, B.I., Yamapi, R., Mokrani, H., 2019. Environmental stochastic effects on phytoplankton–zooplankton dynamics. Nonlinear Dynamics. 96, 2013–2029.

Cao, H., Yang, Z., 2010. Variation in colony size of Microcystis aeruginosa in a eutrophic lake during recruitment and bloom formation. Journal of Freshwater Ecology. 25, 331–335.

Caperon, J., 1969. Time lag in population growth response of isochrysis galbana to a variable nitrate environment. Ecology. 50, 188–192.

Carpenter, S.R., Cole, J.J., Pace, M.L., Wilkinson, G.M., 2016. Response of plankton to nutrients, planktivory and terrestrial organic matter: A model analysis of whole-lake experiments. Ecology letters. 19, 230–239.

Carstensen, J., Henriksen, P., Heiskanen, A.S., 2007. Summer algal blooms in shallow estuaries: definition, mechanisms, and link to eutrophication. Limnology and Oceanography. 52, 370–384.

Chakraborty, S., Tiwari, P.K., Misra, A.K., Chattopadhyay, J., 2015. Spatial dynamics of a nutrient–phytoplankton system with toxic effect on phytoplankton. Mathematical Biosciences. 264, 94–100.

Chang, C.W., Huo, X., Lin, T.F., 2018. Exposure of Microcystis aeruginosa to hydrogen peroxide and titanium dioxide under visible light conditions: Modeling the impact of hydrogen peroxide and hydroxyl radical on cell rupture and microcystin degradation. Water Research. 141, 217–226.

Chattopadhyay, J., Sarkar, R.R., 2003. Chaos to order: preliminary experiments with a population dynamics models of three trophic levels. Ecological Modelling. 163, 45–50.

Chen, M., Fan, M., Kuang, Y., 2017. Global dynamics in a stoichiometric food chain model with two limiting nutrients. Mathematical Biosciences. 289, 9-19.

Chen, M.X., Wu, R.C., Liu, B., Chen, L.P., 2020a. Hopf-Hopf bifurcation in the delayed nutrient-microorganism model. Applied Mathematical Modelling. 86, 460-483.

Chen, Q., Rui, H., Li, W., Zhang, Y., 2014. Analysis of algal bloom risk with uncertainties in lakes by integrating self-organizing map and fuzzy information theory. Science of the Total Environment. 482, 318–324.

Chen, Q.W., Mynett, A.E., 2006. Modelling algal blooms in the Dutch coastal waters by integrated numerical and fuzzy cellular automata approaches. Ecological Modelling. 199, 73–81.

Chen, S.S., Shi, J.P., Wei, J.J., 2013. Time delay-induced instabilities and Hopf bifurcations in general reaction–diffusion systems. Journal of nonlinear science. 23, 1–38.

Chen, S.S., Yang, H., Wei, J.J., 2019. Global dynamics of two phytoplankton-zooplankton models with toxic substances effect. Journal of Applied Analysis & Computation. 9, 796–809.

Chen, Z.W., Tian, Z.Y., Zhang, S.W., Wei, C.J., 2020b. The stationary distribution and ergodicity of a stochastic phytoplankton–zooplankton model with toxin-producing phytoplankton under regime switching. Physica A: Statistical Mechanics and its Applications. 537, 122728.

Chen, Z.W., Zhang, R.M., Li, J., Zhang, S.W., Wei, C.J., 2020c. A stochastic nutrient-phytoplankton model with viral infection and Markov switching. Chaos, Solitons & Fractals. 140, 110109.

Chislock, M.F., Doster, E., Zitomer, R.A., Wilson, A.E., 2013. Eutrophication: causes, consequences, and controls in aquatic ecosystems. Nature Education Knowledge. 4, 10.

Choi, C.J., Brosnahan, M.L., Sehein, T.R., Anderson, D.M., Erdner, D.L., 2017. Insights into the loss factors of phytoplankton blooms: The role of cell mortality in the decline of two inshore Alexandrium blooms. Limnology and Oceanography. 62, 1742–1753.

Cloern, J.E., 2001. Our evolving conceptual model of the coastal eutrophication problem. Marine ecology progress series. 210, 223–253.

Conley, D.J., Paerl, H.W., Howarth, R.W., Boesch, D.F., Seitzinger, S.P., Havens, K.E., Lancelot, C., Likens, G.E., 2009. Controlling Eutrophication: Nitrogen and Phosphorus. Science. 323, 1014–1015.

Crowley, P.H., Martin, E.K., 1989. Functional Responses and Interference within and between Year Classes of a Dragonfly Population. Journal of the North American Benthological Society. 8, 211–221.

Cui, J., Zhang, J., Huo, Y., Zhou, L., Wu, Q., Chen, L., Yu, K., He, P., 2015. Adaptability of free-floating green tide algae in the Yellow Sea to variable temperature and light intensity. Marine pollution bulletin. 101, 660-666.

Cui, Y.J., Liu, D.F., Zhang, J.L., Yang, Z.J., Khu, S.T., Ji, D.B., Song, L.X., Long, L.H., 2016. Diel migration of *Microcystis* during an algal bloom event in the Three Gorges Reservoir, China. Environmental Earth Sciences. 75, 616.

Dacey, J.W., Wakeham, S.G., 1986. Oceanic dimethylsulfide: production during zooplankton grazing on phytoplankton. Science. 233, 1314–1316.

Dai, C.J., Yu, H. G., Guo, Q., Liu, H., Wang, Q., Ma, Z.L., Zhao, M., 2019. Dynamics induced by delay in a nutrient-phytoplankton model with multiple delays. Complexity. 2019, 3879626.

Dai, C.J., Zhao, M., 2020. Bifurcation and patterns induced by flow in a prey-predator system with Beddington-DeAngelis functional response. Physical Review E. 102, 012209.

Dai, C.J., Zhao, M., Yu, H.G., 2016. Dynamics induced by delay in a nutrient–phytoplankton model with diffusion. Ecological Complexity. 26, 29-36.

Dai, C.J., Zhao, M., Yu, H.G., Wang, Y.P., 2015. Delay-induced instability in a nutrient-phytoplankton system with flow. Physical Review E. 91, 032929.

Dalal, N., Greenhalgh, D., Mao, X.R., 2008. A stochastic model for internal HIV dynamics. Journal of Mathematical Analysis and Applications. 341, 1084–1101.

Das, E., Paul, P., Kar, T.K., 2022. Transient indicator of exploited communities at equilibrium in generalist predator–prey models. European Physical Journal Plus. 137, 1221.

Das, K., Ray, S., 2008. Effect of delay on nutrient cycling in phytoplankton-zooplankton interactions in estuarine system. Ecological Modelling. 215, 69–76.

Das, T., Chakraborti, S., Mukherjee, J., Sen, G.K., 2018. Mathematical modelling for phytoplankton distribution in Sundarbans Estuarine System, India. Ecological Modelling. 368, 111–120.

Dawes, J.H.P., Souza, M.O., 2013. A derivation of Holling's type I, II and III functional responses in predator–prey systems. Journal of Theoretical Biology. 327, 11–22.

Dean, A.M., Shnerb, N.M., 2020. Stochasticity-induced stabilization in ecology and evolution: a new synthesis. Ecology. 101, e03098.

DeAngelis, D.L., Goldstein, R.A., O'Neill, R.V., 1975. A Model for Tropic Interaction. Ecology. 56, 881–892.

de la Hoz, F., Vadillo, F., 2012. A mean extinction-time estimate for a stochastic Lotka–Volterra predator–prey model. Applied Mathematics and Computation. 219, 170–179.

Denaro, G., Valenti, D., Cognata, A.L., Spagnolo, B., Bonanno, A., Basilone, G., Mazzola, S., Zgozi, S.W., Aronica, S., Brunet, C., 2013. Spatio-temporal behaviour of the deep chlorophyll maximum in Mediterranean Sea: Development of a stochastic model for picophytoplankton dynamics. Ecological Complexity. 13, 21–34.

Deng, F.Q, Luo, Q., Mao, X.R, Pang, S.L., 2008. Noise suppresses or expresses exponential growth. Systems & Control Letters. 57, 262–270.

Deng, J., Chen, F., Liu, X., Peng, J., Hu, W., 2016. Horizontal migration of algal patches associated with cyanobacterial blooms in an eutrophic shallow lake. Ecological Engineering. 87, 185-193.

Deng, Y.L., Zhao, M., Yu, H.G., Wang, Y., 2015. Dynamical Analysis of a Nitrogen-Phosphorus-Phytoplankton Model. Discrete Dynamics in Nature and Society. 2015, 1–8.

De Silva, M., Jang, S.R.J., 2017. Dynamical behavior of systems of two phytoplankton and one zooplankton populations with toxin producing phytoplankton. Mathematical Methods in the Applied Sciences. 40, 4295–4309.

De Silva, T.M.M., Jang, S.R.J., 2018. Stochastic modeling of phytoplankton–zooplankton interactions with toxin producing phytoplankton. Journal of Biological Systems. 26, 87–106.

Dobramysl, U., Mobilia, M., Pleimling, M., Täuber, U.C., 2018. Stochastic population dynamics in spatially extended predator–prey systems. Journal of Physics A: Mathematical and Theoretical. 51, 063001.

Downing, J.A., Watson, S.B., McCauley, E., 2001. Predicting cyanobacteria dominance in lakes. Canadian Journal of Fisheries and Aquatic Sciences. 58, 1905–1908.

Du, N.H., Kon, R., Sato, K., Takeuchi, Y., 2004. Dynamical behavior of Lotka–Volterra competition systems: non-autonomous bistable case and the effect of telegraph noise. Journal of Computational and Applied Mathematics. 170, 399–422.

Dubey, D., Dutta, V., 2020. Nutrient enrichment in lake ecosystem and its effects on algae and macrophytes. Environmental Concerns and Sustainable Development: Volume 2: Biodiversity, Soil and Waste Management. 81-126.

Duffy, J.E., 2002. Biodiversity and ecosystem function: the consumer connection. Oikos. 99, 201–219.

Duggan, I.C., Wood, S.A., West, D.W., 2015. Brown trout (Salmo trutta) removal by rotenone alters zooplankton and phytoplankton community composition in a shallow mesotrophic reservoir. New Zealand Journal of Marine and Freshwater Research. 49, 356-365.

Edwards, A.M., Brindley, J., 1999. Zooplankton mortality and the dynamical behaviour of plankton population models. Bulletin of mathematical biology. 61, 303–339.

Elliott, J.A., Jones, I.D., Thackeray, S.J., 2006. Testing the sensitivity of phytoplankton communities to changes in water temperature and nutrient load, in a temperate lake. Hydrobiologia. 559, 401–411.

Fan, M., Wang, K., 2000. Global periodic solutions of a generalized n-species Gilpin-Ayala competition model. Computers & Mathematics with Applications. 40, 1141–1151.

Fang, C., Song, K.S., Paerl, H.W., Jacinthe, P.A., Wen, Z.D., Liu, G., Tao, H., Xu, X.F., Kutser, T., Wang, Z.M., Duan, H.T., Shi, K., Shang, Y.X., Lyu, L.L., Li, S.J., Yang, Q., Lyu, D.M., Mao, D., Zhang, B.H., Cheng, S., Lyu, Y.F., 2022. Global divergent trends of algal blooms detected by satellite during 1982–2018. Global Change Biology. 28, 2327-2340.

Fang, S., Del Giudice, D., Scavia, D., Binding, C.E., Bridgeman, T.B., Chaffin, J.D., Evans, M.A., Guinness, J., Johengen, T.H., Obenour, D.R., 2019. A space-time geostatistical model for probabilistic estimation of harmful algal bloom biomass and areal extent. Science of the Total Environment. 695, 133776.

Feng, X.M., Sun, J.X., Wang, L., Zhang, F.Q., Sun, S.L., 2021. Periodic solutions for a stochastic chemostat model with impulsive perturbation on the nutrient. Journal of Biological Systems. 29, 849–870.

Fleming, R.H., 1939. The control of diatom populations by grazing. ICES Journal of Marine Science. 14, 210–227.

Freund, J.A., Mieruch, S., Scholze, B., Wiltshire, K., Feudel, U., 2006. Bloom dynamics in a seasonally forced phytoplankton–zooplankton model: trigger mechanisms and timing effects. Ecological complexity. 3, 129–139.

Fussmann, G.F., Ellner, S.P., Shertzer, K.W., Hairston Jr, N.G., 2000. Crossing the Hopf bifurcation in a live predator-prey system. Science. 290, 1358–1360.

Gajbhiye, S.N., 2002. Zooplankton-Study methods, importance and significant observations. Proc. The National Seminar on Creeks, Estuaries and Mangroves. 21–27.

Gallardo-Rodríguez, J.J., Astuya-Villalón, A., Llanos-Rivera, A., Avello-Fontalba, V., Ulloa-Jofré, V., 2019. A critical review on control methods for harmful algal blooms. Rev Aquacult. 11, 661–684.

Gao, M.M., Jiang, D.Q., Hayat, T., 2019. Stationary distribution and periodic solution of stochastic chemostat models with single-species growth on two nutrients. International Journal of Biomathematics. 12, 1950063.

Gao, M., Shi, H.H., Li, Z.Z., 2008. A planktonic resource–consumer model with a temporal delay in nutrient recycling. Journal of Mathematical Analysis and Applications. 339, 511–516.

Garcés, E., Vila, M., Masó, M., Sampedro, N., Giacobbe, M.G., Penna, A., 2005. Taxon-specific analysis of growth and mortality rates of harmful dinoflagellates during bloom conditions. Marine Ecology Progress Series. 301, 67–79.

Gard, T., 1988. Introduction to Stochastic Differential Equations. Madison Avenue, New York.

Ger, K.A., Naus-Wiezer, S., De Meester, L., Lürling, M., 2019. Zooplankton grazing selectivity regulates herbivory and dominance of toxic phytoplankton over multiple prey generations. Limnology and Oceanography. 64, 1214–1227.

Ghanbari, B., Gómez-Aguilar, J.F., 2018. Modeling the dynamics of nutrient–phytoplankton–zooplankton system with variable-order fractional derivatives. Chaos, Solitons & Fractals. 116, 114–120.

Ghosh, P., Das, P., Mukherjee, D., 2019. Persistence and stability of a seasonally perturbed three species stochastic model of salmonoid aquaculture. Differential Equations and Dynamical Systems. 27, 449–465.

Gianuca, A.T., Pantel, J.H., De Meester, L., 2016. Disentangling the effect of body size and phylogenetic distances on zooplankton top-down control of algae. Proceedings of the Royal Society B: Biological Sciences. 283, 20160487.

Giricheva, E., 2019. Spatiotemporal dynamics of an NPZ model with prey-taxis and intratrophic predation. Nonlinear Dynamics. 95, 875-892.

Godfray, H.C.J., Grenfell, B.T., 1993. The continuing quest for chaos. Trends in Ecology & Evolution. 8, 43–44.

Gökçe, A., Yazar, S., Sekerci, Y., 2020. Delay induced nonlinear dynamics of oxygen-plankton interactions. Chaos, Solitons & Fractals. 141, 110327.

Gourley, S.A., Ruan, S.G., 2003. Spatio-temporal delays in a nutrient-plankton model on a finite domain: linear stability and bifurcations. Applied mathematics and computation. 145, 391–412.

Grattan, L.M., Holobaugh, S., Morris, J.G., 2016. Harmful algal blooms and public health. Harmful Algae. 57, 2–8.

Gray, A., Greenhalgh, D., Hu, L., Mao, X.R., Pan, J., 2011. A stochastic differential equation SIS epidemic model. SIAM Journal on Applied Mathematics. 71, 876–902.

Grill, S., Zykov, V.S., Müller, S.C., 1995. Feedback-Controlled Dynamics of Meandering Spiral Waves. Physical Review Letters. 75, 3368–3371.

Guo, H.J., Chen, L.S., Song, X.Y., 2015. Qualitative analysis of impulsive state feedback control to an algae-fish system with bistable property. Applied Mathematics and Computation. 271, 905–922.

Guo, Q., Dai, C., Wang, L., Liu, H., Wang, Y., Li, J., Zhao, M., 2022. Stochastic periodic solution of a nutrient-plankton model with seasonal fluctuation. Journal of Biological Systems. 30, 695-720.

Guo, Q., Dai, C.J., Yu, H.G., Liu, H., Sun, X.X., Li, J.B., Zhao, M., 2020. Stability and bifurcation analysis of a nutrient-phytoplankton model with time delay. Mathematical Methods in the Applied Sciences. 43, 3018–3039.

Guo, Q., Wang, Y., Dai, C.J., Wang, L.J., Liu, H., Li, J.B., Tiwari, P.K., Zhao, M., 2023. Dynamics of a stochastic nutrient-plankton model with regime switching. Ecological Modelling. 477, 110249.

Guo, S.J, Feng, Y.Y., Wang, L., Dai, M.H., Liu, Z.L., Bai, Y., Sun, J., 2014. Seasonal variation in the phytoplankton community of a continental-shelf sea: the East China Sea. Marine Ecology Progress Series. 516, 103–126.

Häder, D.P., Gao, K.S., 2015. Interactions of anthropogenic stress factors on marine phytoplankton. Frontiers in Environmental Science. 3, 14.

Hallegraeff, G.M., 1993. A review of harmful algal blooms and their apparent global increase. Phycologia. 32, 79–99.

Hallegraeff. G.M., 2010. Ocean climate change, phytoplankton community responses, and harmful algal blooms: a formidable predictive challenge 1. Journal of Phycology. 46, 220–235.

Han, H.W., Xiao, R.S., Gao, G.D., Yin, B.S., Liang, S.K., Lv, X.Q., 2023. Influence of a heavy rainfall event on nutrients and phytoplankton dynamics in a well-mixed semi-enclosed bay. Journal of Hydrology. 617, 128932.

Han, R.J., Dai, B.X., 2019. Spatiotemporal pattern formation and selection induced by nonlinear cross-diffusion in a toxic-phytoplankton–zooplankton model with Allee effect. Nonlinear Analysis: Real World Applications. 45, 822–853.

Hansen, A.M., Hernández-Martínez, C., Falcón-Rojas, A., 2017. Evaluation of Eutrophication Control Through Hypolimnetic Oxygenation. Procedia Earth and Planetary Science. 17, 598–601.

Hassard, B.D., Kazarinoff, N.D., Wan, Y.H., 1981. Theory and applications of Hopf bifurcation. Cambridge University Press, Cambridge.

Hastings, A., Hom, C.L., Ellner, S., Turchin, P., Godfray, H.C.J., 1993. Chaos in ecology: is mother nature a strange attractor?. Annual Review of Ecology and Systematics. 24, 1–33.

Hastings, A., Powell, T., 1991. Chaos in three-species food chain. Ecology. 72, 896–903.

Havens, K.E., Ji, G., Beaver, J.R., Fulton, R.S., Teacher, C.E., 2019. Dynamics of cyanobacteria blooms are linked to the hydrology of shallow Florida lakes and provide insight into possible impacts of climate change. Hydrobiologia. 829, 43-59.

Hder, D.P., Gao, K., 2015. Interactions of anthropogenic stress factors on marine phytoplankton. Frontiers in Environmental Science. 3, 14.

He, P., 2015. Harmful algal blooms. The Algae World. 339-355.

Hernández-Carrasco, I., Orfila, A., Rossi, V., Garçon, V., 2018. Effect of small scale transport processes on phytoplankton distribution in coastal seas. Scientific reports. 8, 8613.

Ho, J.C., Michalak, A.M., 2020. Exploring temperature and precipitation impacts on harmful algal blooms across continental US lakes. Limnology and Oceanography. 65, 992-1009.

Holling, C.S., 1959a. Some characteristics of simple types of predation and parasitism. The Canadian Entomologist. 91, 385–398.

Holling, C.S., 1959b. The Components of Predation as Revealed by a Study of Small-Mammal Predation of the European Pine Sawfly. The Canadian Entomologist. 91, 293-320.

Holmes, E.E., Lewis, M.A., Banks, J.E., Veit, R.R., 1994. Partial differential equations in ecology: spatial interactions and population dynamics. Ecology. 75, 17-29.

Hopcroft, R.R., Clarke, C., Nelson, R.J., Rasko, K.A., 2005. Zooplankton communities of the arctic's canada basin: the contribution by smaller taxa. Polar Biology. 28, 198-206.

Hu, G., Li, X., Wang, Y., 2015. Pattern formation and spatiotemporal chaos in a reaction–diffusion predator–prey system. Nonlinear Dynamics. 81, 265-275.

Huang, J.C., Zhang, Y.J., Huang, Q., Gao, J.F., 2018. When and where to reduce nutrient for controlling harmful algal blooms in large eutrophic lake Chaohu, China. Ecological Indicators. 89, 808–817.

Huang, Y., Luo, L., Xu, K., Wang, X.C., 2019. Characteristics of external carbon uptake by microalgae growth and associated effects on algal biomass composition. Bioresource Technology. 292, 121887.

Huisman, J., Codd, G.A., Paerl, H.W., Ibelings, B.W., Verspagen, J.M.H., Visser, P. M., 2018. Cyanobacterial blooms. Nature Reviews Microbiology. 16, 471–483.

Huisman, J., van Oostveen, P., Weissing F.J., 1999. Species dynamics in phytoplankton blooms: incomplete mixing and competition for light. The American Naturalist. 154, 46–68.

Huisman, J., Pham T.N.N., Karl, D.M., Sommeijer, B., 2006. Reduced mixing generates oscillations and chaos in the oceanic deep chlorophyll maximum. Nature. 439, 322–325.

Huisman, J., Weissing, F.J., 1994. Light-Limited Growth and Competition for Light in Well-Mixed Aquatic Environments: An Elementary Model. Ecology. 75, 507–520.

Huisman, J., Weissing, F.J., 1999. Biodiversity of plankton by species oscillations and chaos. Nature. 402, 407–410.

Hunter-Cevera, K.R., Neubert, M.G., Olson, R.J., Solow, A.R., Shalapyonok, A., Sosik, H.M., 2016. Physiological and ecological drivers of early spring blooms of a coastal phytoplankter. Science. 354, 326–329.

Huppert, A., Blasius, B., Stone, L., 2002. A model of phytoplankton blooms. The American Naturalist. 159, 156–171.

Ibrahim, N.H., Iqbal, A., Mohammad-Noor, N., MR, R., Yanto, D.H.Y., Wilson, L.D., Mahadi, A.H., 2022. A Review on The Biological, Physical and Chemical Mitigation of Harmful Algal Bloom. Squalen Bulletin of Marine and Fisheries Postharvest and Biotechnology. 17, 95-110.

Imhof, L., Walcher, S., 2005. Exclusion and persistence in deterministic and stochastic chemostat models. Journal of Differential Equations. 217, 26–53.

Ittekkot, V., Brockmann, U., Michaelis, W., Degens, E.T., 1981. Dissolved free and combined carbohydrates during a phytoplankton bloom in the northern North Sea. Marine Ecology Progress Series. 4, 299–305.

Jang, S.R.J., Baglama, J., 2005. Nutrient-plankton models with nutrient recycling. Computers & Mathematics with Applications. 49, 375–387.

Jang, S.J., Baglama, J., Rick, J., 2006. Nutrient-phytoplankton-zooplankton models with a toxin. Mathematical and Computer Modelling. 43, 105–118.

Jang, S.R.J., Allen, E.J., 2015. Deterministic and stochastic nutrient-phytoplankton-zooplankton models with periodic toxin producing phytoplankton. Applied Mathematics and Computation. 271, 52–67.

Javidi, M., Ahmad, B., 2015. Dynamic analysis of time fractional order phytoplankton–toxic phytoplankton–zooplankton system. Ecological modelling. 318, 8–18.

Jester, R., Lefebvre, K., Langlois, G., Vigilant, V., Baugh, K., Silver, M.W., 2009. A shift in the dominant toxin-producing algal species in central California alters phycotoxins in food webs. Harmful Algae. 8, 291-298.

Ji, C.Y., Jiang, D.Q., Shi, N.Z., 2011. A note on a predator–prey model with modified Leslie–Gower and Holling-type II schemes with stochastic perturbation. Journal of Mathematical Analysis and Applications. 377, 435–440.

Jiang, L., Xia, M., Ludsin, S.A., Rutherford, E.S., Mason, D.M., Jarrin, J.M., Pangle, K.L., 2015. Biophysical modeling assessment of the drivers for plankton dynamics in dreissenid-colonized western lake erie. Ecological modelling. 308, 18–33.

Jorgensen, S.E., 1995. The growth rate of zooplankton at the edge of chaos: ecological models. Journal of Theoretical Biology. 175, 13–21.

Jorgensen, S.E., Ray, S., Berec, L., Straskraba, M., 2002. Improved calibration of a eutrophication model by use of the size variation due to succession. Ecological Modelling. 153, 269–277.

Kahru, M., Elmgren, R., Kaiser, J., Wasmund, N., Savchuk, O., 2020. Cyanobacterial blooms in the Baltic Sea: Correlations with environmental factors. Harmful Algae. 92, 101739.

Kartal, S., Kar, M., Kartal, N, Gurcan, F., 2016. Modelling and analysis of a phytoplankton–zooplankton system with continuous and discrete time. Mathematical and Computer Modelling of Dynamical Systems. 22, 539–554.

Kauffman, S.A., 1991. Antichaos and adaptation. Scientific American. 265, 78–84.

Kaur, R.P., Sharma, A., Sharma, A.K., 2021. The impact of additional food on plankton dynamics in the absence and presence of toxicity. Biosystems. 202, 104359.

Khasminskii, R., 1980. Stochastic stability of differential equations. Sijthoff and Noordhoff.

Khasminskii, R., 2011. Stochastic stability of differential equations. Springer Science and Business Media.

Kim, K.B., Uranchimeg, S., Kwon, H.H., 2022. A multivariate Chain-Bernoulli-based prediction model for cyanobacteria algal blooms at multiple stations in South Korea. Environmental Pollution. 313, 120078.

Klausmeier, C.A., Litchman, E., Daufresne, T., Levin, S.A., 2004. Optimal nitrogen-to-phosphorus stoichiometry of phytoplankton. Nature. 429, 171–174.

Kumari, N., Mishra, S., Häder, D.P., Sinha, R.P., 2022. Cyanobacterial blooms and their implications in the changing environment. Advances in Environmental and Engineering Research. 3, 1-41.

Landry, M.R., Hassett, R., 1982. Estimating the grazing impact of marine micro-zooplankton. Marine Biology. 67, 283–288.

Lane-Medeiros, L., Puppin-Gonçalves, C.T., Angelini, R., Lira, A.S., Lucena-Frédou, F., Freire, F.A.M., 2023. Macroalgal blooms affect the food web of tropical coastal ecosystems impacted by fisheries. Marine Environmental Research. 184, 105858.

Lauridsen, T.L., Lodge, D.M., 1996. Avoidance by Daphnia magna of fish and macrophytes: Chemical cues and predator-mediated use of macrophyte habitat. Limnology and Oceanography. 41, 794–798.

Lebedeva, L.P., 1972. A model of the latitudinal distribution of the numbers of species of phytoplankton in the sea. ICES Journal of Marine Science. 34, 341–350.

Lee, A.M., Sæther, B.E., Engen, S., 2020. Spatial covariation of competing species in a fluctuating environment. Ecology. 101, e02901.

Leng, R., 2009. The impacts of cultural eutrophication on lakes: A review of damages and nutrient control measures. Freshwater Systems and Society. 20, 37–38.

Leruste, A., Pasqualini, V., Garrido, M., Malet, N., De Wit, R., Bec, B., 2019. Physiological and behavioral responses of phytoplankton communities to nutrient availability in a disturbed Mediterranean coastal lagoon. Estuarine, Coastal and Shelf Science. 219, 176-188.

Levin, S.A., Segel, L.A., 1976. Hypothesis for origin of planktonic patchiness. Nature. 259, 659–659.

Levy, D., Harrington, H.A., Van Gorder, R.A., 2016. Role of seasonality on predator–prey–subsidy population dynamics. Journal of theoretical biology. 396, 163-181.

Li, H., Yu, Z., Cao, X., Song, X., 2023. Chitosan modification and its synergism with clay to mitigate harmful algal blooms. Environmental Technology & Innovation. 29, 103028.

Li, J., Song, Y.Z., Wan, H., Zhu, H.P., 2017. Dynamical analysis of a toxin-producing phytoplankton-zooplankton model with refuge. Mathematical Biosciences & Engineering. 14, 529–557.

Li, L., Liu, Z.C., 2010. Global stability and Hopf bifurcation of a plankton model with time delay. Nonlinear Analysis: Theory, Methods & Applications. 72, 1737–1745.

Li, S., Tao, Y., Zhan, X.M., Dao, G.H., Hu, H.Y., 2020. UV-C irradiation for harmful algal blooms control: A literature review on effectiveness, mechanisms, influencing factors and facilities. Science of The Total Environment. 723, 137986.

Li, X.D., Yang, X.Y., Huang, T.W., 2019. Persistence of delayed cooperative models: Impulsive control method. Applied Mathematics and Computation. 342, 130–146.

Li, X.Y., Jiang, D.Q., Mao, X.R., 2009. Population dynamical behavior of Lotka–Volterra system under regime switching. Journal of Computational and Applied Mathematics. 232, 427–448.

Li, X.Y., Mao, X.R., 2009. Population dynamical behavior of non-autonomous Lotka–Volterra competitive system with random perturbation. Discrete & Continuous Dynamical Systems. 24, 523–545.

Li, X.Y., Yu, R.C., Geng, H.X., Li, Y.F., 2021. Increasing dominance of dinoflagellate red tides in the coastal waters of Yellow Sea, China. Marine Pollution Bulletin. 168, 112439.

Li, Y., Tang, C., Wang, C., Anim, D.O., Yu, Z., Acharya, K., 2013. Improved Yangtze River diversions: are they helping to solve algal bloom problems in Lake Taihu, China? Ecological Engineering. 51, 104–116.

Liao, Q., Chang, H.X., Fu, Q., Huang, Y., Xia, A., Zhu, X., Zhong, N., 2018. Physiological-phased kinetic characteristics of microalgae Chlorella vulgaris growth and lipid synthesis considering synergistic effects of light, carbon and nutrients. Bioresource Technology. 250, 583–590.

Lin, J.N., Yan, T., Zhang, Q.C., Wang, Y.F., Liu, Q., Zhou, M.J., 2014. In situ detrimental impacts of Prorocentrum donghaiense blooms on zooplankton in the East China Sea. Marine Pollution Bulletin. 88, 302–310.

Lind, O., Davalos-Lind, L., Lopez, C., Lopez, M., Bressie, J.D., 2016. Seasonal morphological variability in an in situ Cyanobacteria monoculture: example from a persistent Cylindrospermopsis bloom in Lake Catemaco, Veracruz, Mexico. Journal of Limnology. 75, 66-80.

Liu, C., Liu, M., 2019. Stochastic dynamics in a nonautonomous prey-predator system with impulsive perturbations and Levy jumps. Communications in Nonlinear Science and Numerical Simulation. 78, 104851.

Liu, H., Dai, C.J., Yu, H.G., Guo, Q., Li, J.B., Hao, A.M., Kikuchi, J., Zhao, M., 2021a. Dynamics induced by environmental stochasticity in a phytoplankton-zooplankton system with toxic phytoplankton. Mathematical Biosciences and Engineering. 184, 4101–4126.

Liu, H., Dai, C.J., Yu, H.G., Guo, Q., Li, J.B., Hao, A.M., Kikuchi, J., Zhao, M., 2023. Dynamics of a stochastic non-autonomous phytoplankton–zooplankton system involving toxin-producing phytoplankton and impulsive perturbations. Mathematics and Computers in Simulation. 203, 368–386.

Liu, H., Li, X.X., Yang, Q.S., 2013. The ergodic property and positive recurrence of a multi-group Lotka–Volterra mutualistic system with regime switching. Systems & Control Letters. 62, 805–810.

Liu, M., Bai, C.Z., 2016. Analysis of a stochastic tri-trophic food-chain model with harvesting. Journal of Mathematical Biology. 73, 597–625.

Liu, M., Deng, M.L., 2020. Analysis of a stochastic hybrid population model with Allee effect. Applied Mathematics and Computation. 364, 124582.

Liu, M., Du, C.X., Deng, M.L., 2018. Persistence and extinction of a modified Leslie–Gower Holling-type II stochastic predator–prey model with impulsive toxicant input in polluted environments. Nonlinear Analysis: Hybrid Systems. 27, 177–190.

Liu, M., Wang, K., 2010. Persistence and extinction of a stochastic single-specie model under regime switching in a polluted environment. Journal of Theoretical Biology. 264, 934–944.

Liu, W., Qiu, R.L., 2007. Water eutrophication in China and the combating strategies. Journal of Chemical Technology & Biotechnology: International Research in Process, Environmental & Clean Technology. 82, 781–786.

Liu, X., Chen, L., Zhang, G., Zhang, J., Wu, Y., Ju, H., 2021b. Spatiotemporal dynamics of succession and growth limitation of phytoplankton for nutrients and light in a large shallow lake. Water Research. 194, 116910.

Liu, X.Z., Rohlf, K., 1998. Impulsive control of a Lotka-Volterra system. IMA Journal of Mathematical Control and Information. 15, 269–284.

Lobus, N.V., Kulikovskiy, M.S., 2023. The Co-Evolution Aspects of the Biogeochemical Role of Phytoplankton in Aquatic Ecosystems: A Review. Biology. 12, 92.

Lotka, A.J., 1925. Elements of physical biology. Williams & Wilkins.

Luo, Q., Mao, X., 2007. Stochastic population dynamics under regime switching. Journal of Mathematical Analysis and applications. 334, 69–84.

Lürling, M., 2021. Grazing resistance in phytoplankton. Hydrobiologia. 848, 237-249.

Lürling, M., Mello, M.M.E., Van Oosterhout, F., Domis, L.D.S., Marinho, M.M., 2018. Response of natural cyanobacteria and algae assemblages to a nutrient pulse and elevated temperature. Frontiers in Microbiology. 9, 1851.

Lv, Y., Cao, J., Song, J., Yuan, R., Pei, Y., 2014. Global stability and Hopf-bifurcation in a zooplankton–phytoplankton model. Nonlinear Dynamics. 76, 345–366.

Lv, Y.F., Pei, Y.Z., Gao, S., Li, C.G., 2010. Harvesting of a phytoplankton-zooplankton model. Nonlinear Analysis: Real World Applications. 11, 3608-3619.

Ma, Z., Yu, H., Thring, R., Dai, C., Shen, A., Zhao, M., 2018. Interaction between simulated dense Scenedesmus dimorphus (Chlorophyta) bloom and freshwater meta-zooplankton community. Journal of Limnology. 77, 255-265.

Ma, J.R., Qin, B.Q., Paerl, H.W., Brookes, J.D., Hall, N.S., Shi, K., Zhou, Y.Q., Guo, J.S., Li, Zhe., Xu, H., Wu, T.F., Long, S.X., 2016. The persistence of cyanobacterial (Microcystis spp.) blooms throughout winter in Lake Taihu, China. Limnology and Oceanography. 61, 711–722.

Mackas, D.L., Greve, W., Edwards, M., Chiba, S., Tadokoro, K., Eloire, D., Mazzocchi, M.G., Batten, S., Richardson, A.J., Johnson, C., Head, E., Conversi, A., Peluso, T., 2012.

Changing zooplankton seasonality in a changing ocean: Comparing time series of zooplankton phenology. Progress in Oceanography. 97, 31–62.

Majumder, A., Adak, D., Bairagi, N., 2021. Phytoplankton-zooplankton interaction under environmental stochasticity: Survival, extinction and stability. Applied Mathematical Modelling. 89, 1382–1404.

Malerba, M.E., Connolly, S.R., Heimann, K., 2012. Nitrate–nitrite dynamics and phytoplankton growth: Formulation and experimental evaluation of a dynamic model. Limnology and Oceanography. 57, 1555–1571.

Mandal, S., Ray, S., Roy, S., Jorgensen, S.E., 2006. Order to chaos and vice versa in an aquatic ecosystem. Ecological Modelling. 197, 498–504.

Mandal, A., Tiwari, P.K., Pal, S., 2021a. A nonautonomous model for the effects of refuge and additional food on the dynamics of phytoplankton-zooplankton system. Ecological Complexity. 46, 100927.

Mandal, A., Tiwari, P.K., Pal, S., 2021b. Impact of awareness on environmental toxins affecting plankton dynamics: a mathematical implication. Journal of Applied Mathematics and Computing. 66, 369-95.

Mandal, A., Tiwari, P.K., Samanta, S., Venturino, E., Pal, S., 2020. A nonautonomous model for the effect of environmental toxins on plankton dynamics. Nonlinear Dynamics. 99, 3373–3405.

Mao, X.R., Marion, G., Renshaw, E., 2002. Environmental Brownian noise suppresses explosions in population dynamics. Stochastic Processes and their Applications. 97, 95–110.

Mao, X.R., Yuan, C.G., 2006. Stochastic differential equations with Markovian switching. Imperial college press.

Mao, Z., Gu, X., Cao, Y., Zhang, M., Zeng, Q.F., Chen, H.H., Shen, R.J., Jeppesen, E., 2020. The role of top-down and bottom-up control for phytoplankton in a subtropical shallow eutrophic lake: evidence based on long-term monitoring and modeling. Ecosystems. 23, 1449-1463.

Mars Brisbin, M., Mitarai, S., 2019. Differential gene expression supports a resource‐intensive, defensive role for colony production in the bloom‐forming haptophyte, Phaeocystis globosa. Journal of Eukaryotic Microbiology. 66, 788-801.

May, R.M., 2019. Stability and complexity in model ecosystems. Princeton University Press.

May, R.M., 1974. Biological populations with nonoverlapping generations: Stable points, stable cycles and chaos. Science. 186, 645–647.

May, R.M., 1987. Chaos and the dynamics of biological populations. Proceedings of the Royal Society of London. A. Mathematical and Physical Sciences. 413, 27–44.

Mayersohn, B., Smith, K.S., Mangolte, I., Lévy, M., 2021. Intrinsic timescales of variability in a marine plankton model. Ecological Modelling. 443, 109446.

McCarthy M.J., James, R.T., Chen, Y.W., East, T.L., Gardner, W.S., 2009. Nutrient ratios and phytoplankton community structure in the large, shallow, eutrophic, subtropical Lakes Okeechobee (Florida, USA) and Taihu (China). Limnology. 10, 215–227.

McGillicuddy Jr, D.J., 2010. Models of harmful algal blooms: conceptual, empirical, and numerical approaches. Journal of marine systems: journal of the European Association of Marine Sciences and Techniques. 83, 105–107

McGowan, J.A., Deyle, E.R., Ye, H., Carter, M.L., Perretti, C.T., Seger, K. D., Verneil A.D., Sugihara, G., 2017. Predicting coastal algal blooms in southern California. Ecology. 98, 1419–1433.

Medvinsky, A.B., Petrovskii, S.V., Tikhonova, I.A., Malchow, H., Li, B.L., 2002. Spatiotemporal Complexity of Plankton and Fish Dynamics. SIAM Review. 44, 311–370.

Medvinsky, A.B., Petrovsk, S.V., Tikhonova, I.A., Venturino, E., Malchow, H., 2001. Chaos and regular dynamics in model multi-habitat plankton-fish communities. Journal of Biosciences. 26, 109–120.

Meerson, B., Sasorov, P.V., 2008. Noise-driven unlimited population growth. Physical Review E. 78, 060103.

Mello, F.D., Braidy, N., Marçal, H., Guillemin, G., Nabavi, S.M., Neilan, B.A., 2018. Mechanisms and effects posed by neurotoxic products of cyanobacteria/microbial eukaryotes/dinoflagellates in algae blooms: A review. Neurotoxicity Research. 33, 153-167.

Menden-Deuer, S., Montalbano, A.L., 2015. Bloom formation potential in the harmful dinoflagellate Akashiwo sanguinea: clues from movement behaviors and growth characteristics. Harmful Algae. 47, 75-85.

Meng, X.Y., Li, J., 2020. Stability and Hopf bifurcation analysis of a delayed phytoplankton-zooplankton model with Allee effect and linear harvesting. Mathematical Bioscience and Engineering. 17, 1973–2002.

Meng, X.Y., Wu, Y.Q., Li, J., 2020. Bifurcation analysis of a singular nutrient-plankton-fish model with taxation, protected zone and multiple delays. Numerical Algebra, Control and Optimization. 10, 391-423.

Milman, V.D., Myshkis, A.D., 1960. On the stability of motion in the presence of impulses. Sibirskii Matematicheskii Zhurnal. 1, 233-237.

Mishra, P., Naik, S., Babu, P.V., Pradhan, U., Begum, M., Kaviarasan, T., Vashi, A., Bandyopadhyay, D., Ezhilarasan, P., Panda, U.S., Murthy, M.V.R., 2022. Algal bloom, hypoxia, and mass fish kill events in the backwaters of puducherry, southeast coast of India. Oceanologia. 64, 396–403.

Misra, A., Tiwari, P., Venturino, E., 2016. Modeling the impact of awareness on the mitigation of algal bloom in a lake. Journal of Biological Physics. 42, 147–165.

Mitra, A., 2009. Are closure terms appropriate or necessary descriptors of zooplankton loss in nutrient–phytoplankton–zooplankton type models? Ecological Modelling. 220, 611–620.

Morro, B., Davidson, K., Adams, T.P., Falconer, L., Holloway, M., Dale, A., Aleynik, D., Thies, P.R., Khalid, F., Hardwick, J., Smith, H., Gillibrand, P.A., Rey‐Planellas, S., 2022. Offshore aquaculture of finfish: Big expectations at sea. Reviews in Aquaculture. 14, 791-815.

Moruff, A.K., Patric, A.R., Lawrence, O.O., 2016. Diversity of phytoplankton communities in a Tropical River Basin, Nigeria. Hydro Nepal: Journal of Water, Energy and Environment. 19, 52-56.

Møhlenberg, F., 1999. Effect of meteorology and nutrient load on oxygen depletion in a Danish micro-tidal estuary. Aquatic Ecology. 33, 55–64.

Møller, J.K., Madsen, H., Carstensen, J., 2011. Parameter estimation in a simple stochastic differential equation for phytoplankton modelling. Ecological modelling. 222, 1793–1799.

Mukhopadhyay, B., Bhattacharyya, R., 2006. Modelling phytoplankton allelopathy in a nutrient-plankton model with spatial heterogeneity. Ecological Modelling. 198, 163–173.

Nelson, N.G., Munoz-Carpena, R., Phlips, E.J., Kaplan, D., Sucsy, P., Hendrickson, J., 2018. Revealing biotic and abiotic controls of harmful algal blooms in a shallow subtropical lake through statistical machine learning. Environmental Science & Technology. 52, 3527-3535.

Neutel, A.M., Heesterbeek, J.A.P., de Ruiter, P.C., 2002. Stability in Real Food Webs: Weak Links in Long Loops. Science. 296, 1120–1123.

Nie, L.F., Teng, Z.D., Hu, L., 2011. Existence and stability of periodic solution of a stage-structured model with state-dependent impulsive effects. Mathematical Methods in the Applied Sciences. 34, 1685–1693.

Nwankwegu, A.S., Li, Y., Huang, Y., Wei, J., Norgbey, E., Sarpong, L., Lai, Q.Y., Wang, K., 2019. Harmful algal blooms under changing climate and constantly increasing anthropogenic actions: the review of management implications. 3 Biotech. 9, 1–19.

Odum, H.T., 1988. Self-organization, transformity, and information. Science. 242, 1132–1139.

Ojha, A., Thakur, N.K., 2020. Exploring the complexity and chaotic behavior in plankton–fish system with mutual interference and time delay. BioSystems. 198, 104283.

Orihel, D.M., Schindler, D.W., Ballard, N.C., Graham, M.D., O'Connell, D.W., Wilson, L.R., Vinebrooke, R.D., 2015. The “nutrient pump:” Iron‐poor sediments fuel low nitrogen-to-phosphorus ratios and cyanobacterial blooms in polymictic lakes. Limnology and Oceanography. 60, 856–871.

Otten, T.G., Paerl, H.W., 2011. Phylogenetic inference of colony isolates comprising seasonal Microcystis blooms in Lake Taihu, China. Microbial ecology. 62, 907–918.

Paerl, H.W., Barnard, M.A., 2020. Mitigating the global expansion of harmful cyanobacterial blooms: Moving targets in a human-and climatically-altered world. Harmful Algae. 96, 101845.

Paerl, H.W., Huisman, J., 2008. Blooms like it hot. Science. 320, 57–58.

Paerl, H.W., Otten, T.G., Kudela, R., 2018. Mitigating the expansion of harmful algal blooms across the freshwater-to-marine continuum. Environmental Science & Technology. 52, 5519-5529.

Pal, M., Yesankar, P.J., Dwivedi, A., Qureshi, A., 2020. Biotic control of harmful algal blooms (HABs): A brief review. Journal of Environmental Management. 268, 110687.

Pan, L., Cao, J., Hu, J., 2015. Synchronization for complex networks with Markov switching via matrix measure approach. Applied Mathematical Modelling. 39, 5636-5649.

Passarge, J., Hol, S., Escher, M., Huisman, J., 2006. Competition for nutrients and light: stable coexistence, alternative stable states, or competitive exclusion? Ecological Monographs. 76, 57–72.

Paul, P., Das, E., Kar, T.K., 2021. Reactivity and recovery in an exploited one prey two predators system at equilibrium. European Physical Journal Plus. 136, 1148.

Peng, S.G., Zhu, X.H., 2006. Necessary and sufficient condition for comparison theorem of 1-dimensional stochastic differential equations. Stochastic Processes and Their Applications. 116, 370–380.

Perry, J.N., Woiwod, I.P., Hanski, I., 1993. Using response-surface methodology to detect chaos in ecological time series. Oikos. 68, 329–339.

Peters, R.H., 1983. The Ecological Implications of Body Size. Cambridge University Press, Cambridge.

Pradhan, B., Kim, H., Abassi, S., Ki, J.S., 2022. Toxic Effects and Tumor Promotion Activity of Marine Phytoplankton Toxins: A Review. Toxins. 14, 397.

Raj, K.D., Mathews, G., Obura, D.O., Laju, R.L., Bharath, M.S., Kumar, P.D., Arasamuthu, A., Kumar, T.K.A., Edward, J.P., 2020. Low oxygen levels caused by Noctiluca scintillans bloom kills corals in Gulf of Mannar, India. Scientific Reports. 10, 22133.Ramin, M., Perhar, G., Shimoda, Y., Arhonditsis, G.B., 2012. Examination of the effects of nutrient regeneration mechanisms on plankton dynamics using aquatic biogeochemical modeling. Ecological Modelling. 240, 139–155.

Ralston, D.K., Moore, S.K., 2020. Modeling harmful algal blooms in a changing climate. Harmful Algae. 91, 101729.

Rathore, S.S., Chandravanshi, P., Chandravanshi, A., Jaiswal, K., 2016. Eutrophication: impacts of excess nutrient inputs on aquatic ecosystem. IOSR Journal of Agriculture and Veterinary Science. 9, 89-96.

Raymont, J.E.G.,1980. Plankton and Productivity in the Oceans: Vol. *1: Phytoplankton*. Pergamon Press, New York.

Rehim, M., Imran, M., 2012. Dynamical analysis of a delay model of phytoplankton–zooplankton interaction. Applied Mathematical Modelling. 36, 638–647.

Rehim, M., Zhang, Z.Z., Muhammadhaji, A., 2016. Mathematical analysis of a nutrient–plankton system with delay. SpringerPlus. 5, 1–22.

Reinl, K.L., Harris, T.D., North, R.L., Almela, P., Berger, S.A., Bizic, M., Burnet, S.H., Grossart H.P., Ibelings, B.W., Jakobsson, E., Knoll, L.B., Lafrancois, B.M., McElarney, Y., Morales-Williams, A.M., Obertegger , U., Ogashawara, I., Paule-Mercado, M.C., Peierls, B.L., Rusak, J.A., Sarkar, S., Sharma, S., Trout-Haney, J.V., Urrutia-Cordero, P., Venkiteswaran, J.J., Wain, D.J., Warner, K., Weyhenmeyer, G.A., Yokota, K., 2023. Blooms also like it cold. Limnology and Oceanography Letters.

Rhomad, H., Khalil, K., Neves, R., Bougadir, B., Elkalay, K., 2021. Modeling investigation of the nutrients and phytoplankton dynamics in the Moroccan Atlantic coast: A case study of Agadir coast. Ecological Modelling. 447, 109510.

Righetti, D., Vogt, M., Gruber, N., Psomas, A., Zimmermann, N.E., 2019. Global pattern of phytoplankton diversity driven by temperature and environmental variability. Science advances. 5, eaau6253.

Riley, G.A., Stommel, H., Bumpus, D.F., 1949. Quantitative ecology of the plankton of the western North Atlantic. Bulletin of the Bingham Oceanographic Collection. 12, 1–169.

Ruan, S.G., 1993. Persistence and coexistence in zooplankton-phytoplankton-nutrient models with instantaneous nutrient recycling. Journal of Mathematical Biology. 31, 633–654.

Ruan, S.G., 1995. The effect of delays on stability and persistence in plankton models. Nonlinear Analysis: Theory, Methods & Applications. 24, 575–585.

Ruan, S.G., 2001. Oscillations in plankton models with nutrient recycling. Journal of Theoretical Biology. 208, 15–26.

Ruan, S.G., He, X.Z., 1998. Global stability in chemostat-type competition models with nutrient recycling. SIAM Journal on Applied Mathematics. 58, 170-192.

Ruan, S.G., Wei, J.J., 2003. On the zeros of transcendental functions with applications to stability of delay differential equations with two delays. Dynamics of Continuous Discrete and Impulsive Systems Series A. 10, 863–874.

Ryther, J.H., Dunstan, W.M., 1971. Nitrogen, phosphorus, and eutrophication in the coastal marine environment. Science. 171, 1008–1013.

Sadhu, S., Thakur, S.C., 2017. Uncertainty and predictability in population dynamics of a bitrophic ecological model: Mixed-mode oscillations, bistability and sensitivity to parameters. Ecological Complexity. 32, 196-208.

Sajan., Dubey, B., 2021. Chaos control in a multiple delayed phytoplankton-zooplankton model with group defense and predator's interference. Chaos: An Interdisciplinary Journal of Nonlinear Science. 31, 083101.

Salmaso, N., 2010. Long-term phytoplankton community changes in a deep subalpine lake: responses to nutrient availability and climatic fluctuations. Freshwater Biology. 55, 825–846.

Sandhu, S.K., Morozov, A., Juan, L., 2020. Exploring the role of spatial and stoichiometric heterogeneity in the top-down control in eutrophic planktonic ecosystems. Journal of Theoretical Biology. 499, 110311.

Sandrini, G., Piel, T., Xu, T.S., White, E., Qin, H.J., Slot, P.C., Huisman, J., Visser, P.M., 2020. Sensitivity to hydrogen peroxide of the bloom-forming cyanobacterium Microcystis PCC 7806 depends on nutrient availability. Harmful Algae. 99, 101916.

Sandulescu, M., López, C., Hernández-García, E., Feudel, U., 2007. Plankton blooms in vortices: the role of biological and hydrodynamic timescales. Nonlinear Processes in Geophysics. 14, 443–454.

Sanseverino, I., Conduto, D., Pozzoli, L., Dobricic, S., Lettieri, T., 2016. Algal bloom and its economic impact. European Commission, Joint Research Centre Institute for Environment and Sustainability.

Sarkar, R.R., Pal, S., Chattopadhyay, J., 2005. Role of two toxin-producing plankton and their effect on phytoplankton–zooplankton system–a mathematical study supported by experimental findings. BioSystems. 80, 11–23.

Sarkar, S.K., 2018. Marine Algal Bloom: Characteristics, Causes and Climate Change Impacts (Vol. 4). Berlin/Heidelberg, Germany: Springer.

Schindler, D.E., Scheuerell, M.D., 2002. Habitat coupling in lake ecosystems. Oikos. 98, 177–189.

Schoffman, H., Lis, H., Shaked, Y., Keren, N., 2016. Iron–Nutrient Interactions within Phytoplankton. Frontiers in Plant Science. 7, 1223.

Segel, L.A., Jackson, J.L., 1972. Dissipative structure: An explanation and an ecological example. Journal of Theoretical Biology. 37, 545–559.

Sekerci, Y., Ozarslan, R., 2020. Oxygen-plankton model under the effect of global warming with nonsingular fractional order. Chaos, Solitons & Fractals. 132, 109532.

Sekerci, Y., Petrovskii, S., 2015. Mathematical modelling of plankton–oxygen dynamics under the climate change. Bulletin of mathematical biology. 77, 2325–2353.

Sekerci, Y., Petrovskii, S., 2018. Pattern formation in a model oxygen-plankton system. Computation. 6, 59.

Sengupta, A., Carrara, F., Stocker, R., 2017. Phytoplankton can actively diversify their migration strategy in response to turbulent cues. Nature. 543, 555–558.

Sharma, A., Sharma, A.K., Agnihotri, K., 2014. The dynamic of plankton–nutrient interaction with delay. Applied Mathematics and Computation. 231, 503–515.

Shen, L., Xu, H., Guo, X., 2012. Satellite Remote Sensing of Harmful Algal Blooms (HABs) and a Potential Synthesized Framework. Sensors. 12, 7778–7803.

Shen, X., Zhang, H., He, X., Shi, H., Stephan, C., Jiang, H., Wan, C., Eichholz, T., 2019. Evaluating the treatment effectiveness of copper-based algaecides on toxic algae Microcystis aeruginosa using single cell-inductively coupled plasma-mass spectrometry. Analytical and bioanalytical chemistry. 411, 5531-5543.

Sherratt, J.A., Smith, M.J., 2008. Periodic travelling waves in cyclic populations: field studies and reaction–diffusion models. Journal of the Royal Society Interface. 5, 483–505.

Shi, R., Ren, J., Wang, C., 2020. Stability analysis and Hopf bifurcation of a fractional order mathematical model with time delay for nutrient-phytoplankton-zooplankton. Mathematical Biosciences and Engineering. 17, 3836-3868.

Shu, H.Y., Hu, X., Wang, L., Watmough, J., 2015. Delay induced stability switch, multitype bistability and chaos in an intraguild predation model. Journal of mathematical biology. 71, 1269–1298.

Silva, E., Counillon, F., Brajard, J., Korosov, A., Pettersson, L.H., Samuelsen, A., Keenlyside, N., 2021. Twenty-one years of phytoplankton bloom phenology in the Barents, Norwegian, and north seas. Frontiers in Marine Science. 8, 746327.

Singh, R., Kumar Tiwari, S., Ojha, A., Kumar Thakur, N.,2023. Dynamical study of nutrient - phytoplankton model with toxicity: Effect of diffusion and time delay. Mathematical Methods in the Applied Sciences. 46, 490-509.

Smayda, T.J., 1998. Patterns of variability characterizing marine phytoplankton, with examples from Narragansett Bay. ICES Journal of Marine Science. 55, 562–573.

Smith, V.H., 1983. Low Nitrogen to Phosphorus Ratios Favor Dominance by Blue-Green Algae in Lake Phytoplankton. Science. 221, 669–671.

Sommer, U., 1991. A comparison of the droop and the monod models of nutrient limited growth applied to natural populations of phytoplankton. Functional Ecology. 5, 535–544.

Sommer, U., 2012. Plankton ecology: succession in plankton communities. Springer Science & Business Media.

Song, D., Fan, M., Chen, M., Wang, H., 2019. Dynamics of a periodic stoichiometric model with application in predicting and controlling algal bloom in Bohai Sea off China. Mathematical Biosciences and Engineering. 16, 119–138.

Song, D., Fan, M., Yan, S.H., Liu, M., 2020a. Dynamics of a nutrient-phytoplankton model with random phytoplankton mortality. Journal of Theoretical Biology. 488, 110119.

Song, M.Y., Zuo, W.J., Jiang, D.Q., Hayat, T., 2020b. Stationary Distribution and Extinction of Stochastic Beddington-DeAngelis Predator-prey Model with Distributed Delay. Journal of Nonlinear Modeling and Analysis. 2, 187–204.

Song, Y.L., Wei, J.J., 2005. Local Hopf bifurcation and global periodic solutions in a delayed predator–prey system. Journal of Mathematical Analysis and Applications. 301, 1–21.

Song, Z.G., Zhen, B., Xu, J., 2014. Species coexistence and chaotic behavior induced by multiple delays in a food chain system. Ecological Complexity. 19, 9–17.

Steele, J.H., Henderson, E.W., 1992. The role of predation in plankton models. Journal of Plankton Research. 14, 157–172.

Stelzer, J.A., Mesman, J.P., Gsell, A.S., de Senerpont Domis, L.N., Visser, P.M., Adrian, R., Ibelings, B.W., 2022. Phytoplankton responses to repeated pulse perturbations imposed on a trend of increasing eutrophication. Ecology and evolution. 12, e8675.

Strang, G., 1988. Linear algebra and its applications, thomson learning. Inc. United States.

Sultana, S., Awal, S., Shaika, N.A., Khan, S., 2022. Cyanobacterial blooms in earthen aquaculture ponds and their impact on fisheries and human health in Bangladesh. Aquaculture Research. 53, 5129-5141.

Sun, S.L., Sun, Y.R., Zhang, G., Liu, X.Z., 2017. Dynamical behavior of a stochastic two-species Monod competition chemostat model. Applied Mathematics and Computation. 298, 153–170.

Tang, C., Li, Y., Acharya, K., 2016. Modeling the effects of external nutrient reductions on algal blooms in hyper-eutrophic Lake Taihu, China. Ecological Engineering. 94, 164-173.

Tang, C., Li, Y., He, C., Acharya, K., 2020. Dynamic behavior of sediment resuspension and nutrients release in the shallow and wind-exposed Meiliang Bay of Lake Taihu. Science of the Total Environment. 708, 135131.

Thakur, N.K., Ojha, A., 2020. Complex plankton dynamics induced by adaptation and defense. Modeling Earth Systems and Environment. 6, 907-916.

Thakur, N.K., Ojha, A., Jana, D., Upadhyay, R.K., 2020. Modeling the plankton–fish dynamics with top predator interference and multiple gestation delays. Nonlinear Dynamics. 100, 4003-4029.

Thakur, N.K., Ojha, A., Tiwari, P.K., Upadhyay, R.K., 2021. An investigation of delay induced stability transition in nutrient-plankton systems. Chaos, Solitons & Fractals. 142, 110474.

Tian, C.R., 2012. Delay-driven spatial patterns in a plankton allelopathic system. Chaos. 22, 013129.

Tian, C.R., Ruan, S.G., 2019. Pattern Formation and Synchronism in an Allelopathic Plankton Model with Delay in a Network. SIAM Journal on Applied Dynamical Systems. 18, 531–557.

Tian, R.X., Chen, J.F., Sun, X.W., Li, D.W., Liu, C.X., Weng, H.X., 2018. Algae explosive growth mechanism enabling weather-like forecast of harmful algal blooms. Scientific Reports. 8, 1–7.

Titocci, J., Bon, M., Fink, P., 2022. Morpho-functional traits reveal differences in size fractionated phytoplankton communities but do not significantly affect zooplankton grazing. Microorganisms. 10, 182.

Tiwari, P.K., Roy, S., Misra, A.K., Upadhyay, R.K., 2022. Effect of seasonality on a nutrient-plankton system with toxicity in the presence of refuge and additional food. European Physical Journal Plus. 137, 368.

Tiwari, P.K., Samanta, S., Bona, F., Venturino, E., Misra, A.K., 2019. The time delays influence on the dynamical complexity of algal blooms in the presence of bacteria. Ecological Complexity. 39, 100769.

Treuer, G., Kirchhoff, C., Lemos, M.C., McGrath, F., 2021. Challenges of managing harmful algal blooms in US drinking water systems. Nature Sustainability. 4, 958-964.

Truscott, J., Brindley, J., 1994. Ocean plankton populations as excitable media. Bulletin of Mathematical Biology. 56, 981–998.

Turing, A.M., 1952. On the chemical basis of morphogenesis. Philosophical Transactions of the Royal Society B. 237, 37–72.

Turner, E.L., Bruesewitz, D.A., Mooney, R.F., Montagna, P.A., McClelland, J.M., Sadovski, A., Buskey, E.J., 2014. Comparing performance of five nutrient phytoplankton zooplankton (NPZ) models in coastal lagoons. Ecological Modelling. 277, 13–26.

Upadhyay, R.K., Volpert, V., Thakur, N.K., 2012. Propagation of Turing patterns in a plankton model. Journal of Biological Dynamics. 6, 524–538.

Valenti, D., Denaro, G., Spagnolo, B., Mazzola, S., Basilone, G., Conversano, F., Brunet, C., Bonanno, A., 2016. Stochastic models for phytoplankton dynamics in Mediterranean sea. Ecological Complexity. 27, 84–103.

Vanderley, R.F., Ger, K.A., Becker, V., Bezerra, M.G.T., Panosso, R., 2021. Abiotic factors driving cyanobacterial biomass and composition under perennial bloom conditions in tropical latitudes. Hydrobiologia. 848, 943-960.

Vanni, M.J., 1987. Effects of nutrients and zooplankton size on the structure of a phytoplankton community. Ecology. 68, 624–635.

Vanni, M.J., Layne, C.D., 1997. Nutrient recycling and herbivory as mechanisms in the “top–down” effect of fish on algae in lakes. Ecology. 78, 21–40.

Vellend, M., Srivastava, D.S., Anderson, K.M., Brown, C.D., Jankowski, J.E., Kleynhans, E.J., Kraft, N.J.B., Letaw, A.D., Macdonald, A.A.M., Maclean, J.E., Myers-Smith, I.H., Norris,

A.R., Xue, X.X., 2014. Assessing the relative importance of neutral stochasticity in ecological communities. Oikos. 123, 1420–1430.

Verreydt, D., De Meester, L., Decaestecker, E., Villena, M.J., Van Der Gucht, K., Vannormelingen, P., Vyverman, W., Declerck, S.A.J., 2012. Dispersal-mediated trophic interactions can generate apparent patterns of dispersal limitation in aquatic metacommunities. Ecology Letters. 15, 218–226.

Villacorte, L.O., Tabatabai, S.A.A., Anderson, D.M., Amy, G.L., Schippers, J.C., Kennedy, M.D., 2015. Seawater reverse osmosis desalination and (harmful) algal blooms. Desalination. 360, 61-80.

Volterra, V., 1926. Fluctuations in the abundance of a species considered mathematically. Nature. 118, 558–560.

Wang, B.B., Zhao, M., Dai, C.J., Yu, H.G., Wang, N., Wang, P.F., 2016. Dynamics Analysis of a Nutrient-Plankton Model with a Time Delay. Discrete Dynamics in Nature and Society. 2016, 1–12.

Wang, H., Liu, M., 2020. Stationary distribution of a stochastic hybrid phytoplankton–zooplankton model with toxin-producing phytoplankton. Applied Mathematics Letters. 101, 106077.

Wang, J., Wu, J., 2009. Occurrence and potential risks of harmful algal blooms in the East China Sea. Science of The Total Environment. 407, 4012–4021.

Wang, L., Jiang, D., 2018. Ergodic property of the chemostat: A stochastic model under regime switching and with general response function. Nonlinear Analysis: Hybrid Systems. 27, 341-352.

Wang, Z., Deng, M., Liu, M., 2021. Stationary distribution of a stochastic ratio-dependent predator-prey system with regime-switching. Chaos, Solitons & Fractals. 142, 110462.

Ward, B.A., Dutkiewicz, S., Follows, M.J., 2014. Modelling spatial and temporal patterns in size-structured marine plankton communities: top–down and bottom–up controls. Journal of Plankton Research. 36, 31–47.

Wei, C.J., Fu, Y.J., 2020. Stationary Distribution and Periodic Solution of Stochastic Toxin-Producing Phytoplankton–Zooplankton Systems. Complexity. 2020, 4627571.

Wiles, P.J., van Duren, L.A., Häse, C., Larsen, J., Simpson, J.H., 2006. Stratification and mixing in the Limfjorden in relation to mussel culture. Journal of Marine Systems. 60, 129–143.

Winder, M., Berger, S.A., Lewandowska, A., Aberle, N., Lengfellner, K., Sommer, U., Diehl, S., 2012. Spring phenological responses of marine and freshwater plankton to changing temperature and light conditions. Marine Biology. 159, 2491–2501.

Wootton, K.L., Stouffer, D.B., 2016. Many weak interactions and few strong; food-web feasibility depends on the combination of the strength of species' interactions and their correct arrangement. Theoretical Ecology. 9, 185-195.

Wu, J.H., 1998. Symmetric functional differential equations and neural networks with memory. Transactions of the American Mathematical Society. 350, 4799–4838.

Wu, Z.X., Yu, Z.M., Song, X.X., Yuan, Y.Q., Cao, X.H., Liang, Y.B., 2013. The spatial and temporal characteristics of harmful algal blooms in the southwest Bohai sea. Continental Shelf Research. 59, 10–17.

Xiao, M., Li, M., Reynolds, C.S., 2018. Colony formation in the cyanobacterium Microcystis. Biological Reviews. 93, 1399–1420.

Xiao, Y., Li, Z., Guo, J., Fang, F., Smith, V.H., 2016. Succession of phytoplankton assemblages in response to large-scale reservoir operation: a case study in a tributary of the Three Gorges Reservoir, China. Environmental monitoring and assessment. 188, 1-20.

Xu, C.Q, Yuan, S.L., 2016. Competition in the chemostat: a stochastic multi-species model and its asymptotic behavior. Mathematical Biosciences. 280, 1–9.

Xu, C.Q., Yuan, S.L., Zhang, T.H., 2021. Competitive exclusion in a general multi-species chemostat model with stochastic perturbations. Bulletin of Mathematical Biology. 83, 1–17.

Yamamoto, Y., Shiah, F.K., Chen, Y.L., 2011. Importance of large colony formation in bloom-forming cyanobacteria to dominate in eutrophic ponds. Annales de Limnologie-International Journal of Limnology. 47, 167–173.

Yang, J., Zhao, M., 2012. A mathematical model for the dynamics of a fish algae consumption model with impulsive control strategy. Journal of Applied Mathematics. 2012, 452789.

Yang, Z., Geng, L.L., Wang, W., Zhang, J., 2012. Combined effects of temperature, light intensity, and nitrogen concentration on the growth and polysaccharide content of Microcystis aeruginosa in batch culture. Biochemical Systematics and Ecology. 41, 130-135.

Yang, Z., Wu, F., Gao, X., 2016. Strategy for management of lake-catchment system integrated with natural and anthropogenic factors in China. Physics and Chemistry of the Earth, Parts A/B/C. 96, 26-33.

Yannawar, V.B., 2022. Identification of freshwater zooplankton in Godavari River concerning food chain in aquatic ecosystem of Nanded, Maharashtra, India. International Journal of Agricultural and Natural Sciences. 15, 1-14.

Yu, X.W., Yuan, S.L., Zhang, T.H., 2019a. Asymptotic properties of stochastic nutrient-plankton food chain models with nutrient recycling. Nonlinear Analysis: Hybrid Systems. 34, 209–225.

Yu, X.W., Yuan, S.L., Zhang, T.H., 2019b. Survival and ergodicity of a stochastic phytoplankton–zooplankton model with toxin-producing phytoplankton in an impulsive polluted environment. Applied Mathematics and Computation. 347, 249–264.

Yu, Z., Song, X., Cao, X., Liu, Y., 2017. Mitigation of harmful algal blooms using modified clays: Theory, mechanisms, and applications. Harmful Algae. 69, 48–64.

Yuan, S.L., Zhang, T.H., 2012. Dynamics of a plasmid chemostat model with periodic nutrient input and delayed nutrient recycling. Nonlinear Analysis: Real World Applications. 13, 2104–2119.

Yuan, Y., 2012. A coupled plankton system with instantaneous and delayed predation. Journal of Biological Dynamics. 6, 148–165.

Zhang, F.X., Ye, Q., Chen, Q.L., Yang, K., Zhang, D.Y., Chen, Z.R., Lu, S.S., Shao, X.P., Fan, Y.X., Yao, L.M., Ke, L.N., Zheng, T.L., Xu, H., 2018. Algicidal activity of novel marine bacterium Paracoccus sp. strain Y42 against a harmful algal-bloom-causing dinoflagellate, Prorocentrum donghaiense. Applied and Environmental Microbiology. 84, e01015–18.

Zhang, H., Chen, L.S., Georgescu, P., 2017. Impulsive control strategies for pest management. Journal of Biological Systems. 15, 235–260.

Zhang, M., Song, G., Gelardi, D.L., Huang, L., Khan, E., Mašek, O., Parikh, S.J., Ok, Y.S., 2020. Evaluating biochar and its modifications for the removal of ammonium, nitrate, and phosphate in water. Water Research. 186, 116303.

Zhang, S.Q., Meng, X.Z., Feng, T., Zhang, T.H., 2017a. Dynamics analysis and numerical simulations of a stochastic non-autonomous predator–prey system with impulsive effects. Nonlinear Analysis: Hybrid Systems. 26, 19–37.

Zhang, S.W., Tan, D.J., 2015. Dynamics of a stochastic predator–prey system in a polluted environment with pulse toxicant input and impulsive perturbations. Applied Mathematical Modelling. 39, 6319–6331.

Zhang, Y., Chen, S.H., Gao, S.J., Wei, X., 2017b. Stochastic periodic solution for a perturbed non-autonomous predator–prey model with generalized nonlinear harvesting and impulses. Physica A: Statistical Mechanics and its Applications. 486, 347–366.

Zhao, D.L., 2016. Study on the threshold of a stochastic SIR epidemic model and its extensions. Communications in Nonlinear Science and Numerical Simulation. 38, 172–177.

Zhao, H.Y., Huang, X.X., Zhang, X.B., 2015. Hopf bifurcation and harvesting control of a bioeconomic planktonmodel with delay and diffusion terms. Physica A: Statistical Mechanics and its Applications. 421, 300–315.

Zhao, J.T., Wei, J.J., 2015. Dynamics in a diffusive plankton system with delay and toxic substances effect. Nonlinear Analysis: Real World Applications. 22, 66–83.

Zhao, J.X., Shao, Y.F., 2021. Stochastic periodic solution and permanence of a Holling–Leslie predator-prey system with impulsive effects. Journal of Mathematics. 2021, 6694479.

Zhao, Q.Y., Liu, S.T., Niu, X.L., 2019. Dynamic behavior analysis of a diffusive plankton model with defensive and offensive effects. Chaos, Solitons & Fractals. 129, 94–102.

Zhao, S.N., Yuan, S.L., Wang, H., 2020. Threshold behavior in a stochastic algal growth model with stoichiometric constraints and seasonal variation. Journal of Differential Equations. 268, 5113-5139.

Zhao, Y., Yuan, S.L., Zhang, T.H., 2016. The stationary distribution and ergodicity of a stochastic phytoplankton allelopathy model under regime switching. Communications in Nonlinear Science and Numerical Simulation. 37, 131–142.

Zhao, Y., Yuan, S.L., Zhang, T.H., 2017a. Stochastic periodic solution of a non-autonomous toxic-producing phytoplankton allelopathy model with environmental fluctuation. Communications in Nonlinear Science and Numerical Simulation. 44, 266–276.

Zhao, Z, Pang, L.Y., Song, X.Y., 2017b. Optimal control of phytoplankton–fish model with the impulsive feedback control. Nonlinear Dynamics. 88, 2003–2011.

Zhou, B.Q., Jiang, D.Q., Hayat, T., 2022. Analysis of a stochastic population model with mean-reverting Ornstein–Uhlenbeck process and Allee effects. Communications in Nonlinear Science and Numerical Simulation. 111, 106450.

Zhu, C., Yin, G, 2007. Asymptotic properties of hybrid diffusion systems. SIAM Journal on Control and Optimization. 46, 1155–1179.

Zhu, C., Yin, G., 2009. On competitive Lotka–Volterra model in random environments. Journal of Mathematical Analysis and Applications. 357, 154–170.

Zhuang, K., Li, Y., Gong, B., 2021. Stability Switches and Hopf Bifurcation Induced by Nutrient Recycling Delay in a Reaction-Diffusion Nutrient-Phytoplankton Model. Complexity. 2021, 7943788.

Zohdi, E., Abbaspour, M., 2019. Harmful algal blooms (red tide): a review of causes, impacts and approaches to monitoring and prediction. International Journal of Environmental Science and Technology. 16, 1789-1806.

Zou, X.L., Wang, K., 2014. Optimal harvesting for a stochastic regime-switching logistic diffusion system with jumps. Nonlinear Analysis: Hybrid Systems. 13, 32–44.

Zuo, W.J., Jiang, D.Q., 2016. Periodic solutions for a stochastic non-autonomous Holling–Tanner predator–prey system with impulses. Nonlinear Analysis: Hybrid Systems. 22, 191–201.

APPENDIX A. The proof of Theorem 3.1

Proof. As we have considered zero-flux boundary conditions, let $0 = \mu_0 < \mu_1 < \mu_2 < \cdots$ ($\mu_j = j^2/l^2, j \in \mathbb{N}_0 = \{0,\ 1,\ 2, \ldots\}$) be the eigenvalues of the operator $-\Delta$ on Ω with the homogeneous Neumann boundary condition. Following Dai et al. (2016), model (3.1) can be represented as an abstract functional differential equation in the abstract space $C([-\tau,\ 0],\ W)$. The linear form of model (3.1) around the equilibrium $E^*(N^*,\ P^*,\ Z^*)$ is given by:

$$\frac{dU(t)}{dt} = d\Delta U(t) + \Phi(U_t). \tag{A1}$$

where $D = diag(d_1, d_2, d_3)$ and

$$dom(d\Delta) = \left\{(N,\ P,\ Z)^T:\ N,\ P,\ Z\ \in C^3([0,\ l\pi],\ R),\ \frac{\partial N}{\partial x} = \frac{\partial P}{\partial x} = \frac{\partial Z}{\partial x} = 0,\ x = 0,\ l\pi\right\},$$

$$\Phi(\varphi) = \begin{pmatrix} -[(b + eP^*)\varphi_1(0) + (eN^*)\varphi_2(0)] \\ \beta P^*\varphi_1(-\tau) + \left(\frac{cP^*Z^*}{(h+P^*)^2} - rP^*\right)\varphi_2(0) - \frac{cP^*}{h+P^*}\varphi_3(0) \\ \frac{(d-\rho)hZ^*}{(h+P^*)^2}\varphi_2(0) \end{pmatrix}.$$

Following Wu (1998), the characteristic equation corresponding to Eq. (A1) is rewritten as follows:

$$\lambda y - d\Delta y - \Phi(e^{\lambda} y) = 0,\ y \in dom(d\Delta), y \neq 0. \tag{A2}$$

Define:

$$y = \sum_{j=0}^{+\infty} \Psi_j(x) \begin{pmatrix} y_{1,\ j} \\ y_{2,\ j} \\ y_{3,\ j} \end{pmatrix}, \tag{A3}$$

where $\Psi_j(x)$ composes of the eigenfunctions corresponding to the eigenvalues μ_j. On substituting Eq. (A3) into (A2), one can get:

$$\begin{pmatrix} -(b+eP^*+d_1\mu_j) & -(eN^*) & 0 \\ \beta P^* e^{-\lambda\tau} & \frac{cP^*Z^*}{(h+P^*)^2} - rP^* - d_2\mu_j & -\frac{cP^*}{h+P^*} \\ 0 & \frac{(d-\rho)hZ^*}{(h+P^*)^2} & -d_3\mu_j \end{pmatrix} \begin{pmatrix} y_{1,\,j} \\ y_{2,\,j} \\ y_{3,\,j} \end{pmatrix} = \lambda \begin{pmatrix} y_{1,\,j} \\ y_{2,\,j} \\ y_{3,\,j} \end{pmatrix},$$

$$j = 0,\ 1,\ 2, \ldots.$$

Thus, an equivalent equation of Eq. (A2) is obtained as follows:

$$\lambda^3 + B_j\lambda^2 + C_j\lambda + D_j e^{-\lambda\tau} + E\lambda e^{-\lambda\tau} + F_j = 0, j = 0,\ 1,\ 2, \ldots, \tag{A4}$$

where

$B_j = -(a_{11}+a_{22}) + (d_1+d_2+d_3)\frac{j^2}{l^2}$, $D_j = -a_{21}a_{12}d_3\frac{j^2}{l^2}$, $E = -a_{12}a_{21}$,

$C_j = a_{11}a_{22} - a_{23}a_{32} - (a_{11}d_2 + a_{22}d_1 + a_{11}d_3 + a_{22}d_3)\frac{j^2}{l^2} + (d_1d_3 + d_2d_3 + d_1d_2)\frac{j^4}{l^4}$,

$F_j = a_{11}a_{23}a_{32} + (a_{11}a_{22}d_3 - a_{23}a_{32}d_1)\frac{j^2}{l^2} - (a_{11}d_2d_3 + a_{22}d_1d_3)\frac{j^4}{l^4} + d_1d_2d_3\frac{j^6}{l^6}$,

with

$$a_{11} = -b - eP^*, a_{12} = -eN^*, a_{32} = \frac{(d-\rho)hZ^*}{(h+P^*)^2},$$

$$a_{21} = \beta P^*, a_{22} = \frac{cP^*Z^*}{(h+P^*)^2} - rP^*, a_{23} = -\frac{cP^*}{h+P^*}.$$

For $\tau = 0$, Eq. (A4) reduces to the following form:

$$\lambda^3 + B_j\lambda^2 + (C_j + E)\lambda + D_j + F_j = 0. \tag{A5}$$

Since $a_{21}a_{12} < 0$, one can have $D_j + F_j > 0$ in view of (***H*1**). Obviously, $\lambda = 0$ is not a solution of Eq. (A5). If $b > \max\left\{d - p, \frac{\alpha\beta}{m}\right\}$, then $B_j > 0$ and $C_j + E > 0$ for any $j \in \mathbb{N}_0$. Thus, Eq. (A5) has no positive roots, which yields Theorem 3.1.

This completes the proof.

APPENDIX B. The proof of Lemma 3.1

Proof. For the considered nutrient-plankton model (3.1) with $\tau > 0$. Following Ruan and Wei (2003), we assume $i\omega(\omega > 0)$ is a root of Eq. (A5). Putting $\lambda = i\omega$ into Eq. (A5), one can get the following two equations:

$$\begin{cases} -\omega^3 + C_j\omega = D_j\, sin(\omega\tau) - E\omega\, cos(\omega\tau), \\ -B_j\omega^2 + F_j = -D_j\, cos(\omega\tau) - E\omega\, sin(\omega\tau), \end{cases} \tag{B1}$$

which yields

$$\omega^6 + M_{1,j}\omega^4 + M_{2,j}\omega^2 + Z_j = 0,\ j = 0,\ 1,\ 2, ... \tag{B2}$$

where

$$M_{1,\,j} = B_j^2 - 2C_j,\ M_{2,\,j} = C_j^2 - 2B_jF_j - E^2,\ Z_j = F_j^2 - D_j^2.$$

Let $v = \omega^2$, then we define function $f(v)$ as follows:

$$f(v) = v^3 + M_{1,\,j}v^2 + M_{2,\,j}v + Z_j, \tag{B3}$$

In view of (***H1***), we have $Z_j > 0$, and denote $\Delta_1 = M_{1,\,j}^2 - 3M_{2,\,j}$. Evidently for $\Delta_1 < 0$, Eq. (B3) has no positive roots. However, if there exists $j_0 \in \mathbb{N}_0$ such that $\Delta_1 > 0$, then the equation $f'(v) = 0$ has the following two real roots:

$$x_{j_0,1} = \frac{-M_{1,\,j_0} + \sqrt{\Delta_1}}{3},\ \ x_{j_0,2} = \frac{-M_{1,\,j_0} - \sqrt{\Delta_1}}{3}.$$

For $Z_j > 0$ and $\Delta_1 > 0$, Eq. (B3) has two positive real roots if and only if $x_{j_0,1} > 0$ and $f(x_{j_0,1}) < 0$.

This completes the proof.

APPENDIX C. The proof of Lemma 3.2

Proof. Denote two positive roots of Eq. (B3) by $\chi_{j_0,1}$ and $\chi_{j_0,2}$, then the two positive roots of Eq. (B2) will be $\omega_{j_0,1}=\sqrt{\chi_{j_0,1}}$ and $\omega_{j_0,2}=\sqrt{\chi_{j_0,2}}$. From Eq. (B1), we obtain the critical value of time delay as:

$$\tau_{j_0,p}^{s}=\frac{1}{\omega_{j_0,p}}\left(arccos\frac{E\omega_{j_0,p}^{4}+\left(B_{j_0}D_{j_0}-C_{j_0}E\right)\omega_{j_0,p}^{2}-D_{j_0}F_{j_0}}{{D_{j_0}}^{2}+E^{2}\omega_{j_0,p}^{2}}+2s\pi\right)$$

$$(s=0,\ 1,\ 2,\cdots,\ p=1,\ 2). \tag{C1}$$

Obviously, the right side of Eq. (C1) is an increasing function of s. Thus, we have $\tau_c=min_{p=1,\ 2}\,\tau_{j_0,p}^{0}$. Let $\lambda(\tau)=\mu(\tau)+i\omega(\tau)$ be the root of Eq. (A4) such that

$$\mu\left(\tau_{j_0,p}^{s}\right)=0,\ \ \omega\left(\tau_{j_0,p}^{s}\right)=\omega_k\ ,(s=0,\ 1,\ 2,\ \cdots,\ p=1,\ 2). \tag{C2}$$

On differentiating both sides of Eq. (A4) with respect to τ, we obtain:

$$\left(\frac{d\lambda}{d\tau}\right)^{-1}=\frac{3\lambda^{2}+2B_j\lambda+C_j+Ee^{-\lambda\tau}}{\lambda(D_je^{-\lambda\tau}+E\lambda)e^{-\lambda\tau}}-\frac{\tau}{\lambda}, \tag{C3}$$

then

$$\frac{d\,Re\left(\lambda\left(\tau_{j_0,p}^{s}\right)\right)}{d\tau}=\frac{\omega_k^{2}}{\Delta_2}f'(\omega_k^{2}), \tag{C4}$$

where

$$\Delta_2=\left(D_{j_0}\omega_k\sin\left(\omega_k\tau_{j_0,p}^{s}\right)-E\omega_k^{2}\cos\left(\omega_k\tau_{j_0,p}^{s}\right)\right)^{2}$$

$$+\left(D_{j_0}\omega_k\cos\left(\omega_k\tau_{j_0,p}^{s}\right)+E\omega_k^{2}\sin\left(\omega_k\tau_{j_0,p}^{s}\right)\right)^{2}.$$

For convenience, we assume that $\tau_{j_0,1}^{s}<\tau_{j_0,2}^{s}$. Note that if Lemma 3.1 (ii) holds, then $f'(\chi_{j_0,1})>0$ and $f'(\chi_{j_0,2})<0$. Hence, $\frac{dRe\lambda(\tau)}{d\tau}|_{\tau=\tau_{j_0,1}^{s}}>0$, $\frac{dRe\lambda(\tau)}{d\tau}|_{\tau=\tau_{j_0,2}^{s}}<0,\ s=0,1,2,\ \cdots$.

This completes the proof.

APPENDIX D. The proof of Theorem 3.3

Proof. Let $U = (u, v, w)$, $U_t = (u_t,\ v_t,\ w_t)$, and $\tau = \tau^* + \mu$, $\mu \in R$. We will track the direction of Hopf bifurcation around the positive equilibrium and the stability of the bifurcating periodic solutions by using normal formal theory and the center manifold theorem of differential equations (Hassard et al., 1981).

In space C, Eq. (A1) can be rewritten as

$$\frac{dU}{dt} = \widetilde{D}\Delta U + L_\mu(U_t) + f(\mu, U_t), \tag{D1}$$

where $\widetilde{D} = (\tau^* + \mu)D$, and

$$L_\mu(\varphi) = (\tau^* + \mu)(B_1\varphi(0) + B_2\varphi(-1)), \tag{D2}$$

$f(\mu,\ \varphi) = (\tau^* + \mu) \cdot$

$$\begin{pmatrix} -e\varphi_1(0)\varphi_2(0) + \cdots \\ \beta\varphi_1(-1)\varphi_2(0) + \left(\frac{chZ^*}{(h+P^*)^3} - r\right)\varphi_2{}^2(0) - ch(h+P^*)^{-2}\varphi_2(0)\varphi_3(0) + \cdots \\ (\rho - d)hZ^*(h+P^*)^{-3}\varphi_2{}^2(0) + (d-\rho)h(h+P^*)^{-2}\varphi_2(0)\varphi_3(0) + \cdots \end{pmatrix},$$

$$B_1 = \begin{pmatrix} a_{11} & a_{12} & 0 \\ 0 & a_{22} & a_{23} \\ 0 & a_{32} & 0 \end{pmatrix},\ B_2 = \begin{pmatrix} 0 & 0 & 0 \\ a_{21} & 0 & 0 \\ 0 & 0 & 0 \end{pmatrix},$$

Here, $\varphi = (\varphi_1,\ \varphi_2,\ \varphi_3)^T \in C$. Hence, $\mu = 0$ is the Hopf bifurcation value of Eq. (D1).

On linearizing Eq. (D1) about $(0,\ 0)$, we get

$$\frac{dU}{dt} = \widetilde{D}\Delta U + L_\mu(U_t), \tag{D2}$$

Recall that Eq. (A4) has a pair of purely imaginary roots $\Lambda_j = \{i\omega_j\tau^*,\ -i\omega_j\tau^*\}$ with $\mu = 0$ and other roots have negative real parts. The solution operator of Eq. (D2) is a semigroup whose infinitesimal generator is given by

$$A_\mu\varphi = \begin{cases} \dot{\varphi}(\theta), & \theta \in [-r,\ 0), \\ \widetilde{D}\Delta\varphi(0) + L_\mu(\theta), & \theta \in 0. \end{cases}$$

Hence, Eq. (D2) can be rewritten in the abstract form as,

$$\dot{U}_t = A_\mu U_t + R(\mu,\ U_t), \tag{D3}$$

where

$$R(\mu,\ U_t) = \begin{cases} 0, & \theta \in [-1,0), \\ f(\mu,\ U_t), & \theta = 0. \end{cases}$$

Define $f_j = \left(\beta_j^1,\ \beta_j^2,\ \beta_j^3\right)$, where

$$\beta_j^1 = (b_j,\ 0,\ 0)^T,\ \beta_j^2 = (0,\ b_j,\ 0)^T,\ \beta_j^3 = (0,\ 0, b_j)^T,$$

$$b_j = \frac{cosjx/l}{\|cosjx/l\|},\ \|cos(jx/l)\| = \left(\int_0^{l\pi} cos^2(jx/l)\,dx\right)^{\frac{1}{2}}.$$

Denote by

$$c \cdot f_j = c_1\beta_j^1 + c_2\beta_j^2 + c_3\beta_j^3,\ c = (c_1,\ c_2,\ c_3)^T \in C([-\tau,\ 0], X),$$

and

$$\langle u,\ v\rangle = \int_0^{l\pi} [u_1\bar{v}_1 + u_2\bar{v}_2 + u_3\bar{v}_3]\,dx,$$

where $u = (u_1,\ u_2,\ u_3)$, $v = (v_1,\ v_2,\ v_3)$, $u,\ v \in X$.

For $\varphi = (\varphi_1,\ \varphi_2,\ \varphi_3)^T \in C$, we denote

$$\langle \varphi,\ f_j\rangle = \left(\langle \varphi_1,\ \beta_j^1\rangle,\ \langle \varphi_2,\ \beta_j^2\rangle,\ \langle \varphi_3,\ \beta_j^3\rangle\right)^T.$$

Now, we define

$$A_{\mu,j}\varphi_j b_j = \begin{cases} \dot{\varphi}_j(\theta) b_j, & \theta \in [-1,\ 0), \\ \int_{-r}^0 d\eta_j(\mu,\ \theta)\varphi_j(\theta) b_j, & \theta = 0. \end{cases}$$

Thus, we have

$$-\mu_j \widetilde{D}\varphi_j(0) + L_{\mu,\ j}(\varphi_j) = \int_{-1}^0 d\eta_j(\mu,\ \theta)\varphi_j(\theta), \tag{D4}$$

where

$$\eta_j(\mu,\ \theta) = \begin{cases} -(\tau^* + \mu)B_2, & \theta = -1 \\ 0, & \theta \in (-1,\ 0) \\ (\tau^* + \mu)(B_1 - \mu_j D), & \theta = 0. \end{cases}$$

Define $C^* = C([0,\ \tau],\ X)$ and a bilinear form $(\cdot\ ,\ \cdot)$ on $C^* \times C$ as follows:

$$(\psi, \varphi) = \sum_{k,j=0}^{\infty} (\psi_k,\ \varphi_j)_c \int_0^{l\pi} b_k b_j dx,$$

where $\psi = \sum_{j=0}^{\infty} \psi_j\, b_j \in C^*$, $\varphi = \sum_{j=0}^{\infty} \varphi_j\, b_j \in C$, $\varphi_j \in C$, $\psi_j \in C^*$.

Notice that $\int_0^{l\pi} b_k b_j = 0$ for $k \neq j$. Thus, we have

$$(\psi,\ \varphi) = \sum_{j=0}^{\infty} \left(\psi_j,\ \varphi_j\right)_c \left|b_j\right|^2,$$

where $(\cdot\ ,\ \cdot)_c$ is the bilinear form defined on $C^* \times C$, and satisfies the following equation:

$$\left(\psi_j,\ \varphi_j\right)_c = \bar{\psi}_j(0)\varphi_j(0) - \int_{-1}^{0} \int_0^{\theta} \bar{\psi}_j(\xi - \theta) d\eta_j(0,\ \theta)\varphi_j(\xi) d\xi.$$

Now, we define an adjoint operator A^* as follows:

$$A^*\psi(s) = \begin{cases} -\dot{\psi}(s), & s \in (0,\ 1], \\ \sum_{j=0}^{\infty} \int_{-1}^{0} d\eta_j(0,\ t)\varphi_j(-t) b_j, & s = 0. \end{cases}$$

Let $q(\theta)b_j = (1,\ q_1,\ q_2)^T e^{i\omega_j \tau^* \theta} b_j$, and $q^*(s)b_j = M(q_3,\ q_4,\ 1) e^{i\omega_j \tau^* s} b_j$ be the eigenfunctions of the operators A and A^* corresponding to the eigenvalues $i\omega_j$ and $-i\omega_j$, respectively. Thus, one can obtain the following equations:

$$\begin{pmatrix} i\omega_j - a_{11} + \frac{j^2}{l^2} d_1 & -a_{12} & 0 \\ -a_{21} e^{-i\omega_j \tau^*} & i\omega_j - a_{22} + \frac{j^2}{l^2} d_2 & -a_{23} \\ 0 & -a_{32} & i\omega_j + \frac{j^2}{l^2} d_3 \end{pmatrix} \begin{pmatrix} 1 \\ q_1 \\ q_2 \end{pmatrix} = 0,$$

and

$$\begin{pmatrix} i\omega_j + a_{11} - \frac{j^2}{l^2} d_1 & a_{21} e^{-i\omega_j \tau^*} & 0 \\ a_{12} & i\omega_j + a_{22} - \frac{j^2}{l^2} d_2 & a_{32} \\ 0 & a_{23} & i\omega_j - \frac{j^2}{l^2} d_3 \end{pmatrix} \begin{pmatrix} q_3 \\ q_4 \\ 1 \end{pmatrix} = 0,$$

By direct calculation, we obtain

$$q_1 = \frac{i\omega_j l^2 - a_{11} l^2 + j^2 d_1}{a_{12} l^2},\ q_2 = \frac{a_{32} l^2 \cdot q_1}{i\omega_j l^2 + j^2 d_3};$$

$$q_3 = \frac{l^2 a_{21} e^{-i\omega_j \tau^*} \cdot q_4}{j^2 d_1 - i\omega_j l^2 - a_{11} l^2},\ q_4 = \frac{j^2 d_3 - i\omega_j l^2}{a_{23} l^2}.$$

If we choose M such that $(q^*, q)_c = 1$, $(q^*, \bar{q})_c = 0$, then we have

$$M = \left(q_3 + \bar{q}_1 q_4 + \bar{q}_2 + \tau^* e^{i\omega_j \tau^*} a_{21} q_4\right)^{-1}.$$

This yields the decomposition $C = P \oplus Q$ by Λ_j with

$$P = \{zqb_j + \bar{z}\bar{q}b_j | z \in C\},$$

$$Q = \left\{\varphi \in C \middle| (\bar{q}^* b_j,\ \varphi) = 0\ and\ (q^* b_j,\ \varphi) = 0\right\}.$$

One can rewrite the solution of Eq. (D1) as follows:

$$U_t = (qz + \bar{q}\bar{z}) \cdot f_j + W(z,\ \bar{z}), \tag{D5}$$

where $W = \left(W^{(1)},\ W^{(2)},\ W^{(3)}\right)^T \in Q$. On the center manifold C_0, we have

$$W(t,\ \theta) = W_{20}(\theta)\frac{z^2}{2} + W_{11}(\theta) z\bar{z} + W_{02}(\theta)\frac{\bar{z}^2}{2} + \cdots. \tag{D6}$$

At $\tau = \tau^*$, z satisfies the following relation:

$$\dot{z}(t) = i\omega_j z(t) + \bar{q}^{*T}(0)\langle f(0,\ U_t),\ f_j\rangle. \tag{D7}$$

Next, we define

$$f(0, U_t)|_{C_0} = F(0,\ z,\ \bar{z}) = F''_{zz}\frac{z^2}{2} + F''_{z\bar{z}} z\bar{z} + F''_{\bar{z}\bar{z}}\frac{\bar{z}^2}{2} + \cdots.$$

For convenience, we rewrite Eq. (D7) in the following form:

$$\dot{z} = i\omega_j z + g(z,\ \bar{z}), \tag{D8}$$

where

$$g(z,\ \bar{z}) = g_{20}\frac{z^2}{2} + g_{11} z\bar{z} + g_{02}\frac{\bar{z}^2}{2} + \cdots. \tag{D9}$$

A simple computation will yield the following values:

$$g_{20} = 2\bar{M}\tau^*\left[-eq_1\bar{q}_3 + \beta q_1\bar{q}_4 e^{-i\omega_j\tau^*} + (chZ^*(h+P^*)^{-3} - r)\bar{q}_4 q_1^2 - ch(h+P^*)^{-2} q_1 q_2 \bar{q}_4 +\right.$$

$$\left.(\rho - d)hZ^*(h+P^*)^{-3} q_1^2 + (d-\rho)h(h+P^*)^{-2} q_1 q_2\right] \int_0^{l\pi} b_j^3 dx,$$

$$g_{11} = \bar{M}\tau^*\{-e(q_1 + \bar{q}_1)\bar{q}_3 + \bar{q}_4\left[\beta(\bar{q}_1 e^{-i\omega_j\tau^*} + q_1 e^{i\omega_j\tau^*}) + (chZ^*(h+P^*)^{-3} - r)2q_1\bar{q}_1\right.$$

$$\left.-ch(h+P^*)^{-2}(q_1\bar{q}_2 + \bar{q}_1 q_2)\right] + [(\rho - d)hZ^*(h+P^*)^{-3} 2q_1\bar{q}_1$$

$$+(d-\rho)h(h+P^*)^{-2}(q_1\bar{q}_2+\bar{q}_1q_2)]\}\int_0^{l\pi}b_j^3dx,$$

$$g_{02}=2\bar{M}\tau^*\{-e\bar{q}_1\bar{q}_3+\bar{q}_4[\beta\bar{q}_1e^{i\omega_j\tau^*}+(chZ^*(h+P^*)^{-3}-r)\bar{q}_1^2-ch(h+P^*)^{-2}\bar{q}_1\bar{q}_2]$$

$$+(\rho-d)hZ^*(h+P^*)^{-3}\bar{q}_1^2+(d-\rho)h(h+P^*)^{-2}\bar{q}_1\bar{q}_2\}\int_0^{l\pi}b_j^3dx,$$

$$g_{21}=2\bar{M}\tau^*\left\{\bar{q}_3(-e)\left[W_{11}^{(2)}(0)+\frac{1}{2}W_{20}^{(2)}(0)+\frac{1}{2}W_{20}^{(1)}(0)\bar{q}_1+W_{11}^{(1)}(0)q_1\right]\int_0^{l\pi}b_j^2dx\right.$$

$$+\bar{q}_4\left[\beta\left(W_{11}^{(1)}(-1)q_1+\frac{1}{2}W_{20}^{(1)}(-1)\bar{q}_1+\frac{1}{2}W_{20}^{(2)}(0)e^{i\omega_j\tau^*}+W_{11}^{2}(0)e^{-i\omega_j\tau^*}\right)\right.$$

$$+(chZ^*(h+P^*)^{-3}-r)\left(2q_1W_{11}^{(2)}(0)+W_{20}^{(2)}(0)\bar{q}_1\right)+(-ch(h+P^*)^{-2})$$

$$\times\left.\left(q_1W_{11}^3(0)+\frac{\bar{q}_1W_{20}^{(3)}(0)}{2}+\frac{W_{20}^{(2)}(0)}{2}\bar{q}_2+W_{11}^{(2)}(0)q_2\right)\right]\int_0^{l\pi}b_j^2dx$$

$$+\left[(\rho-d)hZ^*(h+P^*)^{-3}\cdot(2q_1W_{11}^{(2)}(0)+\bar{q}_1W_{20}^{(2)}(0))+(d-\rho)h(h+P^*)^{-2}\right.$$

$$\times\left.\left.\left(q_1W_{11}^{(3)}(0)+\frac{1}{2}W_{20}^{(3)}(0)\bar{q}_1+\bar{q}_2\frac{W_{20}^{(2)}(0)}{2}+q_2W_{11}^{(2)}(0)\right)\right]\int_0^{l\pi}b_j^2dx\right\}.$$

Now, we need to compute $W_{20}(\theta)$ and $W_{11}(\theta)$. From Eq. (D7), we have

$$\begin{aligned}\dot{W}&=\dot{U}_t-\dot{z}qb_j-\dot{\bar{z}}\bar{q}b_j\\&=\begin{cases}AW-2\,Re\{g(z,\ \bar{z})q(\theta)\}b_j & \theta\in[-r,\ 0)\\AW-2\,Re\{g(z,\ \bar{z})q(\theta)\}b_j+F, & \theta=0\end{cases}\\&=AW+H(z,\ \bar{z},\ \theta),\end{aligned}\tag{D10}$$

where

$$H(z,\ \bar{z},\ \theta)=H_{20}(\theta)\frac{z^2}{2}+H_{11}(\theta)z\bar{z}+H_{02}(\theta)\frac{\bar{z}^2}{2}+\cdots,\tag{D11}$$

Further, we obtain

$$H_{20}(\theta)=\begin{cases}-g_{20}q(\theta)b_j+\bar{g}_{02}\bar{q}(\theta)b_j & \theta\in[-r,\ 0),\\-g_{20}q(0)b_j+\bar{g}_{02}\bar{q}(0)b_j+F_{zz}^{''}, & \theta=0,\end{cases}$$

$$H_{11}(\theta)=\begin{cases}-g_{20}q(\theta)b_j+\bar{g}_{11}\bar{q}(\theta)b_j & \theta\in[-r,\ 0),\\-g_{11}q(0)b_j+\bar{g}_{11}\bar{q}(0)b_j+F_{z\bar{z}}^{''}, & \theta=0.\end{cases}$$

After differentiating both sides of Eq. (D6) and comparing the coefficient with Eq. (D10), we get

$$(A_0 - 2i\omega_0 I)W_{20}(\theta) = -H_{20}(\theta), \quad A_0 W_{11}(\theta) = -H_{11}(\theta), \ \cdots \tag{D12}$$

when $\theta \in [-1,\ 0)$. By the definition of A_μ and Eq. (D12), we have

$$W_{20}(\theta) = -\frac{g_{20}}{i\omega_j\tau^*}q(\theta)b_j - \frac{\bar{g}_{02}}{3i\omega_j\tau^*}\bar{q}(\theta)b_j + E_1 e^{2i\omega_j\tau^*\theta},$$

$$W_{11}(\theta) = \frac{g_{11}}{i\omega_j\tau^*}q(\theta)b_j - \frac{\bar{g}_{11}}{i\omega_j\tau^*}\bar{q}(\theta)b_j + E_2. \tag{D13}$$

Denote $E_1 = \sum_{j=1}^{\infty} E_1^j b_j$, $E_2 = \sum_{j=1}^{\infty} E_2^j b_j$. Thus, E_1^j and E_2^j satisfies the following relations:

$$\left(A_0 - 2i\omega_j\tau^* I\right)E_1^j b_j e^{2i\omega_0\tau^*}|_{\theta=0} = -\langle F_{zz}'',\ f_j\rangle b_j,$$

$$A_0 E_2^j b_j|_{\theta=0} = -\langle F_{z\bar{z}}'',\ f_j\rangle b_j, \quad j = 1,\ 2,\ \cdots. \tag{D14}$$

where

$$F_{zz}'' = \sum_{j=1}^{\infty}\langle F_{zz}',\ f_j\rangle b_j,\ F_{z\bar{z}}'' = \sum_{j=1}^{\infty}\langle F_{z\bar{z}}',\ f_j\rangle b_j,$$

$$E_1^j = \left(2i\omega_j\tau^* I - \int_{-1}^{0} e^{2i\omega_j\tau^*\theta}\, d\eta_j(0,\ \theta)\right)^{-1}\langle F_{zz}'',\ f_j\rangle,$$

$$E_2^j = -\left(\int_{-1}^{0} d\eta_j(0,\ \theta)\right)^{-1}\langle F_{z\bar{z}}'',\ f_j\rangle.$$

Thus, we have

$$E_1^j = \begin{pmatrix} 2i\omega_j\tau^* + \frac{j^2 d_1}{l^2} - a_{11} & -a_{12} & 0 \\ -a_{21}e^{-2i\omega_j\tau^*} & 2i\omega_j\tau^* + \frac{j^2 d_2}{l^2} - a_{22} & -a_{23} \\ 0 & -a_{32} & 2i\omega_j\tau^* + \frac{j^2 d_3}{l^2} \end{pmatrix}^{-1} \langle F_{zz}'',\ f_j\rangle,$$

$$E_2^j = \begin{pmatrix} \frac{j^2 d_1}{l^2} - a_{11} & -a_{12} & 0 \\ -a_{21} & \frac{j^2 d_2}{l^2} - a_{22} & -a_{23} \\ 0 & -a_{32} & \frac{j^2 d_3}{l^2} \end{pmatrix}^{-1} \langle F_{z\bar{z}}'',\ f_j\rangle.$$

Thus, one can compute the value of g_{21}. Finally, we will compute the values of the following

quantities:

$$C_1(0) = \frac{i}{2\omega_j}\left(g_{20}g_{11} - 2|g_{11}|^2 - \frac{1}{3}|g_{02}|^2\right) + \frac{g_{21}}{2},$$

$$\mu_2 = -\frac{Re\{C_1(0)\}}{Re\,\lambda'(0)},$$

$$T_2 = -\frac{Im\{C_1(0)\} + \mu_2\, Im\,\lambda'(0)}{\omega_j},$$

$$\beta_2 = 2\,Re\{C_1(0)\},$$

The signs of μ_2, β_2 and T_2 will determine the properties of the Hopf bifurcation. Specifically, μ_2 determines the direction of the Hopf bifurcation, if $\mu_2 > 0 (< 0)$, Hopf bifurcation is supercritical (subcritical); β_2 determines the stability of the bifurcation periodic solutions, with the solutions being stable (unstable) when $\beta_2 < 0 (> 0)$; T_2 determines the period of the bifurcating periodic solutions, such that the period increases (decreases) when $T_2 > 0 (< 0)$.

This completes the proof.

APPENDIX E. Auxiliar Lemmas

Lemma E.1 *(Liu and Bai, 2016). Suppose that* $z(t) \in C(\Omega \times [0, +\infty), R_+)$.

(i) If there exist two positive constants T *and* λ_0 *such that* $\ln z(t) \leq \lambda t - \lambda_0 \int_0^t z(s)\, ds + \sum_{i=1}^n \alpha_i B_i(t)$ *for all* $t \geq T$*, where* $\alpha_i, i = 1, 2, \cdots, n$*, are constants, then*

$$\begin{cases} \lim\limits_{t \to +\infty} \sup t^{-1} \int_0^t Z(s)\, ds \leq \lambda/\lambda_0 \quad a.s., \ \ if \ \ \lambda \geq 0; \\ \lim\limits_{t \to +\infty} z(t) = 0 \quad a.s., \ \ if \ \lambda < 0. \end{cases}$$

(ii) If there exist three positive constants T*,* λ *and* λ_0 *such that* $\ln z(t) \geq \lambda t - \lambda_0 \int_0^t z(s)\, ds + \sum_{i=1}^n \alpha_i B_i(t)$ *for all* $t \geq T$*, then* $\lim\limits_{t \to +\infty} inf\ t^{-1} \int_0^t z(s)\, ds \geq \lambda/\lambda_0$ *a.s.*

Lemma E.2 *(see e.g. Liptser, 1980). Assuming that* $M(t)$*,* $t \geq 0$*, is a local martingale vanishing at time zero. Then*

$$\lim_{t \to +\infty} \rho_M(t) < +\infty \Longrightarrow \lim_{t \to +\infty} \frac{M(t)}{t} = 0 \quad a.s.,$$

where

$$\rho_M(t) = \int_0^t \frac{d\langle M, M\rangle(s)}{(1+s)^2}, \quad t \geq 0,$$

and $\langle M, M\rangle(t)$ *is Meyer's angle bracket process.*

APPENDIX F. The proof of Lemma 4.1

Proof. We consider the following model

$$\begin{cases} dx(t) = \left[r_1 - \beta_1 - b_1 e^{x(t)} - \frac{\alpha(1-m)e^{y(t)}}{n+(1-m)e^{x(t)}}\right] dt + \alpha_1 dB_1(t) \\ dy(t) = \left[r_2 - \beta_2 - \frac{c\alpha e^{y(t)}}{n+(1-m)e^{x(t)}}\right] dt + \alpha_2 dB_2(t) \end{cases} \tag{F1}$$

on $t \geq 0$ with initial value $x(0) = \ln x_1(0)$, $y(0) = \ln x_2(0)$.

Obviously, the coefficients of model (F1) satisfy the local Lipschitz condition, then there exists a unique local solution on $[0, \tau_e)$, where τ_e is the explosion time. Therefore, one can see that $x_1(t) = e^{x(t)}$, $x_2(t) = e^{y(t)}$ is the unique positive local solution to model (4.1) with any initial value $(x_1(0), x_2(0)) \in [0, \tau_e)$. To show this solution is global, we need to verify $\tau_e = +\infty$.

Considering the following auxiliary equations:

$$d\Phi(t) = \Phi(t)\big(r_1 - b_1\Phi(t)\big)dt + \alpha_1\Phi(t)dB_1(t), \Phi(0) = x_1(0); \tag{F2}$$

$$d\psi(t) = \psi(t)\left(r_2 - \frac{c\alpha}{n}\psi(t)\right)dt + \alpha_2\psi(t)dB_2(t), \psi(0) = x_2(0); \tag{F3}$$

$$d\Psi(t) = \Psi(t)\left(r_2 - \frac{c\alpha}{n+(1-m)\Phi(t)}\Psi(t)\right)dt + \alpha_2\Psi(t)dB_2(t), \Psi(0) = x_2(0); \tag{F4}$$

According to the comparison theorem for stochastic equation (Peng and Zhu,2006), one can get the following results for $t \in [0, \tau_e)$,

$$x_1(t) \leq \Phi(t),\ \psi(t) \leq x_2(t) \leq \Psi(t), \text{ a.s.} \tag{F5}$$

By Lemma 4.2 in Bao et al. (2011), Eq. (F2) has the explicit formula

$$\Phi(t) = \frac{\exp\{(r_1-\beta_1)t+\alpha_1 B_1(t)\}}{x_1(0)^{-1}+b_1\int_0^t \exp\{(r_1-\beta_1)s+\alpha_1 B_1(s)\}ds}, \tag{F6}$$

is the unique solution of Eq. (F2). Similarly,

$$\psi(t) = \frac{\exp\{(r_2-\beta_2)t+\alpha_2 B_2(t)\}}{x_2(0)^{-1}+\frac{c\alpha}{n}\int_0^t \exp\{(r_2-\beta_2)s+\alpha_2 B_2(s)\}ds}, \tag{F7}$$

$$\Psi(t) = \frac{\exp\{(r_2-\beta_2)t+\alpha_2 B_2(t)\}}{x_2(0)^{-1}+\int_0^t \frac{c\alpha}{n+(1-m)\Phi(s)}\exp\{(r_2-\beta_2)s+\alpha_2 B_2(s)\}ds} \tag{F8}$$

is the unique solution of Eqs. (F3) and (F4), respectively. It therefore follows that $\Phi(t)$, $\psi(t)$, and $\Psi(t)$ are existent on $t \geq 0$, then we have $\tau_e = +\infty$.

This completes the proof.

APPENDIX G. The proof of Lemma 4.2

Proof. Let T sufficiently large such that $0.5\exp\{(r_1-\beta_1)t\}\geq 1$ for $t\geq T$. Then when $t\geq T$, by Eq. (F6),

$$\Phi(t)=\frac{\exp\{(r_1-\beta_1)t+\alpha_1B_1(t)\}}{x_1(0)^{-1}+b_1\int_0^t\exp\{(r_1-\beta_1)s+\alpha_1B_1(s)\}ds}\leq\frac{\exp\{(r_1-\beta_1)t+\alpha_1B_1(t)\}}{b_1\int_0^t\exp\{(r_1-\beta_1)s+\alpha_1B_1(s)\}ds}$$

$$\leq\frac{\exp\{(r_1-\beta_1)t+\alpha_1B_1(t)\}}{b_1\exp\left\{\min_{0\leq v\leq t}\alpha_1B_1(v)\right\}\int_0^t\exp\{(r_1-\beta_1)s\}ds}=\frac{r_1-\beta_1}{b_1}\frac{\exp\{(r_1-\beta_1)t+\alpha_1B_1(t)\}}{\exp\left\{\min_{0\leq v\leq t}\alpha_1B_1(v)\right\}[\exp\{(r_1-\beta_1)t\}-1]}$$

$$\leq\frac{2(r_1-\beta_1)}{b_1}\frac{\exp\{(r_1-\beta_1)t+\alpha_1B_1(t)\}}{\exp\left\{\min_{0\leq v\leq t}\alpha_1B_1(v)\right\}\exp\{(r_1-\beta_1)t\}}=\frac{2(r_1-\beta_1)}{b_1}\exp\left\{\alpha_1[B_1(t)-\min_{0\leq v\leq t}B_1(v)]\right\}$$

$$\leq\frac{2(r_1-\beta_1)}{b_1}exp\left\{|\alpha_1|[B_1(t)-\min_{0\leq v\leq t}B_1(v)]\right\}.$$

Noting that

$$\exp\left\{|\alpha_1|[B_1(t)-\min_{0\leq v\leq t}B_1(v)]\right\}>1.$$

Consequently, the following equation obtained:

$$\int_T^t\frac{c\alpha}{n+(1-m)\Phi(t)}\exp\{(r_2-\beta_2)s+\alpha_2B_2(s)\}\,ds$$

$$\geq\int_T^t\frac{c\alpha\exp\{(r_2-\beta_2)s+\alpha_2B_2(s)\}}{n+(1-m)\frac{2(r_1-\beta_1)}{b_1}\exp\left\{|\alpha_1|\left[B_1(s)-\min_{0\leq v\leq t}B_1(v)\right]\right\}}ds$$

$$\geq\int_T^t\frac{c\alpha\exp\{(r_2-\beta_2)s+\alpha_2B_2(s)\}}{\left[n+(1-m)\frac{2(r_1-\beta_1)}{b_1}\right]\exp\left\{|\alpha_1|\left[B_1(s)-\min_{0\leq v\leq t}B_1(v)\right]\right\}}ds$$

$$=\frac{b_1c\alpha}{b_1n+(1-m)2(r_1-\beta_1)}\int_T^t\exp\{(r_2-\beta_2)s+\alpha_2B_2(s)\}$$

$$\times\exp\left\{-|\alpha_1|\left[B_1(s)-\min_{0\leq v\leq t}B_1(v)\right]\right\}ds$$

$$\geq\frac{b_1c\alpha}{b_1n+(1-m)2(r_1-\beta_1)}\exp\left\{|\alpha_1|\left(\min_{0\leq v\leq s}B_1(v)-\max_{0\leq v\leq s}B_1(v)\right)\right\}$$

$$\times\exp\left\{\min_{0\leq v\leq s}\alpha_2B_2(v)\right\}\int_T^t\exp\{(r_2-\beta_2)s\}ds$$

$$=H_1(t)[\exp\{(r_2-\beta_2)t\}-\exp\{(r_2-\beta_2)T\}],$$

where

$$H_1(\mathrm{t}) = \frac{b_1 c\alpha}{b_1 n+(1-m)2(r_1-\beta_1)} \exp\left\{|\alpha_1|\left(\min_{0\le v\le s} B_1(v) - \max_{0\le v\le s} B_1(v)\right) + \min_{0\le v\le s} \alpha_2 B_2(v)\right\}.$$

Substituting the above inequality into Eq. (F8), we have

$$\begin{aligned}
\frac{1}{\Psi(t)} &\ge \exp\{-(r_2-\beta_2)(t-T) - \alpha_2\big(B_2(t)-B_2(T)\big)\} \\
&\quad \times [x_2(0)^{-1}(T) + H_1(t)(\exp\{(r_2-\beta_2)t\} - \exp\{(r_2-\beta_2)T\})] \\
&\ge \exp\{-(r_2-\beta_2)t + (r_2-\beta_2)T - \alpha_2 B_2(t) + \alpha_2 B_2(T)\} \\
&\quad \times [H_1(t)(\exp\{(r_2-\beta_2)t\} - \exp\{(r_2-\beta_2)T\})] \\
&= H_1(t)\exp\{(r_2-\beta_2)T - \alpha_2 B_2(t) + \alpha_2 B_2(T)\} \\
&\quad - H_1(t)\exp\{-(r_2-\beta_2)t + 2(r_2-\beta_2)T - \alpha_2 B_2(t) + \alpha_2 B_2(T)\} \\
&\ge \exp\{(r_2-\beta_2)T + \alpha_2 B_2(T)\}(1 - \exp\{-(r_2-\beta_2)(t-T)\}) \\
&\quad \times H_1(t)\exp\left\{-\max_{0\le v\le t} \alpha_2 B_2(v)\right\} \\
&=: M_1(t) \times H_2(t),
\end{aligned}$$

where

$$M_1(t) = \exp\{(r_2-\beta_2)T + \alpha_2 B_2(T)\}(1 - \exp\{-(r_2-\beta_2)(t-T)\}),$$

$$H_2(t) = H_1(t)\exp\left\{-\max_{0\le v\le t} \alpha_2 B_2(v)\right\}.$$

Hence,

$$t^{-1}\ln\Psi(t) \le -t^{-1}\ln M_1(t) - t^{-1}\ln H_2(t). \tag{G1}$$

Since $\alpha_i, i = 1,2$ are bounded, we obtain

$$\lim_{t\to+\infty} \frac{B_i(t)}{t} = 0 \text{ a.s., } i = 1,2, \tag{G2}$$

which implies

$$\lim_{t\to+\infty} t^{-1}\ln M_1(t) = 0, \quad \lim_{t\to+\infty} t^{-1}\ln H_2(t) = 0, \text{ a.s.}$$

Substituting the above identities and Eq. (G2) into Eq. (G1) leads to

$$\lim_{t\to+\infty} \sup t^{-1} \ln x_2(t) \le \lim_{t\to+\infty} \sup t^{-1} \ln \Psi(t) \le 0, \text{ a.s.} \tag{G3}$$

Now we need to prove $\lim_{t\to+\infty} t^{-1} \ln x_2(t) \ge 0$, a.s. Applying Ito's formula to (F4) gives

$$d \ln \psi(t) = \left[r_2 - \beta_2 - \frac{c\alpha}{n}\psi(t)\right] dt + \alpha_2 dB_2(t).$$

One can get that

$$t^{-1} \ln \psi(t) = t^{-1} \ln x_2(0) + r_2 - \beta_2 - t^{-1} \frac{c\alpha}{n} \int_0^t \psi(s)\, ds + \frac{\alpha_2 B_2(t)}{t}. \tag{G4}$$

From Eq. (G3) we obtain that for arbitrary $\varepsilon > 0$, there exist $T > 0$ such that for $t \ge T$,

$$-\varepsilon \le t^{-1} \ln x_2(0) \le \varepsilon,$$

Then it follows from Eq. (G4) that

$$t^{-1} \ln \psi(t) \le r_2 - \beta_2 + \varepsilon - t^{-1} \frac{c\alpha}{n} \int_0^t \psi(s) ds + \frac{\alpha_2 B_2(t)}{t},\ t \ge T, \tag{G5}$$

$$t^{-1} \ln \psi(t) \ge r_2 - \beta_2 - \varepsilon - t^{-1} \frac{c\alpha}{n} \int_0^t \psi(s) ds + \frac{\alpha_2 B_2(t)}{t},\ t \ge T. \tag{G6}$$

Let ε be sufficiently small such that $r_2 - \beta_2 - \varepsilon > 0$, then according to Lemma I.1, Eqs. (G5) and (G6), we have

$$\frac{n(r_2-\beta_2-\varepsilon)}{c\alpha} \le \lim_{t\to+\infty} \inf t^{-1} \int_0^t \psi(s) ds \le \lim_{t\to+\infty} \sup t^{-1} \int_0^t \psi(s) ds \le \frac{n(r_2-\beta_2+\varepsilon)}{c\alpha}, \text{ a.s.}$$

Due to the arbitrariness of ε, then

$$\lim_{t\to+\infty} t^{-1} \int_0^t \psi(s) ds = \frac{n(r_2-\beta_2)}{c\alpha}. \tag{G7}$$

Note that, $\lim_{t\to+\infty} \ln x_2(0)/t = 0$, $\lim_{t\to+\infty} \alpha_2 B_2(t)/t = 0$, and substitute Eq. (G7) into Eq. (G4), then we obtain $\lim_{t\to+\infty} t^{-1} \ln \psi(t) = 0$ a.s. Thus by Eq. (N6), $\lim_{t\to+\infty} \inf t^{-1} \ln x_2(t) \ge \lim_{t\to+\infty} t^{-1} \ln \psi(t) = 0$, a.s.

This completes the proof.

APPENDIX H. The proof of Theorem 4.1

Proof. Applying Ito's formula to model (4.1) gives

$$d\ln x_1(t) = \left[r_1 - \beta_1 - b_1 x_1(t) - \frac{\alpha(1-m)x_2(t)}{n+(1-m)x_1(t)}\right]dt + \alpha_1 dB_1(t),$$

$$d\ln x_2(t) = \left[r_2 - \beta_2 - \frac{c\alpha x_2(t)}{n+(1-m)x_1(t)}\right]dt + \alpha_2 dB_2(t).$$

It follows that

$$\ln x_1(t) - \ln x_1(0) = (r_1 - \beta_1)\,t - b_1\int_0^t x_1(s)\,ds - \alpha\int_0^t \frac{(1-m)x_2(s)}{n+(1-m)x_1(s)}ds + \alpha_1 B_1(t), \quad \text{(H1)}$$

$$\ln x_2(t) - \ln x_2(0) = (r_2 - \beta_2)\,t - c\alpha\int_0^t \frac{x_2(s)}{n+(1-m)x_1(s)}ds + \alpha_2 B_2(t). \quad \text{(H2)}$$

Now we prove (i). According to Eq. (H1)

$$t^{-1}\ln\frac{x_1(t)}{x_1(0)} \le r_1 - \beta_1 - b_1\int_0^t x_1(s)ds + \frac{\alpha_1 B_1(t)}{t}.$$

Note that, $\lim_{t\to+\infty}\frac{B_1(t)}{t} = 0$ a.s. and $r_1 < \beta_1$, thus $\lim_{t\to+\infty} x_1(t) = 0$, a.s. Similarly, if $r_2 < \beta_2$, from Eq. (H2) we have $\lim_{t\to+\infty} x_2(t) = 0$, a.s.

(ii) If $r_1 < \beta_1$, thus (i) implies $\lim_{t\to+\infty} x_1(t) = 0$, a.s. Then, the following inequalities obtained for sufficiently large t

$$\ln x_2(t) - \ln x_2(0) \le (r_2 - \beta_2)\,t - c\alpha\int_0^t \frac{x_2(s)}{n+(1-m)\varepsilon}ds + \alpha_2 B_2(t), \quad \text{(H3)}$$

$$\ln x_2(t) - \ln x_2(0) \ge (r_2 - \beta_2)\,t - c\alpha(\kappa)\int_0^t \frac{x_2(s)}{n-(1-m)\varepsilon}ds + \alpha_2 B_2(t). \quad \text{(H4)}$$

Making use of Lemma E.1 to Eq. (H3) and (H4) respectively, we obtain

$$\frac{(r_2-\beta_2)(n-(1-m)\varepsilon)}{c\alpha} \le \lim_{t\to+\infty}\inf t^{-1}\int_0^t x_2(s)\,ds \le \lim_{t\to+\infty}\sup t^{-1}\int_0^t x_2(s)\,ds \le \frac{(r_2-\beta_2)(n+(1-m)\varepsilon)}{c\alpha},$$

Due to the arbitrariness of ε, $\lim_{t\to+\infty} t^{-1}\int_0^t x_2(s)\,ds = \frac{(r_2-\beta_2)n}{c\alpha}$, a.s.

The proof of (iii) is similar to (ii) and hence is omitted.

Now we prove (iv). By $(\text{H1})\times c - (\text{H2})\times(1-m)$,

$$t^{-1}c\ln\frac{x_1(t)}{x_1(0)} = t^{-1}(1-m)\ln\frac{x_2(t)}{x_2(0)} + c(r_1-\beta_1) - (1-m)(r_2-\beta_2) -$$

$$b_1 c t^{-1}\int_0^t x_1(s)ds + t^{-1}c\alpha_1 B_1(s) - t^{-1}(1-m)\alpha_2 B_2(t) \quad \text{(H5)}$$

Substituting Lemma 4.2 and Eq. (G3) into Eq. (H5), one can see that for sufficiently large t,

$$t^{-1}c\ln x_1(t) \le \varepsilon + c(r_1-\beta_1) - (1-m)(r_2-\beta_2).$$

When $m < 1 - \frac{(r_1-\beta_1)c}{r_2-\beta_2}$, then we can choose ε sufficiently small such that $\varepsilon + c(r_1-\beta_1) - (1-m)(r_2-\beta_2) < 0$, hence $\lim_{t\to+\infty} x_1(t) = 0$, a.s. It therefore follows that $\lim_{t\to+\infty} t^{-1}\int_0^t x_2(s)\,ds = \frac{(r_2-\beta_2)n}{c\alpha}$, a.s.

Finally, let us prove (v). By Eq. (H2) we have

$$t^{-1}\ln x_2(t) - t^{-1}\ln x_2(0) = (r_2-\beta_2) - c\alpha t^{-1}\int_0^t \frac{x_2(s)}{n+(1-m)x_1(s)}ds + \alpha_2 B_2(t)/t.$$

By virtue of Lemma 4.2 and Eq. (G3), one can see that

$$\lim_{t\to+\infty} t^{-1}\int_0^t \frac{x_2(s)}{n+(1-m)x_1(s)}ds = \frac{r_2-\beta_2}{c\alpha}, \text{ a.s.} \quad \text{(H6)}$$

It follows from Eq. (H1) that

$$t^{-1}\ln x_1(t) - t^{-1}\ln x_1(0) = (r_1-\beta_1) - t^{-1}b_1\int_0^t x_1(s)\,ds - t^{-1}\alpha\int_0^t \frac{(1-m)x_2(s)}{n+(1-m)x_1(s)}ds$$

$$+\alpha_1 B_1(t)/t. \quad \text{(H7)}$$

Substituting Eq. (G3) and (H6) into Eq. (H7), for sufficiently large t the following inequalities obtained:

$$t^{-1}\ln x_1(t) \ge (r_1-\beta_1) - \frac{\alpha(1-m)(r_2-\beta_2)}{c\alpha} - \varepsilon - t^{-1}b_1\int_0^t x_1(s)\,ds + \alpha_1 B_1(t)/t, \quad \text{(H8)}$$

$$t^{-1}\ln x_1(t) \le (r_1-\beta_1) - \frac{\alpha(1-m)(r_2-\beta_2)}{c\alpha} + \varepsilon - t^{-1}b_1\int_0^t x_1(s)\,ds + \alpha_1 B_1(t)/t. \quad \text{(H9)}$$

Let ε be sufficiently small such that $(r_1-\beta_1) - \frac{\alpha(1-m)(r_2-\beta_2)}{c\alpha} - \varepsilon > 0$. By Lemma E.1 and the arbitrariness of ε, we obtain

$$\lim_{t\to+\infty} t^{-1}\int_0^t x_1(s)\,ds = \frac{r_1-\beta_1}{b_1} - \frac{(1-m)(r_2-\beta_2)}{b_1 c}, \text{ a.s.}$$

This completes the proof.

APPENDIX I. The proof of Theorem 4.2

Proof. For the deterministic model corresponding to model (4.1), there is an interior equilibrium

$$x_1^* = \frac{r_1 c - r_2(1-m)}{bc},\ x_2^* = \frac{r_2(n+(1-m)x_1^*)}{c\alpha}, \tag{I1}$$

when $r_1 c > r_2(1-m)$.

From Ji et al. (2011), we know that a homogeneous Markov process $X(t)$ that exists in E_l (E_l denotes Euclidean l-space) can be described by the following stochastic equation

$$dX(t) = b(X)dt + \sum_{r=1}^{k} \sigma_r(X) dB_r(t). \tag{I2}$$

The diffusion matrix is

$$A(x) = \left(a_{ij}(x)\right), \qquad a_{ij}(x) = \sum_{r=1}^{k} \sigma_r^i(x)\sigma_r^j(x).$$

Assuming that if there exists a bounded domain $U \subset E_l$ with regular boundary Γ, satisfying the following properties, the Markov process $X(t)$ has a stationary distribution $\mu(\cdot)$ and it is ergodic.

(**B. 1**) In the domain U and some neighborhood thereof, the smallest eigenvalue of the diffusion matrix $A(x)$ is bounded away from zero.

(**B.2**) When $x \in E_l \backslash U$, the mean time τ at which a path issuing from x reaches the set U is finite, and $\sup_{x \in K} E_x \tau < \infty$ for every compact subset $K \subset E_l$.

Remark I.1. From the results in (Gard,1988; Strang, 1988), it is sufficient to prove F is uniformly elliptical in U, where $Fu = b(x)u_x + \frac{[tr(A(x)u_{xx})]}{2}$, that is, there exists a positive number M such that

$$\sum_{i,j=1}^{k} a_{ij}(x)\sigma_i\sigma_j \geq M \mid \sigma \mid^2,\ \ x \in U, \sigma \in R^k,$$

which yields (**B.1**). To verify (**B.2**), we need to prove that there exists some neighborhood U and a non-negative C^2-function such that for any $E_l \backslash U$, LV is negative (Zhu and Yin, 2007).

Remark I.2. According to Eq. (I2), model (4.1) can be written as

$$d\begin{pmatrix}x_1(t)\\x_2(t)\end{pmatrix}=\begin{pmatrix}x_1(t)\left(r_1-b_1x_1(t)-\frac{\alpha(1-m)x_2(t)}{n+(1-m)x_1(t)}\right)\\x_2(t)\left(r_2-\frac{c\alpha x_2(t)}{n+(1-m)x_1(t)}\right)\end{pmatrix}dt+\begin{pmatrix}\sigma_1x_1(t)\\0\end{pmatrix}dB_1(t)+$$

$$\begin{pmatrix}0\\\sigma_2x_2(t)\end{pmatrix}dB_2(t).$$

Here the diffusion matrix is

$$A(x_1,x_2)=\begin{pmatrix}\sigma_1^2x_1^2&0\\0&\sigma_2^2x_2^2\end{pmatrix}.$$

From above analysis, we know that there exists a solution $\left(x_1(t),x_2(t)\right)\in R_+^2$ of model (4.1) for any initial value $\left(x_1(0),x_2(0)\right)\in R_+^2$, and we write $x_1(t)$ and $x_2(t)$ as x_1 and x_2 respectively. Then, we construct a nonnegative function $V\colon E_l=R_+^2\to R_+$ as follows:

$$V(x_1,x_2)=\left[x_1-x_1^*-x_1^*ln\frac{x_1}{x_1^*}\right]+k\left[x_2-x_2^*-x_2^*ln\frac{x_2}{x_2^*}\right]\coloneqq V_1+kV_2,$$

where k is a positive constant to be determined later. It follows from Itô's formula that

$$\begin{aligned}dV_1&=\left(1-\frac{x_1^*}{x_1}\right)dx_1+\frac{1}{2}\frac{x_1^*}{x_1^2}(dx_1)^2\\&=(x_1-x_1^*)\left[\left(r_1-b_1x_1-\frac{\alpha(1-m)x_2}{n+(1-m)x_1}\right)dt+\sigma_1dB_1(t)\right]+\frac{1}{2}x_1^*\sigma_1^2dt\\&=(x_1-x_1^*)\left[\left(b_1x_1^*+\frac{\alpha(1-m)x_2^*}{n+(1-m)x_1^*}-b_1x_1-\frac{\alpha(1-m)x_2}{n+(1-m)x_1}\right)dt+\sigma_1dB_1(t)\right]+\frac{1}{2}x_1^*\sigma_1^2dt\\&=\left[-b(x_1-x_1^*)^2+\frac{\alpha(1-m)^2x_2^*(x_1-x_1^*)^2}{(n+(1-m)x_1^*)(n+(1-m)x_1)}-\frac{\alpha(1-m)(x_2-x_2^*)(x_1-x_1^*)}{(n+(1-m)x_1)}+\frac{1}{2}x_1^*\sigma_1^2\right]dt+\\&\quad\sigma_1dB_1(t)(x-x_1^*)\\&=\left[-b(x_1-x_1^*)^2+\frac{r_2(1-m)^2(x_1-x_1^*)^2}{c(n+(1-m)x_1)}-\frac{\alpha(1-m)(x_2-x_2^*)(x_1-x_1^*)}{(n+(1-m)x_1)}+\frac{1}{2}x_1^*\sigma_1^2\right]dt\\&\quad+\sigma_1dB_1(t)(x-x_1^*),\end{aligned}$$

and

$$dV_2 = \left(1 - \frac{x_2^*}{x_2}\right) dx_2 + \frac{1}{2}\frac{x_2^*}{x_2^2}(dx_2)^2$$

$$= (x_2 - x_2^*)\left[\left(r_2 - \frac{c\alpha x_2}{n+(1-m)x_1}\right)dt + \sigma_2 dB_2(t)\right] + \frac{1}{2}x_2^*\sigma_2^2 dt$$

$$= (x_2 - x_2^*)\left[\left(\frac{c\alpha x_2^*}{n+(1-m)x_1^*} - \frac{c\alpha x_2}{n+(1-m)x_1}\right)dt + \sigma_2 dB_2(t)\right] + \frac{1}{2}x_2^*\sigma_2^2 dt$$

$$= \left[\frac{-c\alpha(x_2-x_2^*)^2}{(n+(1-m)x_1)} + \frac{c\alpha(1-m)x_2^*(x_2-x_2^*)(x_1-x_1^*)}{(n+(1-m)x_1^*)(n+(1-m)x_1)} + \frac{1}{2}x_2^*\sigma_2^2\right]dt + \sigma_2 dB_2(t)(x - x_2^*)$$

$$= \left[\frac{-c\alpha(x_2-x_2^*)^2}{(n+(1-m)x_1)} + \frac{(1-m)r_2(x_2-x_2^*)(x_1-x_1^*)}{(n+(1-m)x_1)} + \frac{1}{2}x_2^*\sigma_2^2\right]dt + \sigma_2 dB_2(t)(x - x_2^*).$$

Then we have

$$dV = dV_1 + kdV_2$$

$$:= LVdt + \sigma_1(x_1 - x_1^*)dB_1(t) + k\sigma_2(x_2 - x_2^*)dB_2(t),$$

where

$$LV = -b(x_1 - x_1^*)^2 + \frac{r_2(1-m)^2(x_1-x_1^*)^2}{c(n+(1-m)x_1)} - \frac{-kc\alpha(x_2-x_2^*)^2}{(n+(1-m)x_1)}$$

$$-\frac{(1-m)(\alpha-kr_2)(x_2-x_2^*)(x_1-x_1^*)}{(n+(1-m)x_1)} + \frac{1}{2}\sigma_1^2 x_1^* + \frac{1}{2}k\sigma_2^2 x_2^*.$$

Let $k = \frac{\alpha}{r_2}$, we have

$$LV = -\frac{(bc(n+(1-m)x_1)-r_2(1-m)^2)(x_1-x_1^*)^2}{c(n+(1-m)x_1)} - \frac{-c\alpha^2(x_2-x_2^*)^2}{r_2(n+(1-m)x_1)} + \frac{1}{2}\alpha_1^2 x_1^* + \frac{1}{2}\frac{\alpha}{r_2}\alpha_2^2 x_2^*$$

$$\leq -\frac{bcn-r_2(1-m)^2(x_1-x_1^*)^2}{c(n+(1-m)x_1)} - \frac{-c\alpha^2(x_2-x_2^*)^2}{r_2(n+(1-m)x_1)} + \frac{1}{2}\alpha_1^2 x_1^* + \frac{1}{2}\frac{\alpha}{r_2}\alpha_2^2 x_2^*.$$

Thus,

$$(n + (1-m)x_1)LV \leq -\frac{bcn-r_2(1-m)^2}{c}(x_1 - x_1^*)^2 - \frac{-c\alpha^2(x_2-x_2^*)^2}{r_2}$$

$$+(n + (1-m)x_1)\left[\frac{1}{2}\sigma_1^2 x_1^* + \frac{1}{2}\frac{\alpha}{r_2}\sigma_2^2 x_2^*\right]$$

$$= -\frac{bcn-r_2(1-m)^2}{c}\left[x_1 - x_1^* - \frac{c}{4(bcn-r_2(1-m)^2)}\left(\sigma_1^2 x_1^* + \frac{\alpha}{r_2}\sigma_2^2 x_2^*\right)\right]^2 -$$

$$\frac{c\alpha^2}{r_2}(x_2 - x_2^*)^2 + \frac{c}{16(bcn - r_2(1-m)^2)}\left(\sigma_1^2 x_1^* + \frac{\alpha}{r_2}\sigma_2^2 x_2^*\right)^2$$

$$+\frac{1}{2}\left[n + \left(1 - m\frac{x_1}{x_1^*}\right)x_1^*\right]\left(\sigma_1^2 x_1^* + \frac{\alpha}{r_2}\sigma_2^2 x_2^*\right)$$

$$:= -\frac{bcn - r_2(1-m)^2}{c}\left[x_1 - x_1^* - \frac{c}{4(bcn - r_2(1-m)^2)}\left(\sigma_1^2 x_1^* + \frac{\alpha}{r_2}\sigma_2^2 x_2^*\right)\right]^2$$

$$-\frac{c\alpha^2}{r_2}(x_2 - x_2^*)^2 + \chi,$$

then if $\chi < \min\left\{\frac{bcn - r_2(1-m)^2}{c}\left[x_1^* + \frac{c}{4(bcn - r_2(1-m)^2)}\left(\sigma_1^2 x_1^* + \frac{\alpha}{r_2}\sigma_2^2 x_2^*\right)\right]^2, \frac{c\alpha^2}{r_2}(x_2^*)^2\right\}$, the ellipsoid $-\frac{bcn - r_2(1-m)^2}{c}\left[x_1 - x_1^* - \frac{c}{4(bcn - r_2(1-m)^2)}\left(\sigma_1^2 x_1^* + \frac{\alpha}{r_2}\sigma_2^2 x_2^*\right)\right]^2 - \frac{c\alpha^2}{r_2}(x_2 - x_2^*)^2 + \chi = 0$ lies entirely in R_+^2. We then choose U to be a neighborhood of the ellipsoid with $\overline{U} \subseteq E_l = R_+^2$, thus we have $LV < -C$(C is a positive constant) for $x_1 \in U \backslash E_l$, which yields condition (B.2). In addition, there is $M > 0$ such that

$$\sum_{i,j=1}^{2} \sigma_{ij}(x_1, x_2)\,\eta_i \eta_j = \sigma_1^2 x_1^2 \eta_1^2 + \sigma_2^2 x_2^2 \eta_2^2 \geq M \mid \eta^2 \mid \text{ all } (x_1, x_2) \in \overline{U}, \eta \in R^2,$$

which leads to condition (B.1). Therefore, the stochastic model (4.1) has a stable stationary distribution $\mu(\cdot)$ and it is ergodic.

This completes the proof.

APPENDIX J. The proof of Lemma 5.1

Proof. Applying Itô's formula to model (5.2) yields that

$$\frac{1}{t}\ln\frac{P(t)}{P(0)} = -\frac{1}{t}\int_0^t \left[c(t) + \frac{1}{2}\sigma_2^2(t) + \frac{\beta(t)Z(s)}{1+m(t)Z(s)+n(t)P(s)}\right] ds + \frac{1}{t}\int_0^t \alpha(t)N(s)\, ds + \frac{M_1(t)}{t}. \tag{J1}$$

$$\frac{1}{t}\ln\frac{Z(t)}{Z(0)} = -\frac{1}{t}\int_0^t \left[b(t) + \frac{1}{2}\sigma_3^2(t) - \frac{\beta(t)P(s)}{1+m(t)Z(s)+n(t)P(s)}\right] ds + \frac{M_2(t)}{t}. \tag{J2}$$

where $M_1(t) = \int_0^t \sigma_2(s)dB_2(s)$, $M_2(t) = \int_0^t \sigma_3(s)dB_3(s)$ are two martingales. Obviously, when $\lim_{t\to+\infty} P(t) = 0$ a.s., for arbitrary $0 < \epsilon < \min\left\{1, b^l + \frac{1}{2}\left(\sigma_3^l\right)^2\right\}$, there exists a measurable set $\Omega_\epsilon \subset \Omega$ with $P(\Omega_\epsilon) \geq 1-\epsilon$ and a constant $T = T(\epsilon) > 0$ such that for $\omega \in \Omega_\epsilon$ and $t > T$

$$\frac{1}{t}\int_0^t \frac{\beta(t)P(s)}{1+m(t)Z(s)+n(t)P(s)} ds + \frac{1}{t}\ln Z(0) < \epsilon, \quad t \geq T.$$

Combine this inequality with Eq. (J2), we have

$$t^{-1}\ln Z(t) = t^{-1}\ln Z(0) - \frac{1}{t}\int_0^t \left[b(s) + \frac{1}{2}\sigma_3^2(s) - \frac{\beta(s)P(s)}{1+m(s)Z(s)+n(s)P(s)}\right] ds + \frac{M_2(t)}{t}$$

$$\leq \epsilon - \frac{1}{t}\int_0^t \left[b\big(r(s)\big) + \frac{1}{2}\sigma_3^2\big(r(s)\big)\right] ds + \frac{M_2(t)}{t},$$

for $t \geq T$. By Lemma E.1 (i), we have $\lim_{t\to+\infty} Z(t) = 0$ a.s. and it follows that the conclusion holds for model (5.2).

This completes the proof.

APPENDIX K. The proof of Theorem 5.1

Proof. From Eqs. (5.3) and (5.4), we have

$$\lim_{t\to+\infty}\frac{M_i(t)}{t}=0 \text{ a.s., } i=1,2.$$

Define $V(N,\ P,\ Z,\ t)=u(t)[N(t)+P(t)+Z(t)]$, then we have the following equation:

$$\begin{aligned}dV(N,P,Z,t)&=u(t)d\big(N(t)+P(t)+Z(t)\big)+u'(t)(N(t)+P(t)+Z(t))dt\\&=\{u(t)D(t)S_0(t)-D(t)u(t)N(t)\}dt+u(t)\sigma_1(t)N(t)dB_1(t)\\&\quad-\big[\big(c(t)-h(t)\big)u(t)\big]P(t)dt+u(t)\sigma_2(t)P(t)dB_2(t)-\big[\big(b(t)-\\&\quad\delta(t)\big)u(t)\big]Z(t)dt+u(t)\sigma_3(t)Z(t)dB_3(t)+u'(t)(N(t)+P(t)+Z(t))dt\\&=\big\{u(t)D(t)S_0(t)-\alpha(t)N(t)-\big[\alpha(t)+\big(c(t)-h(t)-D(t)\big)u(t)\big]P(t)-\\&\quad\big[\alpha(t)+\big(b(t)-\delta(t)-D(t)\big)u(t)\big]Z(t)\big\}dt+u(t)\sigma_1(t)N(t)dB_1(t)+\\&\quad u(t)\sigma_2(t)P(t)dB_2(t)+u(t)\sigma_3(t)Z(t)dB_3(t).\end{aligned}$$

Thus,

$$\frac{1}{t}\int_0^t\alpha(s)\,N(s)ds=-\frac{1}{t}\int_0^t\big[\alpha(s)+\big(c(s)-h(s)-D(s)\big)u(s)\big]\ P(s)ds-\frac{1}{t}\int_0^t\big[\alpha(s)+\big(b(s)-$$

$$\delta(s)-D(s)\big)u(s)\big]Z(s)ds+\frac{1}{t}\int_0^t u(s)D(s)\,S_0(s)ds+\frac{\phi_1(t)}{t},\qquad\text{(K1)}$$

where

$$\begin{aligned}\phi_1(t)&=V(0)-V(t)+\int_0^t u(s)\sigma_1(s)N(s)dB_1(s)+\int_0^t u(s)\sigma_2(s)P(s)dB_2(s)\\&\quad+\int_0^t u(s)\sigma_3(s)Z(s)dB_3(s).\end{aligned}$$

From Eqs. (5.3), (5.4), we have $\lim_{t\to+\infty}\frac{\phi_1(t)}{t}=0$ a.s.

Substituting Eq. (K1) into Eq. (J1) yields

$$\frac{1}{t}\ln\frac{P(t)}{P(0)}=\frac{1}{t}\int_0^t\Big[u(s)D(s)S_0(s)-\Big(c(s)+\frac{1}{2}\sigma_2^2(s)\Big)\Big]ds-\frac{1}{t}\int_0^t\frac{\beta(s)Z(s)}{1+m(s)Z(s)+n(s)P(s)}ds-$$

$$\frac{1}{t}\int_0^t\big[\alpha(s)+\big(c(s)-h(s)-D(s)\big)u(s)\big]P(s)ds-\frac{1}{t}\int_0^t\big[\alpha(s)+\big(b(s)-\delta(s)-$$

$$D(s))u(s)]Z(s)ds + \frac{\phi_2(t)}{t}, \tag{K2}$$

where $\phi_2(t) = M_1(t) + \phi_1(t)$. One can get that $\lim_{t\to+\infty} \frac{\phi_2(t)}{t} = 0$ a.s., it then follows from the periodicity of periodic functions and Eq. (K2), we have

$$\lim_{t\to+\infty} \sup \frac{1}{t} \ln \frac{P(t)}{P(0)} \leq \frac{1}{\theta} \int_0^\theta \left[u(s)D(s)S_0(s) - \left(c(s) + \frac{1}{2}\sigma_2^2(s)\right)\right] ds = \Re_0^\theta \text{ a.s.}$$

Hence, when $\Re_0^\theta < 0$, we have $\lim_{t\to+\infty} P(t) = 0$ a.s. Then $\lim_{t\to+\infty} Z(t) = 0$ a.s. follows from Lemma 5.1.

Next, we prove (ii). From Eq. (K2), we have

$$\frac{1}{t} \ln \frac{P(t)}{P(0)} \leq \frac{1}{t} \int_0^t \left[u(s)D(s)S_0(s) - \left(c(s) + \frac{1}{2}\sigma_2^2(s)\right)\right] ds$$

$$- \frac{1}{t} \int_0^t [\alpha(s) + (c(s) - h(s) - D(s))u(s)] P(s)ds + \frac{\phi_2(t)}{t}, \tag{K3}$$

If $\Re_0^\theta > 0$, then the following result is obtained from Liu and Bai (2016)

$$\lim_{t\to+\infty} \sup \frac{1}{t} \int_0^t P(s)\, ds \leq \frac{\Re_0^\theta}{\vartheta(t)^l} \text{ a.s.} \tag{K4}$$

For Eq. (5.4), we obtain

$$\lim_{t\to+\infty} \sup \frac{1}{t} \ln \frac{Z(t)}{Z(0)} = -\lim_{t\to+\infty} \frac{1}{t} \int_0^t \left[b(s) + \frac{1}{2}\sigma_3^2(s)\right] ds + \lim_{t\to+\infty} \sup \frac{1}{t} \int_0^t \frac{\beta(s)P(s)}{1+m(s)Z(s)+n(s)P(s)} ds$$

$$\leq -\lim_{t\to+\infty} \frac{1}{\theta} \int_0^\theta \left[b(s) + \frac{1}{2}\sigma_3^2(s) - \frac{\beta(s)}{n(s)}\right] ds = \Re_1^\theta. \tag{K5}$$

Obviously, one can get that $\lim_{t\to+\infty} Z(t) = 0$ almost surely if $\Re_1^\theta < 0$. That is, for arbitrary $0 < \epsilon < 1$, there exist a set $\Omega_\epsilon \subset \Omega$ with $\mathbb{P}(\Omega_\epsilon) \geq 1 - \epsilon$ and a constant $\mathcal{F} = \mathcal{F}(\epsilon)$ such that $\max\left\{\frac{1}{t}\int_0^t \eta^u Z(s)ds, \frac{1}{t}\int_0^t \frac{\beta^u Z(s)}{1+m^l Z(s)+n^l P(s)} ds\right\} < \frac{\epsilon}{2}$, for $\omega \in \Omega_\epsilon$ and $t > \mathcal{F}$. By Eq. (K2), we have the following equation for sufficiently large t:

$$\frac{1}{t} \ln \frac{P(t)}{P(0)} \geq \frac{1}{t} \int_0^t \left[u(s)D(s)S_0(s) - \left(c(s) + \frac{1}{2}\sigma_2^2(s)\right) - \epsilon\right] ds$$

$$- \frac{1}{t} \int_0^t [\alpha(s) + (c(s) - h(s) - D(s))u(s)] P(s)ds + \frac{\phi_2(t)}{t},$$

Due to the arbitrariness of ϵ and Lemma E.1, we obtain

$$\lim_{t\to+\infty}\inf\frac{1}{t}\int_0^t P(s)\,ds \geq \frac{\Re_0^\theta}{\vartheta^u} \text{ a.s.}$$

This completes the proof of Theorem 5.1 (ii).

Finally, we prove (iii). By Eq. (5.3), it follows that the left side of Eq. (K5) is nonpositive, from Assumption 1, we have

$$\lim_{t\to\infty}\sup\frac{1}{t}\int_0^t \beta^l P(s)ds \leq \lim_{t\to\infty}\frac{1}{t}\int_0^t \left[b(s)+\frac{1}{2}\sigma_3^2(s)\right]ds + \iota \text{ a.s.} \tag{K6}$$

Then we take upper limit on both sides of Eq. (K2) and combine with Eq. (K6) yields

$$\begin{aligned}\limsup_{t\to\infty}\frac{1}{t}\ln\frac{P(t)}{P(0)} \geq{}& \lim_{t\to\infty}\frac{1}{t}\int_0^t \left[u(s)D(s)S_0(s)-\left(c(s)+\frac{1}{2}\sigma_2^2(s)\right)\right]ds-\frac{\beta^u}{m^l}-\\ &\limsup_{t\to\infty}\frac{1}{t}\int_0^t \vartheta^u P(s)\,ds-\liminf_{t\to\infty}\frac{1}{t}\int_0^t \eta^u Z(s)\,ds\\ \geq{}& \lim_{t\to\infty}\frac{1}{t}\int_0^t \left[u(s)D(s)S_0(s)-\left(c(s)+\frac{1}{2}\sigma_2^2(s)\right)\right]ds\\ &-\frac{\vartheta^u}{\beta^l}\lim_{t\to\infty}\frac{1}{t}\int_0^t \left[b(s)+\frac{1}{2}\sigma_3^2(s)\right]ds-\liminf_{t\to\infty}\frac{1}{t}\eta^u\int_0^t Z(s)\,ds-\frac{\beta^u}{m^l}.\end{aligned}$$

Applying Eq. (J1) again we have

$$\liminf_{t\to\infty}\frac{1}{t}\int_0^t Z(s)\,ds \geq \frac{\Re_0^\theta-\frac{\vartheta^u\frac{1}{\theta}\int_0^\theta\left[b(s)+\frac{1}{2}\sigma_3^2(s)\right]ds}{\beta^l}}{\eta^u}-\frac{\beta^u}{m^l\eta^u}=\frac{\Re_2^\theta}{\eta^u\beta^l}-\frac{\beta^u}{m^l\eta^u}\ a.s.$$

Obviously, $\liminf_{t\to\infty}\frac{1}{t}\int_0^t Z(s)ds > 0$ a.s. if $\Re_2^\theta > \frac{\beta^u\beta^l}{m^l}$.

This completes the proof.

APPENDIX L. The proof of Theorem 5.2

Proof. Since model (5.2) exists a global positive solution, according to Theorem 3.8 in Khasminskii (2011), we need to construct a $\theta-$periodic function $V(t,N,P,Z,t)\in C^2$ and a bounded closed set U_ϵ such that $\mathcal{L}V\le -1$ on $\mathbb{R}^3_+\backslash U_\epsilon$. Let $\underline{D}=\min\{D^l,(c-h)^l,(b-\delta)^l\}$, $(\overline{\sigma})^2=\max\limits_{i\in\{1,2,3\}}\{(\sigma_i^u)^2\}$, $m_3=\frac{\vartheta^u}{\beta^l}$, $m_4=\frac{\lambda^u+\beta^u}{b^l}$. Under $\min\{D^l,(c-h)^l,(b-\delta)^l\}>\frac{1}{2}\max\{(\sigma_1^u)^2,(\sigma_2^u)^2,(\sigma_3^u)^2\}$, there exist a constant $\kappa_2>0$, satisfying $\eta_2=\underline{D}-\frac{1}{2}(\overline{\sigma})^2(\kappa_2+1)>0$. Hence, we construct the C^2-function $V\colon\mathbb{R}^3_+\to\mathbb{R}$ as follows:

$$\begin{aligned}V(N,P,Z,t)&=M_2[-u(t)(N+P+Z)-\ln P-m_3\ln Z+m_4Z+\varpi(t)]\\&\quad-\ln N+\frac{1}{\kappa_2+2}(N+P+Z)^{\kappa_2+2}\\&\equiv M_2V_1+V_2+V_3,\end{aligned}$$

where

$M_2=\frac{2\beta^l}{\Re_2^\theta}\max\{2,r_2\}$,

$r_2=\sup\limits_{(N,P,Z)\in\mathbb{R}^3_+}\Big\{-\frac{1}{2}\eta_2(N^{k_2+2}+P^{k_2+2}+Z^{k_2+2})+m_4\beta^u(P^2+Z^2)+(M_2\vartheta^u+\alpha^u)P+\Gamma_2+D^u+\frac{1}{2}(\sigma_1^u)^2\Big\}$.

Here, Γ_2 is defined as in Eq. (L1), and define $\varpi'=u(t)D(t)S_0(t)-\frac{1}{2}\sigma_2^2(t)-c(t)-m_3\left(b(t)+\frac{1}{2}\sigma_3^2(t)\right)-m_3\Re_2^\theta$. Obviously, ϖ is a $\theta-$periodic function on $[0,+\infty)$ and $V(N,P,Z,t)$ is also $\theta-$periodic satisfying

$$\lim_{\epsilon\to\infty,(N,P,Z)\in\mathbb{R}^3_+\backslash U_\epsilon}\inf V(t,N,P,Z)=+\infty,$$

where $U_\epsilon=\left(\frac{1}{\epsilon},\epsilon\right)\times\left(\frac{1}{\epsilon},\epsilon\right)\times\left(\frac{1}{\epsilon},\epsilon\right)$. We need to find a closed set $U_\epsilon\in\mathbb{R}^3_+$ such that $\mathcal{L}V\le-1$ on $\mathbb{R}^3_+\backslash U_\epsilon$. By Itô's formula, we obtain

$$\mathcal{L}V_1 = -\{u(t)[D(t)(S_0(t)-N)+(h(t)-c(t))P+(\delta(t)-b(t))Z]+u'(t)(N+P+Z)\}-$$

$$\left[\alpha(t)N - c(t) - \frac{\beta(t)Z}{1+m(t)Z+n(t)P} - \frac{1}{2}\sigma_2^2(t)\right]$$

$$-m_3\left[\frac{\beta(t)P}{1+m(t)Z+n(t)P} - b(t) - \frac{1}{2}\sigma_3^2(t)\right] + m_4\left[\frac{\beta(t)PZ}{1+m(t)Z+n(t)P} - b(t)Z\right] + \varpi'(\mathrm{t})$$

$$= [u(t)D(k) - \alpha(t) - u'(t)]N + m_4\frac{\beta(t)PZ}{1+m(t)Z+n(t)P} + \varpi'(\mathrm{t})$$

$$-[u'(t) + (h(t)-c(t))u(t)]P - \frac{m_3\beta(t)P}{1+m(t)Z+n(t)P}$$

$$-[u'(t) + (\delta(t)-b(t))u(t) + m_4 b(t)]Z + \frac{\beta(t)Z}{1+m(t)Z+n(t)P}$$

$$-\left[u(t)D(t)S_0(t) - \frac{1}{2}\sigma_2^2(t) - c(t) - m_3\left(b(t) + \frac{1}{2}\sigma_3^2(t)\right)\right]$$

$$\leq -m_3\Re_2^\theta + m_4\beta^u PZ + \vartheta^u P.$$

Hence,

$$\mathcal{L}V_1 \leq -m_3\Re_2^\theta + m_4\beta^u PZ + \vartheta^u P.$$

Similarly, we have

$$\mathcal{L}V_2 = -\frac{D(t)S_0(t)}{N} + \alpha(t)P - h(t)\frac{P}{N} - \delta(t)\frac{Z}{N} + D(t) + \frac{1}{2}\sigma_1^2(t)$$

$$\leq -\frac{D^l S_0^l}{N} + \alpha^u P + D^u + \frac{1}{2}(\sigma_1^u)^2,$$

and

$$\mathcal{L}V_3 = (N+P+Z)^{k_2+1}[D(t)(S_0(t)-N) + h(t)P + \delta(t)Z - c(t)P - b(t)Z]$$

$$+\frac{1}{2}(k_2+1)(N+P+Z)^{k_2}[\sigma_1^2(t)N^2 + \sigma_2^2(t)P^2 + \sigma_3^2(t)Z^2]$$

$$\leq (N+P+Z)^{k_2+1}\left[D^u S_0^u - \underline{D}(N+P+Z)\right] + \frac{1}{2}(\overline{\sigma})^2(k_2+1)(N+P+Z)^{k_2+2}$$

$$= D^u S_0^u (N+P+Z)^{k_2+1} - \left(\underline{D} - \frac{1}{2}(\overline{\sigma})^2(k_2+1)\right)(N+P+Z)^{k_2+2}$$

$$\leq \Gamma_2 - \frac{1}{2}\eta_2(N+P+Z)^{k_2+2}$$

$$\leq \Gamma_2 - \frac{1}{2}\eta_2(N^{k_2+2} + P^{k_2+2} + Z^{k_2+2}).$$

where

$$\Gamma_2 = \sup_{(N,P,Z)\in\mathbb{R}_+^3} \left\{ D^u S_0^u (N+P+Z)^{k_2+1} - \frac{1}{2}\eta_2 (N^{k_2+2} + P^{k_2+2} + Z^{k_2+2}) \right\} < \infty. \quad \text{(L1)}$$

The above equations yield that

$$\mathcal{L}V(N,P,Z,k) \le -M_2 m_3 \Re_2^\theta + M_2 m_4 \beta^u \mathrm{PZ} + (M_2 \vartheta^u + \alpha^u) P - \frac{D^l S_0^l}{N}$$

$$-\frac{1}{2}\eta_2 (N^{k_2+2} + P^{k_2+2} + Z^{k_2+2}) + \Gamma_2 + D^u + \frac{1}{2}(\sigma_1^u)^2.$$

Define a closed set as follows

$$U_\epsilon = \left\{ (N,P,Z) \in \mathbb{R}_+^3 : \epsilon \le N \le \frac{1}{\epsilon}, \epsilon \le P \le \frac{1}{\epsilon}, \epsilon \le Z \le \frac{1}{\epsilon} \right\},$$

where $\epsilon > 0$ satisfies the following conditions:

$$-\frac{D^l S_0^l}{\epsilon} + \Theta_1 \le 1, \quad \text{(L2)}$$

$$-\frac{1}{4}\frac{2}{\epsilon^{k_2+2}} + \Theta_2 \le -1, \quad \text{(L3)}$$

$$0 < \epsilon < \frac{\Re_2^\theta}{4 m_4 \beta^l \beta^u}, \quad \text{(L4)}$$

$$0 < \epsilon < \frac{1}{M_2}, \quad \text{(L5)}$$

and Θ_1, Θ_2 are constants that are given in the expression (L6) and (L7), respectively.

Divide $\mathbb{R}_+^3 \backslash U_\epsilon$ into six domains:

$$U_\epsilon^1 = \{(N,P,Z) \in \mathbb{R}_+^3 : 0 < N < \epsilon\}, U_\epsilon^2 = \{(N,P,Z) \in \mathbb{R}_+^3 : 0 < P < \epsilon\},$$

$$U_\epsilon^3 = \{(N,P,Z) \in \mathbb{R}_+^3 : 0 < Z < \epsilon\}, U_\epsilon^4 = \left\{ (N,P,Z) \in \mathbb{R}_+^3 : N > \frac{1}{\epsilon} \right\},$$

$$U_\epsilon^5 = \left\{ (N,P,Z) \in \mathbb{R}_+^3 : P > \frac{1}{\epsilon} \right\}, U_\epsilon^6 = \left\{ (N,P,Z) \in \mathbb{R}_+^3 : Z > \frac{1}{\epsilon} \right\}.$$

Obviously, $U_\epsilon^C = \bigcup_{i=1}^6 U_\epsilon^i$. Then, we need to prove that $\mathcal{L}V(N,P,Z,t) \le -1$ on each $U_\epsilon^i \times \mathbb{S}, i = 1,2,\cdots,6$, which is equivalent to the result on $U_\epsilon^i \times \mathbb{S}$.

When $(N,P,Z,t) \in U_\epsilon^1 \times \mathbb{S}$, according to Eq. (L2) we have

$$\mathcal{L}V(N,P,Z,t) \le -M_2\frac{\Re_2^\theta}{\beta^l} + M_2 m_4\beta^u PZ + (M_2\gamma^u + \alpha^u)P - \frac{D^l S_0^l}{N}$$

$$-\frac{1}{2}\eta_2(N^{k_2+2} + P^{k_2+2} + Z^{k_2+2}) + \Gamma_2 + D^u + \frac{1}{2}(\sigma_1^u)^2$$

$$\le -\frac{D^l S_0^l}{N} + \Theta_1 \le -\frac{\hat{D}\hat{S}_0}{\epsilon} + \Theta_1 \le -1,$$

where

$$\Theta_1 = \sup_{(N,P,Z)\in\mathbb{R}_+^3}\Big\{M_2 m_4\beta^u PZ + (M_2\gamma^u + \alpha^u)P - \frac{1}{2}\eta_2(N^{k_2+2} + P^{k_2+2} + Z^{k_2+2}) + \Gamma_2 +$$

$$D^u + \frac{1}{2}(\sigma_1^u)^2\Big\}. \tag{L6}$$

Similarly, when $(N,P,Z,t) \in U_\epsilon^2 \times \mathbb{S}$ or $U_\epsilon^3 \times \mathbb{S}$, using the definition of M_2, Eqs. (L4) and (L5), we obtain

$$\mathcal{L}V \le -\frac{1}{4b^l}M_2\Re_2^\theta \le -1.$$

When $(N,P,Z,t) \in U_\epsilon^4 \times \mathbb{S}$, $U_\epsilon^5 \times \mathbb{S}$ or $U_\epsilon^6 \times \mathbb{S}$, using Eq. (L3), we have

$$\mathcal{L}V \le -\frac{1}{4}\frac{\eta_2}{\epsilon^{k_2+2}} + \Theta_2 \le -1,$$

where

$$\Theta_2 = \sup_{(N,P,Z)\in\mathbb{R}_+^3}\Big\{-\frac{1}{4}\eta_2(N^{k_2+2} + P^{k_2+2} + Z^{k_2+2}) + M_2 m_4\beta^u PZ + (M_2\gamma^u + \alpha^u)P + \Gamma_2 +$$

$$D^u + \frac{1}{2}(\sigma_1^u)^2\Big\}. \tag{L7}$$

Obviously, for a sufficiently small ϵ such that

$$\mathcal{L}V(N,P,Z,t) \le -1, \forall (N,P,Z,k) \in (\mathbb{R}_+^3 \backslash U_\epsilon) \times \mathbb{S}.$$

Then, by Theorem 3.8 in Khasminskii (2011), we obtain that model (5.2) has a nontrivial positive θ −periodic solution.

This completes the proof.

APPENDIX M. The proof of Theorem 6.1

Proof. Clearly, the solution of model (6.2) will remain in $\mathbb{R}_+^3$ for all $t \geq 0$ almost surely. For any $|X(0)| < k$, define a stopping time as

$$\tau_k = \inf\{t \geq 0, |X(t)| > k\}.$$

Then $\tau_k \uparrow \infty$ a.s. as $k \to \infty$. Define a C^2 −function as follows:

$$V(N,P,Z) = e^t\big(N^\theta + P^\theta + Z^\theta\big),$$

where $(N,P,Z) \in \mathbb{R}_+^3$ and $\theta \in (0,1)$. By generalized Itô's formula, we have

$$dV(N,P,Z) = e^t\Big\{\big(N^\theta + P^\theta + Z^\theta\big) + \theta N^{\theta-1}\Big(D\big(r(t)\big)\big(S_0\big(r(t)\big) - N(t)\big) -$$

$$\alpha\big(r(t)\big)P(t)N(t) + h\big(r(t)\big)P(t) + \delta\big(r(t)\big)Z\Big) + \theta P^{\theta-1}\Big(\alpha\big(r(t)\big)PZ - c\big(r(t)\big)P -$$

$$\frac{\beta(r(t))PZ}{1+m\big(r(t)\big)Z+n(r(t))P}\Big) + \theta Z^{\theta-1}\Big(\frac{\beta(r(t))PZ}{1+m\big(r(t)\big)Z+n(r(t))P} - b(r(t))Z\Big) + \frac{\theta(\theta-1)}{2}\big[N^\theta\sigma_1^2(r(t)) +$$

$$P^\theta\sigma_2^2(r(t)) + Z^\theta\sigma_3^2(r(t))\big]\Big\}dt + e^t\theta\big[N^\theta\sigma_1(r(t))dB_1(t) + P^\theta\sigma_2(r(t))dB_2(t) +$$

$$Z^\theta\sigma_3(r(t))dB_3(t)\big] \leq e^t\big\{\big(N^\theta + P^\theta + Z^\theta\big) + \check{D}\check{S}_0 + \big(\check{h} - \hat{c}\big)P + \big(\check{\delta} - \hat{b}\big)Z\big\}dt +$$

$$e^t\theta\big[N^\theta\sigma_1\big(r(t)\big)dB_1(t) + P^\theta\sigma_2\big(r(t)\big)dB_2(t) + Z^\theta\sigma_3\big(r(t)\big)dB_3(t)\big],$$

As $0 < \theta < 1$, there exists a $G(\theta) > 0$ such that

$$dV(N,P,Z) \leq e^t G(\theta)dt$$

$$+ e^t\theta\big[N^\theta\sigma_1\big(r(t)\big)dB_1(t) + P^\theta\sigma_2\big(r(t)\big)dB_2(t) + Z^\theta\sigma_3\big(r(t)\big)dB_3(t)\big].$$

We integrate both sides of the above expression to get

$$\mathbb{E}(V(N(t\wedge\tau_k),P(t\wedge\tau_k),Z(t\wedge\tau_k))) \leq V\big(N(0),P(0),Z(0)\big) + \mathbb{E}\int_0^{t\wedge\tau_k} e^s G(\theta)\,ds,$$

where τ_k is the stopping time. As $k \to +\infty$, we have

$$\mathbb{E}\big(V(N(t),P(t),Z(t)\big) \leq V\big(N(0),P(0),Z(0)\big) + e^t G(\theta),$$

which gives

$$e^{-t}\mathbb{E}(V(N(t),P(t),Z(t))) \le e^{-t}V\big(N(0),P(0),Z(0)\big) + G(\theta).$$

Note that

$$|X(t)|^{\theta} = (N^2(t)+P^2(t)+Z^2(t))^{\frac{\theta}{2}} \le 3^{\frac{\theta}{2}}\max\{N^{\theta},P^{\theta},Z^{\theta}\} \le 3^{\frac{\theta}{2}}\big(N^{\theta}+P^{\theta}+Z^{\theta}\big),$$

Thus,

$$\mathbb{E}|X(t)|^{\theta} \le 3^{\frac{\theta}{2}}\Big(e^{-t}V\big(N(0),P(0),Z(0)\big) + G(\theta)\Big) < +\infty.$$

Setting $\theta = \frac{1}{2}$, then there exists a constant $\delta_1 > 0$, such that

$$\lim_{t\to+\infty}\sup \mathbb{E}|X(t)|^{\frac{1}{2}} \le \delta_1.$$

Using Chebyshev's inequality and taking $\chi = \frac{\delta_1^2}{\varepsilon^2}$ with $0 < \varepsilon < 1$, we obtain

$$\mathbb{P}\{|X(t)| > \chi\} \le \frac{\mathbb{E}|X(t)|^{\frac{1}{2}}}{\chi^{\frac{1}{2}}},$$

which implies that

$$\lim_{t\to+\infty}\sup \mathbb{P}\{|X(t)| > \chi\} \le \frac{\delta_1}{\chi^{\frac{1}{2}}} = \varepsilon.$$

This completes the proof.

APPENDIX N. The proof of Lemma 6.1

Proof. Define a C^2-function from $\mathbb{R}_+^3$ to $\mathbb{R}_+$ as,

$$V(N,P,Z) = \frac{1}{N+P+Z}.$$

By generalized Itô's formula, we have

$$dV(N+P+Z) = \Big\{-V^2\Big[D\big(r(t)\big)S_0\big(r(t)\big) - D\big(r(t)\big)N + \Big(h\big(r(t)\big) - c\big(r(t)\big)\Big)P + \Big(\delta\big(r(t)\big) - b\big(r(t)\big)\Big)Z\Big] + V^3\big[\sigma_1^2\big(r(t)\big)N^2 + \sigma_2^2\big(r(t)\big)P^2 + \sigma_3^2\big(r(t)\big)Z^2\big]\Big\}dt - V^2\big[\sigma_1\big(r(t)\big)NdB_1(t) + \sigma_2\big(r(t)\big)PdB_2(t) + \sigma_3\big(r(t)\big)ZdB_3(t)\big].$$

For any positive constant κ, it follows the differential operator $\mathcal{L}$ acts on $(1+V)^\kappa$ to give

$$\mathcal{L}(1+V)^\kappa = \kappa(1+V)^{\kappa-1}\Big\{-V^2\Big[D\big(r(t)\big)S_0\big(r(t)\big) - D\big(r(t)\big)N + \Big(h\big(r(t)\big) - c\big(r(t)\big)\Big)P + \Big(\delta\big(r(t)\big) - b\big(r(t)\big)\Big)Z\Big] + V^3\big[\sigma_1^2\big(r(t)\big)N^2 + \sigma_2^2\big(r(t)\big)P^2 + \sigma_3^2\big(r(t)\big)Z^2\big]\Big\} + \frac{\kappa(\kappa-1)}{2}(1+V)^{\kappa-2}V^4\big[\sigma_1^2\big(r(t)\big)N^2 + \sigma_2^2\big(r(t)\big)P^2 + \sigma_3^2\big(r(t)\big)Z^2\big]$$

$$= \kappa(1+V)^{\kappa-2}\Big\{-V^2(1+V)\Big[D\big(r(t)\big)S_0\big(r(t)\big) - D\big(r(t)\big)N + \Big(h\big(r(t)\big) - c\big(r(t)\big)\Big)P + \Big(\delta\big(r(t)\big) - b\big(r(t)\big)\Big)Z\Big] + V^3\big[\sigma_1^2\big(r(t)\big)N^2 + \sigma_2^2\big(r(t)\big)P^2 + \sigma_3^2\big(r(t)\big)Z^2\big] + \frac{\kappa+1}{2}V^4\big[\sigma_1^2\big(r(t)\big)N^2 + \sigma_2^2\big(r(t)\big)P^2 + \sigma_3^2\big(r(t)\big)Z^2\big]\Big\}$$

$$= \kappa(1+V)^{\kappa-2}H.$$

where

$$H \le hV - \big(\widehat{D}\widehat{S_0} - h\big)V^2 + V^3[\breve{\sigma}_1^2N^2 + \breve{\sigma}_2^2P^2 + \breve{\sigma}_3^2Z^2] + \frac{\kappa+1}{2}V^4[\breve{\sigma}_1^2N^2 + \breve{\sigma}_2^2P^2 + \breve{\sigma}_3^2Z^2].$$

As

$$V^3[\breve{\sigma}_1^2N^2 + \breve{\sigma}_2^2P^2 + \breve{\sigma}_3^2Z^2] < \max\{\breve{\sigma}_1^2, \breve{\sigma}_2^2, \breve{\sigma}_3^2\}V,$$

we obtain

$$H \le (h + \max\{\breve{\sigma}_1^2, \breve{\sigma}_2^2, \breve{\sigma}_3^2\})V - \Big(\widehat{D}\widehat{S_0} - h - \frac{\kappa+1}{2}\max\{\breve{\sigma}_1^2, \breve{\sigma}_2^2, \breve{\sigma}_3^2\}\Big)V^2.$$

Thus, for a sufficiently small ρ, we have

$$\begin{aligned}\mathcal{L}(e^{\rho t}(1+V)^{\kappa}) &= \rho e^{\rho t}(1+V)^{\kappa} + e^{\rho t}\mathcal{L}(1+V)^{\kappa} \\ &= e^{\rho t}(1+V)^{\kappa-2}(\rho(1+V)^2 + \kappa H) \\ &\leq e^{\rho t}(1+V)^{\kappa-2}(\rho - F_1V^2 + F_2V) \\ &\leq \tfrac{4\rho F_1+F_2^2}{4F_1} e^{\rho t}(1+V)^{\kappa-2},\end{aligned}$$

Where $0 < V \leq \frac{F_2+\sqrt{F_2^2+4F_1\rho}}{2F_1}$. Set $F = (1+V)^{\kappa-2}$. Obviously, F is a monotone increasing function for $\kappa - 2 > 0$ while monotone decreasing function for $0 < \kappa - 2 \leq 0$. Hence, the maximum of the function F takes the form

$$\max\left\{1, \left(\frac{2F_1+F_2+\sqrt{F_2^2+4F_1\rho}}{2F_1}\right)^{\kappa-2}\right\}.$$

Thus, $\mathcal{L}(e^{\rho t}(1+V)^{\kappa})$ can be rewritten as

$$\mathcal{L}(e^{\rho t}(1+V)^{\kappa}) \leq \tfrac{4\rho F_1+F_2^2}{4F_1} e^{\rho t}(1+V)^{\kappa-2} = N_0 e^{\rho t},$$

where

$$N_0 = \tfrac{4\rho F_1+F_2^2}{4F_1} \max\left\{1, \left(\frac{2F_1+F_2+\sqrt{F_2^2+4F_1\rho}}{2F_1}\right)^{\kappa-2}\right\}.$$

Therefore,

$$\mathbb{E}(e^{\rho t}(1+V)^{\kappa}) \leq \big(1+V(0)\big)^{\kappa} + \tfrac{N_0}{\rho}(e^{\rho t}-1).$$

Hence, we have

$$\lim_{t\to+\infty} \sup \mathbb{E}(V(t)^{\kappa}) \leq \lim_{t\to+\infty} \sup \mathbb{E}\big(\big(1+V(t)\big)^{\kappa}\big) \leq \tfrac{N_0}{\rho}.$$

Note that,

$$(N+P+Z)^{\kappa} \leq 3^{\kappa}(N^2+P^2+Z^2)^{\frac{\kappa}{2}} = 3^{\kappa}|X(t)|^{\kappa},$$

Thus, we get

$$\lim_{t\to+\infty} \sup \mathbb{E}\ |X(t)|^{-\kappa} \leq 3^{\kappa} \lim_{t\to+\infty} \sup \mathbb{E}\ (|V(t)|^{\kappa}) \leq \frac{3^{\kappa}N_0}{\rho} = \Pi.$$

This completes the proof.

APPENDIX O. The proof of Theorem 6.2

Proof. According to Theorem 6.1, we have $\lim_{t\to+\infty} \sup \mathbb{P}\{|X(t)| > \chi\} \leq \varepsilon$, which implies that

$$\lim_{t\to+\infty} \sup \mathbb{P}\{|X(t)| \leq \chi\} \geq 1 - \varepsilon.$$

By Lemma 6.1, we have $\lim_{t\to+\infty} \sup \mathbb{E}\,|X(t)|^{-\kappa} \leq \Pi$. Hence, for any given $0 < \varepsilon < 1$ and $\mathrm{K} = \left(\frac{\varepsilon}{\Pi}\right)^{\frac{1}{\kappa}}$, we have

$$\mathbb{P}\{|X(t)| < \mathrm{K}\} = \mathbb{P}\left\{\frac{1}{|X(t)|} > \frac{1}{K}\right\} \leq K^{\kappa}\mathbb{E}|X(t)|^{-\kappa} = \varepsilon,$$

which yields that

$$\lim_{t\to+\infty} \inf \mathbb{P}\{|X(t)| \geq \mathrm{K}\} > 1 - \varepsilon.$$

This completes the proof.

APPENDIX P. The proof of Lemma 6.2

Proof. Eq. (6.4) can be rewritten as

$$HV = A,$$

where $V \in \mathbb{R}^{\mathbb{m}}$, $A = (\alpha_1, \alpha_2, \cdots, \alpha_{\mathbb{m}})^T$ and

$$H = \begin{bmatrix} D(1) - q_{11} & -q_{12} & \cdots & -q_{1\mathbb{m}} \\ -q_{21} & D(2) - q_{22} & \cdots & -q_{2\mathbb{m}} \\ \vdots & \vdots & \vdots & \vdots \\ -q_{\mathbb{m}1} & -q_{\mathbb{m}2} & \cdots & D(\mathbb{m}) - q_{\mathbb{m}\mathbb{m}} \end{bmatrix}.$$

Obviously, $H \in Z^{\mathbb{m}\times\mathbb{m}} \equiv \left\{C = \left(c_{ij}\right)_{\mathbb{m}\times\mathbb{m}} : c_{ij} \le 0, i \ne j\right\}$.

For each $k \in \mathbb{S}$, consider the leading principal sub-matrix

$$H = \begin{bmatrix} D(1) - q_{11} & -q_{12} & \cdots & -q_{1k} \\ -q_{21} & D(2) - q_{22} & \cdots & -q_{2k} \\ \vdots & \vdots & \vdots & \vdots \\ -q_{k1} & -q_{k2} & \cdots & D(k) - q_{kk} \end{bmatrix}.$$

Then we have $H_k \in Z^{k\times k}$, and the sum of each row is

$$D(i) - \sum_{j=1}^{k} q_{ij} = D(i) + \sum_{j=k+1}^{\mathbb{m}} q_{ij} \ge D(i), i = 1, 2, \cdots, k.$$

From Lemma 5.3 in Mao and Yuan (2006), we have $det\, H_k > 0$. It follows from Theorem 2.10 in Mao and Yuan (2006) that H is a nonsingular M-matrix. That is, for any vector $A \in \mathbb{R}_+^{\mathbb{m}}$ the equation $HV = A$ has a unique solution $V = (v(1), v(2), \cdots, v(\mathbb{m}))^T \gg 0$.

This completes the proof.

APPENDIX Q. The proof of Lemma 6.3

Proof. Applying Itô's formula to model (6.2) yields that

$$\frac{1}{t}\ln\frac{P(t)}{P(0)} = -\frac{1}{t}\int_0^t \left[c\big(r(s)\big) + \frac{1}{2}\sigma_2^2\big(r(s)\big) + \frac{\beta\big(r(s)\big)Z(s)}{1+m\big(r(s)\big)Z(s)+n\big(r(s)\big)P(s)}\right] ds$$

$$+\frac{1}{t}\int_0^t \alpha\big(r(s)\big)N(s)\,ds + \frac{M_1(t)}{t}. \tag{Q1}$$

$$\frac{1}{t}\ln\frac{Z(t)}{Z(0)} = -\frac{1}{t}\int_0^t \left[b\big(r(s)\big) + \frac{1}{2}\sigma_3^2\big(r(s)\big) - \frac{\beta(r(s))P(s)}{1+m\big(r(s)\big)Z(s)+n(r(s))P(s)}\right] ds + \frac{M_2(t)}{t}. \tag{Q2}$$

where $M_1(t) = \int_0^t \sigma_2\big(r(s)\big)dB_2(s)$, $M_2(t) = \int_0^t \sigma_3\big(r(s)\big)dB_3(s)$ are two martingales. If $\lim_{t\to+\infty} P(t) = 0$ a.s., then for arbitrary $0 < \epsilon < \min\left\{1, \hat{b} + \frac{1}{2}\hat{\sigma}_3^2\right\}$, there exist a measurable set $\Omega_\epsilon \subset \Omega$ with $P(\Omega_\epsilon) \geq 1-\epsilon$ and a constant $T = T(\epsilon) > 0$ such that for $\omega \in \Omega_\epsilon$ and $t > T$

$$\frac{1}{t}\int_0^t \frac{\beta(r(s))P(s)}{1+m\big(r(s)\big)Z(s)+n(r(s))P(s)}\,ds + \frac{1}{t}\ln Z(0) < \epsilon, \quad t \geq T.$$

Combine the above inequality with Eq. (Q2), we get

$$t^{-1}\ln Z(t) = t^{-1}\ln Z(0) - \frac{1}{t}\int_0^t \left[b\big(r(s)\big) + \frac{1}{2}\sigma_3^2\big(r(s)\big) - \frac{\beta(r(s))P(s)}{1+m\big(r(s)\big)Z(s)+n(r(s))P(s)}\right] ds + \frac{M_2(t)}{t}$$

$$\leq \epsilon - \frac{1}{t}\int_0^t \left[b\big(r(s)\big) + \frac{1}{2}\sigma_3^2\big(r(s)\big)\right] ds + \frac{M_2(t)}{t},$$

for $t \geq T$. By Lemma E.1 (i), we have $\lim_{t\to+\infty} Z(t) = 0$ a.s., and it follows that the conclusion holds for model (6.2).

This completes the proof.

APPENDIX R. The proof of Theorem 6.3

Proof. From Lemma I.2 we have

$$\lim_{t\to+\infty}\frac{M_i(t)}{t}=0 \text{ a.s., } i=1,2.$$

Define $V(N,\ P,\ Z,\ k)=v(k)[N(t)+P(t)+Z(t)]$. By virtue of Lemma 6.2, we get

$dV(N,P,Z,k)$

$=\{v(k)D(k)S_0(k)-[D(k)v(k)-\sum_{l\in\mathbb{S}}q_{kl}\,v(l)]N(t)\}dt+v(k)\sigma_1(k)N(t)dB_1(t)$

$-[(c(k)-h(k))v(k)-\sum_{l\in\mathbb{S}}q_{kl}\,v(l)]P(t)dt+v(k)\sigma_2(k)P(t)dB_2(t)-[(b(k)-$

$\delta(k))v(k)-\sum_{l\in\mathbb{S}}q_{kl}\,v(l)]Z(t)dt+v(k)\sigma_3(k)Z(t)dB_3(t)$

$=\big\{v(k)D(k)S_0(k)-\alpha(k)N(t)-\big[\alpha(k)+\big(c(k)-h(k)-D(k)\big)v(k)\big]P(t)-\big[\alpha(k)+$

$\big(b(k)-\delta(k)-D(k)\big)v(k)\big]Z(t)\big\}dt+v(k)\sigma_1(k)N(t)dB_1(t)+v(k)\sigma_2(k)P(t)dB_2(t)+$

$v(k)\sigma_3(k)Z(t)dB_3(t)$.

Consequently,

$$\frac{1}{t}\int_0^t\alpha\big(r(s)\big)\,N(s)ds=-\frac{1}{t}\int_0^t\Big[\alpha\big(r(s)\big)+\Big(c\big(r(s)\big)-h\big(r(s)\big)-$$

$$D\big(r(s)\big)\Big)\,v\big(r(s)\big)\Big]P(s)ds-\frac{1}{t}\int_0^t\Big[\alpha\big(r(s)\big)+\Big(b\big(r(s)\big)-\delta\big(r(s)\big)-$$

$$D\big(r(s)\big)\Big)\,v\big(r(s)\big)\Big]Z(s)ds+\frac{1}{t}\int_0^t v\big(r(s)\big)D\big(r(s)\big)\,S_0\big(r(s)\big)ds+\frac{\phi_1(t)}{t},\qquad\text{(R1)}$$

where

$$\phi_1(t)=V(0)-V(t)+\int_0^t v\big(r(s)\big)\sigma_1\big(r(s)\big)N(s)dB_1(s)+$$

$$\int_0^t v\big(r(s)\big)\sigma_2\big(r(s)\big)P(s)dB_2(s)+\int_0^t v\big(r(s)\big)\sigma_3\big(r(s)\big)Z(s)dB_3(s).$$

According to Eqs. (6.2) and (6.3), we have $\lim_{t\to+\infty}\frac{\phi_1(t)}{t}=0$ a.s. Substituting Eq. (R1) into Eq. (Q1) yields

$$\frac{1}{t}\ln\frac{P(t)}{P(0)}=\frac{1}{t}\int_0^t\Big[v\big(r(s)\big)D\big(r(s)\big)S_0\big(r(s)\big)-\Big(c\big(r(s)\big)+\frac{1}{2}\sigma_2^2\big(r(s)\big)\Big)\Big]ds-$$

$$\frac{1}{t}\int_0^t \frac{\beta(r(s))Z(s)}{1+m(r(s))Z(s)+n(r(s))P(s)}ds - \frac{1}{t}\int_0^t \Big[\alpha\big(r(s)\big) + \Big(c\big(r(s)\big) - h\big(r(s)\big) - D\big(r(s)\big)\Big)v\big(r(s)\big)\Big]P(s)ds - \frac{1}{t}\int_0^t \Big[\alpha\big(r(s)\big) + \Big(b\big(r(s)\big) - \delta\big(r(s)\big) - D\big(r(s)\big)\Big)v\big(r(s)\big)\Big]Z(s)ds + \frac{\phi_2(t)}{t}, \quad \text{(R2)}$$

where $\phi_2(t) = M_1(t) + \phi_1(t)$. Thus, $\lim_{t\to+\infty} \frac{\phi_2(t)}{t} = 0$ a.s. By the ergodic theorem of Markov chain $r(t)$ and Eq. (R2), we obtain

$$\lim_{t\to+\infty} \sup \frac{1}{t}\ln\frac{P(t)}{P(0)} \le \sum_{k\in\mathbb{S}} \pi_k \Big[v(k)D(k)S_0(k) - \Big(c(k) + \frac{1}{2}\sigma_2^2(k)\Big)\Big] = \Re_0^S \text{ a.s.}$$

Thus, we have $\lim_{t\to+\infty} P(t) = 0$ a.s. if $\Re_0^S < 0$. Consequently, $\lim_{t\to+\infty} Z(t) = 0$ a.s. follows from Lemma 4.3.

Now, from Eq. (R2), we have

$$\frac{1}{t}\ln\frac{P(t)}{P(0)} \le \frac{1}{t}\int_0^t \Big[v\big(r(s)\big)D\big(r(s)\big)S_0\big(r(s)\big) - \Big(c\big(r(s)\big) + \frac{1}{2}\sigma_2^2\big(r(s)\big)\Big)\Big]ds - \frac{1}{t}\int_0^t \Big[\alpha\big(r(s)\big) + \Big(c\big(r(s)\big) - h\big(r(s)\big) - D\big(r(s)\big)\Big)v\big(r(s)\big)\Big]P(s)ds + \frac{\phi_2(t)}{t}, \quad \text{(R3)}$$

If $\Re_0^S > 0$, then we have following result from Liu and Bai (2016)

$$\lim_{t\to+\infty} \sup \frac{1}{t}\int_0^t P(s)\,ds \le \frac{\sum_{k\in\mathbb{S}} \pi_k\Big[v(k)D(k)S_0(k) - \Big(c(k) + \frac{1}{2}\sigma_2^2(k)\Big)\Big]}{\widehat{\gamma}} = \frac{\Re_0^S}{\widehat{\gamma}} \text{ a.s.} \quad \text{(R4)}$$

For Eq. (Q2), we obtain

$$\lim_{t\to+\infty} \sup \frac{1}{t}\ln\frac{Z(t)}{Z(0)} = -\lim_{t\to+\infty} \frac{1}{t}\int_0^t \Big[b\big(r(s)\big) + \frac{1}{2}\sigma_3^2\big(r(s)\big)\Big]ds + \lim_{t\to+\infty} \sup \frac{1}{t}\int_0^t \frac{\beta\big(r(s)\big)P(s)}{1+m\big(r(s)\big)Z(s)+n\big(r(s)\big)P(s)}ds \le -\lim_{t\to+\infty} \frac{1}{t}\int_0^t \Big[b\big(r(s)\big) + \frac{1}{2}\sigma_3^2\big(r(s)\big) - \frac{\beta\big(r(s)\big)}{n\big(r(s)\big)}\Big]ds. \quad \text{(R5)}$$

Thus, one can get that

$$\lim_{t\to+\infty} \sup \frac{1}{t}\ln\frac{Z(t)}{Z(0)} \le -\sum_{k\in\mathbb{S}} \pi_k \Big[b(k) + \frac{1}{2}\sigma_3^2(k) - \frac{\beta(k)}{n(k)}\Big] = \Re_1^S \text{ a.s.}$$

Obviously, $\lim_{t\to+\infty} Z(t) = 0$ a.s. if $\Re_1^S < 0$. That is, for arbitrary $0 < \epsilon < 1$, there exist a set $\Omega_\epsilon \subset \Omega$ with $\mathbb{P}(\Omega_\epsilon) \geq 1 - \epsilon$ and a constant $\mathcal{F} = \mathcal{F}(\epsilon)$ such that

$$\max\left\{\frac{1}{t}\int_0^t \check{\eta} Z(s)ds, \frac{1}{t}\int_0^t \frac{\check{\beta} Z(s)}{1+\hat{m}Z(s)+\hat{n}P(s)}ds\right\} < \frac{\epsilon}{2},$$

for $\omega \in \Omega_\epsilon$ and $t > \mathcal{F}$. By Eq. (R2), for sufficiently large t, we have

$$\frac{1}{t}\ln\frac{P(t)}{P(0)} \geq \frac{1}{t}\int_0^t \left[v\big(r(s)\big)D\big(r(s)\big)S_0\big(r(s)\big) - \left(c\big(r(s)\big) + \frac{1}{2}\sigma_2^2\big(r(s)\big)\right) - \epsilon\right]ds -$$

$$\frac{1}{t}\int_0^t \left[\alpha\big(r(s)\big) + \left(c\big(r(s)\big) - h\big(r(s)\big) - D\big(r(s)\big)\right)v\big(r(s)\big)\right]P(s)ds + \frac{\phi_2(t)}{t},$$

Since ϵ is arbitrary, from Lemma 4 in Liu and Bai (2016), we obtain

$$\lim_{t\to+\infty}\inf\frac{1}{t}\int_0^t P(s)\,ds \geq \frac{\sum_{k\in\mathbb{S}}\pi_k\left[v(k)D(k)S_0(k) - \left(c(k) + \frac{1}{2}\sigma_2^2(k)\right)\right]}{\check{\gamma}} = \frac{\Re_0^S}{\check{\gamma}} \text{ a.s.}$$

This completes the proof.

APPENDIX S. The proof of Theorem 6.4

Proof. By virtue of Assumption 1 and the positive definiteness of the diffusion matrix of model (6.2), and using Theorem 3.13 in Khasminskii (2011), it is obvious that we only need construct a nonnegative function $V \in C^2$ and a bounded closed U_ϵ such that $\mathcal{L}V \leq -1$ for $(N, P, Z, k) \in U_\epsilon^c \times \mathbb{S}$.

For simplicity, we introduce the following notations:

$$\Re_2^S = \hat{\beta}\Re_0^S - \check{\gamma}\sum_{k\in\mathbb{S}}\pi_k\left[\left(b(k) + \frac{1}{2}\sigma_3^2(k)\right)\right],$$

Denoted by

$$D_{min} = \min\{\hat{D}, \hat{c} - \check{h}, \hat{b} - \check{\delta}\}, m_1 = \frac{\check{\gamma}}{\hat{\beta}},$$

$$\sigma_{max}^2 = max_{i\in\{1,2,3\}}\{(\check{\sigma}_i)^2\}, m_2 = \frac{\check{\eta}+\check{\beta}}{\hat{b}}.$$

For $\min\{\hat{D}, \hat{c} - \check{h}, \hat{b} - \check{\delta}\} > \frac{1}{2}\max\{(\hat{\sigma}_1)^2, (\hat{\sigma}_2)^2, (\hat{\sigma}_3)^2\}$, there exists a constant $k_1 > 0$ such that

$$\eta_1 = D_{min} - \frac{1}{2}\sigma_{max}^2(k_1 + 1) > 0.$$

Define a C^2 −function $\tilde{V}: \mathbb{R}_+^3 \times \mathbb{S} \to \mathbb{R}$ by

$$\begin{aligned}\tilde{V}(N, P, Z, k) &= M_1[-v(k)(N + P + Z) - \ln P - m_1 \ln Z + m_2 Z + (\varpi_k + |\varpi|)] \\ &\quad - \ln N + \frac{1}{k_1+2}(N + P + Z)^{k_1+2} \\ &\equiv M_1 V_1 + V_2 + V_3,\end{aligned}$$

where $\varpi = (\varpi_1, \varpi_2, \cdots, \varpi_{\mathbb{m}})^T$ is to be determined later and $M_1 > 0$ is given by

$$M_1 = \frac{2\hat{b}}{\Re_2^S}\max\{2, r_1\},$$

$$\begin{aligned}r_1 = \sup_{(N,P,Z)\in\mathbb{R}_+^3}\Big\{&-\frac{1}{2}\eta_1(N^{k_1+2} + P^{k_1+2} + Z^{k_1+2}) + m_2\check{\beta}(P^2 + Z^2) + (M_1\check{\gamma} + \check{\alpha})P + \Gamma_1 + \\ &\check{D} + \frac{1}{2}(\check{\sigma}_1)^2\Big\}.\end{aligned}$$

with

$$\Gamma_1 = \sup_{(N,P,Z)\in\mathbb{R}_+^3}\left\{\left(\check{D}\check{S}_0\right)(N+P+Z)^{k_1+1} - \frac{1}{2}\eta_1(N^{k_1+2}+P^{k_1+2}+Z^{k_1+2})\right\} < \infty.$$

Obviously, $\tilde{V}(N,P,Z)$ exists a minimum point $(\bar{N},\bar{P},\bar{Z},k)$in $\mathbb{R}_+^3\times\mathbb{S}$. Thus, we can define a nonnegative function $V\colon \mathbb{R}_+^3\times\mathbb{S}\to\mathbb{R}_+$ as follows:

$$V(N,P,Z,k) = \tilde{V}(N,P,Z,k) - \tilde{V}(\bar{N},\bar{P},\bar{Z},k).$$

By Itô's formula, we get

$$\begin{aligned}
\mathcal{L}V_1 = &-\{v(k)[D(k)(S_0(k)-N) + (h(k)-c(k))P + (\delta(k)-b(k))Z(t)] + \\
&\sum_{l\in\mathbb{S}} q_{kl}v(l)(N+P+Z)\} - \left[\alpha(k)N - c(k) - \frac{\beta(k)Z}{1+m(k)Z+n(k)P} - \frac{1}{2}\sigma_2^2(k)\right] - \\
&m_1\left[\frac{\beta(k)P}{1+m(k)Z+n(k)P} - b(k) - \frac{1}{2}\sigma_3^2(k)\right] + m_2\left[\frac{\beta(k)PZ}{1+m(k)Z+n(k)P} - b(k)Z\right] + \sum_{l\in\mathbb{S}} q_{kl}\varpi_l \\
= &[v(k)D(k) - \alpha(k) - \sum_{l\in\mathbb{S}} q_{kl}v(l)]N + m_2\frac{\beta(k)PZ}{1+m(k)Z+n(k)P} + \sum_{l\in\mathbb{S}} q_{kl}\varpi_l \\
&-[\sum_{l\in\mathbb{S}} q_{kl}v(l) + h(k)v(k) - c(k)v(k)]P - \frac{m_1\beta(k)P}{1+m(k)Z+n(k)P} - [\sum_{l\in\mathbb{S}} q_{kl}v(l) + (\delta(k) - \\
&b(k)) + b(k)m_2]Z + \frac{\beta(k)Z}{1+m(k)Z+n(k)P} - \left[v(k)D(k)S_0(k) - \frac{1}{2}\sigma_2^2(k) - c(k) - m_1\left(b(k) + \right.\right. \\
&\left.\left.\frac{1}{2}\sigma_3^2(k)\right)\right] \\
\le &\, m_2\check{\beta}\mathrm{PZ} + \sum_{l\in\mathbb{S}} q_{kl}\varpi_l + \check{\gamma}P - [\sum_{l\in\mathbb{S}} q_{kl}v(l) + (\delta(k)-b(k)) - \beta(k) + b(k)m_2]Z - \\
&\left[v(k)D(k)S_0(k) - \frac{1}{2}\sigma_2^2(k) - c(k) - m_1\left(b(k) + \frac{1}{2}\sigma_3^2(k)\right)\right] \\
= &-\Psi_k + \sum_{l\in\mathbb{S}} q_{kl}\varpi_l + \check{\gamma}P + m_2\check{\beta}PZ,
\end{aligned}$$

where $\Psi_k = v(k)D(k)S_0(k) - \left(c(k) + \frac{1}{2}\sigma_2^2(k)\right) - m_1\left(b(k) + \frac{1}{2}\sigma_3^2(k)\right)$.

Note that $\pi[\Psi - (\pi\Psi)\mathbb{I}_{\mathbb{m}}] = 0$ and $\sum_{k\in\mathbb{S}}\pi_k = 1$, where $\Psi = (\Psi_1,\Psi_2,\cdots,\Psi_{\mathbb{m}})^T$, $\mathbb{I}_{\mathbb{m}} = (1,1,\cdots,1)^T \in \mathbb{R}^{\mathbb{m}}$. By Lemma A. 12 in Khasminskii (2011), the following equation:

$$Q\varpi = \Psi - (\pi\Psi)\mathbb{I}_{\mathbb{m}},$$

has a solution $\varpi = (\varpi_1, \varpi_2, \cdots, \varpi_{\mathbb{m}})^T \in \mathbb{R}^{\mathbb{m}}$. Hence, one can get that

$$-\Psi_k + \sum_{l\in\mathbb{S}} q_{kl}\varpi_l = -\sum_{l\in\mathbb{S}} \pi_k \Psi_k = -\frac{\Re_2^S}{\hat{\beta}}.$$

Thus,

$$\mathcal{L}V_1 \leq -\Psi_k + \sum_{l\in\mathbb{S}} q_{kl}\,\varpi_l + \check{\gamma}P + m_2\check{\beta}PZ = -\frac{\Re_2^S}{\hat{\beta}} + \check{\gamma}P + m_2\check{\beta}PZ.$$

By a direct computation, we get

$$\mathcal{L}V_2 = -\frac{D(k)S_0(k)}{N} + \alpha(k)P - h(k)\frac{P}{N} - \delta(k)\frac{Z}{N} + D(k) + \frac{1}{2}\sigma_1^2(k)$$

$$\leq -\frac{\widehat{D}\hat{S}_0}{N} + \check{\alpha}P + \check{D} + \frac{1}{2}(\check{\sigma}_1)^2$$

$$\mathcal{L}V_3 = (N+P+Z)^{k_1+1}[D(k)(S_0(k)-N) + h(k)P + \delta(k)Z - c(k)P - b(k)Z] + \frac{1}{2}(k_1 +$$

$$1)(N+P+Z)^{k_1}[\sigma_1^2(k)N^2 + \sigma_2^2(k)P^2 + \sigma_3^2(k)Z^2]$$

$$\leq (N+P+Z)^{k_1+1}\left[\check{D}\check{S}_0 - D_{min}(N+P+Z)\right] + \frac{1}{2}\sigma_{max}^2(k_1+1)(N+P+Z)^{k_1+2}$$

$$= \check{D}\check{S}_0(N+P+Z)^{k_1+1} - \left(D_{min} - \frac{1}{2}\sigma_{max}^2(k_1+1)\right)(N+P+Z)^{k_1+2}$$

$$\leq \Gamma_1 - \frac{1}{2}\eta_1(N+P+Z)^{k_1+2}$$

$$\leq \Gamma_1 - \frac{1}{2}\eta_1(N^{k_1+2} + P^{k_1+2} + Z^{k_1+2}).$$

The above inequations yield that

$$\mathcal{L}V(N,P,Z,k) \leq -M_1\frac{\Re_2^S}{\hat{\beta}} + M_1 m_2\check{\beta}PZ + (M_1\check{\gamma} + \check{\alpha})P - \frac{\widehat{D}\hat{S}_0}{N}$$

$$-\frac{1}{2}\eta_1(N^{k_1+2} + P^{k_1+2} + Z^{k_1+2}) + \Gamma_1 + \check{D} + \frac{1}{2}(\check{\sigma}_1)^2. \qquad \text{(S1)}$$

In order to validate that $\mathcal{L}V(N,P,Z,k) \leq -1$ on some $U_\epsilon^c \times \mathbb{S}$, we define a compact subset U_ϵ by

$$U_\epsilon = \left\{(N,P,Z) \in \mathbb{R}_+^3 : \epsilon \leq N \leq \frac{1}{\epsilon}, \epsilon \leq P \leq \frac{1}{\epsilon}, \epsilon \leq Z \leq \frac{1}{\epsilon}\right\},$$

where $\epsilon > 0$ satisfies the following conditions

$$-\frac{\hat{D}\hat{S}_0}{\epsilon}+\Theta_1\le 1, \tag{S2}$$

$$-\frac{1}{4}\frac{\eta_1}{\epsilon^{k_1+2}}+\Theta_2\le -1, \tag{S3}$$

$$0<\epsilon<\frac{\Re_2^S}{4m_2\check{\beta}\hat{\beta}}, \tag{S4}$$

$$0<\epsilon<\frac{1}{M_1}, \tag{S5}$$

Here, Θ_1 and Θ_2 are constants given explicitly in the expression (S6) and (S7), respectively.

We further divide $\mathbb{R}_+^3\backslash U_\epsilon$ into six domains as follows:

$$\mathrm{U}_\epsilon^1=\{(\mathrm{N},\mathrm{P},\mathrm{Z})\in\mathbb{R}_+^3\colon 0<\mathrm{N}<\epsilon\},\mathrm{U}_\epsilon^2=\{(\mathrm{N},\mathrm{P},\mathrm{Z})\in\mathbb{R}_+^3\colon 0<\mathrm{P}<\epsilon\},$$

$$\mathrm{U}_\epsilon^3=\{(\mathrm{N},\mathrm{P},\mathrm{Z})\in\mathbb{R}_+^3\colon 0<\mathrm{Z}<\epsilon\},\mathrm{U}_\epsilon^4=\left\{(\mathrm{N},\mathrm{P},\mathrm{Z})\in\mathbb{R}_+^3\colon \mathrm{N}>\frac{1}{\epsilon}\right\},$$

$$\mathrm{U}_\epsilon^5=\left\{(\mathrm{N},\mathrm{P},\mathrm{Z})\in\mathbb{R}_+^3\colon \mathrm{P}>\frac{1}{\epsilon}\right\},\mathrm{U}_\epsilon^6=\left\{(\mathrm{N},\mathrm{P},\mathrm{Z})\in\mathbb{R}_+^3\colon \mathrm{Z}>\frac{1}{\epsilon}\right\}.$$

Clearly, $U_\epsilon^C=\bigcup_{i=1}^6 U_\epsilon^i$. Next, we prove that $\mathcal{L}V(N,P,Z,k)\le -1$ on each $U_\epsilon^i\times\mathbb{S}, i=1,2,\cdots,6$, which is equivalent to the result on $U_\epsilon^i\times\mathbb{S}$.

For $(N,P,Z,k)\in U_\epsilon^1\times\mathbb{S}$, from Eq. (S1) we have

$$\begin{aligned}\mathcal{L}V(N,P,Z,k)&\le -M_1\frac{\Re_2^S}{\hat{\beta}}+M_1m_2\check{\beta}PZ+(M_1\check{\gamma}+\check{\alpha})P-\frac{\hat{D}\hat{S}_0}{N}\\&\quad-\frac{1}{2}\eta_1(N^{k_1+2}+P^{k_1+2}+Z^{k_1+2})+\Gamma_1+\check{D}+\frac{1}{2}(\check{\sigma}_1)^2\\&\le -\frac{\hat{D}\hat{S}_0}{N}+\Theta_1\le -\frac{\hat{D}\hat{S}_0}{\epsilon}+\Theta_1\le -1,\end{aligned}$$

where

$$\Theta_1=\sup_{(N,P,Z)\in\mathbb{R}_+^3}\left\{M_1m_2\check{\beta}PZ+(M_1\check{\gamma}+\check{\alpha})P-\frac{1}{2}\eta_1(N^{k_1+2}+P^{k_1+2}+Z^{k_1+2})+\Gamma_1+\check{D}+\frac{1}{2}(\check{\sigma}_1)^2\right\}. \tag{S6}$$

Similarly, when $(N,P,Z,k)\in U_\epsilon^2\times\mathbb{S}$ or $U_\epsilon^3\times\mathbb{S}$, using the definition of M_1, Eqs. (S4) and

(S5) yields that

$$\mathcal{L}V \leq -\frac{1}{4\hat{b}} M_1 \Re_2^S \leq -1.$$

For $(N, P, Z, k) \in U_\epsilon^4 \times \mathbb{S}$, $U_\epsilon^5 \times \mathbb{S}$ or $U_\epsilon^6 \times \mathbb{S}$, using Eq. (S3), we have

$$\mathcal{L}V \leq -\frac{1}{4}\frac{\eta_1}{\epsilon^{k_1+2}} + \Theta_2 \leq -1,$$

where

$$\Theta_2 = \sup_{(N,P,Z)\in\mathbb{R}_+^3} \left\{-\frac{1}{4}\eta_1(N^{k_1+2} + P^{k_1+2} + Z^{k_1+2}) + M_1 m_2 \check{\beta} PZ + (M_1\check{\gamma} + \check{\alpha})P + \Gamma_1 + \right.$$

$$\left. \check{D} + \frac{1}{2}(\check{\sigma}_1)^2 \right\}. \tag{S7}$$

Obviously, for a sufficiently small ϵ

$$\mathcal{L}V(N, P, Z, k) \leq -1, \forall (N, P, Z, k) \in (\mathbb{R}_+^3 \backslash U_\epsilon) \times \mathbb{S}.$$

In view of Theorem 3.13 in Zhu and Yin (2007), the stochastic process $(N(t),\ P(t),\ Z(t),\ r(t))$ of model (6.2) is ergodic and it admits a unique stationary distribution in $\mathbb{R}_+^3 \times \mathbb{S}$.

This completes the proof.

APPENDIX T. The proof of Theorem 6.5

Proof. By Eq. (6.3), it follows that the left side of Eq. (R5) is nonpositive, and

$$-\lim_{t\to\infty}\frac{1}{t}\int_0^t\left[b\big(r(s)\big)+\frac{1}{2}\sigma_3^2\big(r(s)\big)\right]ds+\limsup_{t\to\infty}\frac{1}{t}\int_0^t\frac{\beta\big(r(s)\big)P(s)}{1+m\big(r(s)\big)Z(s)+n\big(r(s)\big)P(s)}ds\le 0.$$

From Assumption 2, we have

$$\limsup_{t\to\infty}\frac{1}{t}\int_0^t\hat{\beta}P(s)ds\le\lim_{t\to\infty}\frac{1}{t}\int_0^t\left[b\big(r(s)\big)+\frac{1}{2}\sigma_3^2\big(r(s)\big)\right]ds+\iota \text{ a.s.},$$

Further,

$$\limsup_{t\to\infty}\frac{1}{t}\int_0^t\hat{\beta}P(s)ds\le\sum_{k\in\mathbb{S}}\pi_k\left[b(k)+\frac{1}{2}\sigma_3^2(k)\right]\text{ a.s.}\tag{T1}$$

Taking upper limit on both sides of Eq. (R2) and combine with Eq. (T1), we get

$$\begin{aligned}\limsup_{t\to\infty}\frac{1}{t}\ln\frac{P(t)}{P(0)}\ge&\lim_{t\to\infty}\frac{1}{t}\int_0^t\left[v\big(r(s)\big)D\big(r(s)\big)S_0\big(r(s)\big)-\left(c\big(r(s)\big)+\frac{1}{2}\sigma_2^2\big(r(s)\big)\right)\right]ds-\\&\limsup_{t\to\infty}\frac{1}{t}\int_0^t\frac{\beta(r(s))}{m(r(s))}ds-\limsup_{t\to\infty}\frac{1}{t}\int_0^t\check{\gamma}P(s)\,ds-\liminf_{t\to\infty}\frac{1}{t}\int_0^t\check{\eta}Z(s)\,ds\\\ge&\sum_{k\in\mathbb{S}}\pi_k\left[v(k)D(k)S_0(k)-\left(c(k)+\frac{1}{2}\sigma_2^2(k)\right)\right]\\&-\frac{\check{\gamma}}{\hat{\beta}}\sum_{k\in\mathbb{S}}\pi_k\left[b(k)+\frac{1}{2}\sigma_3^2(k)\right]-\liminf_{t\to\infty}\frac{1}{t}\int_0^t\check{\eta}Z(s)\,ds-\frac{\check{\beta}}{\hat{m}}.\end{aligned}$$

Using Eq. (Q1), we get

$$\liminf_{t\to\infty}\frac{1}{t}\int_0^t Z(s)\,ds\ge\frac{\Re_0^S-\frac{\check{\gamma}}{\hat{\beta}}\sum_{k\in\mathbb{S}}\pi_k\left[b(k)+\frac{1}{2}\sigma_3^2(k)\right]}{\check{\eta}}-\frac{\check{\beta}}{\hat{m}\check{\eta}}=\frac{\Re_2^S}{\check{\eta}\hat{\beta}}-\frac{\check{\beta}}{\hat{m}\check{\eta}}\ a.s.$$

Obviously, $\liminf_{t\to\infty}\frac{1}{t}\int_0^t Z(s)ds>0$ a.s. if $\Re_2^S>\frac{\check{\beta}\hat{\beta}}{\hat{m}}$. Thus, in view of Theorem 6.4, phytoplankton is persistent in mean due to the ergodicity of model (6.2).

This completes the proof.

APPENDIX U. Auxiliary results

We assume that a product equals unity if the number of factors is zero. For a bounded and continuous function $f(t)$, we set

$$f^u = \sup_{t\geq 0} f(t), f^l = \inf_{t\geq 0} f(t).$$

Moreover, if $f(t)$ is integrable, we define

$$\langle f\rangle = \frac{1}{t}\int_0^t f(s)\,ds, \langle f\rangle_T = \frac{1}{T}\int_0^T f(s)\,ds.$$

Now, to facilitate our further discussions, we present the following definitions and lemmas. For an n-dimensional stochastic differential equation,

$$dx(t) = f(x(t),t)dt + g(x(t),t)dB(t),\ \ t \geq t_0 \tag{U1}$$

with initial value $x(t_0) = x_0 \in R^n$, where $B(t)$ is an n-dimensional standard Brownian motion, the associated differential operator $\mathcal{L}$ is defined by

$$\mathcal{L} = \frac{\partial}{\partial t} + \sum_{k=1}^n f_k(x,t)\frac{\partial}{\partial x_k} + \frac{1}{2}\sum_{k,j=1}^n [g^T(x,t)g(x,t)]_{kj}\frac{\partial^2}{\partial x_k \partial_{x_j}}. \tag{U2}$$

Definition U.1 (Zhang and Tan, 2015). Consider the following stochastic-impulsive differential equation:

$$\begin{cases} dX(t) = F\big(t,X(t)\big)dt + G\big(t,X(t)\big)dB(t),\ \ t \neq t_k,\ \ t > 0, \\ X(t_k^+) - X(t_k) = \beta_k X(t_k),\ \ t = t_k,\ \ k = 0,1,2,\cdots \end{cases} \tag{U3}$$

with the initial value $X(0) \in R^n$. Then a stochastic process $X(t) = (X_1(t), X_2(t), \cdots, X_n(t))T$, $t \in [0,\infty)$ is said to be a solution of model (U3) if

(1) $X(t)$ is $\mathcal{F}_t$ adapted, and continuous on $(0,t_1)$ and every interval $(t_k, t_{k+1}) \in R_+$, $k \in N$. $F\big(t,X(t)\big) \in \mathcal{L}^1(R_+;R^n), G(t,X(t)) \in \mathcal{L}^2(R_+;R^n)$, where each $\mathcal{L}^k(R_+;R^n)$ is R^n valued measurable $\mathcal{F}_t$-adapted process $f(t)$ and satisfies $\int_0^T |f(t)|^k\,dt < \infty$ almost surely for every T.

(2) For any t_k, $k \in \mathbb{N}$, $X(t_k^+) = \lim_{t\to t_k^+} X(t)$ exists and $X(t_k^-) = \lim_{t\to t_k^-} X(t)$ with probability one.

(3) For almost every $t \in (0, t_1)$, $X(t)$ obeys the following integral equation:

$$X(t) = X(0) + \int_0^t F(s, X(s))ds + \int_0^t G(s, X(s))dB(s).$$

For all $t \in [t_k, t_{k+1}]$, $k \in \mathbb{N}$, $X(t)$ obeys the following integral equation:

$$X(t) = X(t_k^+) + \int_{t_k}^t F(s, X(s))ds + \int_{t_k}^t G(s, X(s))dB(s).$$

Lemma U.1. *For any $u > 0$, the following inequality holds (Dalal et al., 2008):*

$$u \leq 2(u + 1 - \log u) - (4 - 2\log 2).$$

Proof The proof directly follows from Dalal et al. (2008).

Next, we present the definition of periodic Markovian process.

Definition U.2 (Zhao and Shao., 2021; Zhang et al., 2017b). A stochastic process $\xi(t) = \xi(t, \omega)(-\infty < t < +\infty)$ is said to be periodic with period T if for every finite sequence of numbers $t_1, t_2, \cdots, t_n$, the joint distribution of random variables $\xi(t_1 + h)$, $\xi(t_2 + h)$, ..., $\xi(t_n + h)$ is independent of h, where $h = kT$, $k = \pm 1, \pm 2, \cdots$.

Remark U.1. A Markov process $\xi(t)$ is T -periodic if and only if its transition probability function is T-periodic and the function $P_0(t, A) = P\{\xi(t) \in A\}$ satisfies the following equation:

$$P_0(s, A) = \int_{R^l} P_0(s, dx)\, P(s, x, s + T, A) \equiv p_0(s + T, A)$$

for every $A \in \mathcal{B}$ (Khasminskii, 2011).

Lemma U.2 (Khasminskii, 2011). *Let all the coefficients of the following Itô's differential equation:*

$$dx(t) = b(t, x(t))dt + \sigma(t, x(t))dB(t), \tag{U4}$$

are T-periodic in t, and satisfy the linear growing condition and the Lipschitz condition in every cylinder $U_l \times R_+$ for $l > 0$, where $U_l = \{x : \| x \| \leq l\}$. Further, assume that there exists a function $v = v(t, x)$ which is twice continuously differentiable with respect to x and once

continuously differentiable with respect to t *in* $R^n \times R_+$*, and* T *is periodic in* t *and satisfies the following conditions:*

$$\inf_{\|x\|>R} v(t,x) \to +\infty, as \ \ l \to +\infty, \tag{U5}$$

$$\mathcal{L}v(t,x) \leq -1, outside\ some\ compact\ set, \tag{U6}$$

then there exists a solution of model (U4) which is T*-periodic Markovian process.*

APPENDIX V. The proof of Theorem 7.1

Obviously, for any fixed $t \geq 0$, there exists an integer $n \in \{0, 1, 2, \cdots\}$ such that $nT \leq t \leq (n+1)T$.

As $t_{k+p} = t_k + T$ and $\alpha_k + p = \alpha_k$, we have

$$t_{k+np} = t_{t+(n-1)p} + T = \cdots = t_k + nT, \alpha_{k+np} = \alpha_{k+(n-1)p} = \cdots = \alpha_k.$$

Since $[0, \infty) \cap \{t_k, k \in \mathbb{N}\} = \{t_1, t_2, \cdots, t_p\}$, therefore, there exists a positive integer $r \in \{1, 2, \cdots, p\}$ such that

$$t_{r+np}, t_{r+1+np}, \cdots, t_{p+np} \in [t, (n+1)T),$$

$$t_{1+(n+1)p}, t_{2+(n+1)p}, \cdots, t_{r-1+(n+1)p} \in [(n+1)T, t+T).$$

Following Feng et al. (2021), we will show that model (7.3) has a unique globally positive solution $(y_1(t), y_2(t), y_3(t))$.

Obviously, the coefficients of model (7.3) satisfy the local Lipschitz condition. Thus, there exists a unique local solution of the model on $[0, \tau_e)$, where τ_e is the explosion time. To show that this solution is global, we need to verify $\tau_e = \infty$ a.s. Let $\gamma_0 > 1$ be sufficiently large such that all of the $y_1(0)$, $y_2(0)$ and $y_3(0)$ lie in the interval $[1/\gamma_0, \gamma_0]$. For any positive integer $\gamma(\gamma \geq \gamma_0)$, we define the stopping time as follows:

$$\tau_\gamma = \inf\{t \in [0, \tau_e]: y_1(t) \notin (1/\gamma, \gamma) \ or \ y_2(t) \notin (1/\gamma, \gamma) \ or \ y_3(t) \notin (1/\gamma, \gamma)\}.$$

Now, we set $\inf \emptyset = \infty$ and let τ_γ is increasing when $\gamma \to \infty$. Also, let $\tau_\infty = \lim_{\gamma \to +\infty} \tau_\gamma$. Obviously, if $\tau_\infty = \infty$, then $\tau_\infty \leq \tau_e$ a.s., $\tau_e = \infty$ and $(y_1(t), y_2(t), y_3(t)) \in R_+^3$ a.s. Define a C^3-function $V : R_+^3 \to R_+$ as follows:

$V\big(t_1(t), y_2(t), y_3(t)\big) =$

$$y_1(t) + 1 - \log y_1(t) + y_2(t) + 1 - \log y_2(t) + y_3(t) + 1 - \log y_3(t).$$

For any $T > 0$, employing Itô's formula on $t \in [0, \tau_\gamma \wedge T]$, we get

$$dV\big(t_1(t), y_2(t), y_3(t)\big) = \mathcal{L}V dt + \left(1 - \frac{1}{y_1(t)}\right)\sigma_1(t)y_1(t)dB_1(t)$$
$$+ \left(1 - \frac{1}{y_2(t)}\right)\sigma_2(t)y_2(t)dB_2(t) + \left(1 - \frac{1}{y_3(t)}\right)\sigma_3(t)y_3(t)dB_3(t),$$

where

$$\mathcal{L}V = (y_1(t) - 1)\left(-D(t) + \frac{1}{T}\sum_{j=1}^{p}\log\big(1 + \alpha_{1j}\big) - \frac{m(t)A_2(t)y_2(t)}{a(t)+A_2(t)y_2(t)}\right) + \frac{1}{2}\sigma_1^2(t)$$
$$+(y_2(t) - 1)\left(\frac{n(t)A_1(t)y_1(t)}{a(t)+A_2(t)y_2(t)} + \frac{1}{T}\sum_{j=1}^{p}\log\big(1 + \alpha_{2j}\big) - c(t) - \frac{\beta(t)y_3(t)}{a(t)+A_2(t)y_2(t)}\right) + \frac{1}{2}\sigma_2^2(t)$$
$$+(y_3(t) - 1)\left(\frac{\eta(t)A_2(t)y_2(t)}{a(t)+A_2(t)y_2(t)} - b(t) - \rho(t)y_3(t)\right) + \frac{1}{2}\sigma_3^2(t).$$

On manipulating the terms, we get

$$\mathcal{L}V = -D(t)y_1(t) + D(t) + y_1(t)\frac{1}{T}\sum_{j=1}^{p}\log\big(1 + \alpha_{1j}\big) - \frac{1}{T}\sum_{j=1}^{p}\log\big(1 + \alpha_{1j}\big)$$
$$-\frac{m(t)A_2(t)y_1(t)y_2(t)}{a(t)+A_2(t)y_2(t)} + \frac{m(t)A_2(t)y_2(t)}{a(t)+A_2(t)y_2(t)} + \frac{n(t)A_1(t)y_1(t)y_2(t)}{a(t)+A_2(t)y_2(t)}$$
$$-\frac{n(t)A_1(t)y_1(t)}{a(t)+A_2(t)y_2(t)} + y_2(t)\frac{1}{T}\sum_{j=1}^{p}\log\big(1 + \alpha_{2j}\big) - \frac{1}{T}\sum_{j=1}^{p}\log\big(1 + \alpha_{2j}\big)$$
$$-y_2(t)c(t) + c(t) - \frac{\beta(t)y_2(t)y_3(t)}{a(t)+A_2(t)y_2(t)} + \frac{\beta(t)y_3(t)}{a(t)+A_2(t)y_2(t)}$$
$$+\frac{\eta(t)A_2(t)y_2(t)y_3(t)}{a(t)+A_2(t)y_2(t)} - \frac{\eta(t)A_2(t)y_2(t)}{a(t)+A_2(t)y_2(t)} - b(t)y_3(t) + b(t)$$
$$-\rho(t)y_3(t)^2 + \rho(t)y_3(t) + \frac{1}{2}(\sigma_1^2(t) + \sigma_2^2(t) + \sigma_3^2(t)).$$

From the above, we get

$$\mathcal{L}V \le D^u + c^u + b^u + \frac{1}{2}[(\sigma_1^u)^2 + (\sigma_2^u)^2 + (\sigma_3^u)^2] + y_1(t)\frac{1}{T}\sum_{j=1}^{p}\log\big(1 + \alpha_{1j}\big) + \rho^u y_3(t)$$
$$+ y_2(t)\frac{1}{T}\sum_{j=1}^{p}\log\big(1 + \alpha_{2j}\big) + \frac{m^u A_2^u}{A_2^l} + \frac{n^u A_1^u y_1(t)}{A_2^l} + \frac{\beta^u y_3(t)}{a^l} + \frac{\eta^u A_2^u y_3(t)}{A_2^l}.$$

This yields,

$$\mathcal{L}V \le F_1 + \left(\frac{1}{T}\sum_{j=1}^{p}\log\left(1+\alpha_{1j}\right) + \frac{n^u A_1^u}{A_2^l}\right) y_1(t) + \frac{1}{T}\sum_{j=1}^{p}\log\left(1+\alpha_{2j}\right) y_2(t)$$

$$+\left(\frac{\beta^u}{a^l} + \frac{\eta^u A_2^u}{A_2^l} + \rho^u\right) y_3(t).$$

That is,

$$\mathcal{L}V \le F_1 + 2\left(\tfrac{1}{T}\textstyle\sum_{j=1}^{p}\log\left(1+\alpha_{1j}\right) + \frac{n^u A_1^u}{A_2^l}\right)\left[y_1(t) + 1 - \log y_1(t)\right]$$

$$+\tfrac{2}{T}\textstyle\sum_{j=1}^{p}\log\left(1+\alpha_{2j}\right)\left[y_2(t) + 1 - \log y_2(t)\right]$$

$$+2\left(\frac{\beta^u}{a^l} + \frac{\eta^u A_2^u}{A_2^l} + \rho^u\right)\left[y_3(t) + 1 - \log y_3(t)\right]$$

$$\le F_1 + F_2 V\left(y_1(t), y_2(t), y_3(t)\right),$$

with

$$F_1 = D^u + c^u + b^u + \frac{m^u A_2^u}{A_2^l} + \frac{1}{2}\left[(\sigma_1^u)^2 + (\sigma_2^u)^2 + (\sigma_3^u)^2\right],$$

$$F_2 = 2\left(\tfrac{1}{T}\textstyle\sum_{j=1}^{p}\log\left(1+\alpha_{1j}\right) + \frac{n^u A_1^u}{A_2^l}\right) \vee \tfrac{2}{T}\textstyle\sum_{j=1}^{p}\log\left(1+\alpha_{2j}\right) \vee 2\left(\frac{\beta^u}{a^l} + \frac{\eta^u A_2^u}{A_2^l} + \rho^u\right).$$

Thus, we have

$$dV\left(y_1(t), y_2(t), y_3(t)\right) \le F_1 dt + F_2 V\left(y_1(t), y_2(t), y_3(t)\right) + \sigma_1(t)[y_1(t) - 1]dB_1(t)$$

$$+\sigma_2(t)[y_2(t) - 1]dB_2(t) + \sigma_3(t)[y_3(t) - 1]dB_3(t),$$

Integrating both sides of the above inequality from 0 to $\tau_\gamma \wedge T$ and taking the expectation, we obtain

$$\mathbf{E}V\left(y_1\left(\tau_\gamma \wedge T\right), y_2\left(\tau_\gamma \wedge T\right), y_3\left(\tau_\gamma \wedge T\right)\right) \le V\left(y_1(0), y_2(0), y_3(0)\right) + F_1 T$$

$$+F_2 \mathbf{E}\int_0^{\tau_\gamma \wedge T} V\left(y_1(t), y_2(t), y_3(t)\right)dt.$$

In view of the Gronwall's inequality, we get

$$\mathbf{E}V\left(y_1\left(\tau_\gamma \wedge T\right), y_2\left(\tau_\gamma \wedge T\right), y_3\left(\tau_\gamma \wedge T\right)\right) \le \left(V\left(y_1(0), y_2(0), y_3(0)\right) + F_1 T\right)e^{F_2 T}.$$

Let $\Omega_\gamma(\omega) = \{\omega \in \Omega : \tau_\gamma = \tau_\gamma(\omega) \le T\}$. Then, for $\gamma \ge \gamma_0$, $y_1(\tau_\gamma, \omega)$ or $y_2(\tau_\gamma, \omega)$ or $y_3(\tau_\gamma, \omega)$ equals either γ or $1/\gamma$. Also, we have

$$V\left(y_1(\tau_\gamma, \omega), y_2(\tau_\gamma, \omega), y_3(\tau_\gamma, \omega)\right) \ge (\gamma + 1 - \log\gamma) \vee \left(\frac{1}{\gamma} + 1 + \log\gamma\right) \triangleq H(\gamma),$$

$$\begin{aligned}\left[V(y_1(0), y_2(0), y_3(0)) + F_1 T\right] e^{F_2 T} &\ge \mathbf{E} I_{\Omega_\gamma}(\omega) V\left(y_1(\tau_\gamma, \omega), y_2(\tau_\gamma, \omega), y_3(\tau_\gamma, \omega)\right) \\ &\ge \mathbf{P}\{\tau_\gamma \le T\} H(\gamma),\end{aligned}$$

where I_{Ω_γ} is the indicator function of Ω_γ. Let $\gamma \to \infty$, then $\lim_{\gamma\to\infty} \mathbf{P}\{\tau_\gamma \le T\} = 0$, which implies that $\mathbf{P}\{\tau_\gamma \le T\} = 0$. Since $T > 0$ is arbitrary, we have $\mathbf{P}\{\tau_\infty < \infty\} = 0$. Now, it suffices to show that $\mathbf{P}\{\tau_\infty = \infty\} = 1$, which will ensure that model (7.3) admits a unique positive solution $(y_1(t), y_2(t), y_3(t))$ for all $t \ge 0$ a.s.

Let $N(t) = A_1(t)y_1(t)$, $P(t) = A_2(t)y_2(t)$ and $Z(t) = y_3(t)$. In view of Lemma 7.1, $(N(t), P(t), Z(t))$ is the solution of model (7.2). Obviously, $N(t)$, $P(t)$, and $Z(t)$ are continuous on the intervals $(0, t_1)$ and (t_k, t_{k+1}), $k \in \mathbb{N}$. Also, for $t \ne t_k$, we have

$$\begin{aligned}dN(t) &= A_1'(t)y_1(t)dt + A_1(t)dy_1(t) \\ &= A_1(t)y_1(t)\left[-D(t) - \frac{m(t)A_2(t)y_2(t)}{a(t) + A_2(t)y_2(t)}\right]dt + \sigma_1(t)A_1(t)y_1(t)dB_1(t) \\ &= N(t)\left[-D(t) - \frac{m(t)P(t)}{a(t)+P(t)}\right]dt + \sigma_1(t)N(t)dB_1(t),\end{aligned}$$

$$\begin{aligned}dP(t) &= A_2'(t)y_2(t)dt + A_2(t)dy_2(t) \\ &= A_2(t)y_2(t)\left[\frac{n(t)A_1(t)y_1(t)}{a(t) + A_1(t)y_1(t)} - c(t) - \frac{\beta(t)y_3(t)}{a(t) + A_2(t)y_2(t)}\right]dt \\ &\quad + \sigma_2(t)A_2(t)y_2(t)dB_2(t) \\ &= P(t)\left[\frac{n(t)N(t)}{a(t)+P(t)} - c(t) - \frac{\beta(t)y_3(t)}{a(t)+P(t)}\right]dt + \sigma_2(t)P(t)dB_2(t),\end{aligned}$$

For $t = t_k$, $k \in \mathbb{N}$, we have

$$N(t_k^+) = \lim_{t\to t_k^+} A_1(t)y_1(t) = \left[\prod_{j=1}^{p}\left(1+\alpha_{1j}\right)\right]^{-\left(\frac{t_k}{T}\right)} \prod_{0\le t_j\le t_k}\left(1+\alpha_{1j}\right) y_1(t_k^+)$$

$$= (1+\alpha_{1k})A_1(t_k^+)y_1(t_k^+) = (1+\alpha_{1k})N(t_k),$$

$$N(t_k^-) = \lim_{t\to t_k^-} A_1(t)y_1(t) = \left[\prod_{j=1}^{p}\left(1+\alpha_{1j}\right)\right]^{-\left(\frac{t_k}{T}\right)} \prod_{0\le t_j< t_k}\left(1+\alpha_{1j}\right) y_1(t_k^+) = N(t_k).$$

Similarly, we have

$$P(t_k^+) = (1+\alpha_{2k})P(t_k),\ \ P(t_k^-) = P(t_k).$$

Thus, one can conclude that model (7.2) has a solution $(N(t), P(t), Z(t))$ for $t \ge 0$ with the initial value $(N(0), P(0), Z(0)) \in R_+^2$.

Next, we show that the solution of model (7.2) is unique. For $t \in [0, t_1]$, model (7.2) can be written as follows:

$$\begin{cases} dN(t) = \left[-D(t)N(t) - \frac{m(t)P(t)N(t)}{a(t)+P(t)}\right]dt + \sigma_1(t)N(t)dB_1(t), \\ dP(t) = \left[\frac{n(t)P(t)N(t)}{a(t)+P(t)} - c(t)P(t) - \frac{\beta(t)P(t)Z(t)}{a(t)+P(t)}\right]dt + \sigma_2(t)P(t)dB_2(t), \\ dZ(t) = \left[\frac{\eta(t)P(t)Z(t)}{a(t)+P(t)} - b(t)Z(t) - \rho(t)Z(t)^2\right]dt + \sigma_3(t)Z(t)dB_3(t), \end{cases} \tag{V1}$$

with the initial value $(N(0), P(0), Z(0)) = (N_0, P_0, Z_0)$. The above model can be written as follows:

$$\begin{cases} du(t) = \left[-D(t) - \frac{m(t)e^{v(t)}}{a(t)+e^{v(t)}} - \frac{\sigma_1^2(t)}{2}\right]dt + \sigma_1(t)dB_1(t), \\ dv(t) = \left[\frac{n(t)e^{u(t)}}{a(t)+e^{v(t)}} - c(t) - \frac{\beta(t)e^{w(t)}}{a(t)+e^{v(t)}} - \frac{\sigma_2^2(t)}{2}\right]dt + \sigma_2(t)PdB_2(t), \\ dw(t) = \left[\frac{\eta(t)e^{v(t)}}{a(t)+e^{v(t)}} - b(t) - \rho(t)e^{w(t)} - \frac{\sigma_3^2(t)}{2}\right]dt + \sigma_3(t)dB_3(t), \end{cases} \tag{V2}$$

with the initial value $(u(0), v(0), w(0)) = (\log N_0, \log P_0, \log Z_0)$.

As the coefficients of model (V2) satisfy the local Lipschitz condition, so the model has a unique solution $(u(0), v(0), w(0))$ by the theory of stochastic differential equations. Thus, in the view of Itô's formula, $(N(t), P(t), Z(t)) = (e^u(t), e^v(t), e^w(t))$ is the unique solution of model

(V1).

For $t \in (t_1, t_2]$, model (7.2) can be transformed into the following form:

$$\begin{cases} dN(t) = \left[-D(t)N(t) - \frac{m(t)P(t)N(t)}{a(t)+P(t)}\right]dt + \sigma_1(t)N(t)dB_1(t), \\ dP(t) = \left[\frac{n(t)P(t)N(t)}{a(t)+P(t)} - c(t)P(t) - \frac{\beta(t)P(t)Z(t)}{a(t)+P(t)}\right]dt + \sigma_2(t)P(t)dB_2(t), \\ dZ(t) = \left[\frac{\eta(t)P(t)Z(t)}{a(t)+P(t)} - b(t)Z(t) - \rho(t)Z(t)^2\right]dt + \sigma_3(t)Z(t)dB_3(t), \\ \left(N(t_1^+), P(t_1^+), Z(t_1^+) = (1+\alpha_{11})N(t_1^+), (1+\alpha_{21})P(t_1^+), Z(t_1^+)\right). \end{cases} \quad \text{(V3)}$$

By using the same method, we can show that model (V3) has a unique solution for $t \in (t_1, t_2]$. Thus, by the analogy, we obtain that model (7.2) has a unique solution with the initial value $(N(0), P(0), Z(0))$ for each $t \in (t_k, t_{k+1}]$.

This completes the proof.

APPENDIX W. The proof of Theorem 7.2

In view of Theorem 7.1, it suffices to prove that a periodic solution exists for the equivalent model (7.3) without impulses. Thus, we only need to verify the conditions (U5) and (U6) of Lemma U.2.

Define a C^3-function $V:[0,+\infty)\times R_+^3\to R_+$ as follows:

$$V(t,y_1,y_2,y_3)=\left(\frac{e^{w_1(t)}}{y_1}+\log y_1\right)+\left(\frac{e^{w_2(t)}}{y_2}+\log y_2\right)+\left(\frac{e^{w_3(t)}}{y_3}+\log y_3\right)=V_1+V_2+V_3,$$

where

$$\begin{aligned} w_1'(t)&=\langle D(t)+\sigma_1^2(t)\rangle_T-D(t)-\sigma_1^2(t),\\ w_2'(t)&=\langle c(t)+\sigma_2^2(t)\rangle_T-c(t)-\sigma_2^2(t),\\ w_1'(t)&=-\langle b(t)+\sigma_3^2(t)\rangle_T-b(t)-\sigma_3^2(t). \end{aligned} \tag{W1}$$

Owing to the periodicity of $D(t)$, $c(t)$, $b(t)$, $\sigma1(t)$, $\sigma2(t)$, $\sigma3(t)$, $w1(t)$, $w2(t)$ and $w3(t)$ are T-periodic functions. We can show it by using the approach of Feng et al. (2021).

According to condition (U5) of Lemma U.2, we need to verify that

$$\inf_{(t,y_1,y_2,y_3)\in[0,+\infty)\times(R_+^3\setminus U_\epsilon)} V(t,y)\to\infty,\ \ \epsilon\to\infty,$$

where $U_\epsilon=\left(\frac{1}{\epsilon},\epsilon\right)\times\left(\frac{1}{\epsilon},\epsilon\right)\times\left(\frac{1}{\epsilon},\epsilon\right)$. Note that, this condition trivially holds as

$$\frac{1}{2}+\log z\to+\infty, a.s. z\to 0^+, \frac{1}{z}+\log z\to+\infty, a.s. z\to+\infty.$$

Next, we prove condition (U6) of Lemma U.2. Using Itô formula, we get

$$\mathcal{L}V_1=-\frac{e^{w_1(t)}}{y_1}\left(-w_1'(t)-D(t)+\frac{1}{T}\sum_{j=1}^{p}\log\left(1+\alpha_{1j}\right)-\frac{m(t)A_2(t)y_2(t)}{a(t)+A_2(t)y_2(t)}-\sigma_1^2(t)\right)$$

$$-D(t)+\frac{1}{T}\sum_{j=1}^{p}\log\left(1+\alpha_{1j}\right)-\frac{m(t)A_2(t)y_2(t)}{a(t)+A_2(t)y_2(t)}-\frac{\sigma_1^2(t)}{2}$$

$$\leq-\frac{e^{w_1(t)}}{y_1}\left(-w_1'(t)-D(t)-\sigma_1^2(t)+\frac{1}{T}\sum_{j=1}^{p}\log\left(1+\alpha_{1j}\right)-\frac{m^uA_2^u}{A_2^l}\right)$$

$$+\frac{1}{T}\sum_{j=1}^{p}\log\left(1+\alpha_{1j}\right)-\frac{m^{l}A_{2}^{l}y_{2}(t)}{a^{u}+A_{2}^{u}M_{2}}-D(t)-\frac{\sigma_{1}^{2}(t)}{2},$$

$$\mathcal{L}V_{2}=-\frac{e^{w_{2}(t)}}{y_{2}}\left(-w_{2}'(t)+\frac{1}{T}\sum_{j=1}^{p}\log\left(1+\alpha_{2j}\right)+\frac{n(t)A_{1}(t)y_{1}(t)}{a(t)+A_{2}(t)y_{2}(t)}-c(t)-\right.$$

$$\left.\frac{\beta(t)y_{3}(t)}{a(t)+A_{2}(t)y_{2}(t)}-\sigma_{2}^{2}(t)\right)+\frac{1}{T}\sum_{j=1}^{p}\log\left(1+\alpha_{2j}\right)+\frac{n(t)A_{1}(t)y_{1}(t)}{a(t)+A_{2}(t)y_{2}(t)}-c(t)-$$

$$\frac{\beta(t)y_{3}(t)}{a(t)+A_{2}(t)y_{2}(t)}-\frac{\sigma_{2}^{2}(t)}{2}$$

$$\leq-\frac{e^{w_{2}(t)}}{y_{2}}\left(-w_{2}'(t)-c(t)-\sigma_{2}^{2}(t)+\frac{1}{T}\sum_{j=1}^{p}\log\left(1+\alpha_{2j}\right)-\frac{\beta^{u}M_{3}}{a^{l}}\right)$$

$$-\frac{e^{w_{2}^{l}}n^{l}A_{1}^{l}y_{1}(t)}{M_{2}(a^{u}+A_{2}^{u}M_{2})}+\frac{n^{u}A_{1}^{u}M_{1}}{a^{l}}+\frac{1}{T}\sum_{j=1}^{p}\log\left(1+\alpha_{2j}\right)-c(t)-\frac{\beta^{l}y_{3}(t)}{a^{u}+A_{2}^{u}M_{2}}-\frac{\sigma_{2}^{2}(t)}{2},$$

$$\mathcal{L}V_{3}=-\frac{e^{w_{3}(t)}}{y_{3}}\left(-w_{3}'(t)+\frac{\eta(t)A_{2}(t)y_{2}(t)}{a(t)+A_{2}(t)y_{2}(t)}-b(t)-\rho(t)y_{3}(t)-\sigma_{3}^{2}(t)\right)$$

$$+\frac{\eta(t)A_{2}(t)y_{2}(t)}{a(t)+A_{2}(t)y_{2}(t)}-b(t)-\rho(t)y_{3}(t)-\frac{\sigma_{3}^{2}(t)}{2}$$

$$\leq-\frac{e^{w_{3}(t)}}{y_{3}}\left(-w_{3}'(t)-b(t)-\sigma_{3}^{2}(t)\right)-\frac{e^{w_{3}^{l}}n^{l}A_{2}^{l}y_{2}(t)}{M_{3}(a^{u}+A_{2}^{u}M_{2})}+\rho^{u}e^{w_{3}^{u}}$$

$$+\frac{\eta^{u}A_{2}^{u}}{A_{2}^{l}}-b(t)-\rho^{l}y_{3}(t)-\frac{\sigma_{3}^{2}(t)}{2}.$$

In view of Eq. (W1), we obtain

$$\mathcal{L}V=\mathcal{L}V_{1}+\mathcal{L}V_{2}+\mathcal{L}V_{3}$$

$$\leq\frac{e^{w_{1}(t)}}{y_{1}}\left(\frac{1}{T}\sum_{j=1}^{p}\log\left(1+\alpha_{1j}\right)-\langle D(t)+\sigma_{1}^{2}(t)\rangle_{T}-\frac{m^{u}A_{2}^{u}}{A_{2}^{l}}\right)$$

$$-\frac{e^{w_{2}(t)}}{y_{2}}\left(\frac{1}{T}\sum_{j=1}^{p}\log\left(1+\alpha_{2j}\right)-\langle c(t)+\sigma_{2}^{2}(t)\rangle_{T}-\frac{\beta^{u}M_{3}}{a^{l}}\right)$$

$$-\frac{e^{w_{3}(t)}}{y_{3}}\left(\langle b(t)+\sigma_{3}^{2}(t)\rangle_{T}\right)-\frac{m_{l}A_{2}^{l}y_{2}(t)}{a^{u}+A_{2}^{u}M_{2}}-\frac{e^{w_{2}^{l}}n^{l}A_{1}^{l}y_{1}(t)}{M_{2}(a^{u}+A_{2}^{u}M_{2})}$$

$$-\rho^{l}y_{3}(t)-\frac{\beta^{l}y_{3}(t)}{a^{u}+A_{2}^{u}M_{2}}-\frac{e^{w_{3}^{l}}\eta^{l}A_{2}^{l}y_{2}(t)}{M_{3}(a^{u}+A_{2}^{u}M_{2})}+\frac{1}{T}\sum_{j=1}^{p}\log\left(1+\alpha_{1j}\right)$$

$$+\rho^u e^{w_3^u} + \frac{1}{T}\sum_{j=1}^{p}\log\left(1+\alpha_{2j}\right) + \frac{n^u A_1^u M_1}{a^l} + \frac{\eta^u A_2^u}{A_2^l}$$

$$-D(t) - c(t) - b(t) - \frac{\sigma_1^2(t)}{2} - \frac{\sigma_2^2(t)}{2} - \frac{\sigma_3^2(t)}{2}.$$

Let

$$\varphi^* = \frac{1}{T}\sum_{j=1}^{p}\log\left(1+\alpha_{1j}\right) + \frac{1}{T}\sum_{j=1}^{p}\log\left(1+\alpha_{2j}\right) + \frac{n^u A_1^u M_1}{a^l} + \frac{\eta^u A_2^u}{A_2^l} + \rho^u e^{w_3^u}$$

$$-D^l - c^l - b^l - \frac{\left(\sigma_1^l\right)^2}{2} - \frac{\left(\sigma_2^l\right)^2}{2} - \frac{\left(\sigma_3^l\right)^2}{2}.$$

Thus,

$$\mathcal{L}v \le \varphi^* - \frac{e^{w_1^l}}{y_1}\phi_1 - \frac{e^{w_2^l}}{y_2}\phi_2 - \frac{e^{w_1^l}}{y_1}\left(b^l + \left(\sigma_3^l\right)^2\right) - \frac{m_l A_2^l y_2(t)}{a^u + A_2^u M_2} - \rho^l y_3(t)$$

$$- \frac{e^{w_2^l} n^l A_1^l y_1(t)}{M_2(a^u + A_2^u M_2)} - \frac{\beta^l y_3(t)}{a^u + A_2^u M_2} - \frac{e^{w_3^l}\eta^l A_2^l y_2(t)}{M_3(a^u + A_2^u M_2)} \tag{W2}$$

$$\triangleq \Gamma(y_1, y_2, y_3).$$

Obviously,

$$\Gamma(y_1, y_2, y_3) \to -\infty, a.s. y_1 \to 0^+ \ or \ y_2 \to 0^+ \ or \ y_3 \to 0^+,$$

$$\Gamma(y_1, y_2, y_3) \to -\infty, a.s. y_1 \to +\infty \ or \ y_2 \to +\infty \ or \ y_3 \to +\infty. \tag{W3}$$

From (W2) and (W3), we take ϵ sufficiently small such that

$$\mathcal{L}V \le -1, \ \ for \ (y_1, y_2, y_3) \in R_+^3 \backslash U,$$

where $U = \left[\epsilon, \frac{1}{\epsilon}\right] \times \left[\epsilon, \frac{1}{\epsilon}\right] \times \left[\epsilon, \frac{1}{\epsilon}\right]$. Therefore, the solution $y(t) = (y_1(t), y_2(t), y_3(t))$ of model (7.3) with $y_1(0) > 0$, $y_2(0) > 0$, and $y_3(0) > 0$ is a positive T-periodic Markov process.

The previous analyses yield that

$$N(t) = A_1(t)y_1(t) = \left[\prod_{j=1}^{p}\left(1+\alpha_{1j}\right)\right]^{-\left(\frac{t}{T}\right)} \prod_{0\le t_k<t}(1+\alpha_{1k})\, y_1(t),$$

$$P(t) = A_2(t)y_2(t) = \left[\prod_{j=1}^{p}\left(1+\alpha_{2j}\right)\right]^{-\left(\frac{t}{T}\right)} \prod_{0\le t_k<t}(1+\alpha_{2k})\, y_2(t),$$

$$Z(t) = y_3(t),$$

where $A_1(t)$ and $A_2(t)$ are T-periodic functions. Thus, $(N(t), P(t), Z(t))$ is a positive T-periodic solution of model (7.2).

This completes the proof.